Publishing House ASV

begell house, inc. publishers

PAACH

Scientific coordination is carried out by the Russian Academy of Architecture and Construction Sciences (RAACS)

Volume 19 • Issue 3 • 2023

ISSN 2588-0195 (Online)
ISSN 2587-9618 (Print) Continues ISSN 1524-5845

International Journal for

Computational Civil and Structural Engineering

Международный журнал по расчету гражданских и строительных конструкций

http://ijccse.iasv.ru/index.php/IJCCSE
http://raasn.ru/public.php

DOI: 10.22337/2587-9618
GICID: 71.0000.1500.2830

EXECUTIVE EDITOR

Vladimir I. Travush,
Full Member of RAACS, Professor, Dr.Sc.,
Vice-President of the Russian Academy
of Architecture and Construction Sciences;
Urban Planning Institute
of Residential and Public Buildings;
24, Ulitsa Bolshaya Dmitrovka, 107031, Moscow, Russia

EDITOR-IN-CHIEF

Vladimir N. Sidorov,
Corresponding Member of RAACS, Professor, Dr.Sc.,
National Research Moscow State University of Civil
Engineering; Russian University of Transport
(RUT – MIIT); Moscow Institute of Architecture
(State Academy); Perm National Research Polytechnic
University; 26, Yaroslavskoe Shosse, 129337,
Moscow, Russia

EDITORIAL DIRECTOR

Valery I. Telichenko,
Full Member of RAACS, Professor, Dr.Sc.,
The First Vice-President of the Russian Academy
of Architecture and Construction Sciences;
Honorary President of National Research
Moscow State University of Civil Engineering;
24, Ulitsa Bolshaya Dmitrovka, 107031, Moscow, Russia

MANAGING EDITOR

Nadezhda S. Nikitina,
Professor, Ph.D.,
Director of ASV Publishing House;
National Research Moscow State University
of Civil Engineering;
26, Yaroslavskoe Shosse, 129337, Moscow, Russia

ASSOCIATE EDITORS

Pavel A. Akimov,
Full Member of RAACS, Professor, Dr.Sc.,
Acting Rector of National Research
Moscow State University of Civil Engineering;
Vice-President of the Russian Academy
of Architecture and Construction Sciences;
Tomsk State University of Architecture and Building;
Russian University of Friendship of Peoples;
26, Yaroslavskoe Shosse, 129337, Moscow, Russia

Alexander M. Belostotsky,
Full Member of RAACS, Professor, Dr.Sc.,
Research & Development Center "STADYO";
National Research Moscow State University of Civil
Engineering; Russian University of Transport (RUT –
MIIT); Russian University of Friendship of Peoples;
Perm National Research Polytechnic University;
Tomsk State University of Architecture and Building;
Irkutsk National Research Technical University;
8th Floor, 18, ul. Tretya Yamskogo Polya,
125040, Moscow, Russia

Mikhail Belyi, Professor, Dr.Sc.,
Dassault Systèmes Simulia;
1301 Atwood Ave Suite 101W
02919 Johnston, RI, United States

Vitaly Bulgakov, Professor, Dr.Sc.,
Micro Focus;
Newbury, United Kingdom

Nikolai P. Osmolovskii, Professor, Dr.Sc.,
Systems Research Institute, Polish Academy of Sciences;
Kazimierz Pulaski University
of Technology and Humanities in Radom;
29, ul. Malczewskiego, 26-600, Radom, Poland

Gregory P. Panasenko, Professor, Dr.Sc.,
Equipe d'Analise Numerique; NMR CNRS 5585
University Gean Mehnet;
23 rue. P.Michelon 42023, St.Etienne, France

Scientific coordination is carried out by the Russian Academy of Architecture and Construction Sciences (RAACS)

PUBLISHER

ASV Publishing House
(ООО «Издательство АСВ»)
19/1,12, Yaroslavskoe Shosse, 120338, Moscow, Russia
Tel. +7(925)084-74-24; E-mail: iasv@iasv.ru; Интернет-сайт: http://iasv.ru/

ADVISORY EDITORIAL BOARD

Mojtaba Aslami, Ph.D,
Fasa University; Daneshjou blvd,
Fasa, Fars Province, Iran

Klaus-Jurgen Bathe, Professor
Massachusetts Institute
of Technology;
Cambridge, MA 02139, USA

Alexander T. Bekker,
Academician of RAACS,
Professor, Dr.Sc.,
Far Eastern Federal University;
Russian Academy of Architecture
and Construction Sciences;
8, Sukhanova Street, Vladivostok,
690950, Russia

Tomas Bock, Professor, Dr.-Ing.,
Technical University of Munich,
Arcisstrasse 21, D-80333
Munich, Germany

Jan Buynak, Professor, Ph.D.,
University of Žilina;
1, Univerzitná, Žilina, 010 26,
Slovakia

Vladimir T. Erofeev,
Full Member of RAACS,
Professor, Dr.Sc.,
Ogarev Mordovia State University;
68, Bolshevistskaya Str., Saransk
430005, Republic of Mordovia,
Russia

Victor S. Fedorov,
Full Member of RAACS,
Professor, Dr.Sc.,
Russian University of Transport
(RUT – MIIT);
9b9 Obrazcova Street, Moscow,
127994, Russia

Sergey V. Fedosov,
Full Member of RAACS,
Professor, Dr.Sc.,
Russian Academy of Architecture
and Construction Sciences;
24, Ul. Bolshaya Dmitrovka, 107031,
Moscow, Russia

Sergiy Yu. Fialko,
Professor, Dr.Sc.,
Cracow University of Technology;
24, Warszawska Street, Kraków,
31-155, Poland

Vladimir G. Gagarin,
Corresponding Member
of RAACS, Professor, Dr.Sc.,
Research Institute of Building
Physics of Russian Academy
of Architecture and Construction
Sciences;
21, Lokomotivny Proezd,
Moscow, 127238, Russia

Vyatcheslav A. Ilyichev,
Full Member of RAACS,
Professor, Dr.Sc.,
Russian Academy of Architecture
and Construction Sciences;
Podzemproekt Ltd.;
24, Ulitsa Bolshaya Dmitrovka,
Moscow, 107031, Russia

Marek Iwański,
Professor, Dr.Sc.,
Kielce University of Technology;
7, al. Tysiąclecia Państwa Polskiego
Kielce, 25 – 314, Poland

Sergey Yu. Kalashnikov,
Advisor of RAACS,
Professor, Dr.Sc.,
Volgograd State Technical
University; 28, Lenin avenue,
Volgograd, 400005, Russia

Semen S. Kaprielov,
Academician of RAACS,
Professor, Dr.Sc.,
Research Center of Construction;
6, 2nd Institutskaya St., Moscow,
109428, Russia

Nikolay I. Karpenko,
Full Member of RAACS,
Professor, Dr.Sc.,
Research Institute of Building
Physics of Russian Academy
of Architecture and Construction
Sciences; Russian Academy of
Architecture and Construction
Sciences; 21, Lokomotivny Proezd,
Moscow, 127238, Russia

Vladimir V. Karpov,
Professor, Dr.Sc., Saint Petersburg
State University of Architecture and
Civil Engineering;
4, 2-nd Krasnoarmeiskaya Steet,
Saint Petersburg, 190005, Russia

Galina G. Kashevarova,
Corresponding Member
of RAACS, Professor, Dr.Sc.,
Perm National Research
Polytechnic University;
29 Komsomolsky pros., Perm,
Perm Krai, 614990, Russia

John T. Katsikadelis,
Professor, Dr.Eng, PhD, Dr.h.c.,
National Technical University of
Athens; Zografou Campus
9, Iroon Polytechniou str
15780 Zografou, Greece

Vitaly I. Kolchunov,
Full Member of RAACS,
Professor, Dr.Sc., Southwest State
University; Russian Academy of
Architecture and Construction
Sciences; 94, 50 let Oktyabrya,
Kursk, 305040, Russia

Dmitry V. Kozlov, Dr. Sc.
Engineering, Professor, Head of
the Department of Hydraulics and
Hydrotechnical Construction, NRU
MGSU,
26, Yaroslavskoe Shosse., 129337,
Moscow, Russia

Markus König, Professor
Ruhr-Universität Bochum;
150, Universitätsstraße, Bochum,
44801, Germany

Sergey B. Kositsin,
Advisor of RAACS,
Professor, Dr.Sc.,
Russian University of Transport
(RUT – MIIT); 9b9 Obrazcova
Street, Moscow, 127994, Russia

Sergey B. Krylov,
Corresponding Member
of RAACS, Professor, Dr.Sc.,
Research Center of Construction;
6, 2nd Institutskaya St., Moscow,
109428, Russia

Sergey V. Kuznetsov,
Professor, Dr.Sc.,
Ishlinsky Institute for Problems
in Mechanics of the Russian
Academy of Sciences;
101-1, Prosp. Vernadskogo,
Moscow, 119526, Russia

Vladimir V. Lalin,
Professor, Dr.Sc.,
Peter the Great Saint-Petersburg Polytechnic University;
29, Ul. Politechnicheskaya, Saint-Petersburg, 195251, Russia

Leonid S. Lyakhovich,
Full Member of RAACS, Professor, Dr.Sc., Tomsk State University of Architecture and Building; 2, Solyanaya Sq., Tomsk, 634003, Russia

Rashid A. Mangushev,
Corresponding Member of RAACS, Professor, Dr.Sc., Saint Petersburg State University of Architecture and Civil Engineering;
4, 2-nd Krasnoarmeiskaya Steet, Saint Petersburg, 190005, Russia

Ilizar T. Mirsayapov,
Advisor of RAACS, Professor, Dr.Sc., Kazan State University of Architecture and Engineering; 1, Zelenaya Street, Kazan, 420043, Republic of Tatarstan, Russia

Vladimir L. Mondrus,
Corresponding Member of RAACS, Professor, Dr.Sc., National Research Moscow State University of Civil Engineering;
Yaroslavskoe Shosse 26, Moscow, 129337, Russia

Valery I. Morozov,
Corresponding Member of RAACS, Professor, Dr.Sc., Saint Petersburg State University of Architecture and Civil Engineering;
4, 2-nd Krasnoarmeiskaya Steet, Saint Petersburg, 190005, Russia

Anatoly V. Perelmuter,
Foreign Member of RAACS, Professor, Dr.Sc., SCAD Soft;
Office 1,2, 3a Osvity street, Kiev, 03037, Ukraine

Alexey N. Petrov,
Advisor of RAACS, Professor, Dr.Sc., Petrozavodsk State University; 33, Lenina Prospect, Petrozavodsk, 185910, Republic of Karelia, Russia

Vladilen V. Petrov,
Full Member of RAACS, Professor, Dr.Sc.,
Yuri Gagarin State Technical University of Saratov;
77 Politechnicheskaya Street, Saratov, 410054, Russia

Jerzy Z. Piotrowski,
Professor, Dr.Sc.,
Kielce University of Technology;
al. Tysiąclecia Państwa Polskiego 7, Kielce, 25 – 314, Poland

Chengzhi Qi, Professor, Dr.Sc.,
Beijing University of Civil Engineering and Architecture;
1, Zhanlanlu, Xicheng District, Beijing, China

Vladimir P. Selyaev,
Full Member of RAACS, Professor, Dr.Sc., Ogarev Mordovia State University;
68, Bolshevistskaya Str., Saransk 430005, Republic of Mordovia, Russia

Eun Chul Shin,
Professor, Ph.D.,
Incheon National University;
(Songdo-dong)119 Academy-ro, Yeonsu-gu, Incheon, Korea

D.V. Singh,
Professor, Ph.D,
University of Roorkee;
Roorkee, India, 247667

Wacław Szcześniak,
Foreign Member of RAACS, Professor, Dr.Sc.,
Lublin University of Technology;
Ul. Nadbystrzycka 40, 20-618 Lublin, Poland

Tadatsugu Tanaka,
Professor, Dr.Sc.,
Tokyo University; 7-3-1 Hongo, Bunkyo, Tokyo, 113-8654, Japan

Josef Vican,
Professor, Ph.D,
University of Žilina;
1, Univerzitná, Žilina, 010 26, Slovakia

Zbigniew Wojcicki,
Professor, Dr.Sc.,
Wroclaw University of Technology;
11 Grunwaldzki Sq., 50-377, Wrocław, Poland

Artur Zbiciak, Professor, Dr.Sc.,
Warsaw University of Technology;
Pl. Politechniki 1, 00-661 Warsaw, Poland

Segrey I. Zhavoronok, Ph.D.,
Institute of Applied Mechanics of Russian Academy of Sciences;
Moscow Aviation Institute (National Research University);
7, Leningradsky Prt., Moscow, 125040, Russia

Askar Zhussupbekov,
Professor, Dr.Sc.,
Eurasian National University;
5, Munaitpassov street, Astana, 010000, Kazakhstan

TECHNICAL EDITOR

Taymuraz B. Kaytukov,
Advisor of RAACS,
Associate Professor, Ph.D.,
Vice-Rector of National Research Moscow State University of Civil Engineering;
Yaroslavskoe Shosse 26,
Moscow, 129337, Russia

EDITORIAL TEAM

Vadim K. Akhmetov, Professor, Dr.Sc., National Research Moscow State University of Civil Engineering; 26, Yaroslavskoe Shosse, 129337 Moscow, Russia

Pavel A. Akimov, Full Member of RAACS, Professor, Dr.Sc., Acting Rector of National Research Moscow State University of Civil Engineering; Vice-President of the Russian Academy of Architecture and Construction Sciences; Tomsk State University of Architecture and Building; Russian University of Friendship of Peoples; 26, Yaroslavskoe Shosse, 129337, Moscow, Russia

Alexander M. Belostotsky, Full Member of RAACS, Professor, Dr.Sc., Research & Development Center "STADYO"; National Research Moscow State University of Civil Engineering; Russian University of Transport (RUT – MIIT); Russian University of Friendship of Peoples; Perm National Research Polytechnic University; Tomsk State University of Architecture and Building; Irkutsk National Research Technical University; 8th Floor, 18, ul. Tretya Yamskogo Polya, 125040, Moscow, Russia

Mikhail Belyi, Professor, Dr.Sc., Dassault Systèmes Simulia; 1301 Atwood Ave Suite 101W 02919 Johnston, RI, United States

Vitaly Bulgakov, Professor, Dr.Sc., Micro Focus; Newbury, United Kingdom

Charles El Nouty, Professor, Dr.Sc., LAGA Paris-13 Sorbonne Paris Cite; 99 avenue J.B. Clément, 93430 Villetaneuse, France

Natalya N. Fedorova, Professor, Dr.Sc., Novosibirsk State University of Architecture and Civil Engineering (SIBSTRIN); 113 Leningradskaya Street, Novosibirsk, 630008, Russia

Darya Filatova, Professor, Dr.Sc., Probability, Assessment, Reasoning and Inference Studies Research Group, EPHE Laboratoire CHART (PARIS) 4-14, rue Ferrus, 75014 Paris

Vladimir Ya. Gecha, Professor, Dr.Sc., Research and Production Enterprise All-Russia Scientific-Research Institute of Electromechanics with Plant Named after A.G. Iosiphyan; 30, Volnaya Street, Moscow, 105187, Russia

Taymuraz B. Kaytukov, Advisor of RAACS, Associate Professor, Ph.D, Vice-Rector of National Research Moscow State University of Civil Engineering; 26, Yaroslavskoe Shosse, 129337, Moscow, Russia

Marina L. Mozgaleva, Professor, Dr.Sc., National Research Moscow State University of Civil Engineering; 26, Yaroslavskoe Shosse, 129337 Moscow, Russia

Nadezhda S. Nikitina, Professor, Ph.D., Director of ASV Publishing House; National Research Moscow State University of Civil Engineering; 26, Yaroslavskoe Shosse, 129337 Moscow, Russia

Nikolai P. Osmolovskii, Professor, Dr.Sc., Systems Research Institute Polish Academy of Sciences; Kazimierz Pulaski University of Technology and Humanities in Radom; 29, ul. Malczewskiego, 26-600, Radom, Poland

Gregory P. Panasenko, Professor, Dr.Sc., Equipe d'Analise Numerique NMR CNRS 5585 University Gean Mehnet; 23 rue. P.Michelon 42023, St.Etienne, France

Andreas Rauh, Prof. Dr.-Ing. habil. Carl von Ossietzky Universität Oldenburg, Germany School II - Department of Computing Science Group Distributed Control in Interconnected Systems D-26111 Oldenburg, Germany

Zhan Shi, Professor LPSM, Université Paris VI 4 place Jussieu, F-75252 Paris Cedex 05, France

Marina V. Shitikova, National Research Moscow State University of Civil Engineering, Advisor of RAACS, Professor, Dr.Sc., Voronezh State Technical University; 14, Moscow Avenue, Voronezh, 394026, Russia

Igor L. Shubin, Corresponding Member of RAACS, Professor, Dr.Sc., Research Institute of Building Physics of Russian Academy of Architecture and Construction Sciences; 21, Lokomotivny Proezd, Moscow, 127238, Russia

Vladimir N. Sidorov, Corresponding Member of RAACS, Professor, Dr.Sc., National Research Moscow State University of Civil Engineering; Russian University of Transport (RUT – MIIT); Moscow Institute of Architecture (State Academy); Perm National Research Polytechnic University; 26, Yaroslavskoe Shosse, 129337, Moscow, Russia

Valery I. Telichenko, Full Member of RAACS, Professor, Dr.Sc., The First Vice-President of the Russian Academy of Architecture and Construction Sciences; National Research Moscow State University of Civil Engineering; 24, Ulitsa Bolshaya Dmitrovka, 107031, Moscow, Russia

Vladimir I. Travush, Full Member of RAACS, Professor, Dr.Sc., Vice-President of the Russian Academy of Architecture and Construction Sciences; Urban Planning Institute of Residential and Public Buildings; 24, Ulitsa Bolshaya Dmitrovka, 107031, Moscow, Russia

INVITED REVIEWERS

Akimbek A. Abdikalikov, Professor, Dr.Sc.,
Kyrgyz State University of Construction, Transport and Architecture n.a. N. Isanov;
34 Maldybayeva Str., Bishkek, 720020, Biskek, Kyrgyzstan

Vladimir N. Alekhin, Advisor of RAACS, Professor, Dr.Sc.,
Ural Federal University named after the first President of Russia B.N. Yeltsin;
19 Mira Street, Ekaterinburg, 620002, Russia

Irina N. Afanasyeva, Ph.D., University of Florida; Gainesville, FL 32611, USA

Ján Čelko, Professor, PhD, Ing., University of Žilina; Univerzitná 1, 010 26, Žilina, Slovakia

Tatyana L. Dmitrieva, Professor, Dr.Sc.,
Irkutsk National Research Technical University; 83, Lermontov street, Irkutsk, 664074, Russia

Petr P. Gaidzhurov, Advisor of RAACS, Professor, Dr.Sc.,
Don State Technical University; 1, Gagarina Square, Rostov-on-Don, 344000, Russia

Jacek Grosel, Associate Professor, Dr inz.
Wroclaw University of Technology; 11 Grunwaldzki Sq., 50-377, Wrocław, Poland

Stanislaw Jemioło, Professor, Dr.Sc.,
Warsaw University of Technology; 1, Pl. Politechniki, 00-661, Warsaw, Poland

Konstantin I. Khenokh, M.Ing., M.Sc.,
General Dynamics C4 Systems; 8201 E McDowell Rd, Scottsdale, AZ 85257, USA

Christian Koch, Dr.-Ing., Ruhr-Universität Bochum;
Lehrstuhl für Informatik im Bauwesen, Gebäude IA, 44780, Bochum, Germany

Gaik A. Manuylov, Professor, Ph.D.,
Moscow State University of Railway Engineering; 9, Obraztsova Street, Moscow, 127994, Russia

Alexander S. Noskov, Professor, Dr.Sc.,
Ural Federal University named after the first President of Russia B.N. Yeltsin;
19 Mira Street, Ekaterinburg, 620002, Russia

Grzegorz Świt, Professor, Dr.hab. Inż.,
Kielce University of Technology; 7, al. Tysiąclecia Państwa Polskiego, Kielce, 25 – 314, Poland

AIMS AND SCOPE

The aim of the Journal is to advance the research and practice in structural engineering through the application of computational methods. The Journal will publish original papers and educational articles of general value to the field that will bridge the gap between high-performance construction materials, large-scale engineering systems and advanced methods of analysis.

The scope of the Journal includes papers on computer methods in the areas of structural engineering, civil engineering materials and problems concerned with multiple physical processes interacting at multiple spatial and temporal scales. The Journal is intended to be of interest and use to researches and practitioners in academic, governmental and industrial communities.

ОБЩАЯ ИНФОРМАЦИЯ О ЖУРНАЛЕ

International Journal for Computational Civil and Structural Engineering

(Международный журнал по расчету гражданских и строительных конструкций)

Международный научный журнал "International Journal for Computational Civil and Structural Engineering (Международный журнал по расчету гражданских и строительных конструкций)" (IJCCSE) является ведущим научным периодическим изданием по направлению «Инженерные и технические науки», издаваемым, начиная с 1999 года (ISSN 2588-0195 (Online); ISSN 2587-9618 (Print) Continues ISSN 1524-5845). В журнале на высоком научно-техническом уровне рассматриваются проблемы численного и компьютерного моделирования в строительстве, актуальные вопросы разработки, исследования, развития, верификации, апробации и приложений численных, численно-аналитических методов, программно-алгоритмического обеспечения и выполнения автоматизированного проектирования, мониторинга и комплексного наукоемкого расчетно-теоретического и экспериментального обоснования напряженно-деформированного (и иного) состояния, прочности, устойчивости, надежности и безопасности ответственных объектов гражданского и промышленного строительства, энергетики, машиностроения, транспорта, биотехнологий и других высокотехнологичных отраслей.

В редакционный совет журнала входят известные российские и зарубежные деятели науки и техники (в том числе академики, члены-корреспонденты, иностранные члены, почетные члены и советники Российской академии архитектуры и строительных наук). Основной критерий отбора статей для публикации в журнале − их высокий научный уровень, соответствие которому определяется в ходе высококвалифицированного рецензирования и объективной экспертизы, поступающих в редакцию материалов.

Журнал входит в Перечень ВАК РФ ведущих рецензируемых научных изданий, в которых должны быть опубликованы основные научные результаты диссертаций на соискание ученой степени кандидата наук, на соискание ученой степени доктора наук по научным специальностям и соответствующим им отраслям науки:

- 1.1.8 – Механика деформируемого твердого тела (технические науки),
- 1.2.2 – Математическое моделирование численные методы и комплексы программ (технические науки),
- 2.1.1 – Строительные конструкции, здания и сооружения (технические науки),
- 2.1.2 – Основания и фундаменты, подземные сооружения (технические науки),
- 2.1.5 – Строительные материалы и изделия (технические науки),
- 05.23.07 – Гидротехническое строительство (технические науки),
- 2.1.9 – Строительная механика (технические науки)

В Российской Федерации журнал индексируется Российским индексом научного цитирования (РИНЦ).

Журнал входит в базу данных Russian Science Citation Index (RSCI), полностью интегрированную с платформой Web of Science. Журнал имеет международный статус и высылается в ведущие библиотеки и научные организации мира.

Издатели журнала – *Издательство Ассоциации строительных высших учебных заведений /АСВ/* (Россия, г. Москва) и до 2017 года *Издательский дом Begell House Inc*. (США, г. Нью-Йорк). Официальными партнерами издания является *Российская академия архитектуры и строительных наук* (РААСН), осуществляющая научное курирование издания, и *Научно-исследовательский центр СтаДиО* (ЗАО НИЦ СтаДиО).

Цели журнала – демонстрировать в публикациях российскому и международному профессиональному сообществу новейшие достижения науки в области вычислительных методов

решения фундаментальных и прикладных технических задач, прежде всего в области строительства.

Задачи журнала:

• предоставление российским и зарубежным ученым и специалистам возможности публиковать результаты своих исследований;

• привлечение внимания к наиболее актуальным, перспективным, прорывным и интересным направлениям развития и приложений численных и численно-аналитических методов решения фундаментальных и прикладных технических задач, совершенствования технологий математического, компьютерного моделирования, разработки и верификации реализующего программно-алгоритмического обеспечения;

• обеспечение обмена мнениями между исследователями из разных регионов и государств.

Тематика журнала. К рассмотрению и публикации в журнале принимаются аналитические материалы, научные статьи, обзоры, рецензии и отзывы на научные публикации по фундаментальным и прикладным вопросам технических наук, прежде всего в области строительства. В журнале также публикуются информационные материалы, освещающие научные мероприятия и передовые достижения Российской академии архитектуры и строительных наук, научно-образовательных и проектно-конструкторских организаций.

Тематика статей, принимаемых к публикации в журнале, соответствует его названию и охватывает направления научных исследований в области разработки, исследования и приложений численных и численно-аналитических методов, программного обеспечения, технологий компьютерного моделирования в решении прикладных задач в области строительства, а также соответствующие профильные специальности, представленные в диссертационных советах профильных образовательных организациях высшего образования.

Редакционная политика. Политика редакционной коллегии журнала базируется на современных юридических требованиях в отношении авторского права, законности, плагиата и клеветы, изложенных в законодательстве Российской Федерации, и этических принципах, поддерживаемых сообществом ведущих издателей научной периодики.

За публикацию статей плата с авторов не взымается. Публикация статей в журнале бесплатная. На платной основе в журнале могут быть опубликованы материалы рекламного характера, имеющие прямое отношение к тематике журнала.

Журнал предоставляет непосредственный открытый доступ к своему контенту, исходя из следующего принципа: свободный открытый доступ к результатам исследований способствует увеличению глобального обмена знаниями.

Индексирование. Публикации в журнале входят в системы расчетов индексов цитирования авторов и журналов. «Индекс цитирования» – числовой показатель, характеризующий значимость данной статьи и вычисляющийся на основе последующих публикаций, ссылающихся на данную работу.

Авторам. Прежде чем направить статью в редакцию журнала, авторам следует ознакомиться со всеми материалами, размещенными в разделах сайта журнала (интернет-сайт Российской академии архитектуры и строительных наук (http://raasn.ru); подраздел «Издания РААСН» или интернет-сайт Издательства АСВ (http://iasv.ru); подраздел «Журнал IJCCSE»): с основной информацией о журнале, его целями и задачами, составом редакционной коллегии и редакционного совета, редакционной политикой, порядком рецензирования направляемых в журнал статей, сведениями о соблюдении редакционной этики, о политике авторского права и лицензирования, о представлении журнала в информационных системах (индексировании), информацией о подписке на журнал, контактными данными и пр. Журнал работает по лицензии Creative Commons типа cc by-nc-sa (Attribution Non-Commercial Share Alike) – Лицензия «С указанием авторства – Некоммерческая – Копилефт».

Рецензирование. Все научные статьи, поступившие в редакцию журнала, проходят обязательное двойное слепое рецензирование (рецензент не знает авторов рукописи, авторы рукописи не знают рецензентов).

Заимствования и плагиат. Редакционная коллегия журнала при рассмотрении статьи проводит проверку материала с помощью системы «Антиплагиат». В случае обнаружения многочисленных заимствований редакция действует в соответствии с правилами COPE.

Подписка. Журнал зарегистрирован в Федеральном агентстве по средствам массовой информации и охраны культурного наследия Российской Федерации. Индекс в общероссийском каталоге РОСПЕЧАТЬ − 18076.

По вопросам подписки на международный научный журнал “International Journal for Computational Civil and Structural Engineering (Международный журнал по расчету гражданских и строительных конструкций)” обращайтесь в Агентство «Роспечать» (Официальный сайт в сети Интернет: http://www.rosp.ru/) или в издательство Ассоциации строительных вузов (АСВ) в соответствии со следующими контактными данными:

ООО «Издательство АСВ»

Юридический адрес: 129337, Россия, г. Москва, Ярославское ш., д. 26, офис 705;

Фактический адрес: 129337, Россия, г. Москва, Ярославское ш., д. 19, корп. 1, 5 этаж, офис 12 (ТЦ Соле Молл);

Телефоны: +7 (925) 084-74-24;

Интернет-сайт: www.iasv.ru. Адрес электронной почты: iasv@iasv.ru.

Контактная информация. По всем вопросам работы редакции, рецензирования, согласования правки текстов и публикации статей следует обращаться к главному редактору журнала члену-корреспонденту РААСН *Сидорову Владимиру Николаевичу* (адреса электронной почты: sidorov.vladimir@gmail.com, sidorov@iasv.ru, iasv@iasv.ru, sidorov@raasn.ru) или к техническому редактору журнала советнику РААСН *Кайтукову Таймуразу Батразовичу* (адреса электронной почты: tkaytukov@gmail.com; kaytukov@raasn.ru). Кроме того, по указанным вопросам, а также по вопросам размещения в журнале рекламных материалов можно обращаться к генеральному директору ООО «Издательство АСВ» *Никитиной Надежде Сергеевне* (адреса электронной почты: iasv@iasv.ru, nsnikitina@mail.ru, ijccse@iasv.ru).

Журнал становится технологичнее. Издательство АСВ с сентября 2016 года является членом Международной ассоциации издателей научной литературы (Publishers International Linking Association (PILA)), осуществляющей свою деятельность на платформе CrossRef. Оригинальным статьям, публикуемым в журнале, будут присваиваться уникальные номера (индексы DOI – Digital Object Identifier), что значительно облегчит поиск метаданных и местонахождение полнотекстового произведения. DOI – это система определения научного контента в сети Интернет.

С октября 2016 года стал возможен прием статей на рассмотрение и рецензирование через онлайн систему приема статей Open Journal Systems на сайте журнала (электронная редакция): http://ijccse.iasv.ru/index.php/IJCCSE.

Автор имеет возможность следить за продвижением статьи в редакции журнала в личном кабинете Open Journal Systems и получать соответствующие уведомления по электронной почте.

В феврале 2018 года журнал был зарегистрирован в Directory of open access journals (DOAJ) (это один из самых известных поисковых сервисов в мире, который предоставляет открытый доступ к материалам и индексирует не только заголовки журналов, но и научные статьи), в сентябре 2018 года включен в продукты EBSCO Publishing.

В ноябре 2020 года журнал начал индексироваться в международной базе Scopus.

International Journal for
Computational Civil and Structural Engineering
(Международный журнал по расчету гражданских и строительных конструкций)
Volume 19, Issue 3 ***2023***

Scientific coordination is carried out by the Russian Academy of Architecture and Construction Sciences (RAACS)

CONTENTS

Modeling of Loads From Tsunami Waves on the Structure **14**
Tatiana A. Belash, Anton D. Yakovlev

Statistical Model of Aerodynamic Impact on the Large-Span Coverage
Vladimir I. Erofeev, Aleksandr V. Ilyakhinsky, Elena A. Nikitina, Vladimir M. Rodyushkin, **20**
Pavel A. Khazov, Andrey A. Satanov

Numerical Modeling of the Process of Degradation of Permafrost Soils of the Base of the Railway Roadbed in the Area of Passage of Construction Equipment **31**
Sergey A. Kudryavtsev, Tatyana Yu. Valtseva, Igor I. Gavrilov

Characteristic Method for Solving Filtration Problem **39**
Liudmila I. Kuzmina, Yuri V. Osipov, Artem R. Pesterev

Experimental Studies of the Stability of Thin-Walled Cylindrical Shells of Medium Length Filled with Bulk Material Under Torsion **49**
Mikhail V. Petrov, Alexander I. Kibets, Boris V. Mikhailov, Ekaterina G. Gonik,
Viktor A. Ivanov

Reciprocity Laws for Oscillations of Dissipative Systems **58**
Alexander N. Potapov

Coupled Heat and Mass Transfer Problem with Dependent Heat Conduc-tivity Properties and its Semi-Analytical Solution **69**
Vladimir N. Sidorov, Alim M. Primkulov

Fe Modelling for Capacities of Headed Stud Shear Connectors in Composite Steel Beams with Slabs Concrete **83**
Muthanna Abbu, Doaa Talib Hashim, Hasan M. A. Albegmprli

Seismic Fragility Evaluation of Soil-Pile-Structure Interaction Effects Subjected to Mainshock-Aftershock Records **92**
Souheyla Saddouki, Djarir Yahiaoui, Rafik Demagh

Numerical Modelling of Wind Loads on Windows. Validation For a High-Rise Square Plan Building 114
Oleg S. Goryachevsky

The Effect of Soil Densification on the Attenuation of the Phenomenon of Soil Liquefaction in a Port Project in Morocco 130
Mohamed Bziaz, Lahcen Bahi, Latifa Ouadif, Anas Bahi, Abdehak Sabihi, Hamou Mansouri

Seismic Vulnerability Assessment for Buildings of Port Blair City Using Rapid Visual Screening as a Tool 141
Mr. Adharsh G., Dr. R. Sivakumar, Dr. K.S. Satyanarayanan

Localization of Solution of The Problem of Three-Dimensional The-ory of Elasticity with the Use of B-Spline Discrete-Continual Finite Element Method 155
Marina L. Mozgaleva, Pavel A. Akimov

Numerical Simulation of the Stress-Strain State of a Large-Span Structure with Joints with Gap Under the Seismic Loads in a Transient Dynamic 165
Alexander M. Belostotsky, Andrei S. Pavlov, Alexandr I. Nagibovich

Development of Computational Schemes of Generalized Kinematic Devices that Precisely Regulate the Natural Frequency Spectrum of Elastic Systems with a Finite Number of Degrees of Mass Freedom, in Which the Directions of Motion are Parallel, But Do Not Lie in the Same Plane. Part 1: Theoretical Foundations 173
Leonid S. Lyakhovich, Pavel A. Akimov, Zaur R. Galyautdinov, Andrey S. Plyaskin

International Journal for
Computational Civil and Structural Engineering
(Международный журнал по расчету гражданских и строительных конструкций)
Volume 19, Issue 3 ***2023***

Scientific coordination is carried out by the Russian Academy of Architecture and Construction Sciences (RAACS)

СОДЕРЖАНИЕ

Моделирование нагрузок от волн цунами на сооружение **14**
Т.А. Белаш, А.Д. Яковлев

Статистическая модель аэродинамического воздействия на большепролетное покрытие **20**
В.И. Ерофеев, А.В. Иляхинский, Е.А. Никитина, В.М. Родюшкин, П.А. Хазов, А.А. Сатанов

Численное моделирование процесса деградации многолетнемерзлых грунтов основания земляного полотна железных дорог в зоне проезда строительной техники **31**
С.А. Кудрявцев, Т.Ю. Вальцева, И.И. Гаврилов

Характеристический метод для решения задачи фильтрации **39**
Л.И. Кузьмина, Ю.В. Осипов, А.Р. Пестерев

Экспериментальные исследования устойчивости тонкостенных цилиндрических оболочек средней длины, заполненных сыпучим материалом, при кручении **49**
М.В. Петров, А.И. Кибец, Б.В. Михайлов, Е.Г. Гоник, В.А. Иванов

Соотношения взаимности в динамике диссипативных систем **58**
А.Н. Потапов

Совместная задача тепломассообмена с зависимыми теплопроводящми свойствами и ее полуаналитическое решение **69**
В.Н. Сидоров, А.М. Примкулов

Конечноэлементное моделирование несущей способности по сдвигу стад болтов в сталежелезобетонных балках с бетонными перекрытиями **83**
Мутанна Аббу, Доа Талиб Хашим, Хасан М.А. Альбегмпрли

Оценка сейсмической неустойчивости эффектов взаимодействия грунт-свая-конструкция, подверженных записям основных толчков и афтершоков **92**
Сухейла Саддуки, Джарир Яхиауи, Рафик Демаг

Численное моделирование ветровых давлений на окна. Валидация для типового многоэтажного здания квадратной формы **114**
О.С. Горячевский

Влияние уплотнения почвы на ослабление явления её разжижения в портовом проекте в Марокко **130**
Мохамед Бзиаз, Лахсен Бахи, Латифа Оадиф, Анас Бахи, Абдехак Сабихи, Хаму Мансури

Оценка сейсмической уязвимости зданий в городе порт-Блэр с использованием метода быстрого визуального скрининга **141**
Г. Адхарш, Р. Сивакумар, К.С. Сатьянараянан

Локализация решения трехмерной задачи теории упругости на основе вейвлет-реализации дискретно-континуального метода конечных элементов с использованием в-сплайнов **155**
М.Л. Мозгалева, П.А. Акимов

Численное моделирование напряженно-деформированного состояния большепролетного сооружения с люфтами в опорах с учетом сейсмических воздействий в нелинейной динамической постановке **165**
А.М. Белостоцкий, А.С. Павлов, А.И. Нагибович

Формирование расчетных схем обобщенных кинематических устройств, прицельно регулирующих спектр частот собственных колебаний упругих систем с конечным числом степеней свободы масс, у которых направления движения параллельны, но не лежат в одной плоскости **173**
Л.С. Ляхович, П.А. Акимов, З.Р. Галяутдинов, А.С. Пляскин

DOI:10.22337/2587-9618-2023-19-3-14-19

MODELING OF LOADS FROM TSUNAMI WAVES ON THE STRUCTURE

Tatiana A. Belash [1], Anton D. Yakovlev [2]

[1] JSC Research Center of Construction, Moscow, RUSSIA
[2] KAPproject, Saint Petersburg, RUSSIA

Abstract. Currently, the improvement of methods for calculating building structures is continuing, including, among other things, methods for determining the magnitude of the load. Despite the fact that for most impacts, the principles of determining loads and methods from the application have been formed for a long time, a number of special tasks are sometimes encountered in design practice, for example, the impact of tsunami waves on a structure. This article is devoted to modeling the wave roll on a structure in the "Fluid Flow (Fluent)" module of the ANSYS 2021 software package and comparing the results obtained with the methodology presented in SP 292.1325800.2017 "Buildings and structures in tsunami-prone areas. Design rules". The studies presented in this article have shown that the nature of the propagation of hydrodynamic pressure when modeling wave rolling in ANSYS is similar to that presented in SP 292.1325800.2017: according to a triangular plot with maximum pressure at the bottom. But at the same time, the value of the maximum pressure on the joint venture is about 1.5 times greater than according to the calculation in ANSYS, which is explained by many different factors. But, despite this, modeling of the tsunami waves rolling on the construction site can be performed at the pre-project stage in order to assess the nature of the pressure distribution over the surface of the object, which will allow choosing the most suitable structural and space-planning solutions.

Keywords: calculation of building structures, stress-strain state, tsunami, loads, building structures

МОДЕЛИРОВАНИЕ НАГРУЗОК ОТ ВОЛН ЦУНАМИ НА СООРУЖЕНИЕ

Т.А. Белаш [1], А.Д. Яковлев [2]

АО «НИЦ»Строительство», г. Москва, РОССИЯ
ООО «КАПпроект», г. Санкт-Петербург, РОССИЯ

Аннотация. В настоящее время продолжаются усовершенствование методов расчета строительных конструкций, включающих в себя, в том числе, и способы определения величины нагрузки. Несмотря на то, что для большинства воздействий уже достаточно давно сформировались принципы определения нагрузок и способы из приложения, в проектной практике иногда встречается ряд особых задач, например, воздействие волн цунами на сооружение. Данная статья посвящена моделированию наката волны на сооружение в модуле «Fluid Flow (Fluent)» программного комплекса ANSYS 2021 и сравнению полученных результатов с методикой, представленной в СП 292.1325800.2017 «Здания и сооружения в цунамиопасных районах. Правила проектирования». Исследования, представленные в данной статье, показали, что характер распространения гидродинамического давления при моделировании наката волн в ANSYS аналогичен представленному в СП 292.1325800.2017: по треугольной эпюре с максимальным давлением внизу. Но при этом величина максимального давления по СП примерно в 1,5 раза больше, чем по расчету в ANSYS, что объясняется множеством различных факторов. Но, несмотря на это, моделирование наката волн цунами на объект строительства может выполняться на стадии предпроекта, чтобы оценить характер распределения давления по поверхности объекта, что позволит выбрать наиболее подходящие конструктивные и объемно-планировочные решения.

Ключевые слова: расчет строительных конструкций, напряженно-деформированное состояние, цунами, нагрузки, строительные конструкции

INTRODUCTION

Tsunami is the Japanese name for a system of gravitational waves arising in the sea due to large–scale disturbances of the free surface. Despite all the possible danger of tsunami-prone territories, people have long settled in such territories. Most often these were fishing settlements that were supposed to be organized on the coasts. But with the development of science, humanity manages to reduce the risk of staying in tsunami-prone areas. The evolution of methods for calculating building structures for the impact of tsunami waves plays an important role in this, which leads to the possibility of designing tsunami-resistant buildings. [1, 2]

The purpose of the calculation of building structures is to assess their bearing capacity. For these purposes, software complexes based on the finite element method are currently most often used. This method has high accuracy, but implies solving a large number of equations, so this method has become popular with the spread of computer technology. Thus, at present, designers have a fairly effective way to determine the stress-strain state of structures. But it is important to understand that in order to obtain adequate results, it is necessary to enter adequate initial data, including geometric and stiffness parameters of the structure under study, boundary conditions of the design scheme and, of course, loads (both the way they are applied in the design scheme and their numerical value).

In the global design community, conventions for setting power loads (both permanent and temporary) in the design scheme have been formed for a long time. Such loads are applied to the structural elements, as a rule, in the form of static loads. Also, methods for applying instantaneous dynamic loads (such as wind pulsation or earthquake) have been formed for a long time. Thus, for most loads, it is unambiguously clear how to set them in various computer computing programs. But, in design practice, sometimes there are special tasks, for example, the impact of tsunami waves on a structure.

Strictly speaking, on the territory of the USSR (and further on the territory of the Russian Federation), according to the resolution of the Council of Ministers of the RSFSR No. 19 of January 8, 1964, construction in tsunami-prone areas is prohibited. This led to the fact that in Russia for a long time there were no building codes for the development of sea coasts exposed to the danger of a tsunami. [3, 4]

Only since 2018, the code of rules of SP 292.1325800.2017 "Buildings and structures in tsunami-prone areas" approved by the order of the Ministry of Construction of the Russian Federation No. 915/pr dated June 23, 2017 is put into effect. Design Rules", developed by the working group of the ANO "Regional Alliance for Disaster Analysis and Reduction". [5, 6]

SP 292.1325800.2017 allows you to find the value of the load from the expected tsunami wave, which in the future should be set as a static load in the direction of the expected action of the tsunami wave. However, currently there are a large number of software systems capable of simulating the roll of a wave on a structure, which will allow us to estimate the distribution of pressure from the wave over time. Such programs include Autodesk CFD, XFlow, ANSYS and others.

This article is devoted to modeling the wave roll on the structure in the "Fluid Flow (Fluent)" module of the ANSYS 2021 software package and comparing the results obtained with the methodology presented in SP 292.1325800.2017.

MATERIALS AND METHODS

According to SP 292.1325800.2017, the loads from the tsunami are special and are taken into account in a special combination of loads (clause 5.5.1 of SP 292.1325800.2017). Setting loads of a special combination that takes into account the impact of a tsunami on a structure depends on the purpose and location of this structure (clause 5.1.2 of SP 292.1325800.2017), which makes the

methodology presented in this document universal and applicable for most design cases in tsunami-prone areas.

For example, the specific load on the frontal face of the structure from the impact of boron according to SP 292.1325800.2017 is determined by the formula (1):

$$P = 0{,}33 \cdot \rho \cdot C_1^3 \cdot \exp(1{,}4\mu) \cdot \mu \cdot (3 - \mu) \left(1 - \frac{t}{t_*}\right) \cdot t \cdot K_{\text{пр}} \cdot \sin^3 \varepsilon + 0{,}5 \cdot \rho \cdot g \cdot C_1^2 \cdot t^2 \cdot \mu \cdot K_{\text{пр}}, \quad (1)$$

where C_1 – the speed of the boron front when rolling ashore; μ – dimensionless parameter; t_* – duration of the impact of the boron front on the coastal object; t – wave propagation time; ε – the angle between the direction of propagation of the boron front rolling onto the shore and the frontal face of the structure; $K_{\text{пр}}$ – the permeability coefficient of the face of the structure, equal to the ratio of the material-filled part of the face of the structure to its total part. [6]

As can be seen from formula (1), this document takes into account various factors affecting the magnitude of the load from the tsunami wave on the structure. But, in fact, in this approach, we bring an almost instantaneous shock load to a static one (albeit with a fraction of the duration equal to 0).

The "Fluid Flow (Fluent)" module of the ANSYS 2021 software package allows you to simulate the movement of liquids and gases, including taking into account the interaction with obstacles (in our case, these are buildings and structures). The process of performing calculations is similar to those in most calculation programs (such as Lira or SCAD), but each stage has its own peculiarities.

At the first stage, a calculation scheme is created. It consists of a three-dimensional structure (that is, taking into account the actual dimensions of all building structures that will be exposed to interaction with water). And also the calculated area is modeled – the area of space in which a liquid (or gas) will be generated and interact with obstacles. Figure 1 shows a computational model of a fragment of a bridge structure with a computational domain.

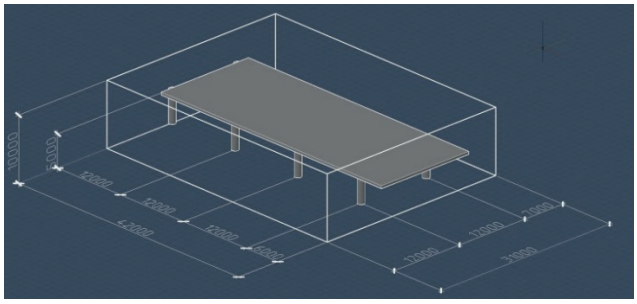


Figure 1. Calculation model

At the next stage, this calculated area is divided into finite elements. ANSYS tools allow you to thicken the grid of finite elements near the boundaries of bodies (bridge structures), which will increase the accuracy of calculations, reducing the calculation time. A fragment of the generated finite element grid is shown in Figure 2.

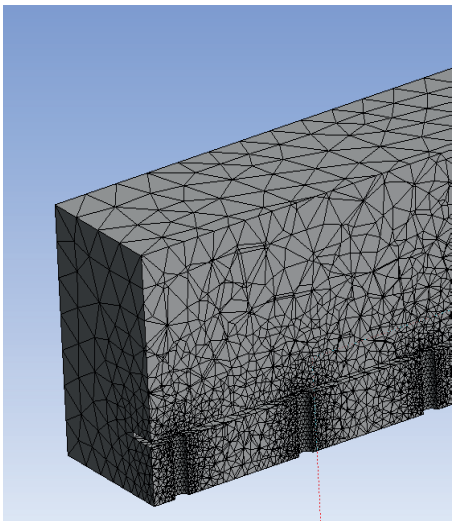


Figure 2. Fragment of finite element grid generation

At the next stage, the initial data is set, of which there is a huge amount in this software package. Initially, the parameters of the input face of the computational domain are set – on which waves will be generated (the blue face in Figure 3). A wave propagation model is chosen for this facet: in this study, the "Short Gravity Waves" model is adopted according to the theory of a cnoidal/solitary wave. This choice is justified by

the fact that all other wave generation mechanisms, which are presented in the "Fluid Flow (Fluent)" module, are designed for medium and large depths, and this study examines the roll of waves on shore structures. Also, the height of the waves (8 m for this calculation) and the speed of their propagation are set here (the speed is taken as in the calculations for SP 292.1325800.2017). Secondly, the output faces (red faces in Figure 3) – from which water can come out either calmly or taking into account resistance to different pressures (atmospheric pressure was established in this study). Thirdly, other faces (gray faces in Figure 3) on which waves will not be generated, but which limit the movement of the wave: these are the faces along the movement of water, the structure itself and the lower face (denoting the ground). If the "No Slip" parameter must be unambiguously set for the faces along the wave motion in order to exclude the loss of wave energy when interacting with them, then it is possible to set roughness for the remaining faces. So, in this scheme, the roughness height (0.2 m) and the constant roughness (0.5) were set, simulating the interaction of the wave with the earth's surface, similar to the parameter n required to determine the dimensionless parameter μ from the formula (1). [6, 7]

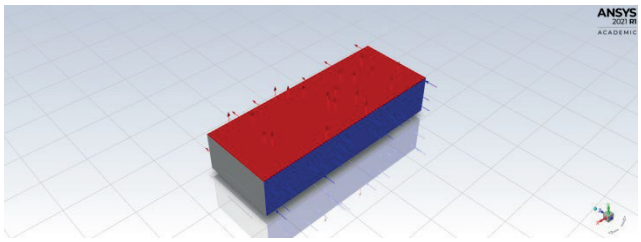


Figure 3. Boundary parameters of the computational domain

In addition to the boundary conditions discussed above, the parameters of the volume of the computational domain itself were also set. The main of these parameters are the presence of gravity (9.81 m/s2) and the multiphase of the model. Monophasicity implies that several different substances (in this case air and liquid) occur in the computational domain. Standard density and viscosity parameters are set for each substance, taken from the default ANSYS program library.

After the calculations, we get a picture of the water distribution in the calculated area at the required time (Figure 4).

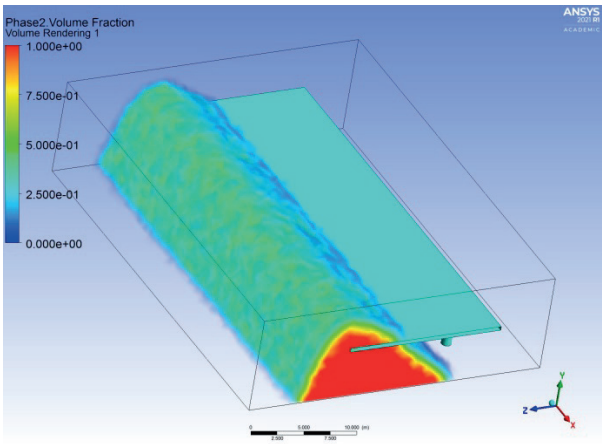


Figure 4. Wave rolling on a bridge fragment

And you can also look at the pressure isofields, at the areas of interest to us, for example, on the surface of the structure under study (Figure 5).

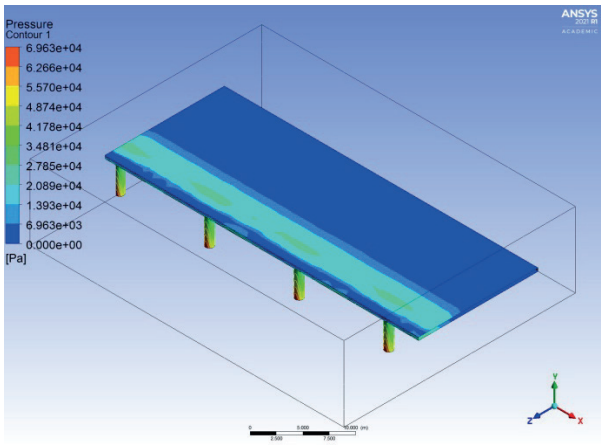


Figure 5. Pressure from the wave on the structure

As can be seen from Figure 5, the nature of pressure propagation is similar to that presented in SP 292.1325800.2017: according to a triangular plot with maximum pressure at the bottom. The maximum pressure value in this calculation is 69630 Pa. At the same time, the

maximum pressure value according to the formula (1) for the same wave is 103590 Pa, which is about 1.5 times more than according to the calculation in ANSYS.

RESULTS

It should be understood that this distribution is characteristic only for this particular case (accepted geometric characteristics of a construction object, accepted wave height, etc.). Another important point is that formula (1) is valid for boron – the most dangerous variant of a tsunami wave is a vertical wall of water, while ANSYS simulates ordinary waves of the desired we need heights. Therefore, it is possible that a special wave propagation model for collecting water will appear in future versions of ANSYS, and then the difference in the results of the joint venture and roll modeling in ANSYS will be even smaller. But at the moment, ANSYS can be considered as an alternative to testing models in the pool – to assess the nature of the interaction of waves with structures of various shapes and sizes, as well as to see the nature of the pressure distribution over the surface of this structure.

CONCLUSION

The magnitude of the load from the tsunami bar when calculated according to the methodology presented in the joint venture is about 1.5 times greater than when modeling the roll in ANSYS, which is explained by many different factors.

Modeling of the tsunami waves rolling on the construction site can be performed at the pre-project stage in order to assess the nature of the pressure distribution over the surface of the object, which will allow choosing the most suitable structural and space-planning solutions.

It is necessary to further develop both methods for calculating loads from tsunami waves and software systems capable of simulating the roll of tsunami waves on various objects. The ultimate goal of this development should be software systems capable of simulating the roll of tsunami waves on building structures with sufficient accuracy, as well as obtaining pictures of the stress-strain state of these structures, which should lead to the design of safe buildings and structures in tsunami-prone areas.

REFERENCES

1. **Syvorotkin V.L.** Tsunami. Space and time. 2011. No. 3. Pp. 144–153.
2. **Helal M.A., Mehanna M.S.** Tsunamis from nature to physics // Chaos, Solitons and Fractals. 2008. Vol. 36. No 4. Pp. 787-796.
3. **Klyachko M.A., Maksimov V.V., Nudner I.A., Filkov V.Yu.** About the interstate standard "Buildings, structures and territories. Safety requirements under the impact of a tsunami" // Collection of materials of the All-Russian conference with international participation "Geodynamic processes and natural disasters. The experience of Neftegorsk". 2015. Pp. 304-306
4. **Klyachko M.A.** On the design standards of buildings and structures in tsunami-prone areas. Fundamental and Applied Hydrophysics. 2017. Vol. 10. No. 3. Pp. 5–25.
5. **Klyachko M.A., Pelinovsky E.N., Kaistrenko V.M.** The concept and rationing of tsunami protection in the Russian Federation // Natural and technogenic risks. Safety of structures. 2017. No.6. p. 72.
6. SP 292.1325800.2017. Buildings and structures in tsunami-prone areas. Design rules. – Introduction. 2017-06-23. - Moscow: Ministry of Construction of Russia, 2017. – 146p.
7. ANSYS Fluent Theory Guide. – Canonsburg (PA) USA.: ANSYS, Inc., 2021. – 1028 p.

СПИСОК ЛИТЕРАТУРЫ

1. **Сывороткин В.Л.** Цунами. / В.Л. Сывороткин // Пространство и Время. – 2011. – № 2(4). – с. 124-137
2. **Helal M.A., Mehanna M.S.** Tsunamis from nature to physics // Chaos, Solitons and Fractals. 2008. Vol. 36. No 4. Pp. 787-796.
3. **Клячко М.А., Максимов В.В., Нуднер И.А., Фильков В.Ю.** О межгосударственном стандарте «Здания, сооружения и территории. Требования безопасности при воздействии цунами» // Сборник материалов Всероссийской конференции с международным участием “Геодинамические процессы и природные катастрофы. Опыт Нефтегорска”. 2015. С. 304-306
4. **Клячко М.А.** О нормах проектирования зданий и сооружений в цунамиопасных районах // ФУНДАМЕНТАЛЬНАЯ и ПРИКЛАДНАЯ ГИДРОФИЗИКА. 2017. Том 10. № 3. С. 5-25
5. **Клячко М.А., Пелиновский Е.Н., Кайстренко В.М.** Концепция и нормирование цунамизащиты в Российской Федерации // Природные и техногенные риски. Безопасность сооружений. 2017. №6. С. 72.
6. СП 292.1325800.2017. Здания и сооружения в цунамиопасных районах. Правила проектирования. – Введ. 2017-06-23. - М.: Минстрой России, 2017. – 146с.
7. ANSYS Fluent Theory Guide. – Canonsburg (PA) USA.: ANSYS, Inc., 2021. – 1028 с.

Tatiana A. Belash, Doctor of Technical Sciences, Professor of the Department of "Building Structures, structures and Materials", JSC Research Center of Construction, 6, 2nd Institutskaya, 109428, Moscow, Russia

Белаш Татьяна Александровна, д.т.н., профессор кафедры «Строительные сооружения, конструкции и материалы» АО «НИЦ»Строительство», эл почта: belashta@mail.ru, 89219910115.

Anton D. Yakovlev, Candidate of Technical Sciences, engineer, KAPproject, 23a, Krasnogvardeysky lane, 197342, Saint Petersburg, Russia

Яковлев Антон Дмитриевич, к.т.н., инженер-конструктор ООО «КАПпроект», эл почта: anton.yakovlev.94@mail.ru.

DOI:10.22337/2587-9618-2023-19-3-20-30

STATISTICAL MODEL OF AERODYNAMIC IMPACT ON THE LARGE-SPAN COVERAGE

Vladimir I. Erofeev [1], Aleksandr V. Ilyakhinsky [1], Elena A. Nikitina [1], Vladimir M. Rodyushkin [1], Pavel A. Khazov [2], Andrey A. Satanov [1]

[1] Mechanical Engineering Research Institute of the RAS – Branch of Federal Research Center «A.V. Gaponov – Grekhov Institute of Applied Physics of the Russian Academy of Sciences», Nizhny Novgorod, RUSSIA
[2] Nizhny Novgorod State University of Architecture and Civil Engineering, Nizhny Novgorod, RUSSIA

Abstract: The aim of the study was to study the possibility of using the Dirichlet distribution as a statistical model of the process of dynamic interaction of large-span structures with aerodynamic load. As an object of research, a model of a hangar building was chosen for the maintenance of two AirbusA-380 aircraft at a scale of 1: 500 blown in a wind tunnel at five directions of wind flow at angles of 0 °, 30 °, 45 °, 60 °, 90 ° to the front of the structure ... It is shown that the statistical model of the Dirichlet distribution has sufficient flexibility and realism and compares favorably with the models built on the basis of the normal distribution, beta distribution, gamma distribution and Poisson distribution when describing the processes of intense dynamic interaction of wind load with structural elements. The problem of finding an integral assessment of the state of the processes of interaction of the wind load with the hangar building for the maintenance of two aircraft was reduced to calculating the self-organization parameter of the distribution over the surface of the building model of the aerodynamic coefficients, which was taken as the ratio of the total weighted amount of the Dirichlet models detected in the analyzed numerical series of the registered signal i-th dimension with negative external entropy to the total weighted number of Dirichlet models with positive external entropy.
The study showed that the dimensionless informational and statistical indicator of self-organization makes it possible from a unified standpoint to assess the states that differ from each other in terms of external signs, the processes of interaction and their dynamics. The integral indicator can be used to rank the efficiency of operating systems and can be useful in assessing the state of the processes of dynamic interaction of the operating pressure and objects and structures of various shapes and purposes.

Keywords: wind load, statistical model, Dirichlet distribution, entropy, self-organization

СТАТИСТИЧЕСКАЯ МОДЕЛЬ АЭРОДИНАМИЧЕСКОГО ВОЗДЕЙСТВИЯ НА БОЛЬШЕПРОЛЕТНОЕ ПОКРЫТИЕ

В.И. Ерофеев [1], А.В. Иляхинский [1], Е.А. Никитина [1], В.М. Родюшкин [1], П.А. Хазов [2], А.А. Сатанов [1]

[1] Институт проблем машиностроения РАН – филиал ФГБНУ «Федеральный исследовательский центр «Институт прикладной физики им. А.В. Гапонова – Грехова Российской академии наук», г. Нижний Новгород, РОССИЯ
[2] Нижегородский государственный архитектурно-строительный университет, г. Нижний Новгород, РОССИЯ

Аннотация: Целью исследования являлось изучение возможности использования распределения Дирихле в качестве статистической модели процесса динамического взаимодействия большепролетных конструкций с ветровыми нагрузками. В качестве объекта исследования был выбран макет здания ангара для технического обслуживания двух самолетов AirbusA-380, разработанный в масштабе 1:500, который подвергалась аэродинамическим воздействиям в аэродинамической трубе по пяти различным направлениям ветрового потока под углами 0°, 30°, 45°, 60°, 90° к передней части конструкции. Показано, что статистическая модель распределения Дирихле обладает достаточной гибкостью, отражает реальную картину и выгодно отличается от моделей, построенных на основе нормального распределения, бета-распределения, гамма-распределения и распределения Пуассона при описании процессов интенсивного динамического воздействия ветра на элементы покрытия. Задача нахождения интегральной оценки состояния процессов взаимодействия ветровой нагрузки со зданием ангара для технического обслуживания

двух самолетов сводилась к вычислению параметра самоорганизации распределения по поверхности макета здания значений аэродинамических коэффициентов, в качестве которого была принята величина отношения суммарного взвешенного количества выявленных в анализируемом числовом ряде зарегистрированного сигнала моделей Дирихле i-ой размерности, имеющих отрицательное значение внешней энтропии, к суммарному взвешенному количеству моделей Дирихле, имеющих положительное значение внешней энтропии.

Проведенное исследование показало, что безразмерный информационно-статистический показатель самоорганизации позволяет с единых позиций оценить состояния, отличающихся между собой по внешним признакам процессы взаимодействия и их динамику. Интегральный показатель может быть использован для ранжирования эффективности действующих систем и может оказаться полезным при оценке состояния процессов динамического взаимодействия действующего давления и различных по форме и назначению объектов и конструкций.

Ключевые слова: ветровая нагрузка, статистическая модель, распределение Дирихле, энтропия, самоорганизация

1. INTRODUCTION

Structural aerodynamics have always been considered quite important and paramount in design. Many works of domestic and foreign authors are devoted to the study of the distribution of aerodynamic loads on various objects and structures using methods of numerical modeling and experiments in a wind tunnel [1-6]. However, there is no unified methodology for assessing the state of the processes of dynamic interaction of the operating pressure and objects and structures of various shapes and purposes. For large objects of complex shape, taking into account the wind profile, this problem is not fully solved even with modern computing means [7-12]. In particular, as shown by the results of experiments, the aerodynamic characteristics for large-span buildings, as a rule, differ for each object [13-18]. The main approach to solving the problem of the distribution of aerodynamic loads consists in setting a mathematical model of a building or structure and solving three-dimensional equations of fluid and gas motion with adequate turbulence models implemented in modern software and computational systems for fluid dynamics, as well as carrying out a physical test of the model in a wind tunnel. At the same time, the question of assessing the nature of the interaction of large-span structures with a complex geometric shape as a whole with the aerodynamic load remains, as a rule, open. Therefore, obtaining an assessment of the state of the processes of interaction of wind load with complex large-span structures based on the use of new information technologies requires further development.

2. MATERIALS AND METHODS

Modern large-span structures are a complex system consisting of a complex of various subsystems, which, in the course of the action of the wind load, through the exchange of energy, are interconnected by processes of intense dynamic interaction. In this system, complex transient processes occur and critical chaotic regimes arise, as a result of which self-organization processes can occur, which means that the system's reactions are determined not only by external forces, but mainly by its structure and internal connections. A large number of interacting elements, the influence of many poorly controlled external factors lead to the fact that the processes that determine the state of such structures reveal a probabilistic nature and can be represented by a statistical model (image) in the form of a probability density function defined on a limited interval by the Dirichlet distribution. The model reflects the result of joint implementation of n-1 independent processes xj, proceeding with speeds (intensities) vj, and the opposite process in the sense of the process, proceeding with a speed vn. In this sense, the distribution is informa-

tionally equivalent to an object of any nature and degree of complexity [19]. The probability density function of the Dirichlet distribution, defined on a k-dimensional simplex, is

$$D(x_1,...,x_k)=\frac{\Gamma(a_n)}{\prod_{i=1}^{n}\Gamma(v_i)}\prod_{i=1}^{k}x_i^{v_i-1}\times(1-\sum_{i=1}^{k}x_i)^{v_n-1} \quad (1)$$

$$0\le\sum x_i\le 1; v_i\ge 0,...,v_n\ge 0; \sum_{i=1}^{n}v_i=a_n; n=k+1$$

In (1) $\Gamma(x)$ is the gamma function. The entropy of the Dirichlet distribution according to the definition

$$H=-\int_x \varphi(x)\log_\alpha \varphi(x)dx \quad (2)$$

up to the base of the logarithm is

$$H(v_1,...,v_n)=\prod_{i=1}^{n}\Gamma(v_i)-\ln\Gamma(\alpha_n)+(\alpha_n-n)\psi(\alpha_n)-\sum_{i=1}^{n}(v_i-1)\psi(v_i) \quad (3)$$

Here in (4) and (5) $\psi(x)=\frac{d}{dx}\ln\Gamma(x)$ is the logarithmic derivative of the gamma function (Euler's psi-function). The entropy of the Dirichlet distribution can be represented as the sum

$$H(D)=H_i(v_1,...,v_n)+H_e(a_n) \quad (4)$$

in which the always positive term

$$H_i(v_1,...,v_n)=\ln\prod_{i=1}^{n}\Gamma(v_i)-\sum_{i=1}^{n}(v_i-1)\psi(v_i) \quad (5)$$

represents the entropy production corresponding to the second law of thermodynamics, and the term

$$H_e(a_n)=-\ln\Gamma(a_n)+(a_n-n)\psi(a_n) \quad (6)$$

represents the entropy flow characterizing the processes of interaction with the external environment. At $n\ge 3$ the entropy flux (6) can take both positive and negative values.

With an unlimited increase in the number of processes proceeding at the same speeds ($v_1=,...,=v_n=v_\gamma$) the Dirichlet distribution can be approximately replaced by a gamma distribution with density

$$\gamma(x) = \frac{x^{v_\gamma - 1}}{\Gamma(v_\gamma)} \exp(-x), x \geq 0, v_\gamma \geq 0 \quad (7)$$

and the entropy

$$H_\gamma = v_\gamma + \ln \Gamma(v_\gamma) - (v_\gamma - 1)\psi(v_\gamma) \quad (8)$$

The expression for the entropy of the gamma distribution does not allow to select any part of it that characterizes the entropy flux. Therefore, the model represented by the gamma distribution corresponds to an isolated system. Consequently, the choice of this model when describing processes in problems of atmospheric sounding [20,21] or in problems of detection [22,23] is incorrect, since an isolated system does not take into account the interaction of an object with the external environment. As a statistical model, the gamma distribution is only to the extent a satisfactory model for observing the state of an object, in which it is possible to implement an infinitely increasing number of processes proceeding at the same speeds.

At $v_\gamma = 1$ (7) it turns into an exponential distribution — a model of observation (but not a mechanism) of radioactive decay.

If the speeds of processes take on discrete values, and the number of processes is large, but of course, then the model will correspond to the Poisson distribution, which has the form:

$$f_p = \frac{v^x}{x!} \exp(-x); v > 0; x = 1,2,... \quad (9)$$

Like the gamma distribution, the Poisson distribution is a fluctuation model, since the mathematical expectation (space-time characteristic) for (9) is by definition equal to the second central moment (impulse-energy characteristic). It can be shown that the expression for the entropy of distribution (9)

$$H_p = v(1 - \ln v) + \ln \Gamma(1 + v) + \frac{v}{2}\psi^I(1 + v) \quad (10)$$

does not allow, as in the case of the gamma distribution, to single out the entropy flux. Consequently, model (11) corresponds to an isolated system with all the ensuing consequences. It should be noted that the normal distribution, defined on an unlimited interval, as a statistical model of the researched process, assumes that the investigated object has physical properties, the parameters of which tend to an infinitely large or small value. Obviously, there are no such properties.

Thus, of all the considered distributions, only the Dirichlet distribution has sufficient flexibility and realism, which favorably distinguishes it from the models built on the basis of the normal distribution, beta distribution, gamma distribution and Poisson distribution.

The object of the study is the projected hangar building for the maintenance of two AirbusA-380 aircraft in Moscow, covered by spatial arches with a span of 227.65 m (Fig. 1).

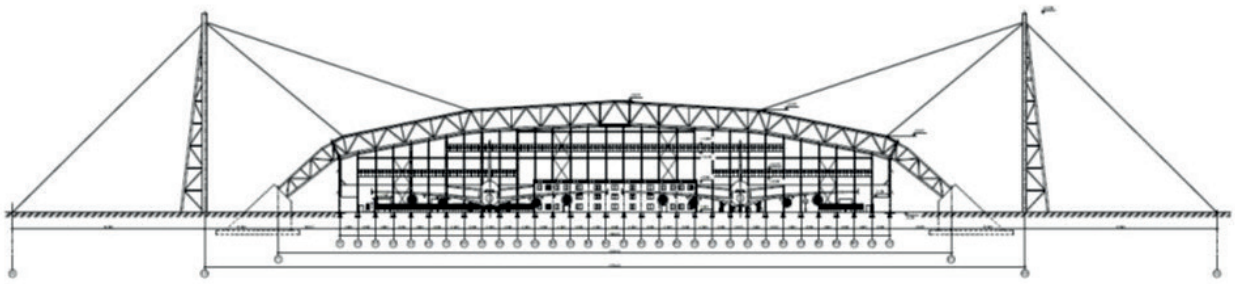


Figure 1. Main section of the hangar for maintenance

For testing in a wind tunnel, a model of the hangar building on a scale of 1: 500 was made on a 3D printer. The pressure measurement at characteristic points of the coating surface was carried out by means of a drainage system of 126 air outlet pipes connected to a micromanometer. The experiment was carried out for five directions of the wind flow, at angles of 0°, 30°, 45°, 60°, 90° with respect to the front of the structure. The tests were carried out in the laboratory of the Department of Heating and Ventilation of NNGASU.

The problem of finding an integral assessment of the state of the processes of interaction of the wind load with the hangar building for the maintenance of two aircraft was reduced to calculating the self-organization parameter of the distribution over the surface of the building model of the values of aerodynamic coefficients (tab. 1-5), which was taken as the value [23]

$$K_c = \frac{\sum iQ^i_{D-}}{\sum iQ^i_{D+}} \qquad (11)$$

of the ratio of the total weighted $\sum iQ^i_{D-}$ number Q of Dirichlet models of i dimension, which have a negative value of the external (flow) entropy, revealed in the analyzed numerical series of the registered signal, to the total weighted $\sum iQ^i_{D+}$ number of Dirichlet models with a positive value of the external entropy.

3. RESULTS AND DISCUSSION

The obtained values of the aerodynamic coefficients Cw=Psur/Po ,where Psur is the pressure measured at the studied point of the surface, and Po is the dynamic pressure exerted by the wind flow on the vertical surface, are given in tables 1-5.

The values of the self-organization parameter of the distribution of aerodynamic coefficients for different directions of the wind load are shown in Fig. 2.

Table 1. The values of the aerodynamic coefficients Cw at a wind flow direction of 0°

-0,15	-0,15	-0,10	-0,12	-0,15	-0,15	-0,15	-0,15	-0,15	-0,15	-0,15	-0,15	-0,12	-0,15
-0,17	-0,17	-0,15	-0,17	-0,17	-0,17	-0,20	-0,20	-0,20	-0,20	-0,17	-0,17	-0,15	-0,17
-0,17	-0,20	-0,20	-0,24	-0,27	-0,27	-0,24	-0,24	-0,27	-0,27	-0,20	-0,20	-0,17	-0,17
-0,22	-0,24	-0,27	-0,32	-0,29	-0,34	-0,37	-0,34	-0,37	-0,34	-0,29	-0,27	-0,24	-0,20
-0,29	-0,34	-0,37	-0,44	-0,41	-0,44	-0,46	-0,44	-0,44	-0,44	-0,41	-0,32	-0,29	-0,27
-0,41	-0,51	-0,51	-0,54	-0,56	-0,56	-0,54	-0,56	-0,54	-0,54	-0,51	-0,46	-0,37	-0,37
-0,54	-0,61	-0,61	-0,61	-0,63	-0,61	-0,61	-0,63	-0,63	-0,63	-0,61	-0,59	-0,51	-0,49
-0,63	-0,68	-0,66	-0,66	-0,68	-0,66	-0,63	-0,66	-0,71	-0,68	-0,68	-0,68	-0,68	-0,59
-0,76	-0,80	-0,73	-0,71	-0,68	-0,68	-0,68	-0,66	-0,73	-0,71	-0,76	-0,76	-0,78	-0,78

Table 2. The values of the aerodynamic coefficients Cw at a wind flow direction of 30°

-0,32	-0,22	-0,22	-0,24	-0,19	-0,14	-0,16	-0,27	-0,16	-0,14	-0,14	-0,14	-0,11	-0,11
-0,38	-0,22	-0,22	-0,27	-0,19	-0,16	-0,22	-0,30	-0,16	-0,14	-0,16	-0,16	-0,11	-0,11
-0,41	-0,22	-0,19	-0,27	-0,16	-0,16	-0,24	-0,35	-0,19	-0,16	-0,19	-0,16	-0,11	-0,11
-0,41	-0,22	-0,22	-0,30	-0,19	-0,19	-0,24	-0,35	-0,19	-0,16	-0,22	-0,16	-0,11	-0,11
-0,41	-0,22	-0,22	-0,27	-0,19	-0,19	-0,24	-0,35	-0,22	-0,19	-0,22	-0,19	-0,11	-0,11
-0,41	-0,22	-0,19	-0,27	-0,19	-0,19	-0,24	-0,38	-0,22	-0,19	-0,22	-0,19	-0,11	-0,08
-0,38	-0,19	-0,19	-0,24	-0,19	-0,16	-0,22	-0,35	-0,19	-0,19	-0,22	-0,19	-0,14	-0,11
-0,32	-0,19	-0,16	-0,24	-0,16	-0,14	-0,22	-0,30	-0,19	-0,16	-0,22	-0,19	-0,14	-0,11
-0,30	-0,16	-0,19	-0,22	-0,14	-0,14	-0,19	-0,30	-0,16	-0,16	-0,19	-0,19	-0,16	-0,14

Table 3. The values of the aerodynamic coefficients Cw at a wind flow direction of 45°

-0,03	-0,13	-0,13	-0,17	-0,17	-0,13	-0,20	-0,17	-0,17	-0,20	-0,23	-0,27	-0,20	-0,27
-0,03	-0,10	-0,10	-0,13	-0,13	-0,10	-0,17	-0,13	-0,10	-0,13	-0,13	-0,17	-0,10	-0,20
-0,03	-0,10	-0,10	-0,13	-0,13	-0,10	-0,13	-0,13	-0,10	-0,10	-0,13	-0,13	-0,07	-0,17
-0,03	-0,10	-0,10	-0,13	-0,13	-0,10	-0,13	-0,13	-0,10	-0,10	-0,10	-0,10	-0,07	-0,13
-0,10	-0,13	-0,13	-0,20	-0,17	-0,13	-0,13	-0,17	-0,10	-0,10	-0,10	-0,07	-0,07	-0,13
-0,13	-0,13	-0,17	-0,23	-0,27	-0,20	-0,27	-0,27	-0,20	-0,17	-0,13	-0,07	-0,07	-0,10
-0,13	-0,17	-0,20	-0,27	-0,33	-0,30	-0,53	-0,53	-0,50	-0,37	-0,30	-0,20	-0,07	-0,10
-0,17	-0,20	-0,23	-0,37	-0,40	-0,43	-0,60	-0,60	-0,63	-0,70	-0,67	-0,63	-0,33	-0,13
-0,23	-0,23	-0,27	-0,40	-0,53	-0,57	-0,60	-0,63	-0,70	-0,87	-1,00	-1,07	-1,10	-0,60

Table 4. The values of the aerodynamic coefficients Cw at a wind flow direction of 60°

-0,04	-0,07	-0,11	-0,15	-0,19	-0,22	-0,26	-0,30	-0,11	-0,22	-0,26	-0,26	-0,15	-0,19
-0,04	-0,07	-0,11	-0,15	-0,15	-0,15	-0,19	-0,26	-0,11	-0,19	-0,19	-0,19	-0,15	-0,22
-0,04	-0,04	-0,07	-0,15	-0,15	-0,15	-0,19	-0,22	-0,07	-0,19	-0,19	-0,19	-0,15	-0,22
-0,04	-0,04	-0,07	-0,15	-0,15	-0,11	-0,19	-0,19	-0,07	-0,15	-0,19	-0,19	-0,15	-0,26
-0,04	-0,04	-0,07	-0,11	-0,15	-0,11	-0,19	-0,19	-0,07	-0,15	-0,19	-0,15	-0,15	-0,22
-0,04	-0,07	-0,07	-0,15	-0,11	-0,11	-0,19	-0,19	-0,07	-0,15	-0,15	-0,15	-0,11	-0,22
-0,04	-0,07	-0,11	-0,15	-0,11	-0,11	-0,22	-0,19	-0,07	-0,15	-0,15	-0,15	-0,11	-0,22
-0,07	-0,11	-0,15	-0,15	-0,15	-0,15	-0,30	-0,19	-0,11	-0,11	-0,15	-0,15	-0,07	-0,19
-0,07	-0,15	-0,22	-0,33	-0,37	-0,33	-0,48	-0,33	-0,30	-0,30	-0,30	-0,15	-0,07	-0,15

Table 5. The values of the aerodynamic coefficients Cw at a wind flow direction of 90°

0,03	0,07	0,14	0,17	0,21	0,21	0,28	0,31	0,28	0,28	0,34	0,38	0,34	0,31
0,03	0,07	0,14	0,17	0,17	0,17	0,24	0,24	0,24	0,24	0,24	0,24	0,24	0,28
0,07	0,07	0,10	0,10	0,14	0,14	0,24	0,17	0,21	0,21	0,21	0,21	0,21	0,24
0,07	0,03	0,07	0,10	0,14	0,14	0,21	0,17	0,21	0,17	0,17	0,17	0,17	0,21
0,07	0,07	0,07	0,10	0,14	0,14	0,21	0,14	0,17	0,17	0,17	0,17	0,17	0,21
0,10	0,10	0,14	0,14	0,14	0,14	0,21	0,14	0,17	0,17	0,17	0,17	0,14	0,17
0,14	0,14	0,24	0,34	0,31	0,31	0,41	0,28	0,28	0,17	0,17	0,14	0,14	0,17
0,14	0,21	0,45	0,59	0,62	0,52	0,69	0,62	0,59	0,48	0,41	0,28	0,14	0,14
0,17	0,24	0,45	0,66	0,69	0,66	0,72	0,69	0,69	0,90	0,93	0,79	0,62	0,24

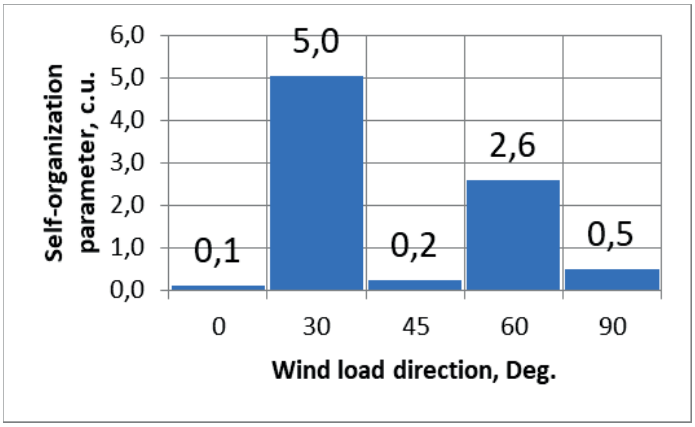


Figure 2. The values of the self-organization parameter of the distribution of aerodynamic coefficients for a hangar building for the maintenance of two aircraft at different directions of wind load

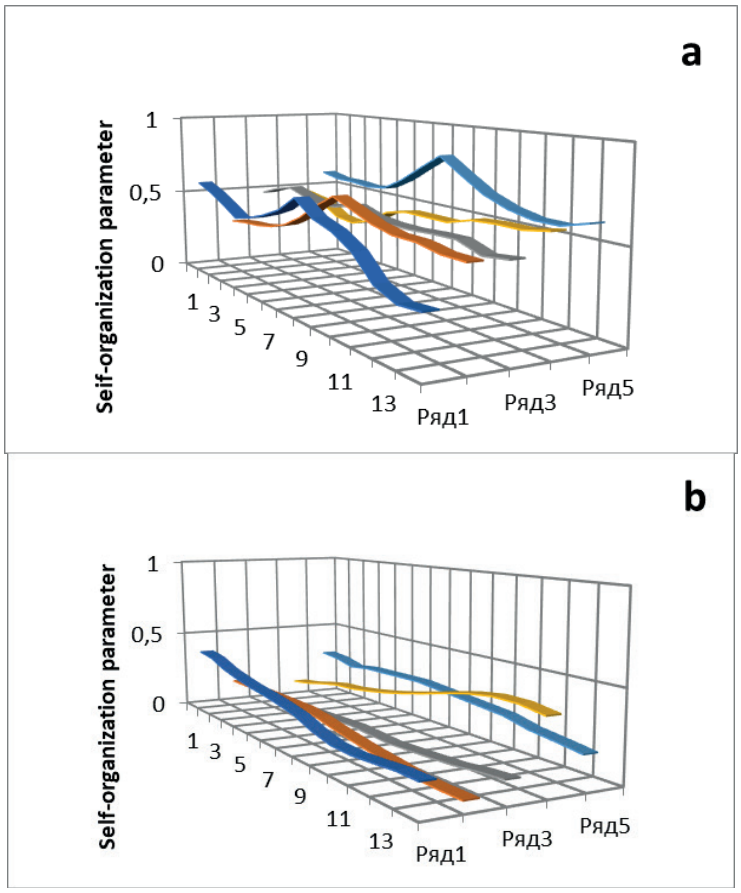


Figure 3. Distribution of the self-organization parameter over the hangar surface for two directions of the wind flow: a – 90 degrees (frontal direction); b – 0 degrees (longitudinal direction)

If we consider self-organization as a process, the essence of which is the formation of a set of actions leading to the creation of a stable system response, then, as follows from Figures 2, 3, the interaction of the wind flow with the object of study is complex. This interaction is greatest at angles of 30 and 60 degrees, and the least at the longitudinal direction of the wind flow. With the frontal direction of the wind flow, the process of interaction between the wind flow and the structure is maximal along the ends of the central part (Fig. 3a).

4. CONCLUSIONS

Our research has shown that a dimensionless informational and statistical indicator makes it possible from a unified standpoint to assess the states that differ from each other in terms of external signs, processes and their dynamics. The integral indicator can be used to rank the efficiency of operating systems and can be useful in assessing the state of the processes of dynamic interaction of the operating pressure and objects and structures of various shapes and purposes.

5. ACKNOWLEDGEMENTS

The work was carried out within the framework of the state assignment of the IAP RAS for fundamental scientific research for 2021-2023 on topic No. 0030-2021-0025.

REFERENCES

1. **Eremeev P.G.** Sovremennije stal'nie konstruktsii bol'sheproletnikh pokritij unikal'nikh zdanij i sooruzhenij [Modern steel structures of large-span roofs of unique buildings and structures]. Moscow, ASV, 2009. 336 p.
2. **Simiu E., Scanlan R.** Wind effects on structures. New York, Wiley,1978. 488 p.
3. **Retter E.I.** Arkhitekturno-stroitelnaya aerodinamika [Architectural and constructional aerodynamics]. Moscow, Stroyizdat, 1984. 294 p.
4. **Savitsky G.A.** Vetrovaya nagruzka na sooruzheniya [Wind load on structures]. Moscow, Izd-vo lit po str-vu, 1972. 111 p.
5. **Hoerner S.F.,** Fluid-dynamic drag: theoretical, experimental and statistical information. - Wachington, 1965. - 455p.
6. **Stankovic, S., Campbell N., Harries A.** Urban Wind Energy - London Taylor &Francis, 2009. - 200p.
7. **Mohamed A.** Comparision of the numerical study of the effect of building protrusion aerodynamics with the results of aerodynamic tests // 15th Australian wind energy society workshop. - Sydney. - 2012.- 4 p.
8. **Mou, B., He, B.-J., Zhao, D.-X., & Chau, K.-W.** (2017). Numerical simulation of the effects of building dimensional variation on wind pressure distribution. Engineering Applications of Computational Fluid Mechanics, 11(1), pp 293–309.
9. **Fevralskikh A.V.** Chislennoe issledovanie aerodinamicheskoy interferentsii startovoy sistemy podduva i kryla ekranoplana [Numerical study of aerodynamic interference of the launch air-inflation system and the wing of a wing-in-groundcraft]. Trudy Krylovskogo gosudarstvennogo nauchnogo tsentra – Transactions of the Krylov State Scientific Center, 2019, Vol. 4(390), Pp. 117-124.
10. **Gnyrya A.I., Korobkov S.V., Koshin A.A., Terekhov V.I.** Modelirovanie vetrovykh nagruzok pri obtekanii vozdushnym potokom sistemy modeley zdaniy pri variatsii ikh raspolozheniya [Simulation of wind loads with air flow around a system of building models with a variation in their location]. Vestnik Tomskogo gosudarstvennogo arkhitekturno-stroitelnogo universiteta – Bulletin of the Tomsk State University of Architecture and Civil Engineering, 2018, No 4, Pp.65-73.
11. **Muschanov V.F., Zubenko A.V., Drozdov A.A.** Issledovanie aerodinamicheskikh koeffitsientov provisayuschikh membrannykh pokrytiy inzhenernykh sooruzheniy [Study of the aerodynamic coefficients of sagging membrane coatings of engineering structures]. Metallicheskie konstruktsii – Steel Constructions, 2017, vol. 23, No 2, Pp. 81-96.
12. **Lampsi B.B., Shilov S.S., Khazov P.A.** Chislennoe i fizicheskoe modelirovanie vetrovyh potokov na bol'sheproletnoe pokrytie [Numerical and physical modeling of wind loads on long-span shell structures]. Vestnik MGSU – (Monthly Journal

on Construction and Architecture, 2022. Vol. 1, Pp. 21-31.
13. **Satanov, A.A., Simonov A.V., Khazov P. A.** Opredelenie aerodinamicheskih harakteristik bol'sheproletnogo zdaniya eksperimental'nymi metodami [Experimental study of the aerodynamic characteristics of the large-span building] // Structural mechanics and structures, 2023. Vol. 1 (36). Pp. 63-74.
14. **Anushchenko A.M., Erofeev V.I., Khazov P.A., Satanov A.A., Fevral'skikh A.V**. Issledovanie obtekaniya vozdushnymi potokami bol'sheproletnoj poverhnosti chislennym i eksperimental'nym metodami [Investigation of the air flow around a large-span surface by numerical and experimental methods] // Privolzhsky Scientific Journal, 2021. Vol. 1. Pp. 9-18.
15. **Tryanina N.Yu., Obletov E.N., Samokhvalov I.A.** Aerodinamicheskoe vozdejstvie na panel'nye antenny bazovyh stancij [Aerodynamic impact on base station panel antennas]. Privolzhsky Scientific Journal, 2022. Vol. 1. Pp. 23-30.
16. **Rajasekarababu K.B., Vinayagamurthy G., and Rajan S.S.** Experimental and computational investigation of outdoor wind flow around a setback building, Build. Simul., 2019, Vol. 12, Pp. 891–904.
17. **Valger, S.A.** On numerical modeling of aerodynamics of urban developments on unstructured computational grids. Thermophys. Aeromech. 28, Pp. 507–522 (2021).
18. **Khazov P.A., Anuschenko A.M., Onischuk E.A., Schyolokova Yu.D.** Chislennoe i eksperimentalnoe issledovanie raspredeleniya vetrovoy nagruzki na krivolineynoe bolsheprolyotnoe pokrytie [Numerical and experimental study of the distribution of the wind load on the curvilinear large-span covering]. Privolzhskiy nauchny zhurnal – Privolzhsky Scientific Journal, 2020. No 1, pp.16-21.
19. **Sereda Yu.S.** Osnovi diagnostiki i prognozirovaniya [Fundamentals of Diagnostics and Forecasting]. Nizhny Novgorod, Tipografiya «Povolzhie», 2005. 188 p.
20. **Ilyakhinsky A.V., Sereda Yu.S**. Statistricheskie modeli v zadachakh zondirovanija [Statistical models in probing problems]. Izvestiya VUZov, Radiofizika – Radiophysics and Quantum Electronics, 1989, vol.32, No 12, pp. 1502-1505.
21. **Egan J.P.** Signal Detection Theory and ROC Analysis, New York, 1975. 277 p.
22. **Vatutin V.A., Televina T.M., Chistiakov V.P**. Veroyatnostniye metodi v fizicheskikh issledovaniyakh [Probabilistic Methods in Physics Research]. Moscow, Nauka,1985. 208 p.
23. **Erofeev V.I., Ilyakhinsky A.V., Nikitina E.A., Pakhomov P.A., Rodyushkin V.M.** Ultrasonic sensing Method for evaluating the limit state of metal structures associated with the onset of plastic deformation. Physical Mesomechanics, 2020, vol. 23, No 3, pp. 241-245.

СПИСОК ЛИТЕРАТУРЫ

1. **Еремеев, П.Г.** Современные стальные конструкции большепролетных покрытий уникальных зданий и сооружений: монография. - М.: АСВ, 2009. - 336 с.
2. **Simiu E., Scanlan R.** Wind effects on structures. New York, Wiley,1978. 488 p. ISBN: 978-0471021759
3. **Реттер, Э.И.** Архитектурно-строительная аэродинамика: монография. - М.: Стройиздат, 1984. - 294 с.
4. **Савицкий Г.А.** Ветровая нагрузка на сооружения. - М.: Изд-во лит. по стр-ву, 1972.- 111 с.
5. **Hoerner S.F.,** Fluid-dynamic drag: theoretical, experimental and statistical information. - Wachington, 1965. - 455p.
6. **Stankovic, S., Campbell N., Harries A**. Urban Wind Energy - London Taylor &Francis, 2009. - 200p.
7. **Mohamed A.** Comparision of the numerical study of the effect of building protrusion aerodynamics with the results of aerodynamic tests // 15th Australian wind energy society workshop. - Sydney. - 2012.- 4 p.

8. **Mou, B., He, B.-J., Zhao, D.-X., & Chau, K.-W.** (2017). Numerical simulation of the effects of building dimensional variation on wind pressure distribution. Engineering Applications of Computational Fluid Mechanics, 11(1), Pp. 293–309.
9. **Февральских А.В.** Численное исследование аэродинамической интерференции стартовой системы поддува и крыла экраноплана / Февральских А.В. // Труды Крыловского государственного научного центра, 2019. – № 3(390). – С. 117-124.
10. **Гныря А.И., Коробков С.В., Кошин А.А., Терехов В.И.** Моделирование ветровых нагрузок при обтекании воздушным потоком системы моделей зданий при вариации их расположения // Вестник Томского государственного архитектурно-строительного университета / Томский гос. архитектур.-строит. ун-т. – Томск, 2018. – № 4. – С. 65-73.
11. **Мущанов В.Ф., Зубенко А.В., Дроздов А.А.** Исследование аэродинамических коэффициентов провисающих мембранных покрытий инженерных сооружений // Металлические конструкции. – Макеевка. - 2017. - №2. - Том 23. - С. 81-96.
12. **Лампси, Б.Б., Шилов С.С., Хазов П.А.** Численное и физическое моделирование ветровых потоков на большепролетное покрытие // Вестник МГСУ. -2022. -Т. 17, № 1. - С. 21-31.
13. **Сатанов А.А., Симонов А.В., Хазов П.А.** Определение аэродинамических характеристик большепролетного здания экспериментальными методами // Строительная механика и конструкции. -2023. - № 1(36). - С. 63-74.
14. **Анущенко А.М., Ерофеев В.И., Хазов П.А., Сатанов А.А., Февральских А.В.** Исследование обтекания воздушными потоками большепролетной поверхности численным и экспериментальным методами // Приволжский научный журнал. - 2021. - № 1. - С. 9-18.
15. **Трянина, Н.Ю. Облетов Е. Н., Самохвалов И. А.** Аэродинамическое воздействие на панельные антенны базовых станций // Приволжский научный журнал. – 2022. – № 1(61). – С. 23-30.
16. **Rajasekarababu K.B., Vinayagamurthy G., and Rajan S.S**. Experimental and computational investigation of outdoor wind flow around a setback building, Build. Simul., 2019, Vol. 12, P. 891–904.
17. **Valger, S.A.** On numerical modeling of aerodynamics of urban developments on unstructured computational grids. Thermophys. Aeromech. 28, 507–522 (2021).
18. **Хазов, П.А., Анущенко А.М., Онищук Е.А, Щелокова Ю.Д**. Численное и экспериментальное исследование распределения ветровой нагрузки на криволинейное большепролетное покрытие // Приволжский научный журнал /Нижегор. гос. архитектур.-строит. ун-т. – Нижний Новгород, 2020. – № 1. – С. 16-21.
19. **Середа Ю.С.** Основы диагностики и прогнозирования // Нижний Новгород Изд. «Типография «Поволжье», 2005. 188 с.
20. **Иляхинский А.В., Середа Ю.С**. Статистические модели в задачах зондирования// Известия высших учебных заведений. Радиофизика. 1989. Т. 32. № 12. С. 1502-1505.
21. **Egan J.P.** Signal Detection Theory and ROC Analysis, New York, 1975. 277 p.
22. **Ватутин В.Л., Телевинова Т.М., Чистяков В.П.** Вероятностные методы в физических исследованиях. - М.: Наука, 1985.- 208 с.
23. **Erofeev V.I., Ilyakhinsky A.V., Nikitina E.A., Pakhomov P.A., Rodyushkin V.M**. Ultrasonic sensing Method for evaluating the limit state of metal structures associated with the onset of plastic deformation. Physical Mesomechanics, 2020, vol. 23, No 3, pp. 241-245.

Vladimir Ivanovich Erofeev, Doctor of Physical and Mathematical Sciences, Professor, Director, Mechanical Engineering Research Institute of the RAS – Branch of Federal Research Center «A.V. Gaponov – Grekhov Institute of Applied Physics of the Russian Academy of Sciences», 85, Belinskogo str., Nizhny Novgorod, 603024, Russia, e-mail: erof.vi@yandex.ru, tel: +7(831) 432-05-76.

Ilyakhinsky Aleksandr Vladimirovich, Senior Researcher, Mechanical Engineering Research Institute of the RAS – Branch of Federal Research Center «A.V. Gaponov – Grekhov Institute of Applied Physics of the Russian Academy of Sciences», 85, Belinskogo str., Nizhny Novgorod, 603024, Russia, tel: +7(831) 432-23-87.

Elena Aleksandrovna Nikitina, Candidate of Technical Sciences, Senior Researcher, Mechanical Engineering Research Institute of the RAS – Branch of Federal Research Center «A.V. Gaponov – Grekhov Institute of Applied Physics of the Russian Academy of Sciences», 85, Belinskogo str., Nizhny Novgorod, 603024, Russia, tel: +7(831) 432-23-87.

Vladimir Mitrofanovich Rodyushkin, Doctor of Technical Sciences, Head of Laboratory, Mechanical Engineering Research Institute of the RAS – Branch of Federal Research Center «A.V. Gaponov – Grekhov Institute of Applied Physics of the Russian Academy of Sciences», 85, Belinskogo str., Nizhny Novgorod, 603024, Russia, e-mail: vlkn2005@yandex.ru, tel: +7(831) 432-23-87.

Khazov Pavel Alekseevich, Candidate of Technical Sciences, Associate Professor of the Department of Theory of Structures and Technical Mechanics, Head of the Laboratory for Continuous Monitoring of the Technical Condition of Buildings and Structures, Nizhny Novgorod State University of Architecture and Civil Engineering, 65, Ilyinkaya str., Nizhny Novgorod, 603950, Russia, e-mail: khazov.nngasu@mail.ru, tel: +7 (951) 919-0-919.

Andrey Andreevich Satanov, post-graduate student, Mechanical Engineering Research Institute of the RAS – Branch of Federal Research Center «A.V. Gaponov – Grekhov Institute of Applied Physics of the Russian Academy of Sciences», 85, Belinskogo str., Nizhny Novgorod, 603024, Russia, e-mail: andrewsatanov@gmail.com, tel: +79101333866.

Владимир Иванович Ерофеев, доктор физико-математических наук, профессор, директор, Институт проблем машиностроения РАН – филиал ФГБНУ «Федеральный исследовательский центр «Институт прикладной физики им. А.В. Гапонова – Грехова Российской академии наук» (ИПМ РАН), Адрес: д. 85, ул. Белинского, г. Нижний Новгород, 603024, Россия, e-mail: erof.vi@yandex.ru, тел. +7(831) 432-05-76.

Александр Владимирович Иляхинский, старший научный сотрудник, Институт проблем машиностроения РАН – филиал ФГБНУ «Федеральный исследовательский центр «Институт прикладной физики им. А.В. Гапонова – Грехова Российской академии наук» (ИПМ РАН), Адрес: д. 85, ул. Белинского, г. Нижний Новгород, 603024, Россия, тел. +7(831) 432-23-87.

Елена Александровна Никитина, кандидат технических наук, старший научный сотрудник, Институт проблем машиностроения РАН – филиал ФГБНУ «Федеральный исследовательский центр «Институт прикладной физики им. А.В. Гапонова – Грехова Российской академии наук» (ИПМ РАН), Адрес: д. 85, ул. Белинского, г. Нижний Новгород, 603024, Россия, тел. +7(831) 432-23-87.

Владимир Митрофанович Родюшкин, доктор технических наук, заведующий лабораторией, Институт проблем машиностроения РАН – филиал ФГБНУ «Федеральный исследовательский центр «Институт прикладной физики им. А.В. Гапонова – Грехова Российской академии наук» (ИПМ РАН), Адрес: д. 85, ул. Белинского, г. Нижний Новгород, 603024, Россия, e-mail: vlkn2005@yandex.ru, тел. +7(831) 432-23-87.

Павел Алексеевич Хазов, кандилат технических наук, доцент кафедры теории сооружений и технической механики, заведующий лабораторией непрерывного контроля технического состояния зданий и сооружений, Нижегородский государственный архитектурно-строительный университет (ННГАСУ), Адрес: д. 65, ул. Ильинсская, г. Нижний Новгород, 603950, Россия, e-mail: khazov.nngasu@mail.ru, тел. +7 (951) 919-0-919.

Андрей Андреевич Сатанов, аспирант, Институт проблем машиностроения РАН – филиал ФГБНУ «Федеральный исследовательский центр «Институт прикладной физики им. А.В. Гапонова – Грехова Российской академии наук» (ИПМ РАН), Адрес: д. 85, ул. Белинского, г. Нижний Новгород, 603024, Россия, e-mail: andrewsatanov@gmail.com, тел. +79101333866.

International Journal for Computational Civil and Structural Engineering, 19(3) 31–38 (2023)

DOI:10.22337/2587-9618-2023-19-3-31-38

NUMERICAL MODELING OF THE PROCESS OF DEGRADATION OF PERMAFROST SOILS OF THE BASE OF THE RAILWAY ROADBED IN THE AREA OF PASSAGE OF CONSTRUCTION EQUIPMENT

Sergey A. Kudryavtsev, Tatyana Yu. Valtseva, Igor I. Gavrilov

Far Eastern State Transport University, Khabarovsk, RUSSIA

Abstract: When studying freezing, permafrost and thawing soils, it is absolutely necessary to develop models of processes occurring in soils and their mathematical description as a basis. This will make it possible to perform a calculated assessment of the "thawing foundation - structure" system during the entire lifetime of the object, which will make it possible to design it correctly. The article considers a soil model that allows us to consider the process of degradation of permafrost soils of the base of the railway roadbed in the zone of passage of construction equipment.

Keywords: numerical modeling, permafrost soils, permafrost degradation, temperature, thawing, freezing

ЧИСЛЕННОЕ МОДЕЛИРОВАНИЕ ПРОЦЕССА ДЕГРАДАЦИИ МНОГОЛЕТНЕМЕРЗЛЫХ ГРУНТОВ ОСНОВАНИЯ ЗЕМЛЯНОГО ПОЛОТНА ЖЕЛЕЗНЫХ ДОРОГ В ЗОНЕ ПРОЕЗДА СТРОИТЕЛЬНОЙ ТЕХНИКИ

Кудрявцев С.А., Вальцева Т.Ю., Гаврилов И.И.

ФГБОУ ВО «Дальневосточный государственный университет путей сообщения», Хабаровск, РОССИЯ

Аннотация: При исследовании промерзающих, многолетнемерзлых и оттаивающих грунтов в качестве основания совершенно необходимой является разработка моделей протекающих в грунтах процессов и их математическое описание. Это позволит выполнить расчетную оценку системы «оттаивающее основание – сооружение» в течение всего срока существования объекта, что даст возможность правильно его спроектировать**.** В статье рассмотрена модель грунта позволяющая рассмотреть процесс деградации многолетнемерзлых грунтов основания земляного полотна железных дорог в зоне проезда строительной техники.

Ключевые слова: численное моделирование, многолетнемерзлые грунты, деградация мерзлоты, температура, оттаивание, промерзание

INTRODUCTION

Russia is rightly considered the coldest country in the world. Its characteristic feature is the presence of permafrost soils occupying more than two-thirds of the total area. In these areas, called the cryolithozone, thawing deformations that develop during the degradation of the base due to an increase in air temperature and permafrost are extremely important. Any design of facilities in regions with permafrost soils begins with thermophysical calculations in order to increase the efficiency of systems regulating the temperature regime of frozen foundations of embankments and recesses on railways and highways [1].

For soil in a frozen state, with an increase in temperature, even in the region of negative values, the strength of ice inclusions decreases, which is accompanied by a decrease in strength

and deformation characteristics. At zero temperature, the ice inclusions thaw and the soil experiences subsidence, which can reach significant values. The thawing process itself and the subsidence caused by it develop over time, which makes it necessary, in addition to the evolution of temperature fields, to consider consolidation during thawing for low-permeable soils.

THE MAIN PROBLEMS OF DESIGNING ON PERMAFROST SOILS

At the end of 2013, engineering and geological survey work began within the framework of the project for the development and construction of the second tracks of the railway infrastructure of the Baikal-Amur Mainline (BAM) and the Trans-Siberian Railway. The research began without scientific support and generalization of the accumulated experience, and for some design organizations this is the first experience of working on permafrost soils. Due to the extremely tight deadlines allowed for the survey of some of the objects, the survey was conducted in winter, since the first design solutions for construction should be issued in the spring.

Taking into account the above, as well as the fact that there are no clear instructions and standard solutions in regulatory documents concerning the design of measures excluding subsequent deformations in the abutment of the existing railway track bed on permafrost soils of the base, we consider it necessary to outline the experience of examination and treatment of the decreeing earthen dam and ways to improve its operational reliability.

The most common deformation of the BAM roadbed is precipitation of embankments (up to 94% of the total length of the roadbed on permafrost soils) [2]. When performing detailed diagnostics, we have to face three main types of deformations of embankments:

- thermal (thawing - compaction) deformations due to thawing during the degradation of permafrost bases;
- plastic (heaving-spreading-squeezing) deformations, due to waterlogged, heaving soils at the base of the embankment, falling into the zone of seasonal freezing-thawing;
- suffusion deformations due to the removal of pulverized clay fractions of soils from the roadbed and the base of the embankment.

Currently, thermal deformations of embankments are most common in the Western and Central sections of the BAM. Here the natural conditions are favorable for the preservation of permafrost rocks. Therefore, a new active layer was formed at the base of the mounds with a height of 1.5-6.0 m 3-5 years after their construction [3] and, despite the increase in average annual air temperatures in recent years, the depth of seasonal thawing and the temperature regime of the soils of the bases change differently depending on the average annual air temperature.

Practically all thermal precipitation of the Western and Central sections is caused by faulty drainage channels and channels of artificial structures, which provoke the development of stagnant water formations, thermokarst, filtration flows through the body of the embankment and eventually the degradation of permafrost (Fig.1).

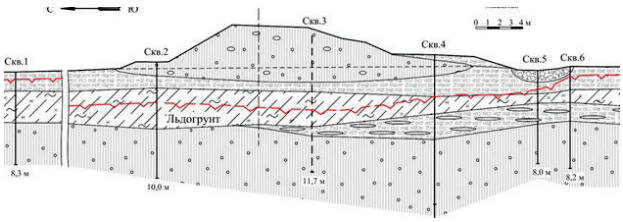


Figure 1. Long-term thawing of underground ice in the base and filtration of water through the body of the embankment

Thermal precipitation of the embankments of the Eastern part of the BAM today occurs only where strongly icy layers of soil and underground ice lie at the base of the roadbed.

Sudden thermal deformations, dangerous for train traffic, were recorded by us during the thawing of the lenses of re-vein ice. With unsecured drainage, the warming filtration flows are concentrated in the relief depressions occupied by re-vein ice. After the thawing of the ice, a

strong sod reinforced with roots and stems of shrubby vegetation prevents the filling of the cavity with the soil of the body of the embankment for some time. The filling of the cavity and the occurrence of dips occurs, as a rule, suddenly, during the passage of trains.

The experience of a detailed survey of the roadbed of the Eastern section of the BAM confirms the predictions of scientists. At the base of the embankments, regardless of their height, a "thawing bowl" with a depth of up to 5 meters or more has formed, the current rate of thawing of permafrost under the embankments does not exceed several centimeters per year.

However, the rates of thawing deformations exceed the predicted 1-2 cm/year, since thermal deformations are replaced by plastic deformations of the watered, heaving soils of the foundations of the roadbed falling into the zone of deep seasonal freezing [2, 3].

The assessment of the deformations of thawing of the base, composed of frozen soils, is aimed at establishing the possibility of allowing thawing during the operation of buildings or structures erected in the cryolithozone. If the value of the final precipitation is less than the maximum permissible, then there is no need to resort to expensive measures to preserve the frozen state of the soil during construction.

The first priority in this case will be the calculation of temperature fields in the base with the determination of the boundary of the thawing bowl within the lifetime of the structure. At the same time, it should be borne in mind that during thawing, which occurs at a constant zero temperature, ice-cement bonds are destroyed, which is accompanied by a sharp decrease in the mechanical characteristics of the base. With rapid thawing, caused, for example, by the action of local heat sources in icy cohesive soils, the stability of the thawed zone of the base can be disrupted, which leads to the extrusion of soils, accompanied by subsidence. In this regard, the most important in such cases will be the assessment of the strength of the foundation, folded thawed soil. For this purpose, the pressure on the thawed soil should be limited by the values of the calculated resistance set for both thawed soils using their characteristics φ and c in the thawed state.

Experimental determination of these characteristics should be carried out according to the unconsolidated shift scheme.

If there is no extrusion of the soil during thawing, and the pressure on the thawing soil does not exceed the calculated resistance of the soil, then the precipitation of the foundations can be determined based on the principle of linear deformability.

At low pressures (according to N.A.Tsytovich up to 400 kPa), the expression for the relative drawdown eth can be represented by a linear function of the form

$$\varepsilon_{th} = A_{th} + \delta_{th}\, p, \qquad (1)$$

where A_{th} is the thawing coefficient; δ_{th} is the compressibility coefficient of the thawing soil due to its compaction by pressure p.

The first term of the formula is called "thermal" precipitation, and the second term is "cargo", which corresponds to the nature of deformations.

NUMERICAL MODELING OF THE PROCESS OF DEGRADATION OF FROZEN SOILS

When studying freezing, permafrost and thawing soils, it is absolutely necessary to develop models of processes occurring in soils and their mathematical description as a basis. This will make it possible to perform a calculated assessment of the "thawing base – structure" system during the entire lifetime of the object, which will make it possible to design it correctly.

Thermophysical and deformation problems in which it is necessary to consider inhomogeneous bases, including layers of thermal insulation of variable thickness, taking into account unilateral heating or cooling of the object, phase transformations in the spectrum of negative temperatures, etc. are available for solution only using numerical methods. Such methods have led to the development of highly efficient pro-

grams capable of calculating temperature fields and deformations in the base.

Naturally, such programs are commercial, which is justified by the great complexity and duration of their creation. At the same time, the most valuable programs are capable, in addition to temperature, to solve the problems of joint calculation of the "foundation – structure" system.

Professors S.A.Kudryavtsev, I.I. Sakharov, V.N. Paramonov for the first time in world practice developed a mathematical model by the finite element method "Termoground" [4], which is an integral part of the software package "FEM models" developed in the company "Georeconstruction", which allows performing complex construction calculations of freezing, frost heaving and thawing processes seasonally freezing and permafrost soils of the foundations of buildings and structures in spatial formulation for scientific, design and construction organizations of the Russian Federation [4].

The freezing-thawing processes are described by the thermal conductivity equation for a non-stationary thermal regime in a three-dimensional ground space:

$$C_{th(f)}\rho_d \frac{\partial T}{\partial t} = \lambda_{th(f)}\left(\frac{\partial^2 T}{\partial x^2} + \frac{\partial^2 T}{\partial y^2} + \frac{\partial^2 T}{\partial z^2}\right) + q_V \quad (2)$$

Where $C_{th(f)}$ is the specific heat capacity of the soil (thawed or frozen), J/kG·K; ρ_d – density of dry soil, kG/m^3; T – temperature, °C; t – time, s; $\lambda_{th(f)}$ – thermal conductivity of the soil (thawed or frozen), W/m·K; x, y, z – coordinates, m; q_V is the power of internal heat sources, W/m^3.

This equation makes it possible to determine the values of the incoming and outgoing heat flow from the elementary volume of the soil, leaving the main flow of the soil volume at a point in time equal to the change in the value of heat turns. In the permafrost soil model, the freezing-thawing processes are estimated non-stationary in time and non-linearly due to changes in thermophysical characteristics depending on changes in soil temperature and humidity. As a result of numerical modeling, temperature and humidity fields in the soil base are determined for each estimated period of time. [3-10].

As is known, when freezing soils, the source of forces are the deformation of heaving. Obviously, if physical experiments do not give an acceptable result, first of all, one should try to determine the heave deformations based on theoretical considerations, starting from obvious facts. One way or another, all deformations during freezing of soils are caused by the transition of water into ice. This is water present in the ground before freezing, as well as brought to the front due to migration. Thus, it is necessary to have an idea of the amount of water present in the ground initially, which is determined by the survey data, and the volume of water delivered from the melt zone.

THE INFLUENCE OF HIGHWAY ROADS ON THE DEGRADATION OF PERMAFROST

To date, extensive experience has been accumulated in the operation of buildings and structures on the Trans-Siberian and Baikal-Amur highways in permafrost conditions. Particular attention was paid to the uneven thawing of extended railway embankments depending on their orientation relative to the cardinal direction of the Earth. Solar energy is distributed in space in the form of a so-called direct directed flow of solar radiation, characterized by itself in the form of a straight line connecting the Sun and the Earth's surface. In view of the presence of the atmosphere and the Earth's surface, solar radiation already enters extended linear structures (railway embankments) in the form of three streams of solar energy: direct, diffuse or scattered and reflected from the Earth's surface.

To ensure the construction of the railway roadbed, temporary highways are being built, designed to transport soil from quarries to embankments being erected. Pritrass highways are built according to the norms of roads of the V category, as a rule, along the entire route, usually within the right-of-way. The type and design of the highway is determined on the basis of a

detailed study of local conditions and taking into account the transported soil.

The Baikal-Amur Highway passes through the territory with severe climatic conditions at 52-56 latitudes, at different angles of light and through areas of permafrost with a depth of 100 to 300 meters and high seismicity up to 9 points. During the construction of the highway and the ongoing modernization, the latest designs are used, new methods of construction and operation of facilities in difficult engineering conditions have been developed and patented.

We have given thermophysical calculations in the annual cycle of the condition of the railway embankment without measures and with measures traced in the latitudinal direction. Monthly solar radiation was taken in accordance with the norms of climatology and data from the nearest weather stations.

Fig. 2 shows the calculation results and shows plots of soil temperatures and zones of frozen soil (blue color) and thawing soil of the construction of the railway roadbed with a highway for the month of October of the tenth year of the forecast without measures to protect the permafrost soils of the base.

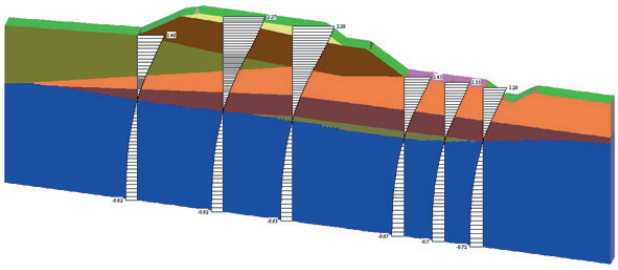


Figure 2. Plot of soil temperatures, ° C and zones of frozen soil (blue) and thawing soil of the structure for the month of October of the tenth year of the forecast without measures to protect the permafrost soils of the base.

These forecast calculations showed that due to the violation of the soil and vegetation layer in the zone of passage of construction equipment during the construction of the structure without additional measures, the degradation of permafrost soils increases by an average of 0.5 m over 10 years.

Fig. 3 shows the design scheme of the railway roadbed with measures to reduce the degradation of permafrost soils of the base in the form of cooling berms with the device of a highway.

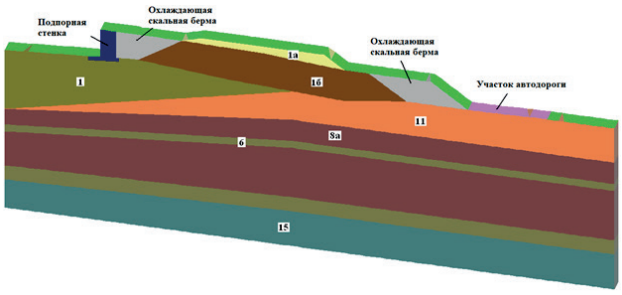


Figure 3. The design scheme of the railway roadbed with measures to reduce the degradation of permafrost soils of the base in the form of cooling berms with the device of a highway and retaining wall

Fig. 4 shows the calculation results and plots of soil temperatures, °C and zones of frozen soil (blue color) and thawing soil of the construction of the railway roadbed with a highway for the month of October of the tenth year of the forecast with measures to protect the permafrost soils of the base in the form of a cooling stone outline and retaining wall.

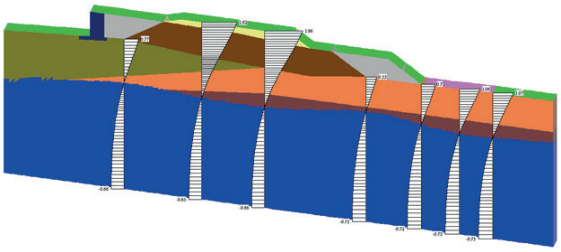


Figure 4. Plots of soil temperatures, °C and zones of frozen soil (blue color) and thawing soil of the construction of the railway roadbed with a highway for the month of October of the tenth year of the forecast with measures to protect the permafrost soils of the base in the form of a cooling stone outline and a retaining wall.

Calculations have shown that due to the violation of the soil and vegetation layer in the zone of the permafrost base of the pritass highway, during the construction of a structure with a cooling rock berm, the degradation of perma-

frost soils continues to occur by an average of 0.4 m over ten years. It is necessary to provide for measures to restore the boundary of permafrost soils in the area of the pre-mass highway for the passage of construction equipment.

To restore the boundary of permafrost soils in the area of the pre-mass highway for the purpose of passing construction equipment, it is advisable to provide a counterbanket of rocky soil, at least 1 m high and more than 5 m wide.

Figure 5 shows the design scheme of the railway roadbed with measures to reduce the degradation of permafrost soils of the base in the form of cooling berms and a counterbanket of rocky soil for the construction of a highway on it.

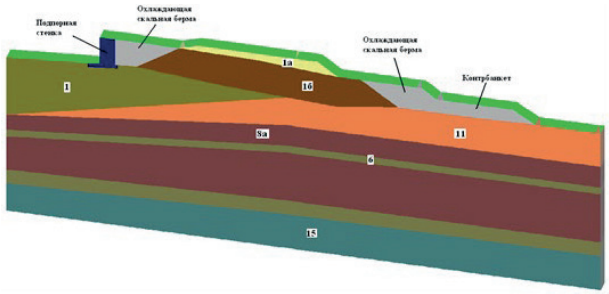


Figure 5. The design scheme of the railway roadbed with measures to reduce the degradation of permafrost soils of the base in the form of cooling berms and a counterbanket of rocky soil for the construction of a highway on it

Fig. 6 shows the calculation results and plots of soil temperatures, °C and zones of frozen soil (blue color) and thawing soil of the construction of the railway roadbed with a highway for the month of October of the tenth year of the forecast with measures to reduce the degradation of permafrost soils of the base in the form of cooling berms and a counterbanket of rocky soil for the device there is a highway on it.

Calculations have shown that the use of a counterbanket made of rocky soil for the construction of a highway on it as an event to stabilize permafrost soils showed a gradual increase in the boundary of permafrost soils by an average of 0.3 m over ten years.

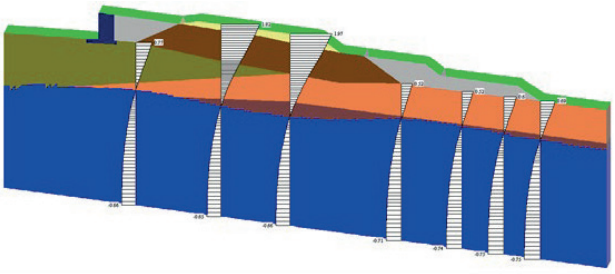


Figure 6. Plots of soil temperatures, °C and zones of frozen soil (blue color) and thawing soil of the construction of the railway roadbed with a pre-track highway for the month of October of the tenth year of the forecast with measures to protect the permafrost soils of the base in the form of a cooling stone outline and a counterbanket of rocky soil for the construction of a pre-track highway and a retaining wall on it walls.

CONCLUSIONS:

1. Any design of objects in regions with permafrost soils is advisable using thermophysical calculations in order to identify rational structures that reduce and regulate the temperature regime of frozen foundations of embankments and recesses on railways and highways.
2. The first priority in thermal engineering forecast calculations is the determination of temperature and humidity fields in the base with the establishment of the boundary of the thawing bowl within the lifetime of the structure.
3. Thermophysical and deformation problems in which it is necessary to consider inhomogeneous bases, including layers of thermal insulation of variable thickness, taking into account unilateral heating or cooling of the object, phase transformations in the spectrum of negative temperatures, etc. are available for solution only using numerical methods.
4. Predictive numerical calculations have shown that due to the violation of the soil and vegetation layer in the zone of passage of construction equipment during the construction of the structure without additional measures, there is an increase in the degradation of permafrost soils by an average of 0.5 m over ten years.

5. Numerical calculations have shown that the use of a counterbanket made of rocky soil for the construction of a highway on it as an event to stabilize permafrost soils showed a gradual increase in the boundary of permafrost soils by an average of 0.3 m over ten years

REFERENCES

1. **Kudryavtsev S.A., Valtseva T.Yu.** Numerical modeling of the process of thawing of permafrost soils of infrastructure railway facilities of the Far East. Actual problems of computer modeling of structures and structures: Abstracts of the VIII-th International Symposium/ Tambov State Technical University. – Tambov, Publishing House of IP Chesnokova A.V., 2023. pp.146-- 147.
2. **Ashpiz E.S.** Development of a program of measures to stabilize the roadbed of railways located on permafrost soils. / Works of reading dedicated to the 105th anniversary of Professor G.M.Shakhunyants, Moscow: MIIT, 2009. – 223 p.
3. **Mironov V.A., Gavrilov I.I**. Temperature monitoring of the earth bed of the BAM zone in modern natural and climatic conditions/ Proceedings of the reading dedicated to the 105th anniversary of Professor G.M. Shakhunyants, Moscow: MIIT, 2009. 223 p
4. **Kudryavtsev S.A**. Calculation of the freezing and thawing process according to the program "Termoground". Urban reconstruction and geotechnical construction. 2004. № 4. p. 83.
5. **Kudryavtsev S.A., Kazharsky A.V., Goncharova E.D., Kotenko Z.I., Grigoriev D.O**. Embankment on the eastern permafrost polygon of the Baikal-Amur mainline. Materials of the International Scientific Conference "Transport Geotechnics and Geoecology" (TGG-2017). Development of technological processes. 2017. pp. 774-782.
6. **Borisova A., Kudryavtsev S.** Investigation of the process of freezing and thawing foundations using seasonal and refrigerating devices. Web conference MATEC. 2018. p. 03040.
7. **Goncharova E.D., Kudryavtsev S.A., Berestyanoy Yu.B.** Design and construction of geotechnical structures from geotechnical materials in the coastal Arctic zone of Russia. Proceedings of the 23rd International Conference on Marine and Polar Engineering. Proceedings of the Symposium on mining in the ocean ISOPE. 2013. No. 2013. p. 562.
8. **Kudryavtsev S.A.** Modeling of the process of freezing, frost heaving and thawing of soils. Foundations, foundations and soil mechanics. 2004. No. 5. p. 21.
9. **Sakharov I.I., Paramonov V.N., Kudryavtsev S.A., Valtseva T.Yu., Kazharsky A.V., Kotenko Zh.I**. Accounting for solar radiation in numerical modeling of thermophysical processes of freezing and thawing of permafrost soils. Construction and Geotechnics. 2020. Vol. 11. No. 4. pp. 20-32.
10. **Sakharov I.I., Paramonov V.N., Kudryavtsev S.A.** The account of frost heave and thawing processes when designing road installations in cold regions. Transportation Soil Engineering in Cold Regions. Proceedings of TRANSOILCOLD 2019. (Series: Lecture Notes in Civil Engineering, volume 49). Singapore, 2020. pp. 19-24.

СПИСОК ЛИТЕРАТУРЫ

1. **Кудрявцев С.А., Вальцева Т.Ю.** Численное моделирование процесса оттаивания многолетнемерзлых грунтов инфраструктурных железнодорожных объектов Дальнего Востока. Актуальные проблемы компьютерного моделирования конструкций и сооружений: Тезисы докладов VIII-го международного симпозиума/ ФГБОУ ВО «Тамбовский государственный технический университет». – Тамбов, Изд-во ИП Чеснокова А.В., 2023. С.146–– 147.
2. **Ашпиз Е.С.** Разработка программы мероприятий по стабилизации земляного по-

лотна железных дорог, расположенных на многолетнемерзлых грунтах. / Труды чтения, посвященные 105-летию профессора Г.М.Шахунянца, М.: МИИТ, 2009. – 223 с.
3. **Миронов В.А., Гаврилов И.И.** Температурный мониторинг земляного полотна зоны БАМ в современных природно-климатических условиях/ Труды чтения, посвященные 105-летию профессора Г.М. Шахунянца, М.: МИИТ, 2009. 223 с
4. **Кудрявцев С.А.** Расчёт процесса промерзания и оттаивания по программе «Termoground» Реконструкция городов и геотехническое строительство. 2004. № 4. С. 83.
5. **Kudryavtsev S.A., Kazharsky A.V.A.V., Goncharova E.D., Kotenko Z.I., Grigoriev D.O.** Embankment on permafrost Eastern polygon of Baikal-Amur mainline. Proceedings of the International Scientific Conference Transportation Geotechnics and Geoecology (TGG-2017). Proceedings Engineering. 2017. С. 774-782.
6. **Borisova A., Kudryavtsev S.** The research of the freezing and thawing process of the foundations with the use of season and cold producing devices. MATEC Web of Conferences. 2018. С. 03040.
7. **Goncharova E.D., Kudryavtsev S.A., Berestyanyy U.B.** Engineering and construction of geotechnical structures with geotechnical materials in coastal arctic zone of Russia. Proceedings of the 23rd international offshore and polar engineering conference. Proceedings of the ISOPE Ocean Mining Symposium. 2013. № 2013. С. 562.
8. **Кудрявцев С.А.** Моделирование процесса промерзания, морозного пучения и оттаивания грунтов. Основания, фундаменты и механика грунтов. 2004. № 5. С. 21.
9. **Сахаров И.И., Парамонов В.Н., Кудрявцев С.А., Вальцева Т.Ю., Кажарский А.В., Котенко Ж.И.** Учет солнечной радиации при численном моделировании теплофизических процессов промерзания и оттаивания вечномерзлых грунтов. Construction and Geotechnics. 2020. Т. 11. № 4. С. 20-32.
10. **Sakharov I.I., Paramonov V.N., Kudryavtsev S.A.** The account of frost heave and thawing processes when designing road embankments in cold regions. Transportation Soil Engineering in Cold Regions. Proceedings of TRANSOILCOLD 2019. (Series: Lecture Notes in Civil Engineering, volume 49). Singapore, 2020. С. 19-24.

Kudryavtsev Sergey Anatolievich, Doctor of Technical Sciences, corresponding member of the RAASN, professor, head of the Department "Bridges, Tunnels and Underground Structures" Far Eastern State Transport University, 680021, 47, Serishev st., Khabarovsk, Russia, room2100. e-mail: olgakudr56@mail.ru, telephone 8(4212)407524

Valtseva Tatyana Urievna, Candidate of Technical Sciences, Associate Professor of the Department "Bridges, Tunnels and Underground Structures " Far Eastern State Transport University, 680021, 47, Serishev st., Khabarovsk, Russia, room 2100. e-mail: vtu25@mail.ru, telephone 8(4212)407524

Gavrilov Igor Ilich, postgraduate student of the Department "Bridges, Tunnels and Underground Structure ", Far Eastern State Transport University, 680021, 47, Serishev st., Khabarovsk, Russia, room 2100. e-mail: iigavrilov@bk.ru, telephone 8(4212)407524

Кудрявцев Сергей Анатольевич, доктор технических наук, член-корреспондент РААСН, профессор, заведующий кафедрой «Мосты, тоннели и подземные сооружения» ФГБОУ ВО «Дальневосточный государственный университет путей сообщения» (ДВГУПС), 680021, г. Хабаровск, ул. Серышева д. 47, ауд.2100. e-mail: olgakudr56@mail.ru. Тел.8(4212)407524

Вальцева Татьяна Юрьевна кандидат технических наук, доцент кафедры «Мосты, тоннели и подземные сооружения» ФГБОУ ВО «Дальневосточный государственный университет путей сообщения» (ДВГУПС), 680021, г. Хабаровск, ул. Серышева д. 47, ауд.2100. e-mail: vtu25@mail.ru. . Тел.8(4212)407524

Гаврилов Игорь Ильич, аспирант кафедры «Мосты, тоннели и подземные сооружения» ФГБОУ ВО «Дальневосточный государственный университет путей сообщения» (ДВГУПС), 680021, г. Хабаровск, ул. Серышева д. 47, ауд.2100. e-mail: iigavrilov@bk.ru. Тел.8(4212)407524

DOI:10.22337/2587-9618-2023-19-3-39-48

CHARACTERISTIC METHOD FOR SOLVING FILTRATION PROBLEM

Liudmila I. Kuzmina [1], Yuri V. Osipov [2], Artem R. Pesterev [2]

[1] HSE University, Moscow, RUSSIA
[2] Moscow State University of Civil Engineering, Moscow, RUSSIA

Abstract: During construction, a liquid solution of a grout or waterproof filler is pumped into porous rock to improve its properties. The filtration of a suspension moving at a variable speed in a porous medium is simulated. A one-dimensional problem of filtration in a homogeneous porous medium with a curvilinear concentration front of suspended and retained particles is considered. For the numerical solution of the problem by the method of finite differences, the method of characteristics is used. The transition to characteristic variables allows one to straighten the front and construct a discrete grid with a constant step. When calculating the solution using an explicit difference scheme, additional points are used that do not coincide with the grid nodes. A detailed description of the algorithm for calculating a solution at the grid nodes and an example of a numerical solution of the problem are given.

Keywords: deep bed filtration, porous medium, suspended and retained particles, finite difference method, method of characteristics, numerical solution

ХАРАКТЕРИСТИЧЕСКИЙ МЕТОД ДЛЯ РЕШЕНИЯ ЗАДАЧИ ФИЛЬТРАЦИИ

Л.И. Кузьмина [1], Ю.В. Осипов [2], А.Р. Пестерев [2]

[1] Национальный исследовательский университет «Высшая школа экономики», г. Москва, РОССИЯ
[2] Национальный исследовательский Московский государственный строительный университет, г. Москва, РОССИЯ

Аннотация: При строительстве для улучшения свойств пористой породы в нее закачивается жидкий раствор укрепителя или водонепроницаемого наполнителя. Моделируется фильтрация суспензии, движущейся с переменной скоростью в пористой среде. Рассматривается одномерная задача фильтрации в однородной пористой среде с криволинейным фронтом концентраций взвешенных и осажденных частиц. Для численного решения задачи методом конечных разностей используется метод характеристик. Переход к характеристическим переменным позволяет выпрямить фронт и построить дискретную сетку с постоянным шагом. При вычислении решения по явной разностной схеме используются дополнительные точки, не совпадающие с узлами сетки. Приведено подробное описание алгоритма построения решения в узлах сетки и пример численного решения задачи.

Ключевые слова: глубинная фильтрация, пористая среда, взвешенные и осажденные частицы, метод конечных разностей, метод характеристик, численное решение

1. INTRODUCTION

Filtration of suspensions in porous media occurs in many construction technologies. To strengthen the foundation, liquid concrete is injected into loose soil, which, when solidified, strengthens the rock. During the construction of underground storage facilities for hazardous liquid waste, watertight partitions are constructed. To do this, a solution of a polymer or bentonite is pumped into the cavity, which, when wetted, expand and fill empty pores. During the reconstruction of roads, a grout is pumped into the eroded cavities under the

roadbed, which is filtered in sand and fine gravel [1-6].

Filtration models describe the transport of suspended particles by a carrier fluid through pores. Under the influence of various forces (electrostatic, gravitational, hydrodynamic, mechanical and others), some particles are deposited on the framework of a porous medium and form an immobile deposit. Depending on the physical and chemical properties of the particles, of the liquid, of the porous medium frame and on the geometry of the pores, one or another mechanism of particle capture predominates. If the sizes of particles and pores are close, then the size-exclusion mechanism is the main one: suspended particles freely pass through large pores and get stuck in the neck of narrow pores [7–11].

Mathematical models of filtration include quasi-linear partial differential equations with various conditions which determine the unique solution. Analytical solutions of such problems are available only in the simplest cases. As a rule, numerical methods are used to obtain the solution [12–16].

The model of pure water displacement by a suspension in a porous medium is given by inconsistent initial and boundary conditions. The solution – the concentration of suspended particles – is discontinuous at the concentration front. It is zero before the front and positive behind the concentration front [17].

For the numerical solution of filtration problems, the finite difference method with a constant step is mainly used [18–20]. This method works well on a rectangular grid. It can be used also on a wedge obtained by cutting off from the rectangle the area before the rectilinear concentration front, where the solution is zero. The ratio between the time and coordinate steps is selected so that the grid nodes lie on the concentration front.

If the suspension velocity changes, then the concentration front becomes curvilinear [21]. In this case, to get the nodes to the concentration front, a variable grid spacing is usually chosen. It is also possible to keep the grid step constant and check each node whether it lies behind the front [22].

The proposed algorithm uses the characteristic variables of the hyperbolic system [23–25]. In these variables, the front becomes rectilinear, which makes it possible to apply the finite difference method with a constant step. The solution in Cartesian variables is obtained by reverse substitution. The algorithm is used to solve the filtration problem with deposit rise. For a variable suspension velocity, this problem has no analytical solution [26, 27].

2. FILTRATION MODEL WITH DEPOSIT EROSION

In the domain $\Omega = \{(x,t):\ x \ge 0,\ \ t \ge 0\}$, a one-dimensional filtration model of a monodisperse suspension moving in a porous medium with a variable speed $v(t) > 0$ is considered

$$\frac{\partial C}{\partial t} + v(t)\frac{\partial C}{\partial x} + \frac{\partial S}{\partial t} = 0, \qquad (1)$$

$$\frac{\partial S}{\partial t} = F(S)C - \varphi(S) \qquad (2)$$

with boundary and initial conditions

$$x = 0: C = 1, \quad t = 0: C = 0,\ S = 0. \qquad (3)$$

Consider (1) as an equation with respect to the unknown $C(x,t)$ for a given solution $S(x,t)$. Let us introduce a characteristic variable τ. The characteristics of equation (1) are given by a system of ordinary differential equations [28]

$$\frac{dt}{d\tau} = 1, \quad \frac{dx}{d\tau} = v(t). \qquad (4)$$

The initial conditions for characteristics (4) depend on their location. For characteristics coming out of the OX axis

$$t(0) = 0, \quad x(0) = x_0,\ \ x_0 > 0, \qquad (5)$$

for characteristics coming out of the *OT* axis

$$t(0)=t_0,\quad x(0)=0,\ t_0>0. \tag{6}$$

Integrating equations (4) with conditions (5) and (6), we obtain two families of characteristics:

$$\begin{array}{l} OX:\ t=\tau,\quad x=\int\limits_0^{\tau} v(t)d\tau+x_0; \\ OT:\ t=\tau+t_0,\quad x=\int\limits_0^{\tau} v(t)d\tau. \end{array}. \tag{7}$$

Since the initial and boundary conditions (3) are not consistent at the origin, the solution *C* has a discontinuity. The discontinuity line Γ – the concentrations front of the suspended and deposited particles is a characteristic emerging from the origin of coordinates. It is given by system (4) with the conditions $t(0)=0,\ x(0)=0.$

In this case $t=\tau$ and the concentration front is determined by the formula

$$x_{\Gamma}(t)=\int\limits_0^{t} v(\varsigma)d\varsigma. \tag{8}$$

Using the method of characteristics, it can be shown that problem (1)-(3) has a zero solution in the domain $\Omega^0=\{(x,t):\ x\ge x_{\Gamma}(t),\ t\ge 0\}$ (before the front), behind the front in the domain $\Omega^+=\{(x,t):\ x<x_{\Gamma}(t),\ t\ge 0\}$ the solution is positive.

Substitute equation (2) into (1). In characteristic variables, equation (1) takes the form

$$\frac{dC}{d\tau}=-\big(F(S)C-\varphi(S)\big). \tag{9}$$

For the uniqueness of a positive solution, the conditions are set on the boundaries of the region Ω^+:

$$C\big|_{\tau=0}=1,\qquad S\big|_{\Gamma}=0. \tag{10}$$

The limit value of the retained concentration at $t\to\infty$ is determined from the ratio

$$F(S)-\varphi(S)=0.$$

3. ALGORITHM FOR NUMERICAL SOLUTION

To effectively use the finite difference method in the domain Ω^+, let's pass to variables $t,\ t_0\ (t\ge t_0)$:

$$\tau=t-t_0,\quad x(t,t_0)=\int\limits_{t_0}^{t} v(\varsigma)d\varsigma. \tag{11}$$

From formulae (11) it follows

$$\frac{dC}{d\tau}=\frac{dC}{dt}.$$

We integrate equation (9) with respect to the variable *t* from *t* to $t+dt$:

$$\begin{array}{l} C\big(x(t+dt,t_0),t+dt\big)-C\big(x(t,t_0),t\big)= \\ =-\int\limits_t^{t+dt}\big(F(S)C-\varphi(S)\big)dt \end{array} \tag{12}$$

Approximate calculation of the integral on the right side of equation (12) is performed using the trapezoid method:

$$\begin{array}{l} \int\limits_t^{t+dt}\big(F(S)C-\varphi(S)\big)dt=\frac{dt}{2}\Big(F\big(S(x(t+dt,t_0),t+dt)\big)C(x(t+dt,t_0),t+dt)- \\ -\varphi\big(S(x(t+dt,t_0),t+dt)\big)+F\big(S(x(t,t_0),t)\big)C(x(t,t_0),t)-\varphi\big(S(x(t,t_0),t)\big)\Big). \end{array} \tag{13}$$

Substitute the integral (13) into equation (12):

$$C\left(x(t+dt,t_0),t+dt\right)= \\ =\frac{\left(2-F\left(S(x(t,t_0),t)\right)dt\right)C\left(x(t,t_0),t\right)+dt\left(\varphi\left(S(x(t+dt,t_0),t+dt)\right)+\varphi\left(S(x(t,t_0),t)\right)\right)}{2+F\left(S(x(t+dt,t_0),t+dt)\right)dt}. \quad (14)$$

To find the value $S(x(t+dt,t_0),t+dt)$, integrate equation (2) over time for a fixed $x=x(t,t_0)$:

$$S(x(t,t_0),t+dt)-S(x(t,t_0),t)=\int_t^{t+dt}\left(F(S)C-\varphi(S)\right)dt. \quad (15)$$

Calculate the integral on the right side of (15) using the left rectangle method:

$$S(x(t,t_0),t+dt)=S(x(t,t_0),t)+\left(F\left(S(x(t,t_0),t)\right)C\left(x(t,t_0),t\right)-\varphi\left(S(x(t,t_0),t)\right)\right)dt. \quad (16)$$

Formulae (14), (16) make it possible to sequentially calculate the discrete values of the solution.

First, consider an example of how the algorithm works on the first few iterations. Denote by dt a constant grid step in variables t, t_0 and let $C_{j,i}$, $S_{j,i}$ be the solution at the node $(t,t_0)=(jdt,idt)$, $0\le j\le N$, $0\le i\le j$. We calculate solutions at the grid nodes by time layers starting from $t=0$.

The layer $t=0$ contains one grid node (0,0), in which the solution values are known from condition (3): $C_{0,0}=1$, $S_{0,0}=0$.

The layer $t=dt$ contains two mesh nodes: $(dt,0)$ and (dt,dt). For $t_0=0$ the point $(x,t)\in\Gamma$ and according to (10) $S_{1,0}=0$. The value of $C_{1,0}$ is obtained from formula (14):

$$C_{1,0}=\frac{\left(2-F(0)dt\right)\cdot 1+2\varphi(0)dt}{2+F(0)dt}.$$

At the point (dt,dt), the coordinate $x=0$ and according to (3) $C_{1,1}=1$. The value $S_{1,1}=S(0,dt)$ is determined by the formula (16):

$$S_{1,1}=S_{0,0}+\left(F(S_{0,0})\cdot 1-\varphi(S_{0,0})\right)dt.$$

The layer $t=2dt$ includes three mesh nodes: $(2dt,0)$, $(2dt,dt)$, $(2dt,2dt)$. For $t_0=0$ the point $(x,t)\in\Gamma$ and $S_{2,0}=0$. The value $C_{2,0}$ is determined by formula (14). At the node $(2dt,2dt)$, the coordinate $x=0$ and $C_{2,2}=1$. The value $S_{2,2}=S(0,2dt)$ is calculated by formula (16):

$$S_{2,2}=S_{1,1}+\left(F(S_{1,1})\cdot 1-\varphi(S_{1,1})\right)dt.$$

Let's define the value $S_{2,1}$ in the node $(2dt,dt)$. First, we find $S\left(x(dt,0),2dt\right)$ by formula (16):

$$S\left(x(dt,0),2dt\right)=S_{1,0}+\left(F(S_{1,0})C_{1,0}-\varphi(S_{1,0})\right)dt.$$

Note that the point (t,t_0) corresponding to the Cartesian coordinates $x=x(dt,0)$, $t=2dt$ lies on the layer $t=2dt$, but generally speaking, does not coincide with the grid nodes. It follows from formula (11) that the point (t,t_0) cannot coincide with the node $(2dt,0)$.

On a layer $t=2dt$ he value $S_{2,1}$ is obtained by linear interpolation in x using two known values $S\left(x(dt,0),2dt\right)$ and $S_{2,0}$:

$$S_{2,1}=\frac{S\left(x(dt,0),2dt\right)\left(x(2dt,dt)-x(2dt,0)\right)+S_{2,0}\left(x(dt,0)-x(2dt,dt)\right)}{x(dt,0)-x(2dt,0)}.$$

The value $C_{2,1}$ is determined by formula (14).

Consider the algorithm in the general case. Let the solution in all $j+1$ nodes of the layer $t=jdt$ is known. Let us find the solution at the nodes of the next layer $t+dt=(j+1)dt$. The node $(j+1,0)$ lies on the front Γ and $S_{j+1,0}=0$, $C_{j+1,0}$ is calculated by the formula (14). The node $(j+1,j+1)$ lies on the axis OT, $C_{j+1,j+1}=1$, $S_{j+1,j+1}$ is obtained from the formula (14). Let the solutions at the nodes $(j+1,0)$, ..., $(j+1,i-1)$ be computed. To obtain the solution at the internal node $(j+1,i)$, $1\le i\le j$, calculate $S\left(x(t,t_0),t+dt\right)$, $t_0=idt$ by formula (16) and linearly interpolate $S_{j+1,i}$ over two values $S\left(x(t,t_0),t+dt\right)$ and $S_{j+1,i-1}$. The value $C_{j+1,i}$ is determined by formula (14).

Since the computational formulae of the algorithm use one time layer, an array of solutions of only one time layer is stored in the computer's RAM.

Note that when passing to Cartesian coordinates x,t, the grid becomes non-uniform, the time step dt is constant, but in the layer $t_j=jdt$ the nodes are distributed non-uniformly due to variable speed $v(t)$:

$$x_i=x(jdt,idt)=\int_{idt}^{jdt}v(\varsigma)d\varsigma.$$

4. RESULTS OF NUMERICAL SIMULATION

The calculation of the filtration problem with sediment rise is performed for system (1), (2) with the functions

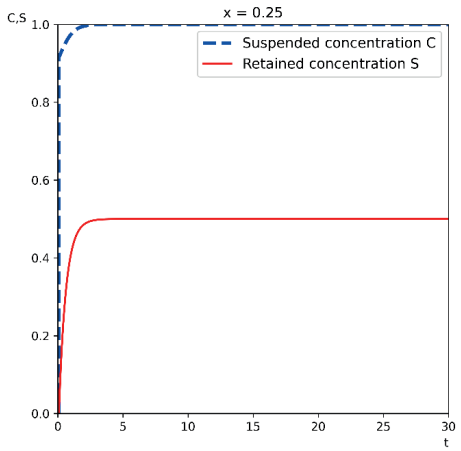
$$v(t)=1.5\left(1+e^{-2t}\right),\ F(S)=1-S,\ \varphi(S)=S.$$

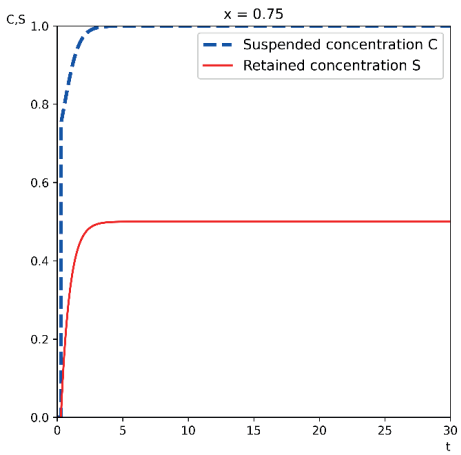
In variables t, t_0 the grid step $dt=0.01$.

Since the step in x is not constant in Cartesian coordinates x,t, the grid nodes, generally speaking, do not lie at the intersection of the time layers of the grid with the lines $x=const$. To plot two-dimensional graphs of solutions at constant x, it is required to interpolate solutions using values at close nodes. The Python software automatically performs interpolation and presents graphs using built-in algorithms of open-source library SciPy [29, 30].

Fig. 1 and 2 show solutions at constant time t and constant coordinate x.

According to Fig. 1 and 2 the deposit concentration is rapidly approaching the limit value $S^*=0.5$.





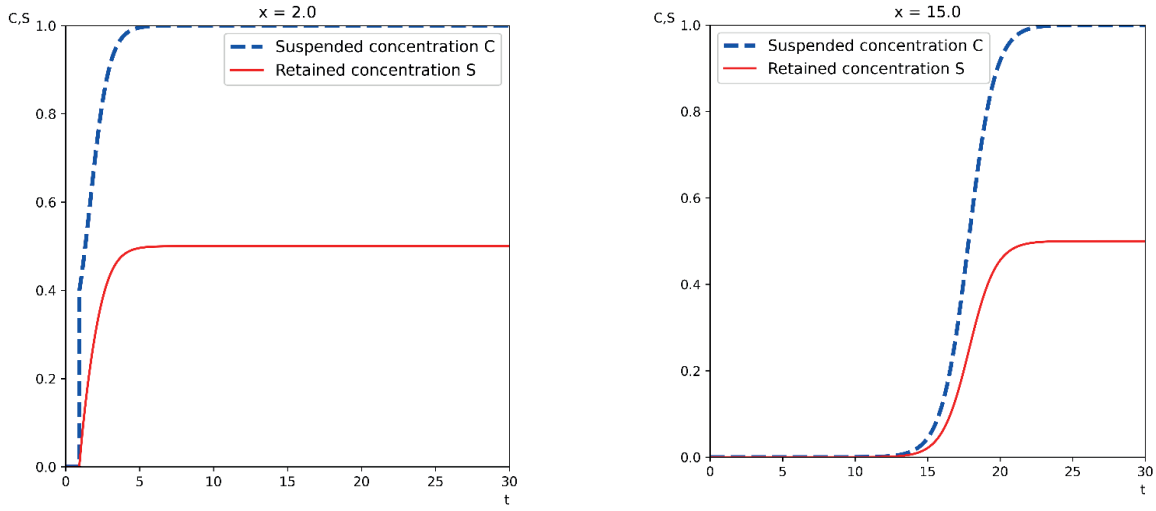


Figure 1. Solutions C and S at constant x.

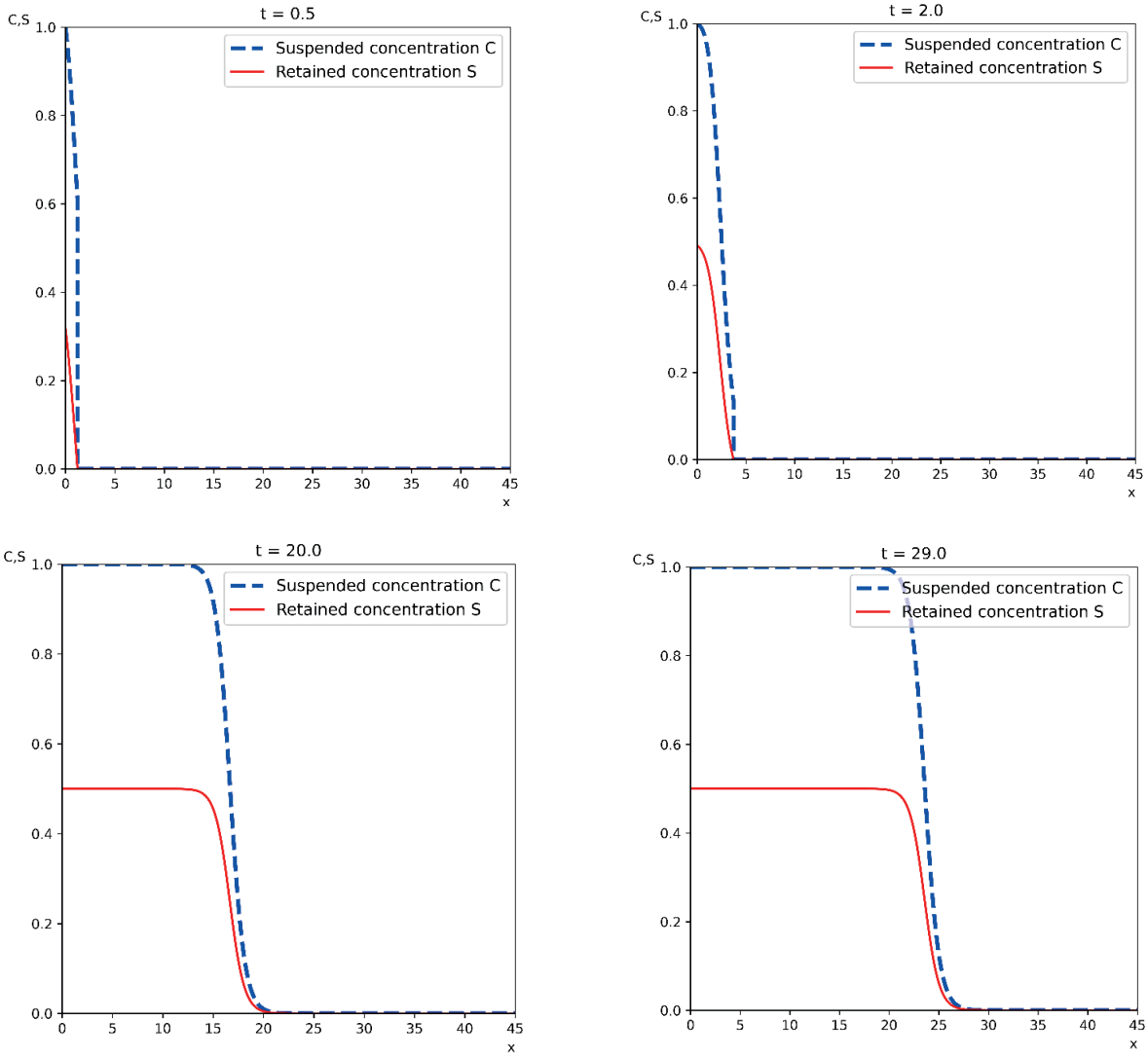


Figure 2. Solutions C and S at constant t

5. DISCUSSION

The change of variables in the system of filtration equations makes it possible to straighten the curvilinear concentration front and construct a discrete grid with a constant step in both new variables. This method is used to derive the lattice Boltzmann equations for solving hydrodynamic problems [31].

There are various options for choosing variables, in which the solution area is limited by straight lines. For example, characteristic variables τ, t_0 can be used. We have chosen variables t, t_0 to simplify both equations of system (1), (2).

In the filtration problem without deposit lifting (in equation (2) $\varphi(S) = 0$), the suspension velocity is reduced to zero. This significantly complicates the computational procedure. However, the proposed method is easily transferred to this case. This problem will be considered separately.

6. CONCLUSIONS

To calculate the filtration problem with a variable suspension speed

- the finite difference method is applied,
- the method of characteristics is used,
- the solution is obtained on a grid with a constant step,
- to find the solution, auxiliary points are used that do not coincide with the grid nodes.

REFERENCES

1. **Zhou Z., Zang H., Wang S., Du X., Ma D., Zhang J.** Filtration Behavior of Cement-Based Grout in Porous Media // Transport in Porous Media, 2018, vol. 125, pp. 435–463.
2. **Tsuji M., Kobayashi S., Mikake S., Sato T., Matsui H.** Post-Grouting Experiences for Reducing Groundwater Inflow at 500 m Depth of the Mizunami Underground Research Laboratory, Japan // Procedia Engineering, 2017, vol. 191, pp. 543–550.
3. **Zhu G., Zhang Q., Liu R., Bai J., Li W., Feng X.** Experimental and Numerical Study on the Permeation Grouting Diffusion Mechanism considering Filtration Effects // Geofluids, 2021, 6613990.
4. **Wang X., Cheng H., Yao Z., Rong C., Huang X., Liu X.** Theoretical Research on Sand Penetration Grouting Based on Cylindrical Diffusion Model of Tortuous Tubes // Water, 2022, vol. 14, 1028, pp. 1–15.
5. **Salnyi I., Stepanov M., Karaulov A.** Experience in strengthening foundations and foundations on technogenic soils // E3S Web of Conferences, 2022, vol. 363(5), 02004.
6. **Christodoulou D., Lokkas P., Droudakis A., Spiliotis X., Kasiteropoulou D., Alamanis N.** The development of practice in permeation grouting by using fine-grained cement suspensions // Asian Journal of Engineering and Technology, 2021, vol. 9(6), pp. 92–101.
7. **Ramachandran V., Fogler H.S.** Plugging by hydrodynamic bridging during flow of stable colloidal particles within cylindrical pores // Journal of Fluid Mechanics, 1999, vol. 385, pp. 129–156.
8. **Rabinovich A., Bedrikovetsky P., Tartakovsky D.** Analytical model for gravity segregation of horizontal multiphase flow in porous media // Physics of Fluids, 2020, vol. 32(4), pp. 1–15.
9. **Tartakovsky D.M., Dentz M.** Diffusion in Porous Media: Phenomena and Mechanisms // Transport in Porous Media, 2019, vol. 130, pp. 105–127.
10. **Santos A., Bedrikovetsky P.** Size exclusion during particle suspension transport in porous media: stochastic and averaged equations // Computational and Applied Mathematics, 2004, vol. 23(2-3), pp. 259–284.

11. **Kuzmina L.I., Osipov Yu.V., Zheglova Yu. G.** Analytical model for deep bed filtration with multiple mechanisms of particle capture // International Journal of Non-Linear Mechanics, 2018, vol. 105, pp. 242–248.
12. **Osipov Yu., Safina G., Galaguz Yu.** Calculation of the filtration problem by finite differences methods // MATEC Web Conference, 2018, vol. 251(3), 04021.
13. **Safina G.L.** Filtration problem with nonlinear filtration and concentration functions // International Journal for Computational Civil and Structural Engineering, 2022, vol. 18(1), pp. 129–140.
14. **Galaguz Y.P.** Realization of the TVD-scheme for a numerical solution of the filtration problem // International Journal for Computational Civil and Structural Engineering, 2017, vol. 13(2), pp. 93–102.
15. **Safina G.L.** Numerical solution of filtration in porous rock // E3S Web of Conferences, 2019, vol. 97, 05016.
16. **Khuzhayorov B.K., Ibragimov G., Saydullaev U., Pansera B.A.** An Axi - Symmetric Problem of Suspensions Filtering with the Formation of a Cake Layer // Symmetry, 2023, vol. 15(6), 1209.
17. **Vyazmina E.A., Bedrikovetskii P.G., Polyanin A.D.** New classes of exact solutions to nonlinear sets of equations in the theory of filtration and convective mass transfer // Theoretical Foundations of Chemical Engineering, 2007, vol. 41(5), pp. 556–564.
18. **Kuzmina L.I., Osipov Yu.V., Vetoshkin N.V.** Calculation of long-term filtration in a porous medium // International Journal for Computational Civil and Structural Engineering, 2018, vol. 14(1), pp. 92–101.
19. **Galaguz Y.P., Safina G.L** Modeling of fine migration in a porous medium // MATEC Web of Conferences, 2016, vol. 86, 03003.
20. **Safina G.L.** Calculation of retention profiles in porous medium // Lecture Notes in Civil Engineering, 2021, vol. 170, pp. 21–28.
21. **Kuzmina L.I., Osipov Y.V.** Exact solution to non-linear filtration in heterogeneous porous media // International Journal of Non-Linear Mechanics, 2023, vol. 150, 104363.
22. **Galaguz Yu.P., Kuzmina L.I., Osipov Yu.V.** Problem of Deep Bed Filtration in a Porous Medium with the Initial Deposit // Fluid Dynamics, 2019, vol. 54(1), pp. 85–97.
23. **Sun N.Z.** Mathematical Modeling of Groundwater Pollution, Springer New York, NY, 2014.
24. **Chaudhry M.H.** Applied Hydraulic Transients, Springer New York, NY, 2013.
25. **Koo B.** Comparison of finite-volume method and method of characteristics for simulating transient flow in natural-gas pipeline // Journal of Natural Gas Science and Engineering, 2022, vol. 98, 104374.
26. **Kuzmina L., Osipov Y.** Filtration in porous medium with particle release // Advances in Transdisciplinary Engineering, 2022, vol. 31, pp. 40–48.
27. **Kuzmina L., Osipov Y.** Particles transport with deposit release in porous media // Lecture Notes in Civil Engineering, 2022, vol. 170, pp. 539–547.
28. **Courant R., Hilbert D.** Partial Differential Equations, Reprint of the 1962 Original, Edited, Wiley-InterScience, New York, 1989.
29. **Alfeld P.** A trivariate Clough-Tocher scheme for tetrahedral data // Computer Aided Geometric Design, 1984, vol. 1(2), pp. 169–181.
30. **Farin G.** Triangular Bernstein-Bezier patches // Computer Aided Geometric Design, 1986, vol. 3(2), pp. 83–127.
31. **Kruger T., Kusumaatmaja H., Kuzmin A., Shardt O., Silva G., Viggen E.M.** The Lattice Boltzmann Method, Springer International Publishing, Switzerland, 2017.

СПИСОК ЛИТЕРАТУРЫ

1. **Zhou Z., Zang H., Wang S., Du X., Ma D., Zhang J.** Filtration Behavior of Cement-Based Grout in Porous Media // Transport in Porous Media, 2018, vol. 125, pp. 435–463
2. **Tsuji M., Kobayashi S., Mikake S., Sato T., Matsui H.** Post-Grouting Experiences for Reducing Groundwater Inflow at 500 m Depth of the Mizunami Underground Research Laboratory, Japan // Procedia Engineering, 2017, vol. 191, pp. 543–550.
3. **Zhu G., Zhang Q., Liu R., Bai J., Li W., Feng X.** Experimental and Numerical Study on the Permeation Grouting Diffusion Mechanism considering Filtration Effects // Geofluids, 2021, 6613990.
4. **Wang X., Cheng H., Yao Z., Rong C., Huang X., Liu X.** Theoretical Research on Sand Penetration Grouting Based on Cylindrical Diffusion Model of Tortuous Tubes // Water, 2022, vol. 14, 1028, pp. 1–15.
5. **Salnyi I., Stepanov M., Karaulov A.** Experience in strengthening foundations and foundations on technogenic soils // E3S Web of Conferences, 2022, vol. 363(5), 02004.
6. **Christodoulou D., Lokkas P., Droudakis A., Spiliotis X., Kasiteropoulou D., Alamanis N.** The development of practice in permeation grouting by using fine-grained cement suspensions // Asian Journal of Engineering and Technology, 2021, vol. 9(6), pp. 92–101.
7. **Ramachandran V., Fogler H.S.** Plugging by hydrodynamic bridging during flow of stable colloidal particles within cylindrical pores // Journal of Fluid Mechanics, 1999, vol. 385, pp. 129–156.
8. **Rabinovich A., Bedrikovetsky P., Tartakovsky D.** Analytical model for gravity segregation of horizontal multiphase flow in porous media // Physics of Fluids, 2020, vol. 32(4), pp. 1–15.
9. **Tartakovsky D.M., Dentz M.** Diffusion in Porous Media: Phenomena and Mechanisms // Transport in Porous Media, 2019, vol. 130, pp. 105–127.
10. **Santos A., Bedrikovetsky P.** Size exclusion during particle suspension transport in porous media: stochastic and averaged equations // Computational and Applied Mathematics, 2004, vol. 23(2-3), pp. 259–284.
11. **Kuzmina L.I., Osipov Yu.V., Zheglova Yu. G.** Analytical model for deep bed filtration with multiple mechanisms of particle capture // International Journal of Non-Linear Mechanics, 2018, vol. 105, pp. 242–248.
12. **Osipov Yu., Safina G., Galaguz Yu.** Calculation of the filtration problem by finite differences methods // MATEC Web Conference, 2018, vol. 251(3), 04021.
13. **Safina G.L.** Filtration problem with nonlinear filtration and concentration functions // International Journal for Computational Civil and Structural Engineering, 2022, vol. 18(1), pp. 129–140.
14. **Galaguz Y.P.** Realization of the TVD-scheme for a numerical solution of the filtration problem // International Journal for Computational Civil and Structural Engineering, 2017, vol. 13(2), pp. 93–102.
15. **Safina G.L.** Numerical solution of filtration in porous rock // E3S Web of Conferences, 2019, vol. 97, 05016.
16. **Khuzhayorov B.K., Ibragimov G., Saydullaev U., Pansera B.A.** An Axi - Symmetric Problem of Suspensions Filtering with the Formation of a Cake Layer // Symmetry, 2023, vol. 15(6), 1209.
17. **Vyazmina E.A., Bedrikovetskii P.G., Polyanin A.D.** New classes of exact solutions to nonlinear sets of equations in the theory of filtration and convective mass transfer // Theoretical Foundations of Chemical Engineering, 2007, vol. 41(5), pp. 556–564.
18. **Kuzmina L.I., Osipov Yu.V., Vetoshkin N.V.** Calculation of long-term filtration in a porous medium // International Journal for

Computational Civil and Structural Engineering, 2018, vol. 14(1), pp. 92–101.
19. **Galaguz Y.P., Safina G.L.** Modeling of fine migration in a porous medium // MATEC Web of Conferences, 2016, vol. 86, 03003.
20. **Safina G.L.** Calculation of retention profiles in porous medium // Lecture Notes in Civil Engineering, 2021, vol. 170, pp. 21–28.
21. **Kuzmina L.I., Osipov Y.V.** Exact solution to non-linear filtration in heterogeneous porous media // International Journal of Non-Linear Mechanics, 2023, vol. 150, 104363.
22. **Galaguz Yu.P., Kuzmina L.I., Osipov Yu.V.** Problem of Deep Bed Filtration in a Porous Medium with the Initial Deposit // Fluid Dynamics, 2019, vol. 54(1), pp. 85–97.
23. **Sun N.Z.** Mathematical Modeling of Groundwater Pollution, Springer New York, NY, 2014.
24. **Chaudhry M.H.** Applied Hydraulic Transients, Springer New York, NY, 2013.
25. **Koo B.** Comparison of finite-volume method and method of characteristics for simulating transient flow in natural-gas pipeline // Journal of Natural Gas Science and Engineering, 2022, vol. 98, 104374.
26. **Kuzmina L., Osipov Y.** Filtration in porous medium with particle release // Advances in Transdisciplinary Engineering, 2022, vol. 31, pp. 40–48.
27. **Kuzmina L., Osipov Y.** Particles transport with deposit release in porous media // Lecture Notes in Civil Engineering, 2022, vol. 170, pp. 539–547.
28. **Courant R., Hilbert D.** Partial Differential Equations, Reprint of the 1962 Original, Edited, Wiley-InterScience, New York, 1989.
29. **Alfeld P.** A trivariate Clough-Tocher scheme for tetrahedral data // Computer Aided Geometric Design, 1984, vol. 1(2), pp. 169–181.
30. **Farin G.** Triangular Bernstein-Bezier patches // Computer Aided Geometric Design, 1986, vol. 3(2), pp. 83–127.
31. **Kruger T., Kusumaatmaja H., Kuzmin A., Shardt O., Silva G., Viggen E.M.** The Lattice Boltzmann Method, Springer International Publishing, Switzerland, 2017.

Liudmila I. Kuzmina, Candidate of Physical and Mathematical Sciences, Associate Professor, Department of Applied Mathematics, National Research University Higher School of Economics, 101000, Russia, Moscow, Myasnitskaya st., 20, tel. +7(495) 77295 90 * 15219, e-mail: lkuzmina@hse.ru.

Yuri V. Osipov, Candidate of Physical and Mathematical Sciences, Professor, Department of Computer Science and Applied Mathematics, Moscow State University of Civil Engineering, 129337, Russia, Moscow, Yaroslavskoe Shosse, 26, tel. +7(499)1835994, e-mail: yuri-osipov@mail.ru.

Artem R. Pesterev, 3rd year bachelor's degree student of the direction of training 01.03.04 of the Institute IDTMC of the National Research Moscow State University of Civil Engineering; 129337, Russia, Moscow, Yaroslavskoe shosse, 26; tel. +7(499)1834674; e-mail: vip.pesterev_a@mail.ru.

Кузьмина Людмила Ивановна, доцент, кандидат физико-математических наук, Департамент прикладной математики, Национальный исследовательский университет «Высшая школа экономики»; 101000, г. Москва, ул. Мясницкая, д. 20, тел. +7(495) 77295 90 *15219; e-mail: lkuzmina@hse.ru.

Осипов Юрий Викторович профессор, кандидат физико-математических наук, кафедра информатики и прикладной математики Национального исследовательского Московского государственного строительного университета; 129337, Россия, г. Москва, Ярославское шоссе, д. 26; тел. +7(499)1835994; e-mail: yuri-osipov@mail.ru.

Пестерев Артем Романович, студент 3 курса бакалавриата направления подготовки 01.03.04 института ИЦТМС Национального исследовательского Московского государственного строительного университета; 129337, Россия, г. Москва, Ярославское шоссе, д. 26; тел. +7(499)1834674; e-mail: vip.pesterev_a@mail.ru.

International Journal for Computational Civil and Structural Engineering, 19(3) 49–57 (2023)

DOI:10.22337/2587-9618-2023-19-3-49-57

EXPERIMENTAL STUDIES OF THE STABILITY OF THIN-WALLED CYLINDRICAL SHELLS OF MEDIUM LENGTH FILLED WITH BULK MATERIAL UNDER TORSION

Mikhail V. Petrov [1], Alexander I. Kibets [2], Boris V. Mikhailov [1], Ekaterina G. Gonik [1], Viktor A. Ivanov [1]

[1] I.N. Ulyanov Chuvash State University, Cheboksary, RUSSIA
[2] Research Institute of Mechanics, N.I. Lobachevsky State University of Nizhny Novgorod, Nizhny Novgorod, RUSSIA

Abstract. Experimental studies were carried out to study the effect of bulk filler on the stability of shells during torsion. In the domestic and foreign literature, we have not found publications where the stability of thin-walled shells filled with bulk material under torsion would be considered. To carry out experiments, a special installation has been developed and manufactured that allows testing samples for torsion, bending and complex loading, loading the samples accordingly. Before the tests, samples were taken for the absence of defects in the form of dents, ovality, diversity, constancy of cross-sectional dimensions. It is known that defects in samples significantly affect stability. The samples were tested with a length of 140 mm, 90 mm, 25 mm. The samples were made by deep drawing from a high-plastic aluminum alloy 3004 in the H19 state. In this case, one end of the samples was rigidly fixed to the installation, a torque was applied to the other end, which increased until the samples lost stability. At the beginning and at the end of the test, the samples were loaded in small portions to catch the beginning of movement and the beginning of loss of stability. The installation made it possible to create various boundary conditions of the samples. In experiments, the torque and the twist angle were measured. Linear dependences of the twisting angle on the torque are constructed. So, stability was lost in elasticity. For samples filled with bulk filler, at the beginning of the twisting process, there was a nonlinear relationship between the torque and the twisting angle. This is due to the occurrence of friction forces between the filler and the inner wall of the samples, which created a counteracting torque. Then the graphs for the empty and filled samples were enlarged parallel to each other.
For empty samples [1], critical stresses, critical twisting angles, the number of waves formed, and their direction were calculated. The convergence of the calculated and experimental parameters within 36% is obtained. The bulk filler, in the form of iron powder, increased the value of the critical torque to 17%.

Keywords: torsion, stability, experiment, sample, installation, filler, torque, voltage

ЭКСПЕРИМЕНТАЛЬНЫЕ ИССЛЕДОВАНИЯ УСТОЙЧИВОСТИ ТОНКОСТЕННЫХ ЦИЛИНДРИЧЕСКИХ ОБОЛОЧЕК СРЕДНЕЙ ДЛИНЫ, ЗАПОЛНЕННЫХ СЫПУЧИМ МАТЕРИАЛОМ, ПРИ КРУЧЕНИИ

М.В. Петров [1], А.И. Кибец [2], Б.В. Михайлов [1], Е.Г. Гоник [1], В.А. Иванов [1]

[1] Чувашский государственный университет имени И.Н. Ульянова, г. Чебоксары, РОССИЯ
[2] НИИ механики Нижегородского госуниверситета им. Н.И. Лобачевского, г. Нижний Новгород, РОССИЯ

Аннотация. Экспериментальные исследования выполнены с целью изучения влияния сыпучего заполнителя на устойчивость оболочек при кручении. В отечественной и зарубежной литературе не обнаружены нами публикации, где рассматривалось бы устойчивость тонкостенных оболочек, заполненных сыпучим материалом, при кручении. Для выполнения экспериментов разработана и изготовлена специальная установка, позволяющая испытывать образцы на кручение, на изгиб и на сложное нагружение, нагружая образцы соответствующим образом. До испытаний производился отбор образцов на отсутствие дефектов в виде вмятин, овальности, разностенности, постоянства размеров поперечного сечения. Известно, что дефекты образцов существенно влияют на устойчивость. Образцы

испытывались длиной 140 мм, 90 мм, 25 мм. Образцы изготавливались глубокой вытяжкой из высокопластичного алюминиевого сплава 3004 в состоянии H19. В данном случае один конец образцов жестко закреплялся к установке, к другому концу прикладывался крутящий момент, который возрастал до потери устойчивости образцов. В начале и в конце испытания нагружали образцы малыми порциями, чтобы уловить начало движения и начало потери устойчивости. Установка позволяла создавать различные граничные условия образцов. В экспериментах измеряли крутящий момент и угол закручивания. Построены линейные зависимости угла закручивания от крутящего момента. Значит устойчивость терялась в упругости. Для образцов, заполненных сыпучим заполнителем, в начале процесса закручивания имело место нелинейная зависимость между крутящим моментом и углом закручивания. Это связано с возникновением сил трения между заполнителем и внутренней стенкой образцов, которые создавали противодействующий крутящий момент. Затем графики для пустых и заполненных образцов увеличивались параллельно друг другу.
Для пустых образцов [1] рассчитывались критические напряжения, критические углы закручивания, число образовавшихся волн, их направление. Получена сходимость расчетных и экспериментальных параметров в пределах 36%. Сыпучий заполнитель, в виде железного порошка увеличивал значение критического крутящего момента до 17%.

Ключевые слова: кручение, устойчивость, эксперимент, образец, установка, заполнитель, крутящий момент, напряжение

INTRODUCTION

Problems of stability of cylindrical shells were considered in numerous works [1-18,22-31, etc.]. In the works of L.H. Donnel, H.M. Mushtari, V.M. Dorevsky and others obtained simple formulas for calculating critical stresses and the number of waves. Studies of the buckling of shells filled with liquid, gas, and other loads were carried out in [12,24,26]. In [9,18,20-23], the stability of shells in bending filled with bulk material was studied. In these studies, the influence of various bulk materials, the geometric dimensions of the shells, the percentage of volume filling on stability was established. The critical bending moment, for shells filled with bulk material, increased by 10-20%. The stability of thin-walled cylindrical shells filled with bulk material during torsion has been little studied [19] and this problem is very relevant. For example, tank semi-trailers are used to transport bulk cargo (flour, grain, sand, etc.). It is much cheaper to transport such goods on tank semi-trailers, they can be transported along rural roads to remote areas. The tank is a thin-walled cylindrical shell, which is attached to the trailer of the car and when the car is moving, it can bend, twist, which leads to loss of stability. **The purpose of this work** is an experimental study of the torsion loss of thin-walled shells filled with bulk material.

EXPERIMENTAL SETUP, SAMPLES, TESTING

A special setup (Figure 1) was made and assembled for the experiments. Sample 1 was rigidly fixed at one end to frame 2. The other end was placed in wall 3, where it could turn, and to stiffen this end, a metal disk was inserted inside, to which rod 4 was attached to create a torque.
Rod 5 was rigidly attached perpendicular to the axis of sample 1, to the end of which a leg of the dial gauge ICH-10 6 was attached to measure displacements and calculate the angle of rotation.
Dynamometers 7 were used to measure the forces. Forces were created by weights 8, which were placed on hangers 9. Hangers 9 were connected by cables 10 by dynamometers 7 and rod 4 at the same distance from the longitudinal axis of the sample. This created torque.
The specimens were made from 3004 aluminum alloy in H19 temper from deep drawn sheets in a die. The samples were of high quality, but before testing they were selected, checked for

the absence of defects in the form of dents, ovality, variation in wall thickness, and constancy of cross-sectional dimensions. The dimensions of the samples are presented in Table 1. The dimensions of the samples are assumed to be similar to tanks manufactured at the enterprises. A photograph of the samples is shown in Figure 2.

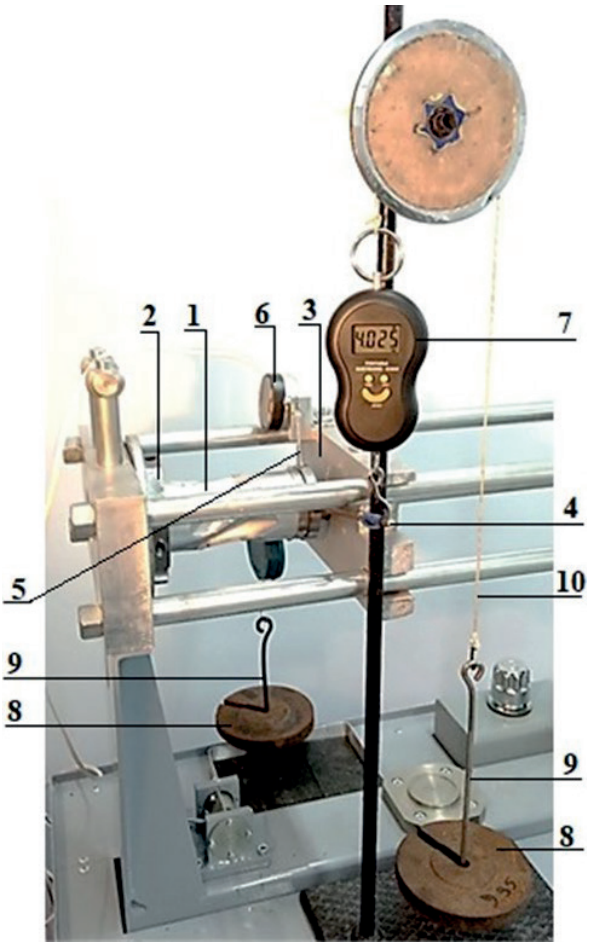


Figure. 1. Test facility.

The samples were tested empty and filled to 90% of the volume with PZh-5 iron powder. Weights 8 were loaded simultaneously from both sides, at the beginning of twisting and when approaching the critical state, they were loaded in small portions.

In the experiments, at each load, the readings of the dynamometers and the indicator of the clock type ICh-10 were recorded.

Table 1. Sample sizes

N series	Radius R, mm	Wall thickness h, mm	Length L, mm	L/R
1	31,5	0,1	140	4,45
2	31,5	0,1	90	2,86
3	31,5	0,1	25	0,79

One end of the sample was pinched, and the other end, when a torque was applied, could only rotate freely, excluding other movements, which is the advantage of the installation. If the wall 3 is removed, bending and bending with torsion tests can be performed



Figure 2. Sample photography: 1-sample before testing, 2-sample 140mm long after testing without loading, 3-sample 90mm long tested with filler, 4-sample 25mm long tested without loading

TESTING

Tests began with a thorough inspection and sampling. The absence of ovality, thickness variation, the presence of dents, scratches, and variation in geometric dimensions was checked. Samples with a dent were immediately rejected. The wall thickness of the samples was 0.1 mm and samples with a wall thickness of 0.11 mm were not allowed for testing. Ovality was not observed. Then the correct fixing of the sample on the installation began. One end of the sample was mounted on the mandrel of frame 2 and crimped from the outside with a clamp to obtain

a rigid fastening. To avoid distortion of the sample during the test, the second end was inserted into the bearing hole installed in wall 3, where it could rotate freely. Then, metal rods 4 were installed on both sides of the sample. The coaxiality of the centers of the circles of the ends of the sample was corrected with a laser beam. Hangers 9 were hung on cables 10 to the ends of the rods 4.

At the beginning and at the end of the tests, weights were loaded with a small mass in order to catch the beginning of twisting and the moment of loss of stability. During the test, the coaxiality of the centers of the circles of the ends of the sample was constantly checked by a laser beam so that the conditions of the torsion test were not violated (there was no bending). In the experiments, the magnitude of the load and the corresponding movement of the indicator leg were recorded.

TEST RESULTS

Each series of samples was tested at least five pieces. Average statistical test results are shown in Table 2.

Table 2. Results of test.

sample series	empty		filled		Mcr·10^{-8}, MN m [1]	n	%
	$M_{cr}\cdot10^{-8}$, MN m	$\varphi_{cr}\cdot10^{-4}$, radian	$M_{cr}\cdot10^{-8}$, MN m	$\varphi_{cr}\cdot10^{-4}$, radian			
1	1094	22,2	1154	37,4	1218	6	11,3
2	1103	29,5	1290	40	1540	8	28,4
3	1745	39,6	1986	46	2294	14	31,5

In table. 2 denotes: M_{cr}-critical torque, φ_{cr}-angle of twist under the action of M_{cr}, n-number of waves after buckling of the sample, %-percentage of divergence of critical torques obtained in experiments and calculated from the literature [1] for empty samples. The percentage of discrepancy increases with decreasing sample length. This is due to the fact that the calculation formulas were obtained for shells of medium length.

As an example, the test results for specimens 90 mm long are shown in Figure.3.

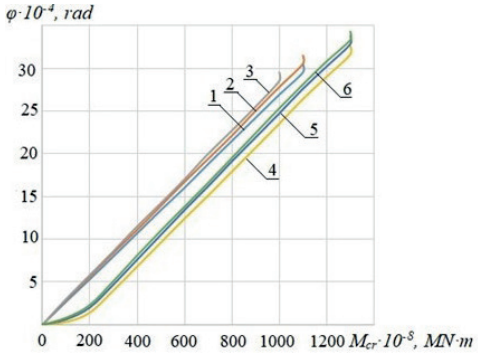


Figure 3. Test results of samples with a length of 90 mm. Graphs 1,2,3 for empty 4,5,6 for filled samples

The angle of twist was calculated as the ratio of the movement of the indicator leg to the distance from the sample axis to the indicator leg.

The graphs are linear, the loss of stability occurred in elasticity. The graphs for empty and filled with iron powder samples are parallel, except for the initial twisting process, where the influence of the friction force between the powder and the inner wall of the sample occurs. The experimental value of the critical shear stress is:

$$\tau_{cr}^{o} = \frac{M_{cr}}{2\pi R^2 h} = \frac{1103\cdot10^{-8}}{2\cdot3{,}14\cdot31{,}5^2\cdot10^{-6}\cdot0{,}1\cdot10^{-3}} = 17{,}7\ МПа. \quad (1)$$

Estimated upper critical shear stress [1]:

$$\tau_{cr} = 0{,}78E\frac{h}{R}\sqrt[4]{\frac{Rh}{L^2}} = 0{,}78\cdot0{,}7\cdot\cdot10^5\frac{0{,}1}{31{,}5}\sqrt[4]{\frac{31{,}5\cdot0{,}1}{90^2}} = 24{,}27\ MPa, \quad (2)$$

where E=0.7 10^5 MPa modulus of elasticity.
The divergence of critical shear stresses is 26.6%.
For samples filled to 90% of the volume with iron powder, the critical torque increased compared to the critical torque for empty samples of the first series by 5.5%, the second series by 17%, and the third series by 14%. The value of M_{cr} increased with decreasing sample length.
The number of generated waves according to [1] for samples of the first series:

$$n = 4{,}2 \cdot \sqrt[8]{1\text{-}\mu^2} \cdot \sqrt{\frac{R}{L}} \cdot \sqrt[4]{\frac{R}{h}} = 4{,}2 \cdot \sqrt[8]{1\text{-}0{,}3^2} \cdot \cdot \sqrt{\frac{31{,}5}{140}} \cdot \sqrt[4]{\frac{31{,}5}{0{,}1}} = 8. \quad (3)$$

In experiments n=6.
Second series: n=10, and in experiments n=6.
Third series: n=22, and in experiments n=14.
In experiments, the number of waves is less than in calculations by 25%, 20%, 36%, respectively. For the filled samples, waves first formed in the upper part, where there was no iron powder. Waves then formed on the rest of the wall.
The angle of inclination of the dents to the axis of the specimens of the first series [1]:

$$\gamma = 1{,}73 \cdot \sqrt[4]{\frac{Rh}{L^2}} = 1{,}73 \cdot \sqrt[4]{\frac{31{,}5 \cdot 0{,}1}{140^2}} = 12{,}6. \quad (4)$$

The second and third series γ=14º and γ=26º respectively. In experiments γ=12º…24º.
The difference between the results is due to the fact that the calculated dependences in [1] were obtained for shells without defects, and the tested samples were not ideal.

CONCLUSION

1. Loose aggregate increases the critical torque value.
2. The stability of the samples is lost in elasticity.
3. When designing and manufacturing tank trucks for the transport of bulk materials, it is necessary to take into account the effect of aggregate on stability.
4. The formulas used in the calculations from [1], which were obtained for shells of medium length, give calculated results for short samples of the third series, which differ significantly from the test results.

REFERENCES

1. **Volmir A.S.** (1967) Ustoichivost deformiruemykh system. Stability of deformable systems. Moscow. Fizmatgiz. 984p.
2. **Grigoliuk E.I.** (1978) Ustoichivost obolochek. Shell Resistance. Moscow. Nauka. 360 p.
3. **Pikul V.V**. (2000) Current State of Shell Theory and Prospects for its Development. The current state of the theory of shells and the prospects for its development. Mekhanika tverdogo tela. no. 2: pp. 153-168.
4. **Konoplev Yu.G**. (1966) Experimental study of the problem of the action of a concentrated force on a cylindrical shell. Experimental study of the problem of the action of a concentrated force on a cylindrical shell. Kazan, KGU. no. 4: pp. 83-90.
5. **Ilgamov M.A**. (1964) Experimental study of the stability of a cantilevered cylindrical shell under the action of a transverse force and internal pressure. Research on the theory of plates and shells. Kazan, KGU, no. 2, pp. 186-191.
6. **Sachenkov A.V**. (1970) Theoretical and experimental method for studying the stability of plates and shells. Research on the theory of plates and shells. – Kazan: Publishing House of Kazan State University. – Issue 617. – pp. 391-433.
7. **Mathon C., Limam A**. (2006) Experimental collapse of thin cylindrical shells submitted to internal pressure and

pure bending. ThinWalled Structures, vol. 44, no. 1, pp. 39-50.
8. **Li L.-Y., Kettle R.** (2002) Nonlinear bending response and buckling of ringstiffened cylindrical shells under pure bending. International Journal of Solids and Structures, vol. 39, no. 3, pp. 765-781.
9. **Boyko D.V., Zheleznov L.P., Kabanov V.V**. (2012) Investigation of nonlinear deformation and stability of reinforced oval cylindrical shells under combined loading by bending moment and marginal transverse force. Solid state mechanics. No. 3. pp. 47-53.
10. **Brazier L.** (1927) On the flexure of thin cylindrical shells and other thin sections. Proc. Roy. Soc. Vol. A116. No. 773. P. 104–114.
11. **Mossakovsky V.I., Manevich L.I., Miltsyn A.M**. (1977) Modeling of the bearing capacity of cylindrical shells. Kiev: Nauk. Dumka. 141 p.
12. **Ilgamov M.A., Ivanov V.A., Gulin B.V**. (1987). Calculation of shells with elastic filler. M.: Nauka. 260 p.
13. **Houliara S., Karamanos S.A**. (2010) Stability of long transversely-isotropic elastic cylindrical shells under bending. International Journal of Solids and Structures, vol. 47, no. 1, pp. 10-14.
14. **Axelrad E.L**. (2000) Shell theory and its specialized branches. Int.J. Solids and struct, vol. 37, no. 10, pp. 1425-1451.
15. **Yan W., Ying J., Chen W.Q**. (2007) The behavior of angle-ply laminated cylindrical shells with viscoelastic interfaces in cylindrical bending. Composite Structures, vol. 78, no. 4, pp. 551-559.
16. **Zeinoddini M., Harding J.E., Parke G.A.R**. (2008) Axially preloaded steel tubes subjected to lateral impacts (a numerical simulation). International Journal of Impact Engineering, no. 35, pp. 1267-1279.
17. **Fajuyitan O.K., Sadowski A.J., Wadee M.A., Rotter J.M**. (2018) Nonlinear behavior of short elastic cylindrical shells under global bending. Thin-Walled Structures, vol. 124, pp. 574-587.
18. **M.V. Petrov, T.G. Fedorova, B. V. Mihaylov, E G. Gonik, N.G. Pfanenshtil** (2018) The influence of imperfections of the geometry of thinwalled cylindrical shells filled with bulk material, their flexural buckling. New in architecture, design construction and renovation: Proceedings of the IV International (X All-Russia) Conference (NADCR-2018). The Chuvash State University, Cheboksary, P. 148 - 156.
19. **Petrov M.V., Mikhailov B.V., Gonik E.G., Ivanov V.A.** (2021). Experimental study of the loss of stability of thin-walled cylindrical shells with bulk filler during torsion. Modern issues of continuum mechanics. collection of articles based on the materials of the III International Conference. Cheboksary: ID "Sreda". P.71-78.
20. **Bazhenov V.G., Gonik E.G., Kibets A.I., Petrov M.V., Fedorova T.G., Frolova I.A**. (2017). Experimental and theoretical study of elastoplastic buckling of cylindrical shells filled with bulk material under the action of a transverse force. Scientific notes of Kazan University. Series of Physical and Mathematical Sciences. vol. 159, no. 2, pp. 231–245.
21. **Bazhenov V.G., Kibets A.I., Petrov M.V., Shoshin D.V**. (2008). Numerical analysis of deformation, loss of stability and supercritical behavior of large-sized containers for automobile transportation of bulk cargo. Problems of strength and plasticity, no. 70. pp. 89-97.
22. **Petrov M.V., Fedorova T.G., Gonik E.G., Pfanenstil N.G**. (2018). Method of approximate calculation for stability during transverse bending of thin-walled cylindrical shells of medium length filled with bulk material. Bulletin of the Chuvash State Pedagogical University. Series: Mechanics of the limit state. No. 4(38). pp. 120-128.

23. **Bazhenov V.G., Gonik E.G., Kibets A.I., Kibets Yu. I., Pavlenkova E.V., Petrov M.V., Fedorova T.G**. (2013). Finite-element solution of the problem of stability and supercritical behavior of tank trucks for bulk cargo transportation. Problems of strength and plasticity. V.75. no.1. pp. 056-062.
24. **Ivanov V.A.** (1983). Research on the theory of shells with a placeholder. Kazan.
25. **Zubchaninov V.G**. (2007). Stability and plasticity. In 2 t. t. 1. Stability. M.: Fizmatlit. 448p.
26. **Safiullin F.H.** (1978). To the bending of cylindrical shells with filler under local loads. Collection: Research on the theory of shells. Tr. of the seminar of the KFTI KFAN of the USSR, Kazan, rel. 10. pp. 97-103.
27. **Rotter J. M., Sadowski A. J., Chen L**. (2014). Nonlinear stability of thin elastic cylinders of different length under global bending. International Journal of Solids and Structures, vol. 51, pp.2826-2839.
28. **Xu Z., Gardner L., Sadowski A.J.** (2017). Nonlinear stability of elastic elliptical cylindrical shells under uniform bending. International Journal of Mechanical Sciences, vol. 128-129, pp. 593-606.
29. **Wang J., Sadowski A. J.** (2018). Elastic imperfect tip-loaded cantilever cylinders of varying length. International Journal of Mechanical Sciences, vol. 140, pp. 200-210.
30. **Fajuyitan O.K., Sadowski A.J., Wadee M.A., Rotter J.M.** (2018). Nonlinear behaviour of short elastic cylindrical shells under global bending. Thin-Walled Structures, vol. 124, pp. 574-587.
31. **Boyko D.V., Zheleznov L.P., Kabanov V.V.** (2012). Investigation of nonlinear deformation and stability of non–circular cylindrical shells under transverse bending. M.: Mechanics of a solid body. No. 2. pp. 59-67.

СПИСОК ЛИТЕРАТУРЫ

1. **Вольмир А.С.** Устойчивость деформируемых систем. М.: Физматгиз, 1967. – 984 с.
2. **Григолюк Э.И.** Устойчивость оболочек. М.: Наука, 1978. – 360 с.
3. **Пикуль В.В.** (2000). Современное состояние теории оболочек и перспективы ее развития. МТТ № 2. С. 153–168.
4. **Коноплев Ю.Г.** (1966). Экспериментальное исследование задачи о действии сосредоточенной силы на цилиндрическую оболочку. Исследования по теории пластин и оболочек. Казань: Изд-во Казан. гос. ун-та № 4. С. 83–90.
5. **Ильгамов М.А.** (1964). Экспериментальное исследование устойчивости консольно закрепленной цилиндрической оболочки под действием поперечной силы и внутреннего давления. Исследования по теории пластин и оболочек. Казань: Изд-во Казан. гос. ун-та № 2. С. 186–191.
6. **Саченков А.В.** (1970). Теоретико-экспериментальный метод исследования устойчивости пластин и оболочек. Исследования по теории пластин и оболочек. Казань: Изд-во Казан. гос. ун-та. Вып. 617. С. 391–433.
7. **Mathon C., Limam A**. (2006) Experimental collapse of thin cylindrical shells submitted to internal pressure and pure bending. ThinWalled Structures, vol. 44, no. 1, pp. 39-50.
8. **Li L.-Y., Kettle R.** (2002) Nonlinear bending response and buckling of ringstiffened cylindrical shells under pure bending. International Journal of Solids and Structures, vol. 39, no. 3, pp. 765-781.
9. **Бойко Д.В., Железнов Л.П., Кабанов В.В.** (2012). Исследование нелинейного деформирования и устойчивости подкрепленных овальных цилиндрических оболочек при комбинированном нагружении изгибающим моментом и краевой поперечной силой. Механика твердого тела. № 3. С. 47–53.
10. **Brazier L.** (1927) On the flexure of thin cylindrical shells and other thin sections.

Proc. Roy. Soc. Vol. A116. No. 773. P. 104–114.

11. **Моссаковский В.И., Маневич Л.И., Мильцын А.М.** Моделирование несущей способности цилиндрических оболочек. Киев: Наук. думка, 1977. – 141 с.
12. **Ильгамов М.А., Иванов В.А., Гулин Б.В.** Расчет оболочек с упругим заполнителем. – М.: Наука, 1987. – 260 с.
13. **Houliara S., Karamanos S.A**. (2010) Stability of long transversely-isotropic elastic cylindrical shells under bending. International Journal of Solids and Structures, vol. 47, no. 1, pp. 10-14.
14. **Axelrad E.L**. (2000) Shell theory and its specialized branches. Int.J. Solids and struct, vol. 37, no. 10, pp. 1425-1451.
15. **Yan W., Ying J., Chen W.Q**. (2007) The behavior of angle-ply laminated cylindrical shells with viscoelastic interfaces in cylindrical bending. Composite Structures, vol. 78, no. 4, pp. 551-559.
16. **Zeinoddini M., Harding J.E., Parke G.A.R**. (2008) Axially preloaded steel tubes subjected to lateral impacts (a numerical simulation). International Journal of Impact Engineering, no. 35, pp. 1267-1279.
17. **Fajuyitan O.K., Sadowski A.J., Wadee M.A., Rotter J.M**. (2018) Nonlinear behavior of short elastic cylindrical shells under global bending. Thin-Walled Structures, vol. 124, pp. 574-587.
18. **М.В. Петров и др.** (2018). Влияние несовершенств геометрии тонкостенных цилиндрических оболочек, заполненных сыпучим материалом, на их устойчивость при изгибе. Новое в архитектуре, проектировании строительных конструкций и реконструкции. Материалы IV Международной (X Всероссийской) конференции НАСКР-2018. Изд-во Чуваш. ун-та, г. Чебоксары. С. 148-156.
19. **М.В. Петров и др.** (2021). Экспериментальное исследование потери устойчивости тонкостенных цилиндрических оболочек с сыпучим заполнителем при кручении. Современные вопросы механики сплошных сред. Сборник статей. по материалам III Международной конференции. Чебоксары: ИД «Среда», 2021. С.71-78.
20. **В.Г. Баженов и др.** (2017). Нестационарное осесимметричное движение упругого моментного полупространства под действием нестационарных нормальных поверхностных перемещений. Учен. зап. Казан. ун-та. Сер. Физ.-матем. науки. Т. 159, кн. 2. С. 231–245.
21. **В.Г. Баженов и др.** (2008). Численный анализ деформирования, потери устойчивости и закритического поведения большегабаритных емкостей для автомобильной транспортировки сыпучих грузов. Проблемы прочности и пластичности. № 70. С. 89-97.
22. **Петров М.В., Федорова Т.Г., Гоник Е.Г., Пфаненштиль Н.Г.** (2018). Способ приближенного расчета на устойчивость при поперечном изгибе тонкостенных цилиндрических оболочек средней длины, заполненных сыпучим материалом / Вестник Чувашского государственного педагогического университета им. И.Я. Яковлева. Серия: Механика предельного состояния. № 4(38). С. 120-128.
23. **В.Г. Баженов и др.** (2013). Конечно-элементное решение задачи устойчивости и закритического поведения автоцистерн для транспортировки сыпучих грузов. Проблемы прочности и пластичности. Т. 75. № 1. С. 056-062.
24. **Иванов В.А**. (1983). Исследования по теории оболочек с заполнителем. Диссертация доктора физико-математических наук: 01.02.04. Казань. 306 с.
25. **Зубчанинов В.Г.** Устойчивость и пластичность. В 2 т. Т. 1. Устойчивость. М.: Физматлит, 2007. – 448 с.
26. **Сафиуллин Ф.Х.** (1978). К изгибу цилиндрических оболочек с заполнителем при локальных нагрузках. Сб.: Исследования по теории оболочек.

Тр. семинара КФТИ КФАН СССР, Казань. Вып. 10. С. 97-103.
27. **Rotter J. M., Sadowski A. J., Chen L**. (2014). Nonlinear stability of thin elastic cylinders of different length under global bending. International Journal of Solids and Structures, vol. 51, pp.2826-2839.
28. **Xu Z., Gardner L., Sadowski A.J.** (2017). Nonlinear stability of elastic elliptical cylindrical shells under uniform bending. International Journal of Mechanical Sciences, vol. 128-129, pp. 593-606.
29. **Wang J., Sadowski A. J.** (2018). Elastic imperfect tip-loaded cantilever cylinders of varying length. International Journal of Mechanical Sciences, vol. 140, pp. 200-210.
30. **Fajuyitan O.K., Sadowski A.J., Wadee M.A., Rotter J.M.** (2018). Nonlinear behaviour of short elastic cylindrical shells under global bending. Thin-Walled Structures, vol. 124, pp. 574-587.
31. **Бойко Д.В., Железнов Л.П., Кабанов В.В**. (2012). Исследование нелинейного деформирования и устойчивости некруговых цилиндрических оболочек при поперечном изгибе. М.: Механика твердого тела №2. С. 59–67.

Petrov Mikhail Vasilyevich (Cheboksary, Russian Federation) - Doctor of Technical Sciences, Ass. Professor, Professor of the Department of Building Structures of the I.N. Ulyanov Chuvash State University (428015, 15, Moskovsky prospect, Cheboksary, Russian Federation), e-mail: 21pmv@mail.ru, ORCID: 0000-0002-7355-8553.

Kibets Alexander Ivanovich (Nizhni Novgorod, Russian Federation) - Doctor of Physics and Mathematics, Professor, Chief Researcher (23, Gagarin Avenue, Nizhni Novgorod, Russian Federation, 603600), e-mail: kibec@mech.unn.ru. ORCID: 0000-0001-8490-5541.

Mikhailov Boris Vasilyevich (Cheboksary, Russian Federation) – PhD in Technical Sciences, Ass. Professor, Department of Building Structures of the I.N. Ulyanov Chuvash State University (428015, 15, Moskovsky prospect, Cheboksary, Russian Federation), e-mail: boris.mihaylov.63@mail.ru. ORCID: 0000-0001-6511-6985.

Gonik Ekaterina Grigoryevna (Cheboksary, Russian Federation) – PhD in Technical Sciences, Department of Building Structures of the I.N. Ulyanov Chuvash State University (428015, 15, Moskovsky prospect, Cheboksary, Russian Federation), e-mail: katya.gonik@mail.ru. ORCID: 0000-0002-7355-8553.

Ivanov Viktor Anatolyevich (Cheboksary, Russian Federation) – senior lecturer of Building Structures of the I.N. Ulyanov Chuvash State University (428015, 15, Moskovsky prospect, Cheboksary, Russian Federation), e-mail: 2605viktor@mail.ru. ORCID: 0000-0003-4684-6741.

Петров Михаил Васильевич (Чебоксары, Россия) - доктор технических наук, доцент, профессор кафедры строительных конструкций Чувашского государственного университета им. И.Н. Ульянова (428015, г. Чебоксары, Московский пр-т, 15), e-mail: 21pmv@mail.ru, ORCID: 0000-0002-7355-8553.

Кибец Александр Иванович (Нижний Новгород) - доктор физико-математических наук, профессор, главный научный сотрудник (603600, Нижний Новгород, пр. Гагарина, 23), e-mail: kibec@mech.unn.ru. ORCID: 0000-0001-8490-5541.

Михайлов Борис Васильевич (Чебоксары, Россия) – кандидат технических наук, доцент, доцент кафедры строительных конструкций Чувашского государственного университета им. И.Н. Ульянова (428015, г. Чебоксары, Московский пр-кт, 15), e-mail: boris.mihaylov.63@mail.ru. ORCID: 0000-0001-6511-6985.

Гоник Екатерина Григорьевна (Чебоксары, Россия) – кандидат технических наук, доцент кафедры строительных конструкций Чувашского государственного университета им. И.Н. Ульянова, (428015, г. Чебоксары, Московский пр-кт, 15), e-mail: katya.gonik@mail.ru. ORCID: 0000-0002-7355-8553.

Иванов Виктор Анатольевич (Чебоксары, Россия) – старший преподаватель кафедры строительных конструкций Чувашского государственного университета им. И.Н. Ульянова (428015, г. Чебоксары, Московский пр-кт, 15), e-mail: 2605viktor@mail.ru ORCID: 0000-0003-4684-6741.

International Journal for Computational Civil and Structural Engineering, 19(3) 58–68 (2023)

DOI:10.22337/2587-9618-2023-19-3-58-68

RECIPROCITY LAWS FOR OSCILLATIONS OF DISSIPATIVE SYSTEMS

A.N. Potapov

South Ural State University, Chelyabinsk, RUSSIA

Annotation: A general method for proving reciprocity relations in an arbitrary elastic discrete dissipative system (DDS) is presented. The method is based on the use of the algebraic theorem of P.L. Pasternak and on the new properties of the Duhamel integral, which are obtained for a dissipative system with internal friction of the material, which is taken into account on the basis of the non-proportional damping model. For displacements, velocities and accelerations, the dynamic reaction equations are written in the form of systems of linear equations and their symmetrical structure is shown. The functional dependence of the force parameters of the calculation model and the corresponding kinematic parameters of the reaction is determined by an arbitrary scalar function of time. An extended interpretation of the reciprocity theorems is given and sufficient conditions for their fulfillment are formulated, which consist in the requirement that the matrix differential operator of the equation of motion be symmetrical. New laws of reciprocity in dissipative systems are formulated and proved. The reciprocity of the product between the velocities / accelerations of masses and nodal forces is established. In contrast to the well-known theorem on the reciprocity of possible work, these laws are theorems on the 1st / 2nd derivative of possible work with respect to time and therefore go beyond the Betti principle. For particular cases of these theorems, the reciprocity of velocities and reciprocity of accelerations is shown. Expressions of general and particular theorems have a fairly simple mathematical form that does not require recourse to integral transformations, and are presented in an analytical form.

Keywords: Duhamel integral, dissipative system, reaction, displacement, velocity, acceleration

СООТНОШЕНИЯ ВЗАИМНОСТИ В ДИНАМИКЕ ДИССИПАТИВНЫХ СИСТЕМ

А.Н. Потапов

ФГАОУ ВО «Южно-Уральский государственный университет» (НИУ), г. Челябинск, РОССИЯ

Аннотация: Приведен общий метод доказательства соотношений взаимности в произвольной упругой дискретной диссипативной системе (ДДС), основанный на использовании алгебраической теоремы П.Л. Пастернака и новых свойствах интеграла Дюамеля, которые получены для диссипативной системы с внутренним трением материала, учитываемым на основе модели непропорционального демпфирования. Для перемещений, скоростей и ускорений уравнения динамической реакции записаны в форме систем линейных уравнений и показана их симметричная структура. Функциональная зависимость силовых параметров расчетной модели и соответствующих кинематических параметров реакции определяется произвольной скалярной функцией времени. Дана расширенная трактовка теорем взаимности и сформулированы достаточные условия их выполнения, заключающиеся в требовании симметрии матричного дифференциального оператора уравнения движения. Сформулированы и доказаны новые законы взаимности в диссипативных системах. Установлена взаимность произведения между скоростями / ускорениями масс и узловыми силами. В отличие от известной теоремы о взаимности возможных работ данные законы представляет собой теоремы о 1-й / 2-й производной возможной работы по времени и поэтому выходят за рамки принципа Бетти. Для частных случаев этих теорем показана взаимность скоростей и взаимность ускорений. Выражения общих и частных теорем имеют достаточно простую математическую форму записи, не требующую обращения к интегральным преобразованиям, и представляются в аналитическом виде.

Ключевые слова: интеграл Дюамеля, диссипативная система, реакция, перемещение, скорость, ускорение

INTRODUCTION

The main provisions on the issues of reciprocity in elastic systems were formulated in the works of Maxwell, Betty, Rayleigh and other scientists. These problems are most fully elucidated in the works of Rayleigh, who for the first time extended the results of his research to dissipative systems, introducing the scattering function for this purpose [1].

In deriving reciprocity relations, Rayleigh considered systems with a finite number of degrees of freedom, referred to below as discrete systems. As sources of perturbation of a discrete dissipative system (DDS), he took periodic forces of a harmonic type and given mass displacements, which also obey the harmonic law.

In his proofs, Rayleigh relied on the analysis of the potential and kinetic energies of the DDS, which are homogeneous quadratic functions of generalized coordinates and velocities. As a result, a general law of reciprocity was obtained (the theorem of reciprocity of work in the form of a product of forces and displacements), regardless of the Italian scientist Betty, who formulated this law a year earlier (1872). Rayleigh also proved all particular reciprocity theorems: displacements, reactions, reactions and displacements. In addition, for a conservative system that has only kinetic energy, a work reciprocity theorem was obtained in the form of a product of impulses of forces and mass velocities and a particular theorem on the reciprocity of impulses.

In [2], a purely algebraic interpretation of the principle of reciprocity was given, according to which reciprocity was considered as a property characteristic of any system of n linear equations with a symmetric structure of coefficients.

Reciprocity theorems are used in various fields of science and technology: acoustics, electrical engineering, geophysics, etc. In the field of practical applications of elastodynamics [3], reciprocity theorems are used in microelectromechanical devices, which are typical structural elements of building mechanics. In miniature, they are thin bodies such as beams, plates, shells and membranes. In the field of nanotechnologies (nano- and metamaterials) [4], an approach is used that makes it possible to apply the Betti–Rayleigh reciprocity theorem to calculate scattered fields in the form of plane waves at the interface between a homogeneous medium and a metamaterial.

The principle of reciprocity assumes the invariance of the characteristics of the frequency functions between any two material points during the replacement between the source and the receiver. This fact laid the foundation for many practical studies on ground vibrations caused by traffic [5], in seismic exploration [6], and problems of soil dynamics [7–10].

In [5], a problem related to soil dynamics was solved by checking a numerical model of vibration caused by road roughness during the movement of a vehicle such as a car. Rayleigh surface waves, generated by vertical vibrations from dynamic loads on the axle and propagating in the soil, are studied. Soil response in the free field was calculated using the dynamic Betty-Rayleigh reciprocity theorem using the transfer function between road and receiver. In the field of geophysics, in particular, seismic exploration [6], a method has been developed for detecting underground cavities using special dynamic test procedures designed to determine the characteristics of underground anomalies. The studies were carried out using active or passive sources and receivers placed on the earth's surface or inside wells for Rayleigh surface waves scattered from inhomogeneities in layered half-spaces. Discrete analytic expressions for the Green's functions are obtained on cavities using the thin layer method based on the Betti–Rayleigh reciprocity theorem.

Estimates of the levels of vibrations of the surface of the soil medium from a point source located inside the half-space were carried out in [7] based on the theorem on the reciprocity of displacements. The same theorem was used in studies on assessing the risk of damage to buildings due to sedimentation of the soil surface during shield penetration [8], when moving high-speed vehicles (trains, cars) [9]. The article

[10] considers the case of the impact of a seismic wave on a rigid foundation located in difficult soil conditions. The assessment of seismic load on a rigid foundation was carried out in the frequency range using the reciprocity theorem.

The papers [11, 12] provide proofs of reciprocity theorems for an arbitrary dynamic load without taking into account [11] and taking into account internal friction [12]. In the latter case, the damping matrix was adopted on the basis of the proportional damping model, which made it possible to write the differential equations of motion in a separated form.

For dynamic problems of the theory of elasticity, an approach [13] to the derivation of the reciprocity theorem based on the variational principle was proposed, in contrast to the generally accepted method of deriving reciprocity relations, which used the integral Laplace transform. When writing the equation of motion, the internal friction of the material is not taken into account. In [14], reciprocity relations were obtained in differential form for differential operators of elasticity theory and, for a particular discrete case, transitions to classical reciprocity relations between the coefficients of the force method, displacement method, and the mixed method were shown.

A number of works on reciprocity relations were carried out in the field of nonlinear problems of building mechanics, in particular, for nonlinear elastic systems it was shown [15] that reciprocity relations follow from the conditions of conservative properties of the system. The article [16] developed a technique applicable to discrete or continuous systems with smooth or non-smooth nonlinearities using the Betti-Maxwell reciprocity theorem.

A large cycle of works relates to the elastodynamics of Rayleigh surface waves in solids, where an effect associated with the violation of reciprocity in an elastic medium was discovered. In works [17, 18], devoted to the study of the propagation of Rayleigh waves with masses arranged in the form of a hexagonal and triangular lattice, this effect is explained by the lack of symmetry in the modes of natural oscillations, which manifested itself in the asymmetry of responses in the form of displacement fields in the direction of the medium. Also, the effect of the lack of symmetry in the modes of natural oscillations was noted in [19]. In [20], the violation of reciprocity in the elastodynamics of linear time-invariant acoustic waveguides was studied, which, according to the authors, is possible only due to violation of the time reversal symmetry at the microlevel.

1. Research method

A more general and at the same time simpler method for proving reciprocity theorems, which does not require the use of integral transformations, is described in the articles [21, 22]. The approach is based on new properties of the Duhamel integral, obtained by analyzing the equation of motion of the DDS and its characteristic equation. The interpretation of well-known theorems is extended, proofs of new reciprocity theorems are obtained, and conditions are formulated that ensure reciprocity properties in DDS.

The differential equation of motion of the DDS and its characteristic equation corresponding to the homogeneous equation have the form:

$$M\ddot{Y}(t) + C\dot{Y}(t) + KY(t) = P(t) \qquad (1)$$

$$MS^2 + CS + K = 0, \qquad (2)$$

where $M = \text{diag}\,(m_1,\ldots, m_n)$, C, K – are real and symmetric matrices of masses, damping and stiffness; $Y(t) = [y_j(t)]$, $P(t) = [p_j(t)]$ ($j = 1, \ldots, n$) – displacement and external load vectors; $S \in M_n(\mathbf{C})$ – the required matrix of dynamic characteristics of DDS; n is the number of degrees of freedom. The transition from equation (1) to (2) is performed using the fundamental matrix $\Phi(t) = e^{St}$.

When analyzing the characteristic equation (2), an arbitrary type of damping is considered, which is determined by the matrix C. Here, the only mandatory condition is the requirement for the symmetry of the matrix $C = C^{\mathrm{T}}$. In the presence of symmetry of the matrix C, the type of damping can be adopted based on any model

(proportional or non-proportional) damping, and then the solution of equation (2) is written as:

$$S = M^{-1}(-C + V + U)/2 \in M_n(\mathrm{C}), \qquad (3)$$

where: $V = -V^{\mathrm{T}}$, $U = U^{\mathrm{T}}$. With a small dissipation characteristic of conventional building structures, additional properties are valid: V, $iU \in M_n(\mathrm{R})$ (i – imaginary unit).

The vector $P(t)$ is represented as a product of an arbitrary scalar function of time $\xi(t)$, which specifies the shape of the dynamic load, and the amplitude vector $P_0 = [p_{0j}]$ ($j = 1, \ldots, n$):

$$P(t) = \xi(t)P_0. \qquad (4)$$

In this case, the reaction equations of the system - displacement vectors (Duhamel integral), velocities and accelerations, take the form:

$$\left.\begin{aligned} Y(t) &= 2\mathrm{Re}\ \{I(t)\}P_0, \\ \dot{Y}(t) &= 2\mathrm{Re}\{SI(t)\}P_0, \\ \ddot{Y}(t) &= 2\mathrm{Re}\{S^2I(t)\}P_0 + M^{-1}P(t), \end{aligned}\right\} \qquad (5)$$

where

$$I(t) = \{U^{-1}\int_{t_0}^{t}\Phi\,(t-\tau)^{\mathrm{T}}\xi(\tau)\,\mathrm{d}\tau\}. \qquad (6)$$

It follows from the analysis of equation (2) in [23] that solution (3) satisfies the equalities:

$$S^{\mathrm{T}}U = US, \quad \Phi(t)^{\mathrm{T}}U = U\Phi(t), \qquad (7)$$

which establish the fact of symmetry of matrices US, $U\Phi(t)$. This fact regarding the second equation in (7) is based on the property of the exponential matrix $\Phi(t) = e^{St}$ to be expanded into an infinite series in powers of the matrix argument S:

$$\Phi(t) = \sum_{k=0}^{\infty}\frac{(St)^k}{k!}.$$

Indeed, the equality $US = S^{\mathrm{T}}U$ implies a whole class of equalities related to any integer power of the matrix S: $US^k = (S^k)^{\mathrm{T}}U$ ($k = 0, \pm1, \pm2, \ldots$). From here one can obtain any linear combination of such equalities, and hence a combination containing the coefficients of the expansion series of the fundamental matrix $\Phi(t)$. This leads to an important symmetry property of the auxiliary matrix functions $S^kU^{-1}\Phi(t-\tau)^{\mathrm{T}}$ ($k = 0, \pm1, \pm2, \ldots$), from which it is sufficient to choose only the dependencies for $k = 0, 1, 2$:

$$U^{-1}\Phi(t-\tau)^{\mathrm{T}},\ SU^{-1}\Phi(t-\tau)^{\mathrm{T}},\ S^2U^{-1}\Phi(t-\tau)^{\mathrm{T}}.$$

These matrices are contained in the structure of equations (5). They coincide up to a scalar factor with the corresponding expressions, which are under the integral sign in (5). Note that for elastic vibrations of the system, the matrices U^{-1}, SU^{-1} и S^2U^{-1} do not depend on the integration variable and, therefore, can be introduced under the integral sign (6) in equations (5).

Generalizing these results, we represent the vector form of equations (5) in the form:

$$\left.\begin{aligned} Y(t) = D(t)P(t),\ \ \dot{Y}(t) &= V(t)P(t), \\ \ddot{Y}(t) &= A(t)P(t), \end{aligned}\right\} \qquad (8)$$

where

$$\left.\begin{aligned} D(t) = D(t)^{\mathrm{T}} &= 2\mathrm{Re}\ \{I(t)\}\xi(t)^{-1}, \\ V(t) = V(t)^{\mathrm{T}} &= 2\mathrm{Re}\ \{SI(t)\}\xi(t)^{-1}, \\ A(t) = A(t)^{\mathrm{T}} &= 2\mathrm{Re}\ \{S^2I(t)\}\xi(t)^{-1} + M^{-1}, \end{aligned}\right\} \qquad (9)$$

2. Results and discussion

In view of the symmetry (9), these relations express special cases of reciprocity in a dissipative system, representing the displacement reciprocity theorem (Maxwell's theorem, first equation): $D(t) = D(t)^{\mathrm{T}}$, the velocity reciprocity theorem (second equation): $V(t) = V(t)^{\mathrm{T}}$ and the acceleration reciprocity theorem (third equation): $A(t) = A(t)^{\mathrm{T}}$.

Velocity reciprocity theorem in DDS:

The speed $V_{ik}(t)$, imparted to the mass mi from the action of a unit force given by the law $P_k(t) = 1\cdot\xi(t)$ and applied to the mass m_k, is equal to

the same speed $V_{ki}(t) = V_{ik}(t)$, that occurs when moving mass m_k, as a result of the action of a unit force $P_k(t) = 1 \cdot \xi(t)$, applied to the mass m_i.

The theorem of reciprocity of accelerations in DDS:

The acceleration $A_{ik}(t)$, arising from the movement of the mass m_i from the action of a unit force given by the law $P_k(t) = 1 \cdot \xi(t)$ and applied to the mass m_k, is equal to the same acceleration $A_{ki}(t) = A_{ik}(t)$, arising during the movement of the mass m_k, caused by the action of a unit force $P_i(t) = 1 \cdot \xi(t)$, applied in the mass m_i.

The presence of reciprocity of accelerations is recognized by many experts as a fact [11], although there is no proof of the existence of this theorem in the scientific literature.

According to the physical meaning, the elements of matrices (9) are, respectively, the dynamic displacements, velocities and accelerations of the DDS nodes. The dynamic nature of these quantities and reciprocity relations is indicated by the scalar function $\xi(t)$ of the load form, which is included in all expressions of matrices (9). These matrices have a fairly simple mathematical form of notation, represented by analytical expressions and do not require recourse to integral transformations.

It should be noted that Rayleigh in his studies initially considered periodic effects of both force and kinematic types, taking as a scalar harmonic function of time $\xi(t) = \sin(\vartheta t + \varphi)$, where the angular frequency ϑ and the initial phase φ of the periodic effect were considered constant values for all nodes of the discrete system. In this case, Rayleigh considered only steady-state oscillations. Indicative, in this regard, is his statement, which has the character of insight: “If the force is not a harmonic function of time, then the types of oscillations in different parts of the system generally differ from each other and from the type of force oscillation” [1]. That is, Rayleigh well understood that with an arbitrary law of acting forces, the oscillatory process in the system becomes too complicated to study the emerging "types of oscillations" and requires more advanced methods of analysis, which at that time were not available.

Systems of equations (8) at any fixed moment of time are considered as systems of algebraic equations with a symmetric structure of coefficients, for which the property of reciprocity can be shown based on the theorem of prof. P.L. Pasternak [2]. We present a scheme for proving the law of reciprocity using the first equation in (8) as an example.

Let some other group of new forces $p_j(t)'$ ($j = 1, \dots, n$) represented by the vector $P(t)'$ act on the same n-mass dissipative system, then from formula (4) we have $P(t)' = \xi(t)P_0'$, where $P_0' = [p_{0j}']$ ($j = 1, \dots, n$). This action will cause the response of the elastic system in the form of a new displacement vector $Y(t)' = [y_j(t)']$ ($j = 1, \dots, n$). This set of forces and displacements will correspond to the equation $Y(t)' = D(t)P(t)'$, which is converted to the form $P(t)' = D(t)^{-1}Y(t)'$. After the operation of transposing the first equation in (8) $Y(t)^{\mathrm{T}} = P(t)^{\mathrm{T}}D(t)$ and term by term multiplication of the left and right parts of the obtained equalities as a row by a column, we obtain an equation. This equation expresses the equality of possible works (the Betti principle) performed in an elastic dissipative system by the force vectors $P(t)$ and $P(t)'$ on displacements represented by the corresponding vectors $Y(t)'$, $Y(t)$:

$$Y(t)^{\mathrm{T}}P(t)' = Y(t)'^{\mathrm{T}}P(t). \qquad (10)$$

Similarly, for two other linear systems in (8) with symmetric matrices $V(t)$ and $A(t)$, reciprocity relations are constructed according to the above scheme:

$$\left.\begin{aligned} \dot{Y}(t)^{\mathrm{T}}P(t)' &= \dot{Y}(t)'^{\mathrm{T}}P(t), \\ \ddot{Y}(t)^{\mathrm{T}}P(t)' &= \ddot{Y}(t)'^{\mathrm{T}}P(t). \end{aligned}\right\} \qquad (11)$$

Relations (11) represent new laws of reciprocity in the dynamics of dissipative systems. These laws are outside the scope of the Betty principle (10), since their expressions do not represent possible work. The first relation in (11) has the dimension "kN·m/s" and it can be considered as a theorem on the reciprocity of the 1st deriva-

tive of the possible work with respect to time, the second relation (with the dimension "kN·m/s^2") - as the reciprocity theorem 2nd derivative of possible work with respect to time.

Laws (11) establish *the reciprocity of the product of velocities / accelerations of masses in one state of the system and the nodal forces in its other state*. In this case, the proof of particular cases of reciprocity relations (9) follows from the property of the Duhamel integral based on the symmetric structure of the integrands (6). To construct general reciprocity laws (10), (11), Pasternak's theorem is used, which is based on systems of equations (8), which have a proven symmetric structure of coefficients.

Thus, the prerequisite for the existence of reciprocity relations in a dissipative system is due to the presence of symmetry of the differential operator of the equation of motion (1), which is a sufficient condition for the fulfillment of the reciprocity laws shown above. Less obvious is the necessity of a condition for the fulfillment of these laws.

Indeed, symmetry breaking in the structure of a differential operator, for example, when using a damping model with a non-symmetric matrix $C \neq C^{\mathrm{T}}$, will affect the properties of the characteristic equation (2) and auxiliary equalities (7). This will affect the structure of the expression for the dynamic response of the system (5), (6). With this formulation of the problem, the laws of reciprocity will be formulated in a more complex, generalized form. This indicates that in the field of dissipative systems there are still many problematic issues that need to be resolved.

An illustration of the reciprocity theorems is given on the example of vibrations of a rigidly clamped steel I-beam (№ 50, J_x = 39727 cm^4) for its various states (Fig. 1, 2, 3). The beam length is l = 1500 cm, point masses m_i = 0.5282 kNs^2/cm at n = 7.

The damping matrix is adopted in accordance with the non-proportional damping model used in the author's works [23]: $C = \frac{1}{2}(KT + TK)$, where T = diag (t_1, …, t_7); $t_i = \frac{\delta}{\pi}\sqrt{\frac{m_j}{r_{jj}}}$; m_j, r_{jj} – diagonal elements of matrices M, K (δ = 0.07 – logarithmic oscillation decrement).

Parameters of natural oscillations of a steel beam: the frequency of the fundamental tone of oscillations was ω_{min} = 52.78 rad/s, the period of oscillations was T = 0.12 s.

The reciprocity of velocities and accelerations is shown in fig. 1 for the case of action of single rectangular pulses $P_k(t) = 1\cdot\xi(t)$ with a length of 0.1 s (pulse shape $\xi(t) = 1$). In the first state, the reaction of the beam at the 3rd node from the action of the impulse $1\cdot\xi(t)$ applied to the mass m_6 is shown. Oscillograms of velocities and accelerations are red (Fig. 1). The scale of accelerations (dashed line) is reduced by 50 times. In the second state, the same reactions (blue color) occur at the 6th node from the action of the impulse $1\cdot\xi(t)$ applied to the mass m_3.

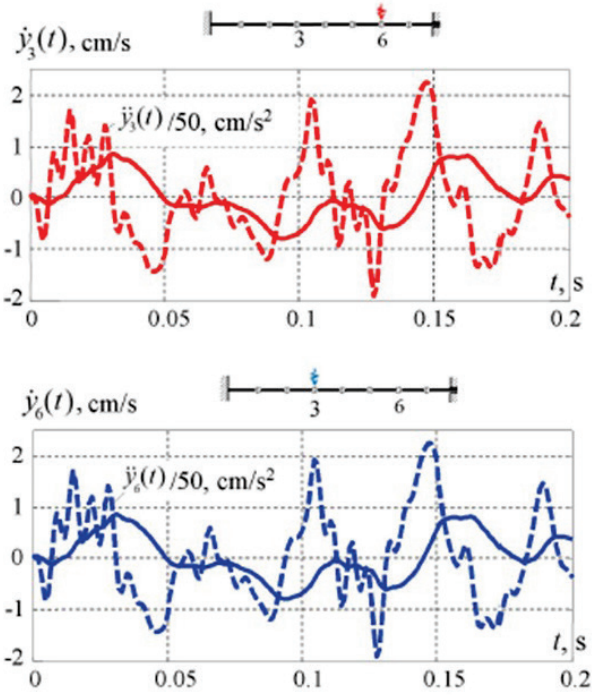


Figure 1. Oscillograms of velocities (solid line) and accelerations (dotted line) in a rigidly clamped beam under the action of a rectangular pulse equal to 1 in two states of the system: at the 6th node (response at the 3rd node - red) and at the 3rd node (response at the 6th node - blue)

On Figure 2, the action of vibrational forces with an angular frequency of 300 s^{-1} is consid-

ered: $P(t) = \xi(t)P_0$, where $\xi(t) = \sin 300t$. The reciprocity of the 1st derivative of the possible work with respect to time is shown. Flat curves on the graphs are plotted only for the peak load values shown on the right side of Figure 2. In the first state, the amplitudes of the forces p_{04}, p_{06} are multiplied by the speeds of the same nodes, caused by the amplitudes of the forces of the second state: p_{02}, p_{03}, p_{05}. The given oscillogram of the 1st derivative of the possible work (red color) coincides with a similar value (blue color) obtained by multiplying the amplitudes of the forces of the 2nd state at the speed of nodes 2, 3, 5, caused by the amplitudes of the forces of the 1st state.

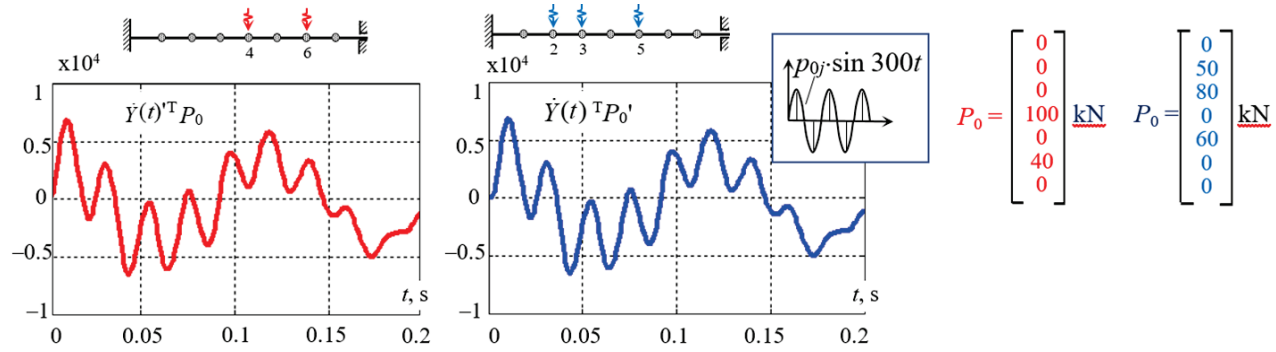


Figure 2. Reciprocity of the 1st derivative of the possible work under the action of vibrational forces in a rigidly clamped beam

On Figure 3 shows a spatial plot of the surface of the 2nd derivative of the possible work from the action of a sinusoidal impulse load $P(t) = \xi(t)P_0$, where $\xi(t) = \sin \pi t/t_1$, $t_1 = 0.1$ s is the pulse length. The pulse amplitudes have the same values as under the action of the vibration load in the previous example.

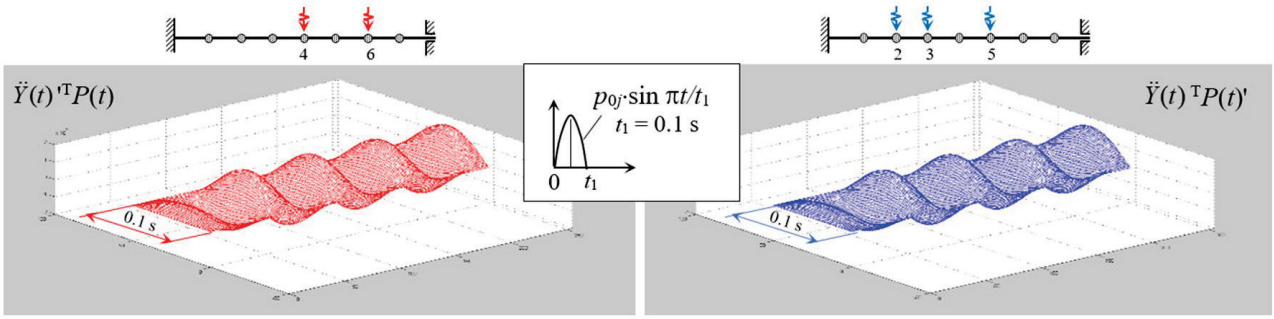


Figure 3. Surfaces of the 2nd derivative of the possible work under the action of sinusoidal pulses

CONCLUSION

1. Thus, a general method for proving reciprocity relations is given, based on the properties of the Duhamel integral and the algebraic theorem of Professor P.L. Pasternak.
2. In the formulation of the problem according to the reciprocity theorems, the following is allowed: the form of the external load is determined by an arbitrary scalar function of time; fluctuations can be both steady and unsteady; DDS damping type can also be arbitrary (proportional, non-proportional).
3. Obtained and proved particular laws of reciprocity of velocities and accelerations in dissipative systems. The expressions of the symmetric matrices of velocities and accelerations have

an analytical form of notation that does not require recourse to integral transformations.

4. The area of application of the laws of reciprocity, which go beyond the framework of the Betty principle, has been expanded. General reciprocity theorems about the 1st and 2nd derivatives of possible work with respect to time are proved.

The proposed approach indicates that the Duhamel integral is not only a tool for analyzing DDS, on the basis of which quantitative estimates of reaction parameters are built, but also an effective tool for studying such systems in order to obtain qualitative estimates. The revealed properties of symmetry in the structure of the reaction equations open up new possibilities for studying and understanding the theoretical foundations of the ongoing processes hidden in the nature of the oscillations of dissipative systems. In the field of fundamental research, which includes problems of reciprocity relations, the solution of these problems is highly topical and is of exceptional importance for practical use.

REFERENCES

1. **Strutt J.W.** (Lord Rayleigh) Sound Theory [Teoriya zvuka] // translation from English. 3rd edition P.N. Uspensky, S.A. Kamenetsky under total. ed. CM. Rytova, K.F. Teodorchik. M.; L.: Gostekhizdat, 1940. T. 1. 500 p.
2. **Pasternak P.L.** Berechnung vielfach statisch unbestimmter biegefester Stab- und Flächentragwerke. I. Teil / Dreigliedrige Systeme: Grundlagen und Anwendungen. Zürich: Leemann, 1927. 43 p.
3. **Giannakopoulos A.E., Amanatidou E., Aravas N.** A reciprocity theorem in linear gradient elasticity and the corresponding Saint-Venant principle // International Journal of Solids and Structures. 2006. Vol. 43(13). P. 3875-3894. doi.org/10.1016/j.ijsolstr.2005.05.048
4. Scattering of in-plane elastic waves at metamaterial interfaces / A.A. Mokhtari, Yan Lu, Q. Zhou, A.V. Amirkhizi, A. Srivastava // International Journal of Engineering Science. Vol. 150. 2020. 103278. doi.org/10.1016/j.ijengsci.2020.103278
5. **Lombaert G., Degrande G.** Experimental validation of a numerical prediction model for free field traffic induced vibrations by in situ experiments // Soil Dynamics and Earthquake Engineering, 2001, Vol. 21(6). P. 485-497. doi.org/10.1016/S0267-7261(01)00017-3
6. Some theoretical and numerical observations on scattering of Rayleigh waves in media containing shallow rectangular cavities / Hua-You Chai, Kok-Kwang Phoon, Siang-Huat Goh, Chang-Fu Wei // Journal of Applied Geophysics. 2012, Vol. 83. P. 107-119. doi.org/10.1016/j.jappgeo.2012.05.005
7. **Kurbatsky E.N.** Using the reciprocity theorem to estimate the levels of vibrations of the surface of an elastic half-space from a point source located inside the half-space [Ispol'zovaniye teoremy vzaimnosti dlya otsenki urovney vibratsiy poverkh-nosti uprugogo poluprostranstva ot] // Bulletin of the Moscow Institute of Engineers. 2005. Issue. 13. C. 32-37.
8. **Elgaev V.S.** Ensuring the safety of buildings during high-speed tunneling using the shield [Obespecheniye bezopasnosti zdaniy pri skorostnoy prokhodke tonneley shchitovym sposobom] // method: Ph.D. dis. … cand. tech. Sciences. M., 2013.
9. **Nguyen Chong Tam**. Application of the reciprocity theorem for assessing oscillations created by moving loads [Prilozheniye teoremy vzaimnosti dlya otsenki kolebaniy, sozdavayemykh po-dvizhnymi nagruzkami] // Theory and Practice of Calculation of Buildings, Structures and Structural Elements. Analytical and numerical methods: Sat. report Int. scientific-practical. conf., dedicated 80th anniversary of the d.r. prof. D.N. Sobolev. Moscow, 16 Dec. 2014. M.: MGSU, 2014. S. 240-248.
10. **Tyapin A.G.** Application of the reciprocity theorem in the frequency range to deter-

mine the seismic load on a rigid foundation in difficult soil conditions [Primeneniye teoremy vzaimnosti v chastotnom diapazone dlya opredeleniya sey-smicheskoy nagruzki na zhestkiy] / Part II: limit transitions and numerical implementation. Stroitelnaya mekhanika i raschet sooruzheniy. 2015. N 1. S. 46-52.

11. **Zylev V.B.** Reciprocity theorems in structural dynamics [Teoremy vzaimnosti v dinamike konstruktsiy] // Stroitel'naya mekhanika i raschet sooruzheniy. 2006. N 5. S. 10-15.
12. **Zylev V.B.** Reciprocity theorems for the dynamics of systems with damping [Teoremy vzaimnosti dlya dinamiki sistem s dempfirovaniyem] / Bulletin of the department of building sciences. Moscow-Orel-Kursk: RAASN, 2011. N 15. S. 86-92.
13. **Ainola L.Ya.** The reciprocity theorem for dynamic problems of the theory of elasticity [Teorema vzaimnosti dlya dinamicheskikh zadach teorii uprugosti] // Applied Mathematics and Mechanics. 1967. T. 31, Issue. 1. S. 176-177.
14. **Kuznetsov E.N.** Reciprocity relations for differential operators of the theory of elasticity [Sootnosheniya vzaimnosti dlya differentsial'nykh operatorov teorii upru-gosti] // Applied Mathematics and Mechanics. 1967. T. 31, Issue. 3. S. 500-502.
15. **Rabinovich I.M.** Reciprocity relations for non-linear elastic systems arising from the condition of conservatism [Sootnosheniya vzaimnosti dlya nelineyno-uprugikh sistem, vytekayushchiye iz usloviya konservativnosti] // Studies in the theory of structures. M.: Stroyiz-dat, 1974. Issue. 20. S. 3-11.
16. Methodology for nonlinear quantification of a flexible beam with a local, strong nonlinearity / C.A. Herrera, D.M. McFarland, L.A. Bergman, A.F. Vakakis // Journal of Sound and Vibration, 2017, Vol. 388. P. 298-314. doi.org/10.1016/j.jsv.2016.10.037
17. Transient response of a gyro-elastic structured medium: Unidirectional waveforms and cloaking / M. Garaua, M.J. Nieves, G. Carta, M. Brun // International Journal of Engineering Science, 2019, Vol. 143. P. 115-141. www.elsevier.com/locate/ijengsci
18. Rayleigh waves in micro-structured elastic systems: Non-reciprocity and energy symmetry breaking / M.J. Nieves, G. Carta, V. Pagneux, M. Brun // International Journal of Engineering Science, 2020, Vol. 156. 103365. doi.org/10.1016/j.ijengsci.2020.103365
19. **Zhao Y., Zhou X., Huang G**. Non-reciprocal Rayleigh waves in elastic gyroscopic medium // Journal of the Mechanics and Physics of Solids. 2020. Vol. 143. 104065. doi.org/10.1016/j.jmps.2020.104065
20. **Blanchard A., Sapsis Th. P., Vakakis A.F.** Non-reciprocity in nonlinear elastodynamics // Journal of Sound and Vibration. 2018. Vol. 412. P. 326-335. doi.org/10.1016/j.jsv.2017.09.039
21. **Potapov A.N.,** Reciprocity relations in dissipative systems [Sootnosheniya vzaimnosti v dissipativnykh sistemakh] // A.N. Potapov. – Izvestiya vuzov. Construction. Novosibirsk, 2001. № 11(515). C. 22-28.
22. **Potapov A.N., Ufimtsev E.M.** Reciprocal Relations in Oscillations of Dissipative Systems // Procedia Engineering. 2015. Vol. 117. P. 296-303.
23. **Potapov A.N.** Dynamic analysis of discrete dissipative systems under nonstationary influences [Dinamicheskij analiz diskretnyh dissipativnyh sistem pri nestacionarnyh vozdejstviyah] / A.N. Potapov. – Chelyabinsk: SUSU Publ., 2003. 167 p.

СПИСОК ЛИТЕРАТУРЫ

1. **Стрэтт Дж. В.** (Лорд Рэлей) Теория звука: перевод с англ. 3-е издание П.Н. Успенского, С.А. Каменецкого под общ. ред. С.М. Рытова, К.Ф. Теодорчика. М.; Л.: Гостехиздат, 1940. Т. 1. 500 с.
2. **Pasternak P.L.** Berechnung vielfach statisch unbestimmter biegefester Stab- und Flächentragwerke. I. Teil / Dreigliedrige Systeme: Grundlagen und Anwendungen. Zürich: Leemann, 1927. 43 p.

3. **Giannakopoulos A.E., Amanatidou E., Aravas N.** A reciprocity theorem in linear gradient elasticity and the corresponding Saint-Venant principle // International Journal of Solids and Structures. 2006. Vol. 43(13). P. 3875-3894. doi.org/10.1016/j.ijsolstr.2005.05.048
4. Scattering of in-plane elastic waves at metamaterial interfaces / A.A. Mokhtari, Yan Lu, Q. Zhou, A.V. Amirkhizi, A. Srivastava // International Journal of Engineering Science. Vol. 150. 2020. 103278. doi.org/10.1016/j.ijengsci.2020.103278
5. **Lombaert G., Degrande G.** Experimental validation of a numerical prediction model for free field traffic induced vibrations by in situ experiments // Soil Dynamics and Earthquake Engineering, 2001, Vol. 21(6). P. 485-497. doi.org/10.1016/S0267-7261(01)00017-3
6. Some theoretical and numerical observations on scattering of Rayleigh waves in media containing shallow rectangular cavities / Hua-You Chai, Kok-Kwang Phoon, Siang-Huat Goh, Chang-Fu Wei // Journal of Applied Geophysics. 2012, Vol. 83. P. 107-119. doi.org/10.1016/j.jappgeo.2012.05.005
7. **Курбацкий Е.Н.** Использование теоремы взаимности для оценки уровней вибраций поверхности упругого полупространства от точечного источника, расположенного внутри полупространства // Вестник Московского института инженеров тр-та. 2005. Вып. 13. С. 32-37.
8. **Елгаев В.С.** Обеспечение безопасности зданий при скоростной проходке тоннелей щитовым способом: автореф. дис. … канд. техн. наук. М., 2013.
9. **Нгуен Чонг Там.** Приложение теоремы взаимности для оценки колебаний, создаваемых подвижными нагрузками // Теория и практика расчета зданий, сооружений и элементов конструкций. Аналитические и численные методы: сб. докл. Межд. науч.-практ. конф., посв. 80-летию со д. р. проф. Д.Н. Соболева. Москва, 16 дек. 2014 г. М.: МГСУ, 2014. С. 240-248.
10. **Тяпин А.Г.** Применение теоремы взаимности в частотном диапазоне для определения сейсмической нагрузки на жесткий фундамент в сложных грунтовых условиях. Часть II: предельные переходы и численная реализация // Строительная механика и расчет сооружений. 2015. N 1. С. 46-52.
11. **Зылев В.Б.** Теоремы взаимности в динамике конструкций // Строительная механика и расчет сооружений. 2006. N 5. С. 10-15.
12. **Зылев В.Б.** Теоремы взаимности для динамики систем с демпфированием / Вестник отделения строительных наук. Москва-Орел-Курск: РААСН, 2011. N 15. С. 86-92.
13. **Айнола Л.Я.** Теорема взаимности для динамических задач теории упругости // Прикладная математика и механика. 1967. Т. 31, Вып. 1. С. 176-177.
14. **Кузнецов Э.Н.** Соотношения взаимности для дифференциальных операторов теории упругости // Прикладная математика и механика. 1967. Т. 31, Вып. 3. С. 500-502.
15. **Рабинович И.М.** Соотношения взаимности для нелинейно-упругих систем, вытекающие из условия консервативности // Исследования по теории сооружений. М.: Стройиздат, 1974. Вып. 20. С. 3-11.
16. Methodology for nonlinear quantification of a flexible beam with a local, strong nonlinearity / C.A. Herrera, D.M. McFarland, L.A. Bergman, A.F. Vakakis // Journal of Sound and Vibration, 2017, Vol. 388. P. 298-314. doi.org/10.1016/j.jsv.2016.10.037
17. Transient response of a gyro-elastic structured medium: Unidirectional waveforms and cloaking / M. Garaua, M.J. Nieves, G. Carta, M. Brun // International Journal of Engineering Science, 2019, Vol. 143. P. 115-141. www.elsevier.com/locate/ijengsci
18. Rayleigh waves in micro-structured elastic systems: Non-reciprocity and energy symmetry breaking / M.J. Nieves, G. Carta, V. Pagneux, M. Brun // International Journal

of Engineering Science, 2020, Vol. 156. 103365.
doi.org/10.1016/j.ijengsci.2020.103365

19. **Zhao Y., Zhou X., Huang G.** Non-reciprocal Rayleigh waves in elastic gyroscopic medium // Journal of the Mechanics and Physics of Solids. 2020. Vol. 143. 104065.
doi.org/10.1016/j.jmps.2020.104065
20. **Blanchard A., Sapsis Th. P., Vakakis A.F.** Non-reciprocity in nonlinear elastodynamics // Journal of Sound and Vibration. 2018. Vol. 412. P. 326-335. doi.org/10.1016/j.jsv.2017.09.039
21. **Потапов А.Н.** Соотношения взаимности в диссипативных системах // Известия вузов. Строительство. Новосибирск, 2001. № 11(515). С. 22-28.
22. **Potapov A.N., Ufimtsev E.M.** Reciprocal Relations in Oscillations of Dissipative Systems // Procedia Engineering. 2015. Vol. 117. P. 296-303.
23. **Потапов А.Н.** Динамический анализ дискретных диссипативных систем при нестационарных воздействиях. – Челябинск: Изд. ЮУрГУ, 2003. 167 с.

Alexander N. Potapov, Corresponding Member of RAACS, Doctor of Technical Sciences, Professor. Department of Building Technologies and Structural Engineering. South Ural State University (76, Lenin Ave., Chelyabinsk, 454080.). South Ural State University (NRU), Chelyabinsk, 76, Lenin Prospect, 454080, Russia
phone: +7(919)343-71-29. E-mail: potapov.alni@gmail.com. ORCID – 0000-0002-9079-2667

Потапов Александр Николаевич, член-корреспондент Российской академии архитектуры и строительных наук (РААСН), профессор, доктор технических наук, профессор кафедры «Строительное производство и теория сооружений». ФГБОУ ВО «Южно-Уральский государственный университет (национальный исследовательский университет)», 76, прос. Ленина, Челябинск, 454080. E-mail: potapov.alni@gmail.com. тел: +7(919)343-71-29.
ORCID – 0000-0002-9079-2667
ScopusID – AAF-2331-2020
AuthorID – 745600

International Journal for Computational Civil and Structural Engineering, 19(3) 69–82 (2023)

DOI:10.22337/2587-9618-2023-19-3-69-82

COUPLED HEAT AND MASS TRANSFER PROBLEM WITH DEPENDENT HEAT CONDUCTIVITY PROPERTIES AND ITS SEMI-ANALYTICAL SOLUTION

Vladimir N. Sidorov, Alim M. Primkulov

Moscow State University of Civil Engineering, Moscow, RUSSIA

Abstract: Present paper proposes a computation method for a coupled heat and mass transfer problem within the porous media where the heat conductivity properties of the media undergo changes caused by the mass transfer. Heat and mass transfer processes are coupled through the inclusion of evaporation and condensation phenomena which in turn require the solution to an another the vapour transfer problem. This complex coupled problem results in a system of both linear and non-linear second order partial differential equations that are spatially discretized by Finite Element Method. Temporal integration is carried out analytically. Thus, the proposed system of equations covering linear vapor transfer problem, linear filtration problem and non-linear heat transfer problem is transformed into a system of both linear and non-linear first order ordinary differential equations being solved by semi-analytical method. Picard approach of successive iterations is used for linearization of the equations. Convergent solution is achieved which is demonstrated on a sample problem herein below. Proposed method gives good insight on the processes taking place within the structures being subjected to temperature and vapor pressure gradients, including the residual effects of moisture accumulation, and assesses its impact on heat conductivity of materials that the structures consist of. Present study is a part of more extensive research on the application of semi-analytical methods in heat transfer problems, therefore it is not exhaustive and complete. Shortcomings of the method and its possible work-arounds as well as the topics for further studies are discussed in Conclusions and Further Studies section.

Keywords: Heat and mass transfer problem, coupled problem, non-linear, finite element method, semi-analytical method

СОВМЕСТНАЯ ЗАДАЧА ТЕПЛОМАССООБМЕНА С ЗАВИСИМЫМИ ТЕПЛОПРОВОДЯЩМИ СВОЙСТВАМИ И ЕЕ ПОЛУАНАЛИТИЧЕСКОЕ РЕШЕНИЕ

В.Н. Сидоров, А.М. Примкулов

Национальный исследовательский Московский государственный строительный университет, г. Москва, РОССИЯ

Аннотация: В настоящей работе предлагается метод расчета связанной задачи тепломассопереноса в пористых средах, когда свойства теплопроводности сред претерпевают изменения, вызванные массопереносом. Процессы тепло- и массопереноса связаны явлениями испарения и конденсации, что, в свою очередь, требует решения другой проблемы переноса пара. Эта сложная проблема приводит к системе как линейных, так и нелинейных дифференциальных уравнений в частных производных второго порядка, которые дискретизируются в соответствии с алгоритмом метода конечных элементов. Интегрирование по временной переменной выполняется аналитически. Таким образом, система дифференциальных уравнений, включающая линейное уравнение паропереноса, линейную задачу фильтрации и нелинейное уравнение теплопереноса, преобразуется в систему как линейных, так и нелинейных дифференциальных уравнений первого порядка, решаемых полуаналитическим путем. Для линеаризации уравнений используется подход Пикара последовательных итераций. Достигается сходящееся решение, что демонстрируется на примере задачи. Предложенный метод позволяет получить представление о теплофизических процессах, происходящих в конструкциях с учетом градиентов температуры и давления пара, в том чис-

ле об остаточных явлениях накопления влаги и оценить их влияние на теплопроводность материалов, из которых изготовлены конструкции. Настоящее исследование является частью более обширного исследования применения полуаналитических методов в задачах теплообмена, поэтому оно не является исчерпывающим и полным. Недостатки метода и его возможные обходные пути, а также темы для дальнейших исследований обсуждаются в разделе «Выводы и дальнейшие исследования».

Ключевые слова: задача тепломассопереноса, связанная задача, нелинейный метод, метод конечных элементов, полуаналитический метод.

1. INTRODUCTION

Multi layered exterior wall structures are widely used in modern buildings as they allow to achieve proper insulation properties as well as to have the desired interior and exterior appearance meanwhile be elegant, lightweight and be of sufficient strength and resilience. On the other hand, the study of physical processes taking place within such kind of walls are becoming, obviously, more complicated as the significantly varying material properties cause those physical processes to occur differently comparing to the homogenous single material wall structures. Multi-layered structures have extensively been studied both domestically and internationally with respect to their responses to varying indoor and outdoor conditions which have been reflected in building codes and manufacturer's design guidelines. Present study though, proposes a mathematical model that can quantitatively describe the processes in such structures with due account of their interactions and interdependence under the given boundary conditions.

In particular it reviews the heat transfer phenomenon within multi-layered wall structure in conjunction with the vapor transfer and the filtration occurring simultaneously and accounts their interactions.

Mathematical model that uses semi-analytical computation techniques is proposed to describe the process in such wall structures. Spatially, the model utilizes the Finite Element Method whereas the temporal variations are solved analytically.

Building Codes and Standards [1] contain various simplified computation methods for practical problems that, with due safety margin, account all negative factors that may develop within the structures thus allowing to design such structures in compliance with the serviceability requirements. The idea in those standard methods is to determine composition and geometric proportions of the structures that would withstand the extreme weather conditions of the region, assuming that at all other intermediate states of the weather the structure would perform adequately.

Main objective of present study is to couple the major physical processes happening in the wall within proposed mathematical model that will allow to calculate the immediate state of the structure under the given indoor and outdoor climate condition and including residual factors remained from the previous actions and solve such coupled problem. Hence the difference of the proposed heat and mass transfer model from standard computation methods is that the model describes accurately the immediate state of the wall.

2. RESEARCH METHODS

2.1. Wall Model

As a practical example let consider tri-layered wall structure consisting of inner and outer blockwork walls and heat insulation layer sandwiched in between. This structure is seemingly good case of the composite wall where the water condensation is very likely to occur. The insulation layer in the middle of the structure retains the majority of the heat thus causing the outer blockwork layer to be cooled down till almost the outdoor temperature. On the other hand, the same outer brickwall has a vapor transmissivity apparently lower than that of the middle insulation layer. These two factors jointly, under certain combination of boundary con-

ditions, result in vapor condensation within the wall, that will consequentially adversely effect the heat transfer phenomena. Evaporation and condensation processes non-uniformly distribute the moist throughout the wall which creates a moisture gradient. Having the material filtration properties this gradient induces the filtration process within the wall. Condensation, evaporation and filtration processes combined form the ultimate moisture content distribution within the wall.

One dimensional mathematical model, where the spatial argument varies along the thickness of the wall might be used to build the relationships between the processes. Physical model of above-mentioned tri-layered wall structure is depicted in Fig.1. The total wall thickness is L whereas the width of each individual layer is $\frac{L}{3}$.

Left hand side of the composite wall faces with the indoor environment varying within the range of positive temperatures while the right-hand side contacts the outdoor environment with the range of temperatures that may have also the negative values.

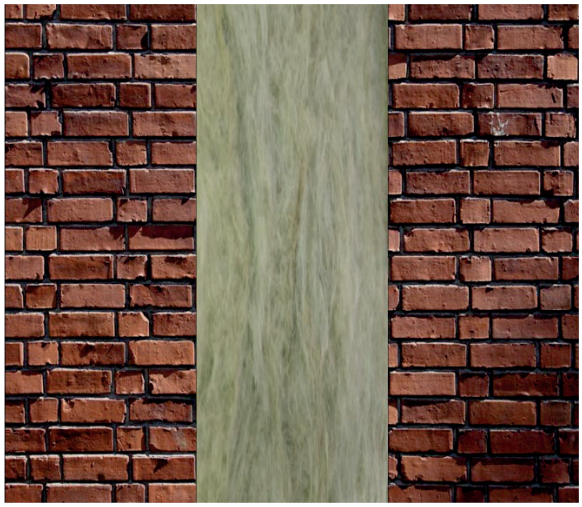


Figure 1. Multi layered wall structure

Indoor and outdoor temperatures are not constant with time as was noted earlier. Let assume that they are given as functions of time:

$$\phi_{in} = \Phi_{in}(t) \quad (1)$$
$$\phi_{out} = \Phi_{out}(t) \quad (2)$$

where, ϕ_{in}, ϕ_{out} - indoor and outdoor temperatures; Φ_{in}, Φ_{out} - some functions of t; t - time.

Similarly, the indoor and outdoor partial vapor pressures are varying with time and can be described as:

$$p_{v,in} = P_{v,in}(t) \quad (3)$$
$$p_{v,out} = P_{v,out}(t) \quad (4)$$

where $p_{v,in}, p_{v,out}$ - indoor and outdoor vapor pressures; $P_{v,in}, P_{v,out}$ - some functions of t; t - time.

All major material properties such as heat conductivities, vapor transmission resistivities, liquid moist filtration properties that appear as parameters in mathematical model are also known and given.

2.2. Physical Processes

The physical model as it is shown on Fig.1 can be described as a finite domain consisting of:

- porous media composed of inner blockwork wall, heat insulation and outer blockwork wall all with its own individual properties - the skeleton;
- moist in its liquid phase (water) which defines the moisture content of the skeleton;
- humid air (binary gas) consisting of air and water vapor mixture.

Having the boundary conditions as specified in section 2.1 above, the processes taking place within the wall can be described as follows:

Mass transfer

This process includes the transfer of the binary gas and liquid water through the skeleton as well as the moist phase changes such as condensation as transformation of vapor into liquid water and the evaporation as transformation of liquid water into vapor. This mass transfer may happen due to the following causes:

a) At microscopic level (so called molecular transfer):

– Diffusion due to temperature gradient (as per Fick's law);

– Diffusion due to vapor concentration gradient;

– Diffusion due to chemical potential gradient;

– Osmosis caused transfers.

b) At macroscopic level (so called convection transfer):

– Capillarity adsorption transfer;

– Pressure gradient transfer (including hydraulic gradient);

– Gravity induced transfer.

Heat transfer

Heat transfer within the same domain occurs due to the following factors:

a) At microscopic level (so called molecular transfer):

– Heat diffusion induced by the difference of temperatures between the skeleton, the air/vapor and/or the liquid water;

– Heat transfer due to change in Enthalpy of the skeleton in the result of moisture content change;

b) At macroscopic level (so called convection transfer):

– Heat transfer induced by temperature gradient and the conductive properties of the media;

– Heat transfer due to moisture phase change (evaporation/condensation);

– Heat transfer due to radiation;

– Heat sink/sources at the boundaries of the domain (derivative boundary conditions).

Detailed discussion of each of above listed processes can be found in [2].

2.3. Heat and Mass Transfer Equations

Physical processes described in 2.1 - 2.2 may occur simultaneously or in various combinations thereof. Also, each of them may have impact in different magnitude on the temperature distribution in the wall. General approach in heat and mass transfer practical problems is to select the relevant processes individually, considering the particularities of that specific problem and evaluating the effect that the process may have on the result. Nonetheless the common property of all those processes is that they can be easily incorporated into the governing equation as a separate term. Hence, in most general form the equations describing heat and mass transfer can be written as:

$$\lambda_{m1,m2,m3}\frac{\partial u_{(1,2,3)}}{\partial t} = -\frac{\partial}{\partial x}\left(\sum_{i=1}^{N_m} D_{(m1,m2,m3)_i}\frac{\partial u}{\partial x}\right) - \sum_{i=1}^{M_m} V_{(m1,m2,m3)_i}\frac{\partial u}{\partial x} + \sum_{i=1}^{K_m} Q_{(m1,m2,m3)_i} \quad (5)$$

$$\lambda_h\frac{\partial \phi}{\partial t} = \frac{\partial}{\partial x}\left(\sum_{i=1}^{N_h} D_{(h)_i}\frac{\partial \phi}{\partial x}\right) - \sum_{i=1}^{M_h} V_{(h)_i}\frac{\partial \phi}{\partial x} + Q_h \quad (6)$$

where, m1, m2, m3 indices denote the mass transfer of vapor, liquid and solid masses respectively; u - mass being transferred; N_m, M_m, K_m - number of physical processes included into mass transfer problem, viz. N_m – number of processes occurring due to diffusion, M_m – number of processes occurring due to convection, K_m– number of processes occurring due to mass source or sinks (see mass transfer in 2.2); $\lambda_{m1,m2,m3}, D_{(m1,m2,m3)}, V_{(m1,m2,m3)}$ - material properties of relevant physical process of the mass transfer (e.g. $\lambda_{m1,m2,m3}$ – retarding coefficients of mass transfer, $D_{(m1,m2,m3)}$ – mass transfer permeability coefficients, $V_{(m1,m2,m3)}$ – mass transfer velocity); $Q_{(m1,m2,m3)}$ - mass source/sink (e.g. evaporation, condensation rates etc.) along the model and at the boundaries; h index denotes the heat transfer problem; ϕ - temperature; N_h, M_h - number of physical processes included into heat transfer problem (see heat transfer in 2.2); λ_h, D_h, V_h - material properties of relevant physical process of the heat transfer; Q_h - heat source/sink rate; t - temporal variable; x - spatial variable.

For the sake of simplicity, the present paper focuses on macroscopic level processes only as they have more significant effect on temperature distribution within the topic problem, namely: convection due to temperature gradient; mass transfer due to vapor pressure and hydraulic gradients. However, it is straightforward to incorporate all the others processes as well with its associated physical parameters. Having this simplification made, the governing equations shall take the following form:

Liquid phase moisture transfer - filtration.

$$\frac{\partial h}{\partial t} = k_f\frac{\partial^2 h}{\partial x^2} + Q_f \overset{FEM}{\Longrightarrow} \{\dot{h}\} = [C_h]\{h\} + \{F\} \quad (7)$$

where, h - mass content of liquid water, in kg per unit volume in m^3 of the skeleton; k_f - permeability coefficient, constant value for each material and does not change in time, in $\frac{m}{sec}$; Q_f - liquid water source/sink – a function accounting the incoming or outgoing moist, in m^3/sec; $\overset{FEM}{\Longrightarrow}$ - Finite element (matrix) transformation of the governing differential equation; $\{h\}, \{\dot{h}\}$ - vectors of mass contents and its time derivatives values at the finite element nodes; $[C_h], \{F\}$ - Finite Element transformed matrix and vector that discretely models $k_f \frac{\partial^2}{\partial x^2}$ operator and water source/sink function Q_f in filtration equation.

Partial vapor pressure distribution

$$\frac{\partial p}{\partial t} = k_v \frac{\partial^2 p}{\partial x^2} + Q_p \overset{FEM}{\Longrightarrow} \{\dot{p}\} = [C_p]\{p\} + \{P\} \qquad (8)$$

where, p - partial vapor pressure, in Pa; k_v - vapor conductivity coefficient, constant value for each material and does not change in time, in $\frac{kg}{m\ sec\ Pa}$; Q_p - boundary condition function that accounts the variation of partial vapor pressure at the boundaries, contact surfaces with indoor and outdoor environments, in $\frac{Pa}{sec}$; $\overset{FEM}{\Longrightarrow}$ - Finite element (matrix) transformation of governing differential equation; $\{p\}, \{\dot{p}\}$ - vectors of vapor pressures and its time derivatives values at the finite element nodes; $[C_p], \{P\}$ - Finite Element transformed matrix and vector that discretely models $k_v \frac{\partial^2}{\partial x^2}$ operator and the boundary condition function Q_p in partial vapor pressure equation.

Heat transfer.

$$\frac{\partial \phi}{\partial t} = \frac{\partial}{\partial x}\left(D(f(\phi))\frac{\partial \phi}{\partial x}\right) + Q_h \overset{FEM}{\Longrightarrow} \overset{FEM}{\Longrightarrow} \{\dot{\phi}\} = [C_t(t)]\{\phi\} + \{T\} \qquad (9)$$

where, ϕ – temperature, in °C; $D(f(\phi))$ - heat conductivity depending on some function of ϕ, individual for each material, in $\frac{W}{m\,°C}$; Q_h - heat source/sink that accounts the boundary conditions and heat transfer due to evaporation or condensation, in $\frac{kcal}{m^3 \cdot hr}$; $\overset{FEM}{\Longrightarrow}$ - Finite element (matrix) transformation of governing heat transfer differential equation; $\{\phi\}, \{\dot{\phi}\}$ - vectors of temperatures and its time derivatives values at the finite element nodes; $[C_\phi], \{T\}$ - Finite Element transformed matrix and vector that discretely model $\frac{\partial}{\partial x}\left(D(f(\phi))\frac{\partial}{\partial x}\right)$ operator and Q_h function in heat transfer equation.

Heat transfer equation (9) shows the heat conductivity coefficient D being dependent on a function of temperature ϕ. Fig. 2 depicts the variation of heat conductivity property of a material with its moisture content as proposed by T.I. Rubashkina [6]. Similar relations are also given in other resources [2]. In order to establish the function D, it is necessary to build the relationship between the moisture content W and the temperature ϕ, as it will be shown later.

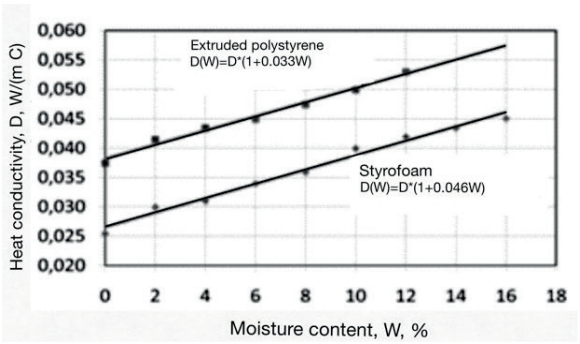


Figure 2. Heat conductivity D as a function of moisture content W

As it can be seen from Fig. 2 the moisture content of the wall material, which is, in our case, the solution to equation (7), changes the heat conductivity linearly. Then the solution to (9) explicitly depends on the solution of (7). Thus (7) and (9) should be solved jointly to obtain the temperature distribution within the media being adjusted to the moisture content. Linear relationship of material moisture content and its thermal conductivity can be defined as:

$$D\left(\frac{h(t)}{\rho_m}\right) = D_k \frac{h(t)}{\rho_m} + D_f \tag{10}$$

where, D_k, D_f - proportionality coefficients of linear relationship as in Fig.2 which are the constant values for each material; $h(t)$ - mass content of liquid water as a function of time t, to be determined by the solution of (7); ρ_m - dry density of the material.

Equation (7) includes the condensation/evaporation function Q_f which in turn depends on temperature. Hence the thermal conductivity D eventually non-linearly depends on temperature ϕ.

Moisture transfer problem (7) can be simplified by assuming that D_f is the heat conductivity property valued at the time $t = 0$, then the initial values for this problem will be a vector of zeros.

$$h(x, t = 0) = 0 \tag{11}$$

Accordingly, the solution of (7) will define the variation of moisture content throughout the wall at any given time $t = t_d$ in comparison to the initial values which are the moisture content at $t = 0$.

2.4. Evaporation and Condensation

In order to calculate the amount of moisture that condenses or evaporates within the wall a model proposed by Dalton [2] shall be utilized. Using the notation of the paper it can be expressed as:

$$\frac{dM}{dt} = \Theta A \left(x_p(t) - x_T(t)\right) \tag{12}$$

where, $\frac{dM}{dt}$ - rate of change of moisture in $\frac{kg}{hr}$; $\Theta = (25 + 19v)$ - evaporation/condensation coefficient in $\frac{kg}{m^2 hr}$, where v - air flow velocity which is negligibly small for the topic problem and can be set to zero; A - contact area, assumed as unity, in m^2; $x_p(t)$ - air humidity as a ratio of vapor mass to dry air mass, in $\frac{kg}{kg}$; $x_T(t)$ - maximum air humidity as a ratio of saturated vapor mass at a given temperature to a dry air mass, in $\frac{kg}{kg}$.

Dalton model states that the condensation happens when $x_p(t) > x_T(t)$, or mass change rate $\frac{dM}{dt}$ is positive valued and the evaporation happens otherwise, when $\frac{dM}{dt}$ is negative valued.

It is a routine to show that $x_p(t)$ and $x_T(t)$ can be expressed by the following formulas, based on the ideal gas theory [5]:

$$x_p(t) = \frac{0.0022 k_B}{p_{atm} m} p(t) \tag{13}$$

$$x_T(t) = \frac{0.0022 k_B}{p_{atm} m} p_{vs}(t) \tag{14}$$

where, t – time, in hr; p_{atm} - absolute pressure (atmospheric pressure), assumed as 100 kPa; m - molecular mass of dry air, circa 4.81×10^{-26}kg; k_B - Bolzmann constant, $1.380649 \times 10^{-23}\ \frac{J}{°K}$; $p(t)$ – partial vapor pressure distribution within the wall, which is a solution to (8), in Pa; $p_{vs}(t)$ - saturated partial vapor pressure for a given temperature, in Pa, can be calculated by using the following formula in kPa (Magnus formula):

$$p_{vs}(t) = 610.94 e^{\left(\frac{17.625\phi}{\phi + 243.04}\right)} \tag{15}$$

where, ϕ - the temperature in °C; Equation (15) makes the saturated vapor pressure $p_{vs}(t)$ and consequently maximum air humidity $x_T(t)$ in (14) dependent on the temperature ϕ, hence the rate of change of moisture $\frac{dM}{dt}$ in (12) is also depends on temperature. Once equation (12) is established it can be incorporated into mass transfer problem (7) in form of mass sink or source function. Here the "sink" means the evaporation whereas "source" - the condensation. Namely:

$$Q_f = \frac{1}{\rho_w}\frac{dM}{dt} = \frac{1}{\rho_w}\Theta A \left(x_p(t) - x_T(t)\right) \tag{16}$$

where, ρ_w- density of water, in $\frac{kg}{m^3}$.
Function (16) accounts such phenomena as vapor transmission via its $x_p(t)$ term and heat transfer via its $x_T(t)$ term, while itself appears in mass transfer (filtration) problem (7). The filtration equation (7) in turn, redistributes the moisture within the wall due to hydraulic gradients and effects the heat conductivity value through (10).
The evaporation and the condensation phase change processes are also associated with the heat transfer as they are either endothermic as in case of evaporation consuming the heat from its surroundings, or exothermic as in condensation releasing the heat to its surroundings. Amount of heat consumed or released, is proportional to the amount of mass of water evaporated or condensed, i.e. it is proportional to (16). Then the heat sink/source function Q_h appearing in (5) can be written as:

$$Q_h = rQ_f \tag{17}$$

where, Q_f – moisture phase change (16); r - specific evaporation/condensation heat.
In [2] it is recommended the specific evaporation/condensation heat to be calculated as:

$$r = 595 - 0.55\phi \tag{18}$$

where, r - evaporation/condensation heat in kcal/kg; ϕ - temperature in °C.
Should r be assumed as a constant, say 595 kcal/kg, this simplification creates an error in the range of 2.0% - 2.5% in r value, which might be ignored. Alternatively (18) can be fully used in the calculations then an additional term occurs in (9) which needs to be handled as per finite element method procedure. Present study uses constant value for r.

2.5. Vapor Transfer

Vapor transfer problem, as it is defined in (8), with the boundary conditions (3), (4), after the finite element discretization, becomes a system of linear ordinary first order differential equations that have an analytical solution:

$$\{\dot{p}\} = [C_p]\{p\} + \{P\} \xrightarrow{solution}$$
$$\{p(t)\} = e^{[C_p]t}\{p_0\} + \int_0^t e^{[C_p](t-\xi)}\{P(\xi)\}\,d\xi \tag{19}$$

where, $\{p_0\}$ - is a vector of initial values (partial vapor pressure distribution within the wall at t = 0), which can be assumed as a linear interpolation between $p_{v,in}(0)$ and $p_{v,out}(0)$ as per given boundary conditions (3) and (4).
Vector notation $\{\cdot\}$ means that (19) results in a vector of nodal vapor pressure functions of time of the corresponding finite element model.
Boundary conditions (3) and (4) are assumed to be essential or Dirichlet boundary conditions.

2.6. Heat and Mass Transfer

Mass transfer or filtration problem (7) has the following finite element form:

$$\{\dot{h}\} = [C_p]\{h\} + \{F\} \tag{20}$$

Here the vector $\{F\}$ is a finite element transformed form of (16) thus it also depends on temperature through the link between (15) → (14) → (16). Therefore, in order to establish this function and solve (7) for a given time t_d, it is necessary to have the temperature distribution function $\phi(t)$. Should this function be guessed or somehow estimated then semi-analytical solution to (7) can be found as follows:

$$\{h^{\langle 0\rangle}(t)\} = e^{[C_h]t}\{h_0\} + \int_0^t e^{[C_h](t-\xi)}\{F^{\langle 0\rangle}(\xi)\}\,d\xi \tag{21a}$$
$$\{h^{\langle 0\rangle}(t)\} = \int_0^t e^{[C_h](t-\xi)}\{F^{\langle 0\rangle}(\xi)\}\,d\xi \tag{21b}$$

as $\{h^{\langle 0\rangle}(t)\} = \{0\}$ according to (11), then (21b) can be used instead of more general (21a). As the function $h(t)$ depends on $\phi(t)$, which is the function we are looking for, then we have a non-linearity, as according to relationship (10), $h(t)$ values are needed to determine heat conductivity properties of the media. This nonlinearity is resolved by using Picard iterative approach method. Angle brackets $\langle\cdot\rangle$ in $h^{\langle 0\rangle}(t)$ denote the iteration number.

In order to achieve the rapid convergence of the solution one may use the linear heat transfer equation to obtain the temperature distribution function as first iteration for Picard method. Namely, the equation can be assumed as:

$$\frac{\partial \phi}{\partial t} = D_f \frac{\partial^2 \phi}{dx^2} + Q_{hBC} \overset{FEM}{\Longrightarrow} \{\dot{\phi}\} = [C_\phi]\{\phi\} + \{T_{BC}\} \quad (22)$$

where, Q_{hBC} - are the function that includes only the boundary conditions (1) and (2); D_f - see (10); see (9) for others.

Unlike in (9) the matrix $[C_\phi]$ in (22) is not time dependent and just a matrix of constants

Semi-analytical solution to (22) has the following form:

$$\{\phi^{\langle 0 \rangle}(t)\} = e^{[C_\phi]t}\{\phi_0\} + \int_0^t e^{[C_\phi](t-\xi)}\{T_{BC}(\xi)\}\, d\xi \quad (23)$$

where, $\{\phi_0\}$ - is a vector of initial temperature distribution in the wall at time $t = 0$. Similarly to $\{p_0\}$, the initial values of $\{\phi_0\}$ in discrete nodes might be assumed as linear interpolation between $\left[\left(\phi_{in} = \Phi_{in}(0)\right) \cdots \left(\phi_{out} = \Phi_{out}(0)\right)\right]$ as per (1) and (2).

Having determined the temperature distribution function at first iteration by (23), one may define the mass transfer function by using (21b).

Each following iteration for heat transfer problem requires the solution of (9) which is linearized by the results of previous iteration and becomes the second order partial differential equation with variable coefficients. The solution to this equation has the form of:

$$\{\phi^{\langle i+1 \rangle}(t)\} = e^{\int_0^t [C^{\langle i \rangle}(\tau)]d\tau}\{\phi_0\} + e^{\int_0^t [C^{\langle i \rangle}(\tau)]d\tau} \int_0^t e^{-\int_0^\xi [C^{\langle i \rangle}(\tau)]d\tau} \{T^{\langle i \rangle}(\xi)\} d\xi \quad (24)$$

where, $[C^{\langle i \rangle}(\tau)]$ - the matrix which elements are the functions of time via (10); $\{T^{\langle i \rangle}(\xi)\}$ - a vector which elements are the functions of time that include the boundary conditions and heat source/sink as per (17); i - iteration number.

Both (22) and (9) have non-essential or Neumann boundary condition as given by (1) and (2).

2.7. Assumptions

All formulation described in sections above are based on the following assumptions:

a) At any given point within the domain and at any given moment of time, the porous media, the moisture in its vapor and liquid phases are all in local thermodynamic equilibrium, i.e. have the same temperatures along with other properties;

b) Porous media is none-deformable and homogeneous within each element of the material of the wall;

c) Gas phase (air and vapor) obeys the ideal gas law;

d) Heat transfer by radiation is negligible and ignored;

e) Moisture transfer due to gravity is ignored;

f) Condensation and evaporation phenomena do not change the initial moisture content of the skeleton significantly such that the degree of saturation of the porous media might be assumed as a constant within time $t \in [0 \cdots t_d]$, where t_d - is the design time.

2.8. Computation Workflow

Proposed formulation has been converted into a computation workflow that then is used for developing of the computer program. Conversion of governing partial differential equations into finite element equations is omitted here, as this can be found in many resources [3].

Computation steps:

Step 1

Form three finite element models with the identical spatial discretization, one for each of problems, i.e. vapor transmission, heat transfer and filtration problem;

Step 2

For a given initial vapor pressure distribution $\{p_0\}$ establish a function of $\{p\} = \{p(t)\}$ by using (19);

Step 3

For a given initial temperature values $\{\phi_0\}$ and by using (23) establish a function of $\{\phi\} = \{\phi^{\langle i \rangle}(t)\}$ where $i = 0$;

Step 4
Having the functions of $\{p\} = \{p(t)\}$ and $\{\phi\} = \{\phi^{\langle i \rangle}(t)\}$ determined on the current iteration, establish the functions $Q_f = Q_f(t)$ and $Q_h = Q_h(t)$ as per (16) and (17) accordingly;
Step 5
Solve filtration problem by using (21) to establish $\{h\} = \{h^{\langle i \rangle}(t)\}$;
Step 6
Establish the functions $D = D(\{h\})$ for the material conductivities by using (10);
Step 7
Solve the heat transfer problem with variable coefficients by using (24) incorporating the conductivity functions as per *Step 6* and the heat sink/source functions $Q_h = Q_h(t)$ as per *Step 4*;
Step 8
Compare the temperature distribution values for a given time $t = 0 + t_d$ using the results of *Step 7* with the values of temperature distribution function used at *Step 4*. Should the difference between the values are in excess of acceptable limit, return to *Step 4* at the following iteration $(i = i + 1)$ where use temperature distribution function $\{\phi\} = \{\phi^{\langle i+1 \rangle}(t)\}$ as it is obtained in *Step 7*. If the difference is less than the acceptable limit then the problem is solved.
Above workflow assumes the linearization of differential equation (9) by Picard method. This method has been preferred comparing to any others because it allows to monitor the iterative progress of every physical phenomenon happening within the model, be it filtration or heat transfer; and interpret them in the framework of boundary conditions and material properties.

3. PROBLEM DEFINITION, RESULTS AND DISCUSSIONS

3.1. Problem Definition

Wall model is assumed to be as in Fig.1. The goal is to calculate the distribution of temperatures within the wall at the given moment of time.

***Given*:**
Inner brickwall thickness $\frac{20}{3}$ m
Insulation thickness $\frac{20}{3}$ m
Outer brickwall thickness $\frac{20}{3}$ m
Structure thicknesses are deliberately selected as wide in order to demonstrate the non-linear behavior.
Brickwall properties:
Heat conductivity $D_f = 0.340\frac{W}{m°C}$ and $D_m = 0.375\frac{W}{m°C}$
Unit weight $\gamma_{wall} = 400\frac{kg}{m^3}$
Vapor conductivity $k_{v_{wall}} = 0.17\frac{mgr}{m\ hr\ Pa}$
Filtration permeability $k_{f_{wall}} = 0.17\frac{m}{hr}$
Insulation layer properties:
Heat conductivity $D_f = 0.033\frac{W}{m°C}$ and $D_m = 0.121\frac{W}{m°C}$
Unit weight $\gamma_{wall} = 150\frac{kg}{m^3}$
Vapor conductivity $k_{v_{wall}} = 0.5\frac{mgr}{m\ hr\ Pa}$
Filtration permeability $k_{f_{wall}} = 1.5\frac{m}{hr}$
Vapor pressure boundary conditions:

$$p_{v,in} = 873 + 50\sin\left(\frac{\pi t}{12}\right), \text{ in } Pa$$
$$p_{v,out} = 378 + 314\sin\left(\frac{\pi t}{50}\right), \text{ in } Pa$$

Temperature boundary conditions:

$$\phi_{in} = 20 + 4\sin\left(\frac{\pi t}{12}\right), \text{ in } °C$$
$$\phi_{out} = -5 + 15\sin\left(\frac{\pi t}{12}\right), \text{ in } °C$$

Design time period $t_d = 20hr$.
Below are the figures showing the temperatures, vapor pressure and moisture change variations throughout the wall in their successive iterations.

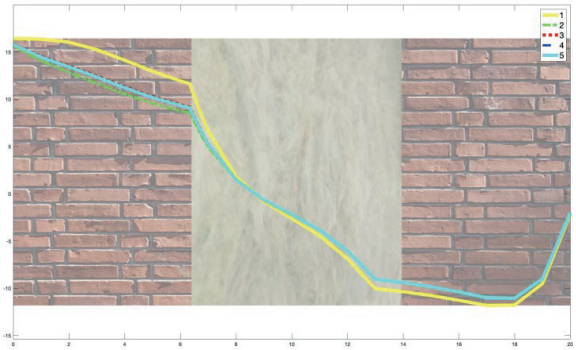


Figure 3. Temperature distribution within the wall at time $t = 20hr$. 1,2,3,4,5 – distribution curves for respective iteration.

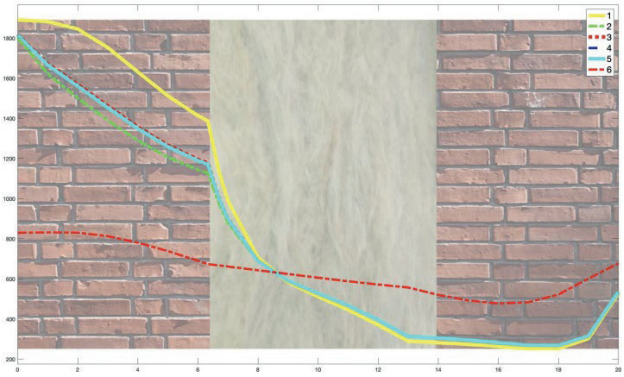


Figure 4. Saturated vapor pressure distribution within the wall at time $t = 20hr$. 1,2,3,4,5 – distribution curves for respective iteration. 6 - vapor pressure distribution as per vapour transit problem.

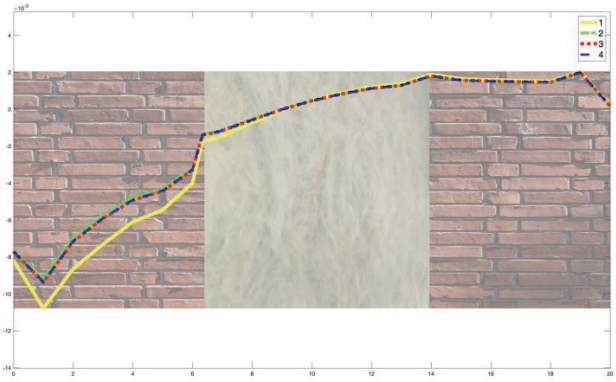


Figure 5. Moisture content variation curves at $t = 20hr$. 1,2,3,4,5 – distribution curves for respective iteration.

Calculation is considered as converged and completed when the following criterion is satisfied:

$$\frac{\left\|\phi^{\langle i\rangle}(t_d) - \phi^{\langle i-1\rangle}(t_d)\right\|_2}{\left\|\phi^{\langle i\rangle}(t_d)\right\|_2 + 1} \leq \epsilon_r$$

where, $\phi^{\langle i\rangle}(t_d), \phi^{\langle i-1\rangle}(t_d)$ – are i^{th} and $(i-1)^{th}$ iterations for temperature distribution functions evaluated at $t = t_d$; ϵ_r – allowable error (assumed to be 0.001); $\|\cdot\|_2$ - second norm of respective vector.

3.2. Discussions

The problem solved in Section 3.1 above has demonstrated how the solution iteratively has been found as per proposed workflow. Red dashed line 6 in Fig.4 represents the vapor pressure distribution at time $t_d = 20hr$ obtained by solving vapour transit problem (19). Yellow solid line 1 (Fig.4) is the saturated vapor pressure values being calculated based on linear heat transfer problem (see yellow line 1 in Fig. 3). The difference between red line 6 and yellow line 1 constitutes the evaporation if it is negative valued and condensation if it is positive valued. Point of intersection corresponds to the Dew Point temperature. The filtration problem (7) solved by accounting this difference results in moisture variation distribution as shown by yellow line 1 in Fig.5.

As the linear relationship is proposed in (Fig.2), the moisture content defines the heat conductivity property of respective material in tri-layered wall structure.

When all corrected values of heat conductivities D and heat sink/source functions Q_h are entered into heat transfer problem (9) and solved by (24) the temperature distribution curve in second iteration is obtained, which is represented by green dashed curve 2 in Fig.3 and as the saturated vapor pressure distribution curve 2 in Fig.4. As it can be seen, the temperatures within the wall from inner face till Dew Point location (a point of intersection of 1,2,3,4,5 curves with curve 6 in Fig.4) have decreased, comparing to the previous iteration, thereafter the temperatures are increased. This can be explained as follows:

- The wall, up until the Dew Point location experiences the evaporation which results in drying out of the wall material thus decreasing its conductivities as per (10). The lower the heat conductivity the higher the resistance to heat transfer, and the better its insulation properties. Also, the heat is partially consumed to compensate the evaporation heat. Therefore, the combined effect of reduced moisture content and the evaporation heat consumption explains why the temperature drops within this zone of the wall.
- Once the Dew Point location is crossed, evaporation changes into the condensation which increases the moisture content which in

turn increases the conductivity. The higher the conductivity the more the heat is transferred. Additionally, there is a heat expel due to the condensation process. Yet again, the combined effect of these two processes results in increase of the wall temperature comparing to its previous iteration.

Having calculated the temperature distribution functions by solving the non-linear problem in $t \in [0, t_d]$, these functions are used for the next iteration. The iterations fine-tune the evaporation and condensation amounts until the stabilized temperature distribution is achieved. These iterations are shown in different colors on the respective figures.

4. CONCLUSIONS

Proposed semi-analytical formulation and computation workflow give a powerful tool to calculate practical the mass and heat transfer problems in multi-layered structures taking into account the interaction in between the key physical processes. Finite element conversion of differential equations allows to define and incorporate many other phenomena mentioned in section 2.1 above thus making the formulation a universal tool.

However, the formulation has also some shortcomings that should be kept in mind while using it. They are briefly discussed below:

a) Unrestricted Moisture Content Change

Linear relationship as defined in (10) is continuous with practically no upper and lower bounds. Computationally the argument of (10) may take such a value that would make the heat conductivity value or the total moisture content less than minimum allowable values. Similarly, the moisture content may rise largely such that the material would not be able to hold that amount of liquid water.

The problem of excessive and negative valued moisture content in the model can be overcame by introducing the limiting values for moisture content for each material comprising the wall structure. In such case the equation (10) shall take the following form:

$$D\left(\frac{h(t)}{\rho_m}\right) = \begin{cases} D_{min};\ \forall W = \dfrac{h(t)}{\rho_m} < W_{min} \\ D_k \dfrac{h(t)}{\rho_m} + D_f;\ \forall W = \dfrac{h(t)}{\rho_m} \in [W_{min}, W_{max}] \\ D_{max};\ \forall W = \dfrac{h(t)}{\rho_m} > W_{min} \end{cases} \quad (25)$$

where, W_{min}, W_{max} - are respectively minimum and maximum moisture content that respective material may have; D_{min}, D_{max} - are respectively minimum and maximum heat conductivity coefficients of respective material.

b) Limitation of Saturation Degree during the Evaporation and the Condensation

Among the other assumptions made in formulation, one regarding the constant degree of saturation is arguable. Excessive condensation and evaporation will inevitably either fill in the voids of the material fully (till maximum degree) or dry it out till minimum possible moisture content. Dalton's model, as described in section 2.4, defines the amount of condensation or evaporation based on the contact area A as noted in (12) which is an area of interface surface between the liquid water and the air. Having assumed the saturation degree as constant, the contact area A becomes constant throughout the material as well. However, the saturation degree and thus the contact area at evaporation zone of the model may decrease, whereas it may increase at the condensation zone. Accordingly, the total amount of moist being evaporated should decrease as the material becomes drier and is actually less than that obtained by proposed calculation, whereas the total amount of condensation should increase and be more that it is calculated. This has an effect on temperature distribution as well. By intuition one may assume that the temperatures all throughout the wall would be slightly higher comparing to those obtained by proposed calculation.

The way to overcome this shortcoming is to introduce a function that would calculate the saturation degree in space and time and incorporate that function into the computation workflow.

Apparently, the saturation degree should be a function of moisture content $h(t)$ or $Sr = Sr(h)$, where Sr is a saturation degree having its value within a range of $[0 \cdots 1]$. Assuming at time $t = 0$ the saturation degree of the material to be $Sr = Sr_0$ then (16) can be rewritten as:

$$Q_f = \frac{1}{\rho_w}\frac{dM}{dt} = \underbrace{\frac{1}{\rho_w}\Theta A S r_0\left(x_p(t) - x_T(t)\right)}_{1^{st}\ term-sink/soource\ function} + \underbrace{\frac{1}{\rho_w}\Theta \mathrm{A}\left(x_p(t) - x_T(t)\right) Sr(h)}_{2^{nd}\ term-to\ be\ included\ into\ FEM} \quad (26)$$

Here, 1^{st} term in (26) is similar to (16) and is included into filtration calculations in accordance with proposed workflow. 2^{nd} term can be further developed by assumption:

$$Sr(h) = \alpha h \quad (27)$$

where, α - is some proportionality coefficient. Then second term will change the filtration governing equation (7) to the following form:

$$\frac{\partial h}{\partial t} = k_f \frac{\partial^2 h}{\partial x^2} + G(t)h + Q_{f1} \quad (28)$$

where,

$$G(t) = \frac{1}{\rho_w}\Theta \mathrm{A}\alpha\left(x_p(t) - x_T(t)\right)$$

Q_{f1}- is first term of right-hand side of (26).

This modification to filtration equation makes it a differential equation with variable coefficients. Accordingly, it will require the relevant solution method.

c) Filtration Formulation in Unsaturated Media

Filtration equation (16), even with the modifications as proposed in (b) above, does not accurately describe the flow happening within the wall. In [2] it is proposed to use the specific moisture content which is equal to

$$u = \frac{h(t)}{\rho_m}$$

and use relevant mass transfer coefficient of the media that includes the pore saturation degree as well. This is a kind of generalization of filtration phenomenon. However, should the filtration within the unsaturated media (the skeleton) be described in form of the equation similar to (7) that equation would become more complicated and non-linear. By intuition one may say that the proposed computation method gives conservative results as it assumes that flow occurs in a constant saturation degree, thus this non-linearity is ignored and the computation is simplified. The evaporation/condensation rate may account the saturation degree effect, if the modification as proposed in (b) is used, whereas for filtration problem the saturation degree effect is ignored posing inconsistency. The numerous computations being run for various initial conditions and using the materials properties that are common in construction industry, showed that mass transfer due to filtration is relatively small comparing to the condensation and evaporation, therefore one may assume that the saturation degree effect, if ignored in filtration problem only, may constitute an error within the permissible limits. Nonetheless this topic has to be investigated further.

d) Ice formation

Another phenomenon that has not been included into calculations is the ice formation within the part of the wall which has negative Celsius temperatures as well the liquid water properties within porous media which may vary at low temperature. In [1] it is proposed to introduce a coefficient ϵ_{ice} that reduces the function (16) at low temperatures such that it is correcting both filtration and heat transfer problems. Further investigations on the way how to include these factors into the calculations need to be done.

REFERENCES

1. SP 50.13330.2012 Thermal protection of buildings.
2. **A.B. Lykov**, Teoriya teploprovodnosti. [Heat transfer theory] // High Education, Moscow 1967. (In Russian).

3. **L.J. Segerlind.** Applied Finite Element Analysis. New York: John Wiley & Sons., 1984.
4. **C.H. Forsberg.** Heat Transfer Principles and Applications. London: Academic Press, Elsevier Inc., 2021.
5. ***Van P. Carey***. Liquid-Vapor Phase-Change Phenomena. An Introduction to the Thermophysics of Vaporization and Condensation Processes in Heat Transfer Equipment. 3rd edition. CRC Press, 2020.
6. **V.N. Kupriyanov, A.M. Yuzmukhametov, I.Sh. Safin**. Vliyaniye vlagi na teploprovodnost' steno-vykh materialov. Sostoyaniye voprosa. [Influence of moisture on the thermal conductivity of wall materials. Question status.] // Proceedings of KSUAU No. 1(39). Building structures of buildings and structures. 2017.
7. **H.P. Langtangen, K.A. Mardal.** Introduction to Numerical Methods for Variational Problems. Cham: Springer Nature Switzerland, 2019.
8. **P.V. O'Neil.** Advanced Engineering Mathematics. Boston: PWS Publishing Company, 1995.
9. **J.N. Reddy.** An Introduction to Nonlinear Finite Element Analysis with applications to heat transfer, fluid mechanics, and solid mechanics. 2nd edition. Oxford University Press, Oxford, 2015.
10. **K.P. Zubarev.** Using Discrete-Continuous Approach for the Solution of Unsteady-State Moisture Transfer Equation for Multilayer Building Walls. International Journal for Computational Civil and Structural Engineering. v.17, i.2, 2021, pp. 50 -57.
11. ***V.N. Sidorov, S.M. Mackewicz.*** Solving Unsteady Boundary Value Problems Using Discrete-Analytic Method for Non-Iterative Simulation of Temperature Processes in Time. Key Engineering Materials, Vol. 685, pp. 211-216, Trans Tech Publications Ltd., 2016 ISSN: 1013-9826 DOI: 10.4028/www.scientific.net/KEM.685.211

СПИСОК ЛИТЕРАТУРЫ

1. СП 50.13330.2012 Тепловая защита зданий.
2. **А.В Лыков**. Теория теплопроводности. Высшая школа, М., 1967.
3. ***L.J. Segerlind***. Applied Finite Element Analysis. New York: John Wiley & Sons., 1984.
4. **C.H. Forsberg**. Heat Transfer Principles and Applications. London: Academic Press, Elsevier Inc., 2021.
5. **Van P.Carey**. Liquid-Vapor Phase-Change Phenomena. An Introduction to the Thermophysics of Vaporization and Condensation Processes in Heat Transfer Equipment. 3rd edition. CRC Press, 2020.
6. **В.Н. Куприянов, А.М. Юзмухаметов, И.Ш. Сафин**. Влияние влаги на теплопроводность стеновых материалов. Состояние вопроса. // Известия КГАСУ №1(39). Строительные конструкции здания и сооружения. 2017.
7. **H.P. Langtangen, K.A. Mardal**. Introduction to Numerical Methods for Variational Problems. Cham: Springer Nature Switzerland, 2019.
8. **P.V. O'Neil.** Advanced Engineering Mathematics. Boston: PWS Publishing Company, 1995.
9. **J.N. Reddy.** An Introduction to Nonlinear Finite Element Analysis with applications to heat transfer, fluid mechanics, and solid mechanics. 2nd edition. Oxford University Press, Oxford, 2015.
10. **К.П. Зубарев.** Использование дискретно-континуального подхода к решению уравнения нестационарного влагопереноса в многослойных стенах зданий.
11. **V.N. Sidorov, S.M. Mackewicz.** Solving Unsteady Boundary Value Problems Using Discrete-Analytic Method for Non-Iterative Simulation of Temperature Processes in Time. Key Engineering Materials, Vol. 685, pp. 211-216, Trans Tech Publications Ltd., 2016 ISSN: 1013-9826. DOI: 10.4028/www.scientific.net/KEM.685.211

Vladimir N. Sidorov, Doctor of Engineering Science, member of Russian Academy of Architecture and Construction Sciences, head of a department, Department of Computer Science and Applied Mathematics, Moscow State University of Civil Engineering (MGSU), 26, Yaroslavl highway, Moscow, 129337, SidorovVN@mgsu.ru, 8-495-183-59-94;

Alim M. Primkulov, Master of Science, postgraduate student, Department of Computer Science and Applied Mathematics, Institute of Digital Technologies and Modeling in Construction, Moscow State University of Civil Engineering (MGSU), 26, Yaroslavl highway, Moscow, 129337, a.primkulov@prodim.ru, +7(926)907-75-94.

Владимир Николаевич Сидоров, доктор технических наук, член-корреспондент РААСН, заведующий кафедрой, кафедра информатики и прикладной математики, Федеральное государственное бюджетное образовательное учреждение высшего образования "Национальный исследовательский Московский государственный строительный университет" (НИУ МГСУ), 129337, г. Москва, Ярославское шоссе, д. 26, SidorovVN@mgsu.ru, 8-495-183-59-94;

Алим Махмудович Примкулов, аспирант, кафедра информатики и прикладной математики, Институт цифровых технологий и моделирования в строительстве, Федеральное государственное бюджетное образовательное учреждение высшего образования "Национальный исследовательский Московский государственный строительный университет" (НИУ МГСУ), 129337, г. Москва, Ярославское шоссе, д. 26, a.primkulov@prodim.ru, +7(926)907-75-94.

International Journal for Computational Civil and Structural Engineering, 19(3) 83–91 (2023)

DOI:10.22337/2587-9618-2023-19-3-83-91

FE MODELLING FOR CAPACITIES OF HEADED STUD SHEAR CONNECTORS IN COMPOSITE STEEL BEAMS WITH SLABS CONCRETE

Muthanna Abbu, Doaa Talib Hashim, Hasan M. A. Albegmprli

Northern Technical University (NTU), Mosul, IRAQ

Abstract. This study examines the performance of shear studs in composite steel beams. The ANSYS APDL program was used to investigate the impact of lateral horizontal pressure. The structure under analysis consists of a composite steel beam with a concrete slab. The beam section measures 254 x 254 (73 kg/m) and supports a slab measuring 1600 mm in length, 1200 mm in width, and 150 mm in height. It is embedded with 6 headed studs having a diameter of 19 mm, each measuring 100 mm in height, with a single row of pointed studs spaced at 150 mm intervals. Firstly, the study positioned itself 200 mm away from the end of the slabs on each side. The pertinent dimensions for this study were the headed studs and the limited load value. Only one parameter was altered, which was the load value. The simulated composite steel beam was analyzed for every alteration in the parameters. These results were then compared to those ones obtained from the experiment, revealing an alternative analysis that incorporated the aforementioned changes. Additionally, the Von Mises stresses and stress intensity were investigated in this study. Structural analysis indicated that the studs demonstrated resistance against horizontal slipping caused by lateral compressive loading. A parametric analysis of four composite steel beams was conducted using ANSYS Language of Design (APDL) to evaluate each parameter and eliminate other factors. The structure's performance was examined through the constructed software.

Keywords: composite steel beam, Finite Element, ANSYS, shear studs

КОНЕЧНОЭЛЕМЕНТНОЕ МОДЕЛИРОВАНИЕ НЕСУЩЕЙ СПОСОБНОСТИ ПО СДВИГУ СТАД БОЛТОВ В СТАЛЕЖЕЛЕЗОБЕТОННЫХ БАЛКАХ С БЕТОННЫМИ ПЕРЕКРЫТИЯМИ

Мутанна Аббу, Доа Талиб Хашим, Хасан М.А. Альбегмпрли

Северный технический университет (СТУ), г. Мосул, ИРАК

Аннотация. В данной работе рассматриваются общие характеристики сопротивления срезу болтов в композитной стальной балке. Работа композитной балки моделировалась с помощью программы ANSYS APDL. При этом учитывалось влияние бокового горизонтального давления. Анализируемая конструкция представляет собой композит балка-перекрытие. Сечение балки составляет 254 x 254 (73 кг/м), плитная часть имеет длину 1600 мм, ширину 1200 мм и высоту 150 мм и 6 стад-болтов диаметром 19 мм и высотой 100 мм в одном ряду, расположенных с интервалом 150 мм. Сначала исследовались участки конструкции на расстоянии 200 мм от торца плиты с обеих сторон. Величина предельной нагрузки на стад-болты являлась предметом данного исследования. При моделировании варьировалась только величина нагрузки на конструкцию. Для каждой композитной балки был выполнен анализ изменения параметров. Полученные результаты сравнивались с экспериментальными данными, что предоставило возможность дополнительного анализа рассматриваемых изменений параметров. Кроме того, были исследованы напряжения Фон-Мизеса и интенсивность напряжений. В результате выполненного структурного анализа было установлено, что в области стад-болтов возникают напряжения, вызванные сопротивлением сдвигу по горизонтальной поверхности от действия боковой нагрузки. Параметры оценивались в каждой из

четырех композитных балок. Для параметрического исследования использовалась программа ANSYS. Для исследования работы конструкции был использован язык проектирования (APDL).

Ключевые слова: сталежелезобетонная композитная балка, конечные элементы, ANSYS, стад-болты

1. INTRODUCTION

Steel structures have a significant market share in building construction. They are frequently used in combination with various types of precast concrete floors. By 2020, precast concrete floors are predicted to be utilized in 50% of multi-story steel frames, with this percentage expected to be significantly higher in several sectors such as hotels, residential buildings, and parking garages, according to the International Precast Concrete Association. As an alternative to traditional "down stand beam" construction, precast slabs can be used in both an "upstand beam" configuration (with slabs on top of beams) and as "upstand slabs". Wide spans between supporting beams can be achieved using precast units in both situations, providing a level soffit and lengthy spans [1].
Flatness was maintained throughout the entire floor area. The mechanical action of the shear connectors transmitted longitudinal shear force through the steel flange of the concrete slabs, which made contact in the steel concrete composite beams. The ability of the shear connections to transmit these longitudinal shear forces was determined by their strength, as well as the resistance of the concrete slab to the longitudinal cracking produced by the high concentration of shear forces. However, most of the research on composite construction has focused on conventional reinforced concrete and metal deck construction, with little information available on the shear capacity of precast hollow-core slabs with pointed studs [2].
The efficiency of structures can be increased through composite action, which involves combining structural components into a single composite section. Construction of composite beam designs is less expensive since it requires less material, allows for deeper floor depths to be kept to a minimum, and is quicker to complete. Furthermore, when compared to no composite alternatives, this technology is well known for the stiffness and strength improvements that may be achieved. It is essential to consider the degree of connection and interaction that exists between of the steel section and concrete slab when developing the structural behavior and design of composite beams. In engineering, a "shear connection" is a connection between two components that is capable of withstanding all stresses applied to them. This is probably the most common occurrence; nevertheless, the widespread usage of beams in building construction over the past two decades has led in more instances when the interconnection is unable to resist the full force of the forces applied to it partial shear connection. In this case, the connection may be break in shear before any of the other components reaches their respective failure states. When the connection between the components is considered to be eternally stiff, the situation is referred to as full interaction in the context of composite beams at their serviceability limit. However, although this is often assumed in design, it is theoretically unattainable, and situations where the stiffness of the link is restricted (partial contact) must be addressed. Depending on the circumstances, the connection itself may flex, producing relative movement along the steel concrete contact and increased the shear deformation throughout the beam.
Since the mid-nineteenth century, composite steel concrete systems have been used in a variety of applications. Mechanical interactions between concrete components and steel sections are represented by connections, dents or bumps

that are created either by friction or adhesion between the two materials. Typically, composite beams are constructed from a steel section (typically "I" shaped), which is situated in the majority of the tensioned zone, and a concrete slab, which is located in the majority of the compressed zone. They are metal devices that allow mechanical binding to be accomplished. Significant functions of shear connections include enabling slab/beam new the material joint operations, limiting longitudinal the slip and of the vertical displacements of interface components, and taking shear loads. Integrating steel and concrete in this way makes it possible to reap advantages of both the materials functioning in concert. Thus, from the viewpoint of material strength, it is possible to utilize steel sections to support tension loads while concrete is used to support compressive pressures. In addition to greater structural stiffness and reduced structural sections, this combination also results in a lighter foundation design, better material performance, and cheaper construction costs.

Shear connections are using to connect the solid concrete slab to the steel beam in the oldest kind of composite beams application. When headed studs were first introduced onto the market, channel connections were extensively utilized in the construction of bridges and buildings. (Ollgaard et al., 2010) [3] was the first to evaluate of shear capacity the headed stud. In order to do this, 48 'small scale' pushout specimens with the solid concrete slab were cast and tested, and the results were published. When designing the studs, it was important to consider their diameters (16 and 19 mm) as well as the quantity of studs per slab. The aggregates used in normal weight concrete and light weight concrete were two different kinds. Significant concrete features include the strength the concrete and its density. Modulus of the elasticity and split of concrete are also important. Concrete strength, density, modulus of elasticity, and split the tensile strength are all factors to consider. As a result of implanting the headed studs in light-weight concrete, test results of revealed a significant reduction in shear connection resistance from (15 to 25 percent), leading to the conclusion that shear stud of capacity was primarily controlled by the modulus of elasticity and concrete's compressive strength. In addition, it was discovered that cross sectional size of the studs was a function of shear the strength in testing. The following experimental equation for estimating the shear of capacity the headed studs implanted in solid concrete slab was established as a result of this research for structural design purposes.

According to literature, demountable of shear connections have been the subject of very little investigation. In the 1960s, 1970s, and 1980s (Dallam, 1968) [4] and (Marshall et al., 1971) [5] were the first to explore the use of bolted shear connections in addition to (Dedic & Klaiber, 1984) [6], and (Hawkins, 1987) [7]. As previously indicated, high the strength-friction a grip bolts in the solid of concrete slab were the investigated using the push out method as well as full scale composite beams test as part of the previously mentioned research endeavors. The post-installation method was often used to put these bolts into the concrete slab after it had been cast, and this was a common practice. It takes more time to complete the post-installation process, on the other side. By using the push test method, Dallam [4] has examined the behavior of high the strength of grip bolt ASTM A325 and A449 in the composite the structures with three a different the diameters, (12.7 mm, 15.9 mm, and 19.9 mm) and a height (102 mm). The formwork for a bolt placement was not immediately noticeable. At serviceability limit stage, there was no evidence of sliding, and of ultimate the shear strength was almost double, that of weld studs, indicating that the design was successful.

Composite components were produced by connecting the concrete slabs and steel segments

together, utilizing shear connectors. (Anju and Smitha 2016) [8] have used four different kinds of shear connections were investigated, and best of connector for the certain composite beams, was selected based on its performance under static stress, with the loading and quantity steel in connector serving as of common variable. The (FE) was using to analyze of various types the steel shear connections in the composite beams. In this experiment, nodal displacements were applied in increments at a load of 155 kN, and the resulting displacements were compared with each other. Following the findings of the finite element FE research, it was discovered that channel type of shear, connection has low displacement than other the types, while the perfobond types connectors has the most displacement the applied loads.

2. MATERIAL AND METHODS

The experimental study of (Lam, 2007) [9] has been used to conduct a modeling using software program. The analyzed structure was the composite beam slab, beam section (254 X 254 X 73 kg/m) with slab (1600 mm X 1200 mm) and 6 headed studs 19 mm diameter with 100 mm high with the single row of studs with headed spaced at 150 mm distance. The first stud was 200 mm from the end of the slabs. The headed studs and the value of the limited load were the most relevant dimensions for the aims of this study. One parameter was changed the change was in load value. The resulting composite steel was analyzed for each change in a parameter. The results were compared to those from the experimental, which revealed a possible alternate analysis that included the selected changes. In this parametric investigation, the experimental analysis was also examined for a constant slip of studs. The influence of load on slab was ignored in this section, and just the cross-section parameters were studied. Also, keep in mind that in the analysis, we selected a different load for each model that was almost equal to the experimental concentrated load values. Four composite steels were evaluated at each parameter and would chick with other factors.

3. FE MODELS

Composite beam slab models were simulated using an ANSYS finite element software [10]. The pressure was applied to measure the slip in the studs. Construction of a composite slab concrete with steel beam consists of three major parts: the concrete of slab, the structural steel beam and the connection stud. Three-dimensional line elements were used to represent these three components. A three-dimensional linear frame element was used to model the composite structure. The models were simulated using ANSYS, a commercial finite element software. Figure. 1 and Figure. 2 show the FE model, which was built using solid elements in both the slab and steel beam sections as well as, link element for the stud connection. The slab was attached to the steel beam by stud connectors. Solid185 components were utilized in the 3-D modeling of the slab concrete and steel beam in the model. It was necessary to model a stud connector using the TARGE170 element, and the CONTA173 element was required to model a point connection between slab concrete and the stud connector. A horizontal load was applied to the slab and the changes that occur in the screw were studied [11].

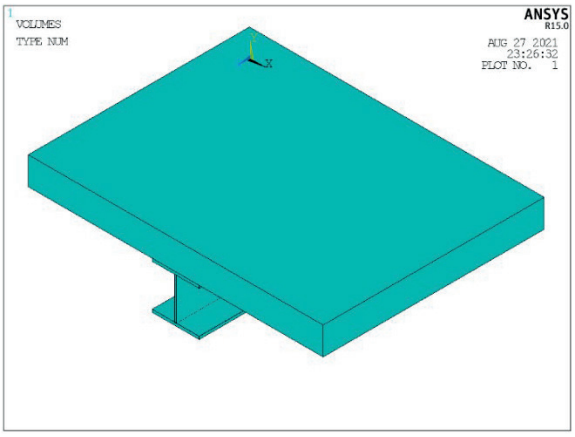


Figure 1. Showing the model beam steel with slab concrete

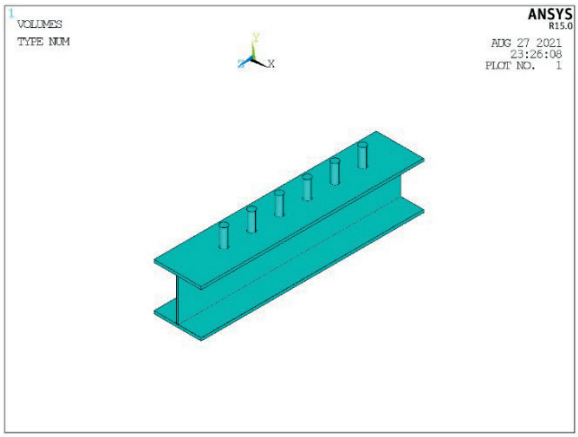


Figure 2. Showing the steel section with studs

4. RESULTS FOR VARIATIONS OF CROSS SECTION PARAMETERS

Figure 3 shows the deformation and the un-deformed model for the horizontal pressure on it. Table.1 and Figures. 4, 5, 6, and 7 show the results of the Finite Element Analysis (FEA) employing RC1, RC2, RC3 and RC4 along with the results of the loading tests, and design values. The design study showed that the stresses and horizontal movement obtained during the loading test were overstated. A composite structures behavior may be determined by using displacements and stresses obtained from finite element models. It's also possible to compare stress profiles with it. The slip studs in RC1 during the experiment was 3.7 mm, while it was 4.14 mm in an analysis done at a load of 71.7 kN for model RC1 by using ANSYS program. As well as the rest of the models as shown in the table.

Through the curve diagrams shown in the Figures 8 and 9, there is a small difference by following the curve between the experimental work and by the ANSYS which it caused by the difference of some laboratory conditions that led to the difference in the results, but the results of the slip were somewhat close to the experimental results. It was noticed that the increase in the slip has a direct relationship with the applied load as shown in the Table. 2. Table. 2 shows the values of slip (mm), at each applied load (KN), where random loading points were selected and slipping was determined.

Table 1. slip value results for FE models

Model Name	Maximum load to stud (kN)	Slip at Maximum load (mm) Experimental	Slip to Maximum load (mm) Simulation by ANSYS
RC1	71.7	3.7	4.14
RC2	102.6	6.3	5.93
RC3	101.6	6.9	5.88
RC4	100.1	6.2	5.79

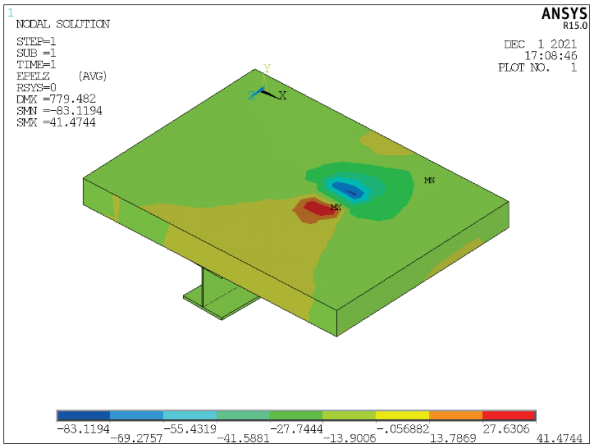


Figure 3. Deformed shape with undeformed model

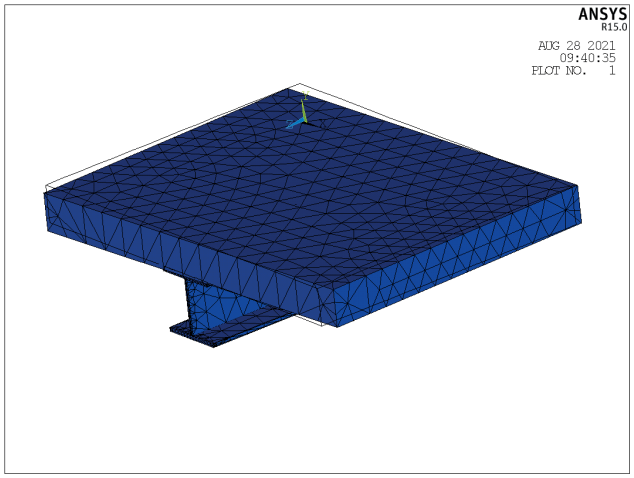


Figure 4. Slip value of numerical model RC1

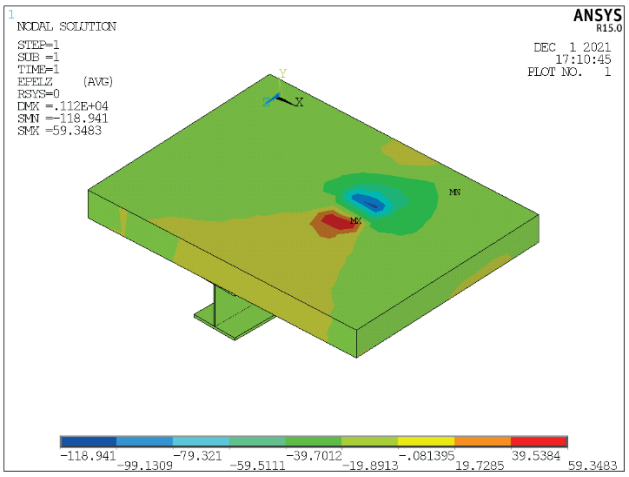


Figure 5. Slip value of numerical model RC2

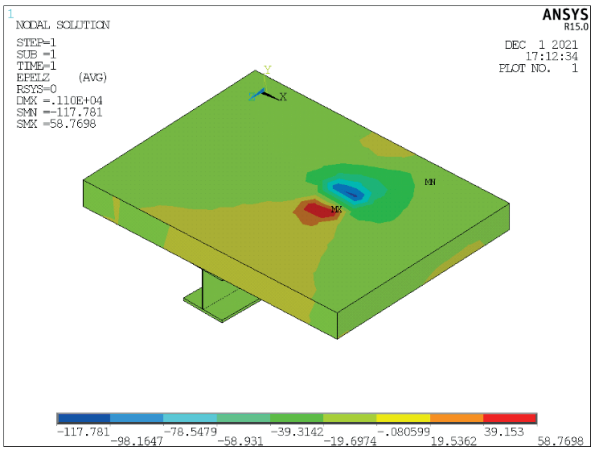


Figure 6. Slip value of numerical model RC3

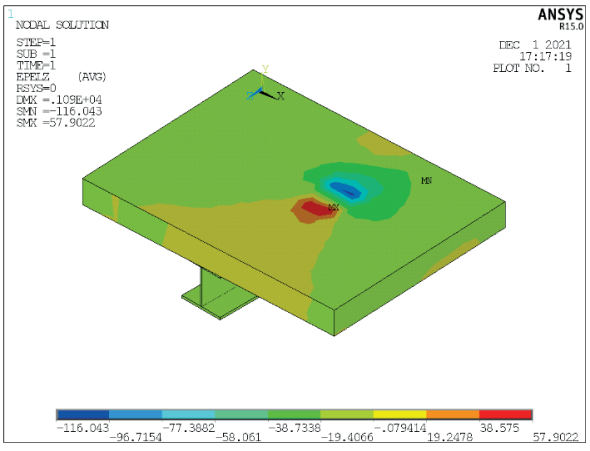


Figure 7. Slip value of numerical model RC4

Table 2. slip values with deferent loads

RC1	Load (kN)	0	3	16	30	38	53	60	67	71.7
	Slip (mm)	0	0.173	0.925	1.735	2.19	3.065	3.471	3.875	4.147
RC2	Load (kN)	0	10	21	33	45	67	80	95	102.6
	Slip (mm)	0	0.578	1.214	1.908	2.602	3.875	4.627	5.495	5.934
RC3	Load (kN)	0	7	18	31	49	62	75	90	101.6
	Slip (mm)	0	0.404	1.041	1.793	2.834	3.586	4.338	5.206	5.876
RC4	Load (kN)	0	5	17	25	41	58	72	83	100.1
	Slip (mm)	0	0.29	0.983	1.146	2.371	3.354	4.164	4.801	5.79

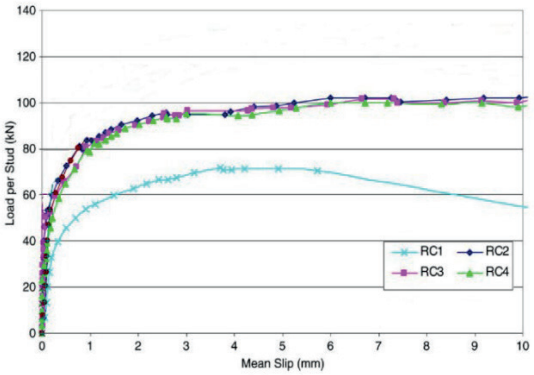


Figure 8. Showing experimental curve

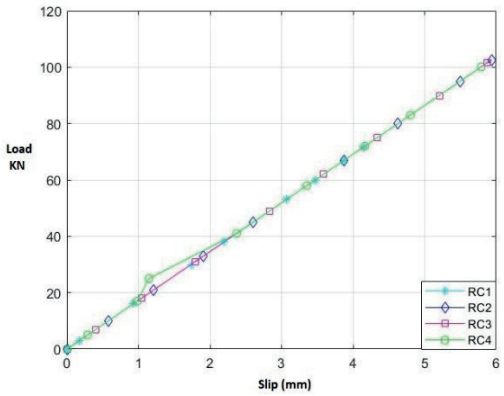


Figure 9. Showing ANSYS curve

5. RESULTS AND DISCUSSIONS

A computer program depended on finite element method for simulating the behavior of composite beam slab was used. The composite beam slab was modeled as three-dimensional structures using commercially available software. The parameters considered in the study include flange thickness, web thickness, span length, haunch ratio, concrete depth and web box depth. The aim of this study is to present a detailed description and explanation of the behavior of composite beam slab at several types of models under variety loads. Comparisons were made between stresses obtained for the composite beam slab according to many changes in the variety of the load. Finally, the parametric investigations were performed on the composite beam slab model, to evaluate of effects the several important parameters on behavior the composite beam slab. The results from this study would enable structures engineers to design composite beam slab more reliably and economically.

The results obtained from ANSYS FEM, were compared with the experimental results in the case of slip. It found that they were very close to reality and this indicated the correct work of the program.

6. CONCLUSIONS

The analyzed structure was a composite beam slab, beam section (254*254*73 kg/m) with slab (1600mm* length, 1200mm* width and 150mm high) and 6 headed studs 19mm diameter with 100mm high consisting of a single row of pointed studs spaced 150mm apart. The first stud is 200mm from the end of the slabs. The headed studs and the value of the limited load were the most relevant dimensions for the aims of this study. One parameter was changed the change was in load value. The resulting composite steel was analyzed for each change in a parameter. The results were compared to those from the experimental, which revealed a possible alternate analysis that included the selected changes. Using software utilizing Parametric analysis using ANSYS. Language of Design (APDL) is constructed to examine the behavior of the structure.

REFERENCES

1. **Markham P.** Temporary Works Toolkit, Part 3:Integration of permanent and temporary works. // The Structural Engineer, 2016.
2. **Queiroz, F. D., Vellasco, P. C. G.S., Nethercot, D. A.** Finite element modelling of composite beams with full and partial shear connection. // Journal of Constructional Steel Research, 2007, 63(4), 505–521.
3. **Ollgaard, J. G., Slutter, R. G., Fisher, J. W.** (2010). Shear strength of stud connectors in lightweight and normal weight concrete. // AISC Eng'g Jr., 2010, (71-10). Fritz Laboratory Reports. Paper.
4. **Dallam, L. N.** High strength bolt shear connectors-pushout tests. // Journal Proceedings, 1968, 65(9), 767–769.
5. **Marshall, W. T., Nelson, H. M., Banerjee, H. K.** An Experiment Study of the Use of High-Strength Friction Grip Bolts as Shear Connectors In Composite Beams. // *Structural Engineer*, 1971.
6. **Dedic, D. J., Klaiber, F. W.** High-strength bolts as shear connectors in rehabilitation work. // Concrete International, 1984, 6(7), 41–46.
7. **Hawkins, N. M.** Strength in shear and tension of cast-in-place anchor bolts. // Special Publication, 1987, 103, 233–256.
8. **Anjua, T., Smitha, K. K.** Finite Element Analysis of Composite Beam with Shear Connectors. // Procedia Technology, 2016, Volume 24, Pages 179-187.
9. **Lam, D.** Capacities of headed stud shear connectors in composite steel beams with precast hollowcore slabs. // Journal of Constructional Steel Research, 2007, 63(9), 1160–1174.
10. **Ansys, I.** Programmer's Manual for Mechanical APDL. // 2009, Canonsburg, PA.
11. **Abbu, M., Ekmekyapar, T., Özakça, M.** 3D FE Modeling of Composite Box Girder Bridge.// 2nd International Balkans Conference on Challenges of Civil Engineering, 2013, May, 23–25.

СПИСОК ЛИТЕРАТУРЫ

12. **Markham P.** Temporary Works Toolkit, Part 3:Integration of permanent and temporary works. // The Structural Engineer, 2016.
13. **Queiroz, F. D., Vellasco, P. C. G.S., Nethercot, D. A.** Finite element modelling of composite beams with full and partial shear connection. // Journal of Constructional Steel Research, 2007, 63(4), 505–521.
14. **Ollgaard, J. G., Slutter, R. G., Fisher, J. W.** (2010). Shear strength of stud connectors in lightweight and normal weight concrete. // AISC Eng'g Jr., 2010, (71-10). Fritz Laboratory Reports. Paper.

15. **Dallam, L. N.** High strength bolt shear connectors-pushout tests. // Journal Proceedings, 1968, 65(9), 767–769.
16. **Marshall, W. T., Nelson, H. M., Banerjee, H. K.** An Experiment Study of the Use of High-Strength Friction Grip Bolts as Shear Connectors In Composite Beams. // *Structural Engineer*, 1971.
17. **Dedic, D. J., Klaiber, F. W.** High-strength bolts as shear connectors in rehabilitation work. // Concrete International, 1984, 6(7), 41–46.
18. **Hawkins, N. M.** Strength in shear and tension of cast-in-place anchor bolts. // Special Publication, 1987, 103, 233–256.
19. **Anjua, T., Smitha, K. K.** Finite Element Analysis of Composite Beam with Shear Connectors. // Procedia Technology, 2016, Volume 24, Pages 179-187.
20. **Lam, D.** Capacities of headed stud shear connectors in composite steel beams with precast hollowcore slabs. // Journal of Constructional Steel Research, 2007, 63(9), 1160–1174.
21. **Ansys, I.** Programmer's Manual for Mechanical APDL. // 2009, Canonsburg, PA.
22. **Abbu, M., Ekmekyapar, T., Özakça, M.** 3D FE Modeling of Composite Box Girder Bridge.// 2nd International Balkans Conference on Challenges of Civil Engineering, 2013, May, 23–25.

DOI:10.22337/2587-9618-2023-19-3-92-113

SEISMIC FRAGILITY EVALUATION OF SOIL-PILE-STRUCTURE INTERACTION EFFECTS SUBJECTED TO MAINSHOCK-AFTERSHOCK RECORDS

Souheyla Saddouki, Djarir Yahiaoui, Rafik Demagh

LGC-ROI, Department of Civil Engineering, Faculty of Technology, University of Batna 2, Batna, ALGERIA

Abstract: In most current seismic design on bridges, only mainshock actions are considered without incorporating the effect of mainshock-aftershock (MA) sequences and interaction soil-pile. However, a large mainshock usually triggers numerous aftershocks in a short period. This paperstudy the effect of mainshock-aftershock sequences on the behavior of interaction Soil-pile-structure system (**ISPS**). abeam on nonlinear Winkler foundation (BNWF) model is usingand subjected to non-linear static analysis and incremental dynamic analysis (IDA) leading finally to the fragility curves which are developed. These analyses aim to capture the collapse state of structures under aftershock events preceded by various mainshock levels. Results obtained from capacity curve, incremental dynamic and fragility curves of ISSP system. The analytical results show that in the MA sequences, for dense soil the vulnerable of mainshock-aftershock (MS-AS) loading are more damage due to mainshock loading for all diameter of the pile and the mass. For soft soil are more vulnerable to damage due to mainshock-aftershock (MS-AS) loading. But in the stiff clay the effect of mainshock-aftershock (MS-AS) loading for all the diameter of pile and for masse are neglected.

Keywords: bridge, interaction soil-pile-structure, Winkler foundation, dynamic analysis, fragility curves, mainshock-aftershock

ОЦЕНКА СЕЙСМИЧЕСКОЙ НЕУСТОЙЧИВОСТИ ЭФФЕКТОВ ВЗАИМОДЕЙСТВИЯ ГРУНТ-СВАЯ-КОНСТРУКЦИЯ, ПОДВЕРЖЕННЫХ ЗАПИСЯМ ОСНОВНЫХ ТОЛЧКОВ И АФТЕРШОКОВ

Сухейла Саддуки, Джарир Яхиауи, Рафик Демаг

LGC-ROI, Департамент гражданского строительства, Технологический факультет Университета Батны 2, г. Батна, АЛЖИР

Аннотация: В большинстве современных сейсмических расчетов мостов учитываются только основные толчки без учета воздействия последовательностей основных толчков и афтершоков (MA) и взаимодействия грунта и сваи. Однако сильный главный толчок обычно вызывает многочисленные повторные толчки за короткий период. В данной статье исследуется влияние последовательностей основных толчков и афтершоков на поведение системы взаимодействия «грунт-свая-сооружение» (ИСПС). балка на нелинейном фундаменте Винклера (BNWF) используется и подвергается нелинейному статическому анализу и инкрементному динамическому анализу (IDA), что в конечном итоге приводит к построению кривых хрупкости. Эти анализы направлены на то, чтобы зафиксировать состояние обрушения конструкций при афтершоковых событиях, которым предшествовали основные толчки различных уровней. Результаты, полученные из кривой емкости, кривых инкрементной динамики и кривых хрупкости системы ISSP. Аналитические результаты показывают, что в последовательностях MA для плотного грунта уязвимые нагрузки основного удара-афтершока (MS-AS) являются более разрушительными из-за нагрузки основного удара для всего диаметра. ворса и массы. Для мягкого грунта они более уязвимы к повреждениям из-за основного удара-афтершока (MS-AS). Но в жесткой глине влиянием главного ударно-афтершокового (MC-AC) нагружения по всему диаметру сваи и по массе пренебрегают.Ключевые слова: мост, взаимодействие грунт-свая-конструкция, фундамент Винклера, динамический расчет, кривые хрупкости, главный толчок-афтершок.

Ключевые слова: мост, взаимодействие грунт-свая-конструкция, фундамент Винклера, динамический расчет, кривые хрупкости, главный толчок-афтершок

1. INTRODUCTION

An earthquake-prone region has the potential to release several extreme earthquake events within a few decades. In one violent earthquake sequence, numerous strong aftershocks occur within several hours or days after the mainshock. For example, On February 6, around 4:15 a.m. local time, a magnitude 7.8 earthquake struck south-central Turkey (Türkiye) near the Turkey/Syria border. Just 11 minutes later, it was followed by a magnitude 6.7 aftershock. The largest aftershock at the time of writing was a M7.5 aftershock which struck 95 km (~60 miles) to the north. USGS observations and analyses indicate all these events are occurring within the East Anatolian fault system.

Bridges are required to withstand a disastrous earthquake without collapses, and retain sufficient capacity along emergency routes prior to/during potential aftershocks in order to promptly dispatch emergency vehicles to the impacted area [2]. In seismically active areas, bridges are subjected to the combined effect of a mainshock (MS) and a series of aftershocks. For example, the March 2011 Tohuku, Japan, earthquake with a moment magnitude (Mw) of 9 was succeeded by hundreds of aftershocks with at least thirty of them greater than Mw 6 [3]. Compared to the MS, the aftershocks (AS) may have significant intensity with a longer effective duration, and different spectral shape, energy content and specific energy density [4].

The diversity of the bridge constitutive components accentuates the need to consider a vast range of interactions, including deck-abutment, abutment embankment [5, 6] and soil-foundation-pier [7, 8] where the Soil-Structure Interaction (SSI) is deemed to represent the most prominent factor in modifying the dynamic response and seismic performance of bridges [9]. Owing to the multi-parametric nature of the soil domain, however, the impact (either favorable or unfavorable) of SSI on the seismic response of bridges is scarce and findings in this domain are conflicting [10]. Until recently, the consensus amongst researchers was that SSI effects are beneficial to the seismic response of bridges by providing a natural isolation layer beneath the bridge with additional flexibility and damping [11]. Mylonakis and Gazetas explored the performance of a simplified bridge-foundation system under a set of actual ground motion records on soft soil and concluded that the elongated period and increased damping of the system has an adverse effect on the imposed seismic demands [9]. In another study, Jeremic et al. conducted a comprehensive finite element analysis on the seismic performance of the I-880 viaduct in California and concluded that depending on the characteristics of the input excitation, SSI can be both beneficial and detrimental [12]. Several other studies have been carried out on the effect of SSI on the seismic response of bridges and shown that SSI has a conspicuous effect on the bridges having relatively light superstructures and heavy substructures regardless of the soil stiffness [10]. The influence of SSI on the seismic performance of the bridge system is a function of the adopted modeling approach of the underlying soil domain. These approaches can be categorized as (a) linear or nonlinear lumped springs at the column bases representing the dynamic characteristics of the of bridge foundations and the supporting soil deposit [13,14]; (b) coupled comprehensive 3D representation of the entire soil-foundation-bridge system [15,16]; and (c) employing the concept of Beam on a Nonlinear Winkler Foundation (BNWF) using a set of distributed dynamic soil springs (p-y, t-z, and q-z) to account for the nonlinear interaction along the length of the piles [17,18]. While the inherent nonlinearity and frequency-dependent nature of the soil is prohibitive in using lumped springs, and the computational cost of analyzing an integrated finite element model of the entire

soil-bridge system is cumbersome, BNWF is discerned to be the most easy-to-manipulate yet accurate approach for simulating the soil domain [17]. Numerous studies have investigated the influence of SSI on the seismic performance of conventionally designed bridges [15;19]. However, there are few publications available in the literature on the extent to which the SSI affects the structural response of seismically isolated bridges [20].

Seismic fragility analysis is a crucial approach to assess the earthquake performance of soil-pile interaction in order to improve the seismic design, retrofitting, and enhancing reliable decision-making on structural engineering. More recently, Ajamy et al.(2018)[21] have worked on an analytical approach to develop seismic fragility curves for an existing Jacket Type Offshore Platforms (JTOP) located in the Persian Gulf using the same data set as described in Ajamy et al. (2014)[22]. The approach used for developing the seismic fragility curves is based on the IDA global interaction method that takes intoaccount the effects of both epistemic and random uncertainties on the expected probability seismic performance of the JTOP. Shafieezadeh et al. (2013)[23] and Su et al. (2017) have used three-dimensional nonlinear FE models to evaluate the seismic performance of dock structures.

Su et al.(2017)[24]have used uncertainties in structural and soil properties as part of a numerical analysis to investigate the variability of seismic behavior of pile-supported wharves.Chara et al. (2016) [25]and Stefanidou et al. (2017) have estimated the effects of SSI on seismic fragility of bridges and building structures respectively. Xiaowei Wang et al.(2019)[26] have identified parameter sensitivity rankings for the evaluation of the seismic performance of bridges supported by groups of piles in liquefiable soils undergoing scour potentials

The primary goal behind the present study is to interrogate the prevailing perception that incorporating the ISSP effects mitigate the probability of damage to a bridge system and its comprising components subjected to mainshock and aftershocks seismic excitations. This research study aims to identify the structural and soil parameters (types of the sand, pile diameter and mass) that have the most and least sensitive effects on theseismic fragility of ISSP system. To reach this objective, a soil-pile-structure finite element (FE) model and a pushover analysis are used to determine the curve of capacity of the ISPS, define the damage condition criteria, and finally generate the fragility curves.

2. NUMERICAL TOOL AND MODELING STRATEGIES

The numerical analyses developed and described in this paper with different nonlinear modeling strategies were studied using the computer program SeismoStruct v7 (SeismoSoft and 2022)[27]. The program includes models for the representation of the behavior of spatial frames and soil under static and/or dynamic loading, considering both material and geometric nonlinearities. With this software, seven types of analyses can be performed, namely: dynamic and static time history (analysis, conventional and adaptive pushover, incremental dynamic analysis, modal analysis, and static analysis (possibly nonlinear) under quasi-permanent loading.

2.1. The Finite Element Model Of Frames

In this study, the elements with distributed inelasticity and all the elements are based on force formulations. In this approach, the entire member is modeled as an inelastic element, the source of such in elasticity beingdefined at the sectional level. The global inelasticity of the frame is obtained by integration of the contribution provided by each controlling section (Fig. 1). A major advantage of such models is the nonexistence of a predetermined length where the inelasticity can occur, because all the sections can have excursions in this field

of response. Though this approach is a closer approximation to reality, it also requires more computational capacity; that is, more analysis time, as well as memory and disk space (Calabrese et al. 2010) [28].

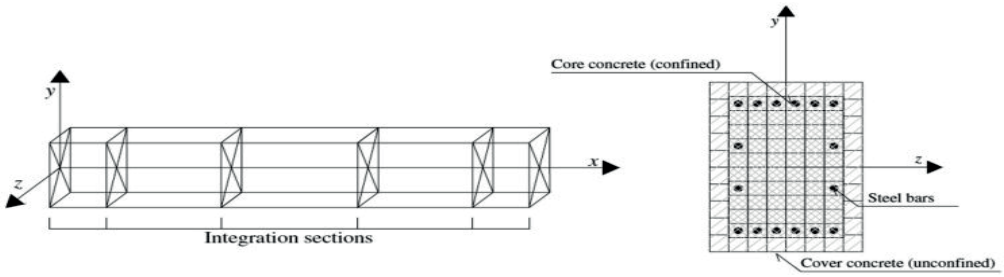


Figure 1. Example of controlling sections along the element and b section fiber discretization

The Material concrete of Mander model was used; to simulate concrete behavior with tensile strength and linear tension softening. For confined concrete material parameters, the equations proposed by Mander et al [29]. were used as represented in Esq.(2) and (3).

$$f_c = K f_c \left[\frac{2\varepsilon_c}{0.002K} - \left(\frac{\varepsilon_c}{0.002K}\right)^2\right]$$

$$K = 1 + \frac{\rho_s f_{\text{yh}}}{f_c}$$

Wherefyhis the hoops yield strength, ρs is the ratio of the volume of hoop reinforcement to the volume of the concrete core, fc, and εc are the concrete longitudinal compressive stress and strain. variable Kf'cand εcu are the ultimate compressive strength and compressive Strain of the confined concrete.

The cyclic behavior of the steel bars is simulated using the classical Menegotto and Pinto (1973) [30]model with kinematic hardening and possibility to take into account buckling by introducing a negative modulus slope in compression depending on the transverse steel reinforcement spacing. The monotonic behavior is defined through the initial Young's modulus (Es), the plastic threshold (esy, rsy), the ultimate strength and strain (eu, ru) and the yielding slope (Eh). The unloading and reloading process, is guided by analytic relations (Eq corresponding to a set of curves ranging between the elastic and the yielding asymptotes

$$\sigma^* = b\varepsilon^* + \left[\frac{1-b}{(1+(\varepsilon^*)^R)^{1/R}}\right]$$

where:

$$\sigma^* = \frac{\sigma_s - \sigma_r}{\sigma_0 + \sigma_r}$$

$$\varepsilon^* = \frac{\varepsilon_s - \varepsilon_r}{\varepsilon_0 + \varepsilon_r}$$

$$R = R_0 - \frac{A_i \xi}{A_j + \xi}$$

Tension: i = 1 and j = 2; Compression: i = 3 and j = 4. (rs, es) is the studied point; (ro, eo) is the crossing point of the elastic and yielding slopes; (rr, er) are the coordinates of the previous point of load reversion; b is the Eh/Es ratio; R is a shape parameter; n is the ratio between the maximum reached strain during loading; eo, Ro, Ai and Aj are material constants that can be obtained from experimental results. A detailed description of the model is presented in Menegotto and Pinto (1928)[31].

2.2. Definiton Ofpy Curves

The backbone curve defined in this model is a multilinear curve defined by fitting a given (theoretical or experimental) non-linear force displacement curve, namely a p-y curve. It is constituted by four segments that can either

simulate monotonic or post-peak behavior (Each slope is determined by the ratio to the initial stiffness of the backbone curve defined by the parameter K0. Cyclic behavior is achieved by introducing specific unload-reload rules. Fig. 2b shows the unloadingcurve, termed the General Unloading Curve (GUC) (segments 5 – 6) and the reloading curve, termed the Standard Reload Curve (SRC) (segments 7 – 8 – 9 – 10), derived by scaling the backbone curve by a factor based on the force at the beginning of reloading or unloading [32] andon the current cyclic degradation factor [33], i.e.

$$\kappa = 1 \pm \frac{p_{ur}}{\delta_s p_f}$$

in which pur is the current force at the onset of unloading or reloading, δs is the strength degradation parameter (described in more detail in the next paragraph) and pf is the ultimate force. The plus (+) and minus (-) signs denote unloading and reloading, respectively. The model simulates either progressive gapping with depth and with the number of load cycles, or pile moving through the slack zone. The Direct Reload Curve (DRC) simulates the soil reaction when the pile moves through the slack zone and is designed as a convex strain-hardening curve controlled by a limiting-force parameter related to the past maximum force. Fig. 2c depicts the formation of pure gap (segment 11), or slack zone (segment 12 characterized by a strain-hardening behavior simulating the densification of the loose caved-in soil).

A generalized fatigue formulation is implemented for simulating the cyclic soil hardening/degradation of both stiffness and strength wheresoil failure conditions and damage evolution functions are dealt separately. The failure condition curve (e.g., S–N curve from cyclic hardening/degradation function [32], used to estimate both the stiffness and strength hardening/degradation factors

$$\delta = 1 + (\delta - 1)\left[1 - (1 - D)^{\theta}\right]^{1/\theta_5}$$

where the subscript ζ stands for either k, the stiffness degradation factor, or s, the strength degradation factor. δ mζ represents the minimum or maximum amount of degradation, D the current cumulative damage and θζ the curve shape parameter. Fig. 3a shows the hardening factor, θζ, versus the number of cycles, N, the maximum hardening factor of δ mζ (> 1) can be achieved by either a concave (θζ< 1) or a linear (θζ =1) or a convex (θζ> 1) curve shape parameter. In Fig. 3b the degradation factor, θζ, versus the number of cycles, N; the minimum degradation factor of δ mζ (< 1) can be attained by either a concave (θζ> 1) or a linear (θζ =1) or a convex (θζ< 1) curve shape parameter. The hardening/degradation factor remains constant as δ mζ is reached. It is worth mentioning that the cyclic soil degradation and hardening is linked to an increase or decrease in the mean effective confining pressure due to the void ratio and pore pressurechanges. The fatigue model used in this paper might be also used for simulating the effects of the liquefaction in terms of degrading behaviour (Allotey and El Naggar[33,34]) but neglects the lateral spreading that can be accounted for by adding further inertial loads tothe pile (e.g. see Brandenburg et al.[35]). In this paper, non-liquefiablesoil deposits are considered.

2.3. Pile-Soil Interaction Analysis With Bnwf

The soil-pile interaction is evaluated using a BNWF model, which approximates the soil-pile interaction using non-linear (p-y) springs in parallel with stiffness proportional dampers. This allows estimating the relative displacements between soil and pile due to the free-field motion. In the BNWF model the pile itself is modelled as a series of beam-column elements, each with discrete springs connecting the pile to the soil, and the freefield motion obtained within the deposit is applied to the p-y springs as excitation to the system.

In this paper, the BNWF model proposed by Allotey and El Naggar[34]is employed for investigating the effect of soil nonlinearity on

the seismic performance of a single pile. This BNWF model is able to simulate generalized dynamic normal force-displacement relationships, accounting for cyclic soil degradation/hardening, soil and structural yielding, slack zone development and radiation damping. In addition, this BNWF model was revised [33] to account for the build-up of pore pressure due to cyclic loading and the different compaction levels of the soil in the vicinity of the pile in a simplified fashion. In particular, a generalized fatigue model based on the total stress method has been developed for simulating cyclic hardening/degradation of stiffness and/ or strength that can account implicitly for several hysteretic soil-pilebehaviours. Finally, results demonstrating the effects of soil non-linearity and the duration of strong motion on the seismic behaviour of piles are compared to the results obtained by the linear soil-pile interaction model defined by Dezi et al. [36,37].

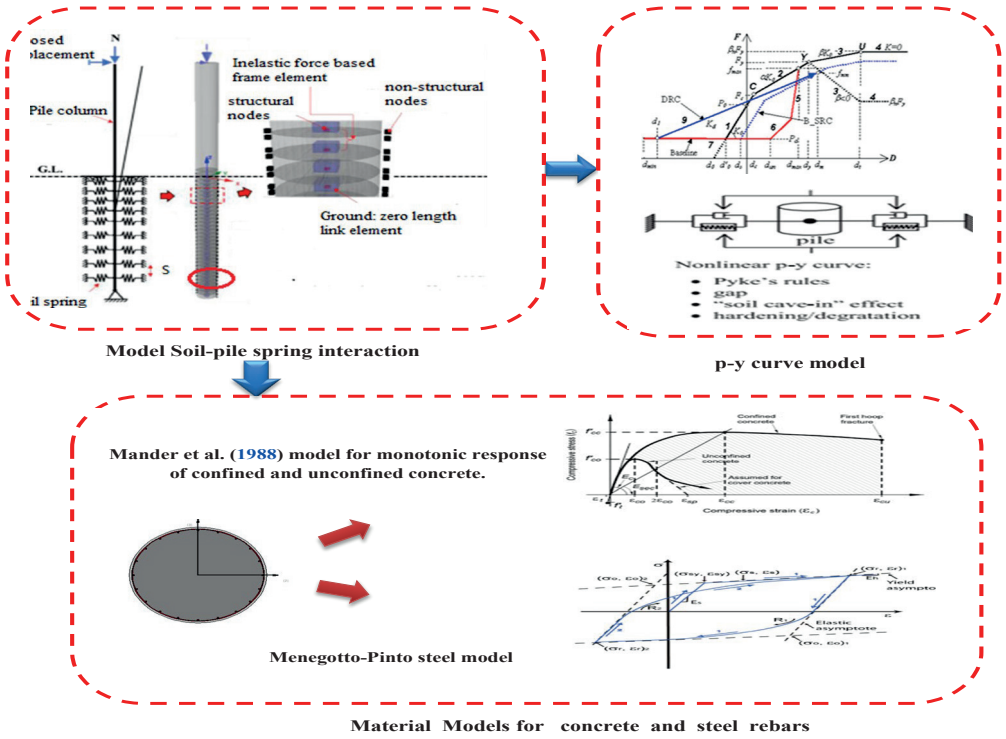


Figure 2. Numerical Tool and Modeling Strategie

3. INCREMENTAL DYNAMIC ANALYSIS AND FRAGILITY ASSESSMENT

IDA is a parametric analysis method that is used to estimate the structural performance under certain earthquake record (see [38]for details). It consists of the development of one curve, under each ground motion, for a specific damage measure (i.e. drift) versus a specific intensity measure of the ground motion (i.e. peak ground acceleration, PGA). The main objectives of IDA are simply to provide deep understanding of the response versus the potential level of the ground motion records and better understanding of the relation of the structural response versus the intensity of the ground motion (maximum displacement, strength, stiffness). This method has been widely used by several researchers in a nonlinear dynamic analysis (see[39;40], for example) as well as in studying pounding phenomenon (see [41-42] for example).

Fragility is the probability of reaching or exceeding a specified damage state. It is expressed in terms of a certain seismic parameter,such as spectral acceleration, spectral

displacement, peak ground velocity and PGA [43-44] Some researchers have provided historical background on the development of the fragility curves (see ,[45-46], forexample). Four different methods can be used to develop the fragility curves, i.e. the expert-based or judgmental method (it depends on the estimates and opinions of experts), empirical method (it is based on thedamage data reported from previous earthquakes - see Ioannou et al.,[47]for example), analytical method (it is based on the time history analyses), andhybrid method (it involves both experimental and numerical analysis [48]). Billah and Alam[49]described the advantages and disadvantages of each method. Among all of them, the analytical method is the most often used one since no experimental or damage datais required for it. One of the most simplest approaches among the analytical methods is the method developed by Ibrahim and El-Shami[50].

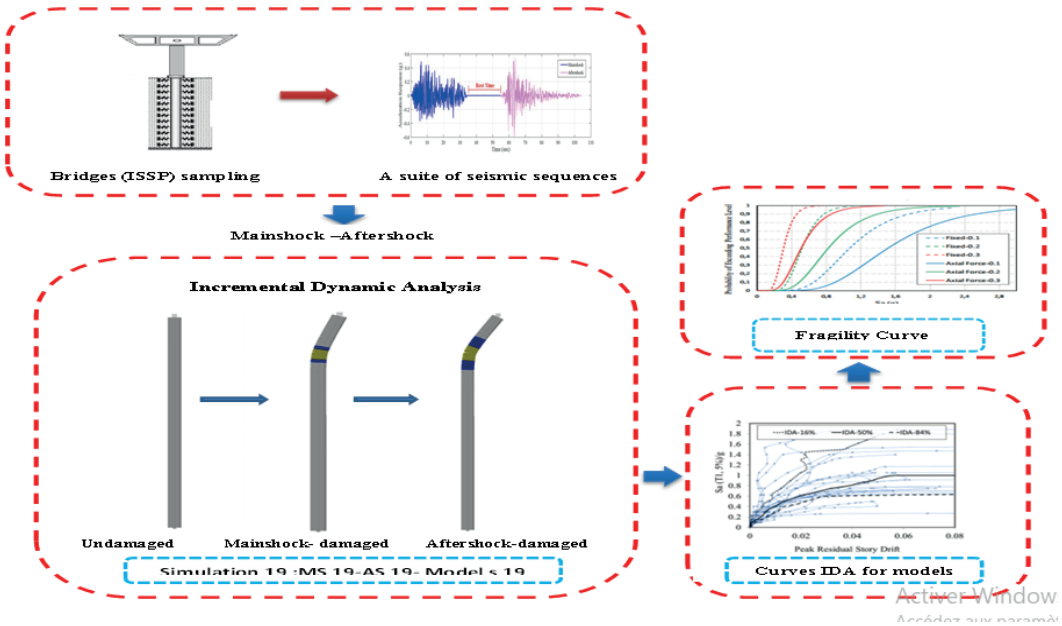


Figure 3. Incremental dynamic analysis method

In this method, the conditional probability of a structure to reach or exceed a specific damage state, D, given the PGA, is defined inEq. (3):

$$P(D/PGA) = \Phi((\ln(PGA) - \mu)/\sigma)$$

whereΦ is the standard normal cumulative distribution function; $\mu$and $\sigma$are the mean value and standard deviation of the natural logarithm of PGA at which the building reaches the threshold of a specific damage state or performance level, D.

Eq. (3) was developed based on the work of Shinozuka et al. [51] where the analytical fragility curves were constructed based on the nonlinear dynamic analysis and the fragility curves were represented by using two-parameter lognormal distribution functions estimated by the maximum likelihood method. The cumulative distribution functions were calculated by dividing the number of data points that reached or exceeded a particular damage state by the number of data points of the whole sample [52]. The accuracy of the use of the mean and standard deviation was investigated and the analytical interpretation of randomness and uncertainty associated with the mean was also provided [51]. Five different damage states/performance levels have been described in the literature, i.e. the operational performance (OP), immediate occupancy (IO), damage control (DC), life safety (LS), and collapse prevention (CP). These

performance levels are defined by certain damage measure, mainly the interstorey drift ratios (or percentages). The maximum allowable interstate drifts for each performance level may differ because it depends on the opinion of the expert. One of the most often used recommendations are the suggestions of Xue et al. [53] which are summarised in Table 1.

Table 1. Limit states considered in this study

Limit state	Transverse drift ratio %
occupancy (IO),	0.7
life safety (LS),	1.5
collapse prevention (CP).	2.5

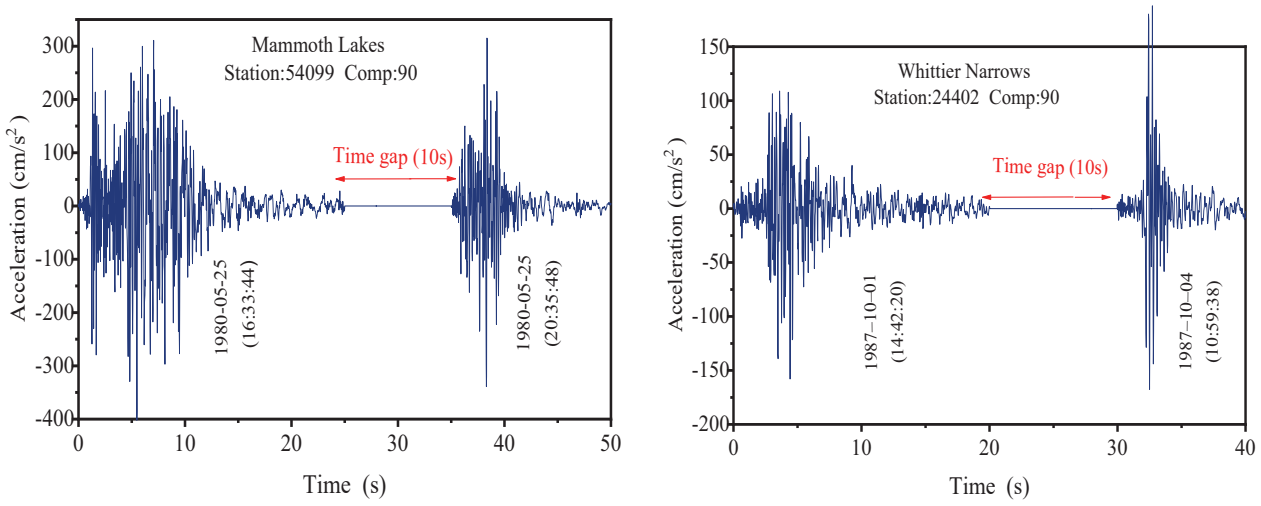
4. GROUND MOTIONS USED IN THE DYNAMIC ANALYSIS

In order to investigate the nonlinear behavior of the mainshockdamaged concrete gravity the ISPS systems for bridge subjected to strong aftershocks, seismic sequences including the mainshock and one major aftershock are needed for performing the nonlinear dynamic analyses. In this study, as-recorded mainshock–aftershock seismic sequences are selected according to the following criteria: (a) the magnitude of the mainshocks isequal to or greater than 5.5 and that of the major aftershocks is equal to or greater than 4.0, (b) accelerograms are recorded at stations, which are located in free fields or low-rise buildings, and (c) the predominant period (Tp) of the mainshocks is less than 0.4 s, which corresponds to the typical dam sites. With these criteria, 19 as-recorded mainshock–- aftershock seismic sequences shown in Table 2, which were recorded at the same station and in the same direction, are selected from the strong motion database of the COSMOS [54]. The data sample includes wellknown earthquakes with strong seismic activities, such as the Mammoth Lakes (1980), Kozani (1995), Whittier Narrows (1987), and Cape Mendocino/Petrolia (1992) events. For each of the 19 sequentialground motion records, the time gap between the mainshock and the aftershock seismic events is set to be 10 s as illustrated in Fig. 4, whichshows the aforementioned four representative mainshock–aftershock seismic sequences. This gap has zero acceleration ordinates and is adequate to allow the structure to cease moving after the previous seismic event.

Table2. List of mainshock-aftershock seismic sequences considered in this investigation

No	Seismicsequences	Station location	Comp.	Date	Mag	R (km)	Recorded PGA (cm/s2)	PredominantPeriod (s)	Duration (5–95%) (s)
1	Mammoth Lake	54099	90	1980-05-25(16:33:44) 1980-05-25 (20:35:48)	6.1(M_L) 5.7(M_L)	9.1 3.4	402.19 338.87	0.22 0.16	8.96 3.54
2	Mammoth Lake	54301	270	1980-05-25(16:33:44) 1980-05-25 (16:49:27)	6.06(M_L) 5.94(M_L)	14.1 14.4	303.97 372.42	0.1 0.25	7.72 3.42
3	ChalfantValley	54428	270	1986–07–21(14:42:26) 1986–07–21(14:51:09)	6.4(M_L) 5.6(M_L)	18.5 27.9	435.80 156.56	0.20 0.12	7.26 7.66
4	ChalfantValley	54428	360	1986–07–21(14:42:26) 1986–07–21(14:51:09)	6.4(M_L) 5.6(M_L)	18.5 27.9	394.60 101.54	0.24 0.12	8.16 11.16

5	ChalfantValley	54171	180	1986–07–21(14:42:26) 986–07–31(07:22:40)	6.4(M_L) 5.6(M_L)	23.7 15.5	249.10 179.66	0.24 0.34	12.76 14.16
6	ChalfantValley	54171	270	1986–07–21(14:42:26) 986–07–31(07:22:40)	6.4(M_L) 5.6(M_L)	23.7 15.5	169.00 121.44	0.36 0.24	17.04 17.18
7	Imperial Valley	0952	140	1979-10-15 (23:16:53) 1979-10-15(23:19:35)	6.5(M_w) 5.01(M_L)	5.2 13.9	539.78 221.36		
8	Imperial Valley	5055	225	1979–10–15(23:16:53) 1979–10–15(23:19:35)	6.5(M_w) 5.01(M_L)	8.8 12.3	242.96 112.67	0.19 0.22	13.32 12.84
9	Imperial Valley	5055	315	1979–10–15(23:16:53) 1979–10–15(23:19:35)	6.5(M_w) 5.01(M_L)	8.8 12.3	209.4 246.96	0.22 0.22	13.22 12.84
10	Kozani	ITSAK	0	1995–05–13(08:47:00) 1995–05–17(04:14:00)	6.1(M_L) 5.3(M_L)	19.5 12.1	211.03 126.19	0.20 0.22	5.84 5.41
11	Kozani	ITSAK	90	1995–05–13(08:47:00) 1995–05–17(04:14:00)	6.1(M_L) 5.3(M_L)	19.5 12.1	136.00 119.26	0.20 0.14	7.72 5.63
12	Whittier Narrows	24400	270	1987–10–01(14:42:20) 1987–10–04(10:59:38)	6.1(M_w) 5.3(M_w)	14.2 16.3	399.10 333.30	0.20 0.14	7.94 5.18
13	Whittier Narrows	24400	360	1987–10–01(14:42:20) 1987–10–04(10:59:38)	6.1(M_w) 5.3(M_w)	14.2 16.3	420.10 308.60	0.18 0.16	7.14 6.2
14	Whittier Narrows	24402	0	1987–10–01(14:42:20) 1987–10–04(10:59:38)	6.1(M_w) 5.3(M_w)	19.4 18..2	299.30 266.00	0.10 0.14	4.54 2.14
15	Whittier Narrows	24402	90	1987–10–01(14:42:20) 1987–10–04(10:59:38)	6.1(M_w) 5.3(M_w)	19.4 18..2	157.90 187.90	0.22 0.14	8.1 3.04
16	Whittier Narrows	24461	270	1987–10–01(14:42:20) 1987–10–04(10:59:38)	6.1(M_w) 5.3(M_w)	13.9 14.8	374.3 210	0.15 0.14	5.72 4.5
17	Northridge	Castaic-Oldridge route	90	1994-01-17 1994-01-17	6.69 5.93		568 138		
18	Northridge	Rinaldi Receiving Sta	318	1994-01-17 1994-03-20	6.69 5.28		472 476		
19	Northridge	0637	270	1994-01-17 1994-01-17	6.69 5.28				



(a) *(b)*

Figure 4. Four representative as-recorded mainshock–aftershock seismic sequence:(a) Mammoth Lakes, Station: 54099-Comp;(b) WhittierNarrows, Station: 24402-Comp

5. NUMERICAL MODELS OF BUILDINGS

Figure 5 shows a single column that extend to5m above and 30m below ground. The column has a uniform section and steel reinforcement. SeismoStruct v7 (SeismoSoft and 2022) software allows for strength and stiffness degradation in the components by providing the force deformation criteria for hinges used in the numerical analyses. The material properties of the structure, piles and soils are given in Tables 3and 4

Table 3. The problem investigated and the two types of presumed soil deposits

	Loose sand φ=30°	Dense sand φ=45°	Soft clay	Stiff clay
Kpy (below water table) (MN/m3)	5.4	12.66	0.5	30.

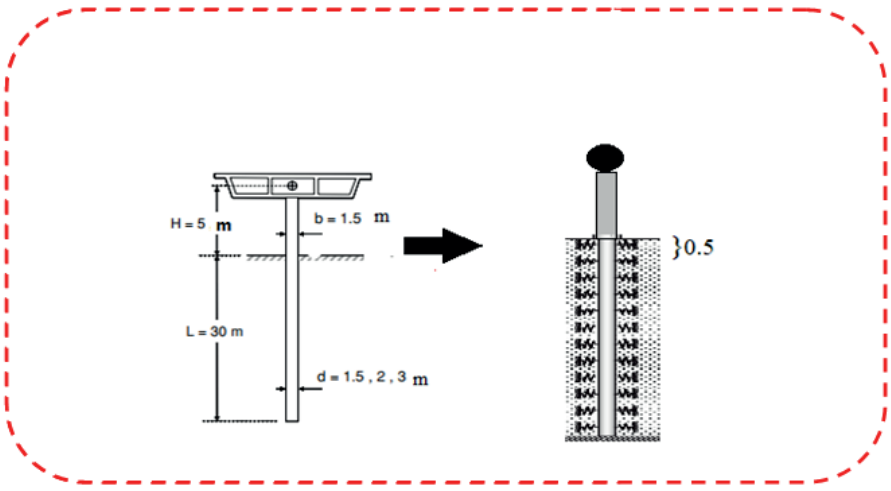


Figure 5. Interaction of soil-pile-structure configuration

Table 4. Parametric cases

Parameter	M(t)	Pile diameter, D (m)	Type of soil
Value	**150;350; 700**	**1.5 ; 2 ;3**	**(Loose,Dense)sand (soft,stiff) clay**

5.1. Pushover Results

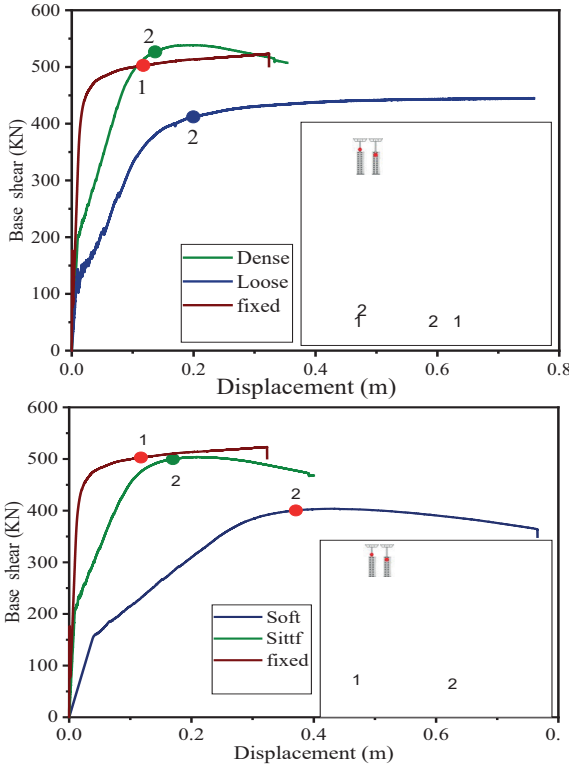


Figure 6. Lateral load-Displacement behaviour: the ISPS system and the fixed: a) sand; b) clay

Figure 6 show Lateral load-Displacement behaviour the ISPS system: a) sand; b) clay The results indicate that the lateral capacity of the dense sand more capacity and less ductility compared the loose sand and the fixed ,note in the result the lateral capacity of the soft caly gives a lower lateral capacity and more ductility compared the stiff clay

5.2. Ida Results

The figure 7 presented the IDA results obtained with nonlinearanalysis of 19 earthquakes for the two extreme cases (mainshock only and mainshock - aftershock) for ISPS system with dens soil type. In order to show the effect of earthquakes with the two extreme cases, after the end of IDA analysis, we take the average results of the acceleration for each displacement.

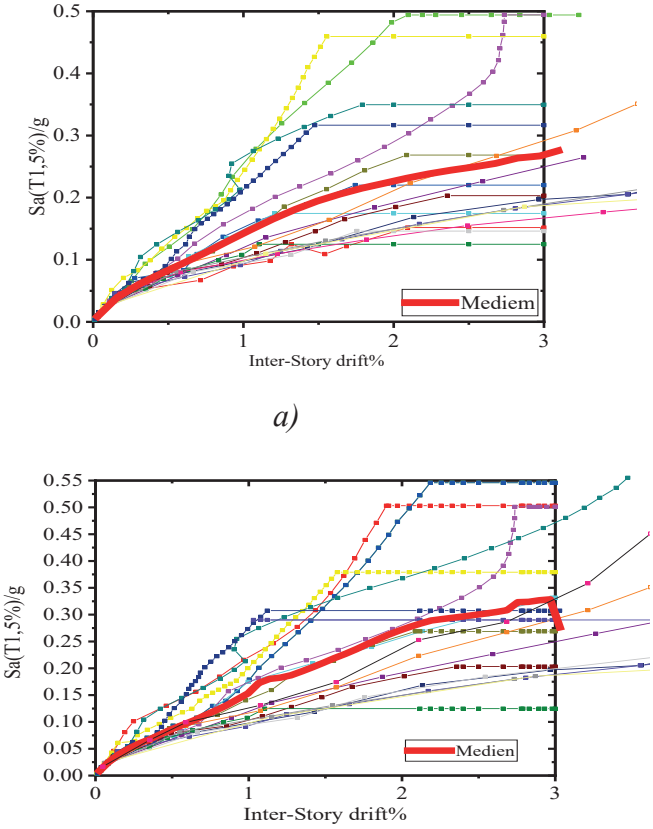
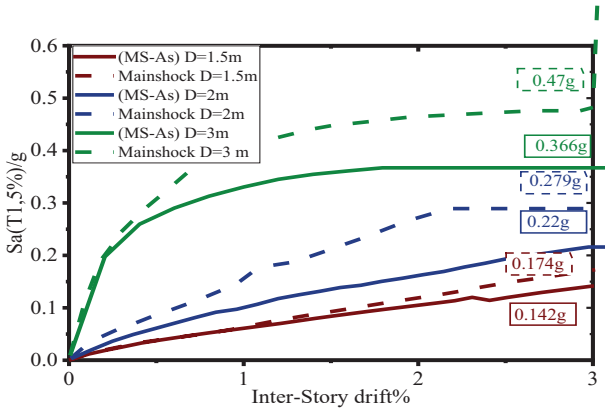


Figure 7. IDA results in ISPS system (a) Mainshock+Aftershock; (b) Mainshock

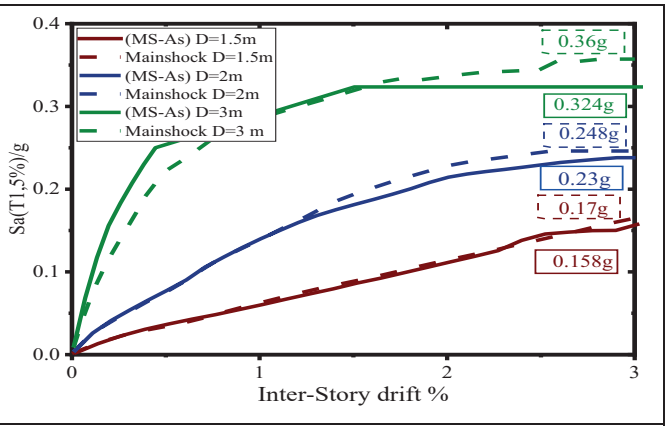
Effects of the Section of Pile

The average IDA curves for the ISPS systems for dense soil and Losse soil are presented in the Figs 8 The results indicated that the effect of the aftershock damage on ISPS are negative and depend on the diameter of the pile. For the dense soil, the results show the decrease in the values of acceleration after adding the aftershock earthquake with the percentage

18.3%, 21.5% and 23.04% for diameters 1.5m, 2m and 3m respectively. For the losses soil, the results show the slight decrease in the values of acceleration after adding the aftershock earthquake with the percentage 7.01%, 8.26% and 10.04% for diameters 1.5m, 2m and 3m respectively.

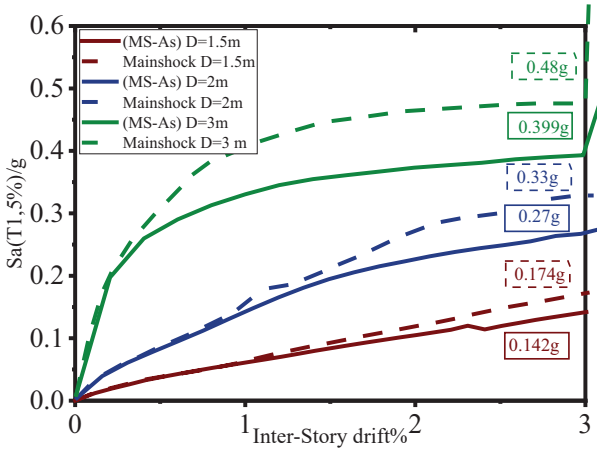


(a)Dense

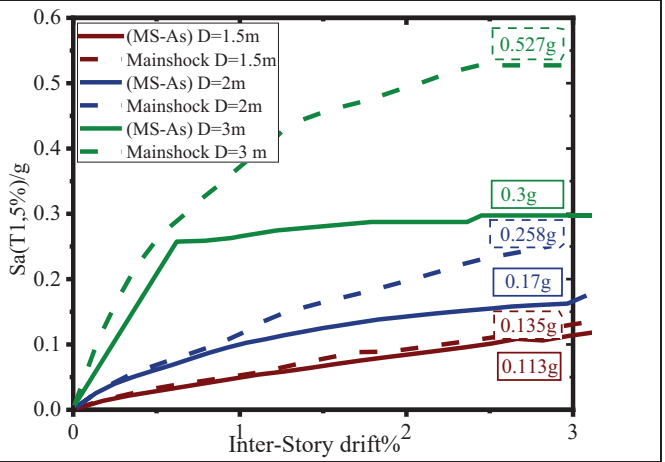


(b) Loose

Figure 8. Average IDA curves of in ISPS system different section :Mainshock+Aftershock; and Mainshock for Dense soil and Losse soil



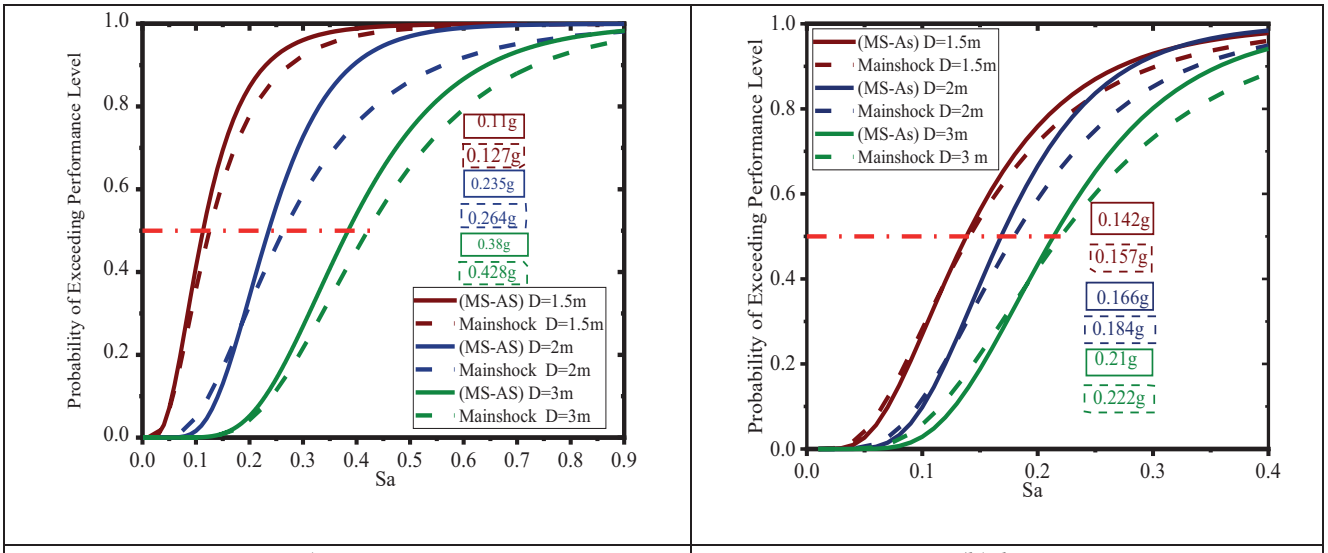
a) Soft



b) Stiff

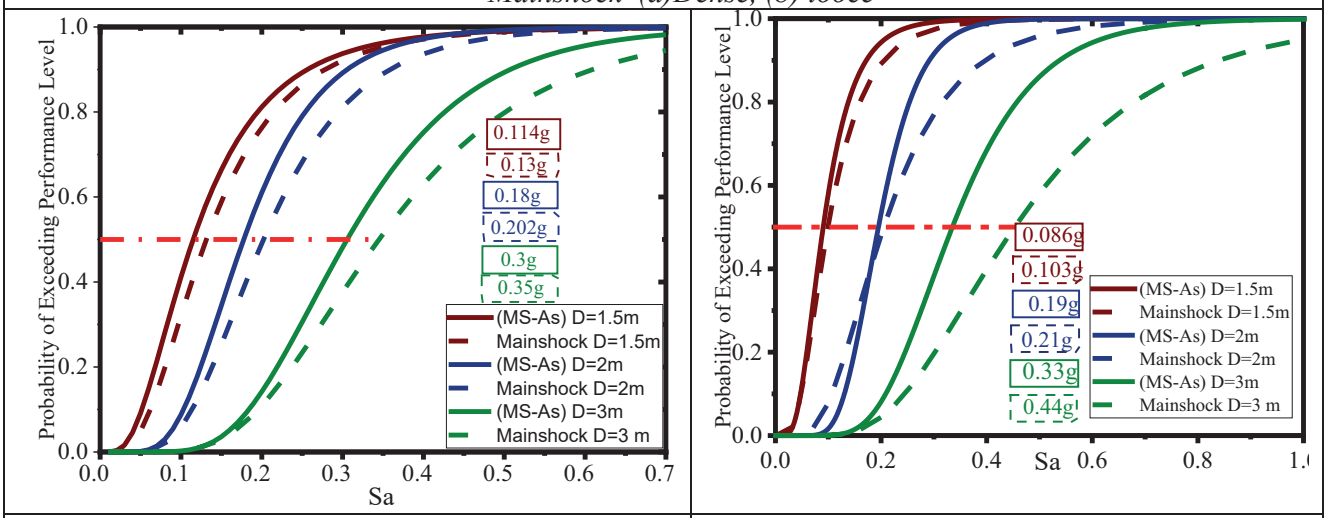
Figure 9. Average IDA curves of in ISPS system different section :Mainshock+Aftershock; and Mainshock for Soft and Stiff soils

Figure 9 The average IDA results forISPS systems for soft soil and stiff! soil shows that the consideration of aftershocks The influence can be seen in the differences between the median curves;increases the extent of ISPS systems responses and depend on the diameter of the pile; For the soft soil, the results show the decrease in the values of acceleration after adding the aftershock earthquake with the percentage 12.2%, 15.77% and 23.5% for diameters 1.5m, 2m and 3m respectively. For the stiff soil, the results show the decrease in the values of acceleration after adding the aftershock earthquake with the percentage 16.3%, 34.1% and 43.64% for diameters 1.5m, 2m and 3m respectively



a) Dense *(b) loose*

Figure 10. Fragility curves of theSPS system different section :Mainshock+Aftershock; and Mainshock (a)Dense, (b) looce



(a) Soft *(b) stiff*

Figure 11. Fragility curves of theSPS system different section :Mainshock+Aftershock; and Mainshock (a) Soft, (b) Stiff.

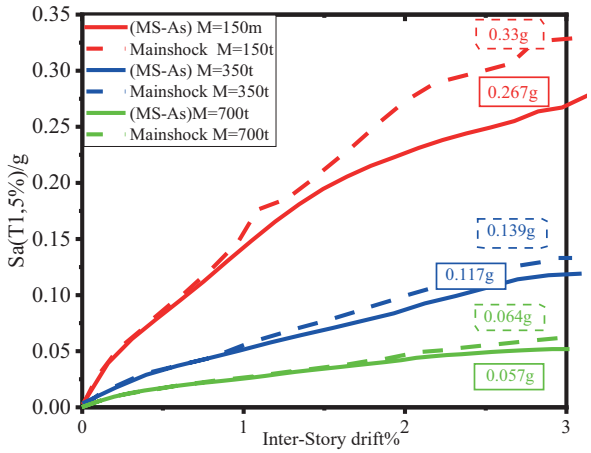
Figure 10 and 11 show the fragility curve under loading of Mainshock+Aftershock and Mainshock with variation of the pile section for Dense, loose, soft and stiff soil.For the probability of exceeding equal to 50%, when add aftershock and increase in the diameter of pile the damage state becomes more serious,for the dense sand the medium intensity S_{ct} are increased with 0.017g, 0.029g, 0.04g for 1.5 m, 2 m and 3 m diameters, respectively. As in the loose sand Sct are increased with 0.015g, 0.018g, 0.0212g for 1.5 m, 2 m and 3 m diameters, respectively. As for the soft caly are increased with 0.016g, 0.022g, 0.05g for 1.5 m, 2 m and 3 m diameters, respectively.

And for stiff clay the medium intensity Sct are increased with 0.017g, 0.02g, 0.11g for 1.5 m, 2 m and 3 m diameters, respectively.

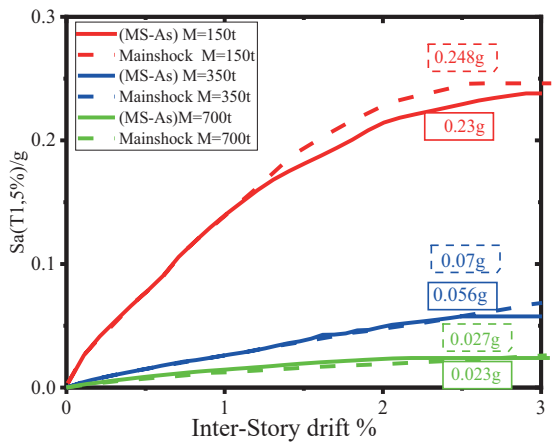
Effects of the mass

Fig. 12 shows the average IDA curves for ISPS systems for different types of sand (dense sand loose sand) under mainshock-only and the mainshock-aftershock loading with the varying of the masse (150t , 350t ,700t). Can be seen that the effect of the mainshock-aftershock loading are neglected when the inter-story drift as low as to 1%, but when the inter-story drift grate to 1% the effect it depends on sand types and masse.

For dense sand the results gives a decrease with 10.33% .15.83% and 18.57% for masse 150t, 350t and 700t respectively, and for loose sand with masse 150t the results give a decrease with 7.26% but for masse 350t and 700t the effect of aftershockare neglected.



(a)Dense



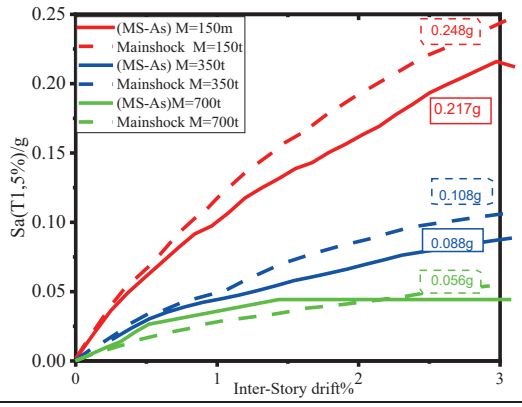
(b) Loose

Figure 12. Average IDA curves of in ISPS system different mass :Mainshock+Aftershock; and Mainshock: (a)Dens (b)Loose

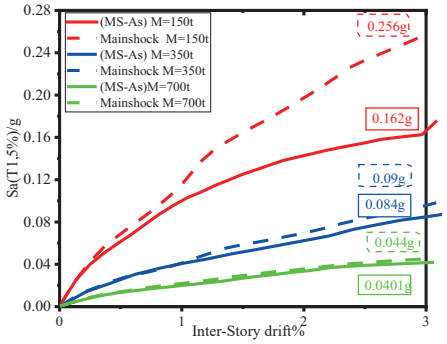
Fig. 12 shows the average IDA curves for ISPS systems for different types of clay (soft clay stiff clay) under mainshock-only and the mainshock-aftershock loading with the varying of the masse (150t , 350t ,700t). Can be seen that the effect of the mainshock-aftershock loading are neglected when the inter-story drift as low as to 1%, but when the inter-story drift grate to 1% the effect it depends on sand types and masse.

For soft clay the results gives a decrease with 12.5% 22.7% and for masse 150t, 350t and and 700t the effect of aftershockare neglected, and for stiff clay with masse 150t the results give a decrease with 36.7% but for masse 350t and 700t the effect of aftershockare neglected.

For the dense sand, the medium intensity S_{ct} are increased with 0.029g, 0.014g, 0.008g for 150t, 350t and 700t masse, respectively. As in the loose sand Sct are increased with 0.027g, 0.013g, 0.009g for 150t, 350t and 700t mass, respectively. As for the soft caly are increased with 0.022g, 0.017g, 0.015g for for 150t, 350tand 700t masse, respectively. And for stiff clay the medium intensity S_{ct} are increased with 0.012g, 0.009g, 0.008g for 150t, 350tand 700t masse respectively.In globale the results indicat that the efect of the masse and type of soil are effected by mainshock-aftershock.

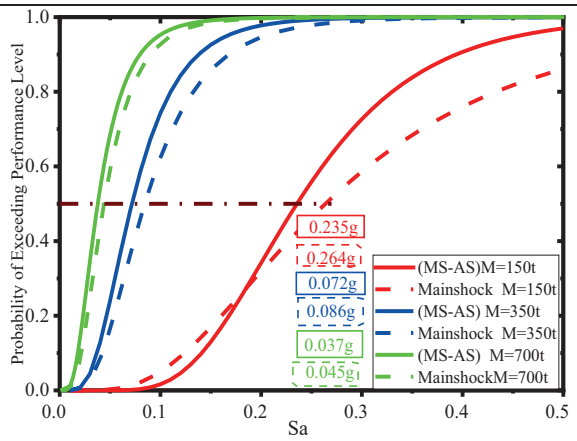


(a) Soft

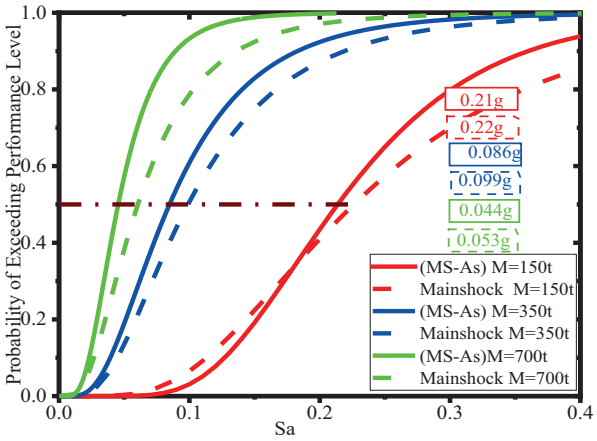


(b)Stiff

Figure 13. Average IDA curves of in ISPS system different mass :Mainshock+Aftershock; and Mainshock: (a) Soft ;(b)stiff

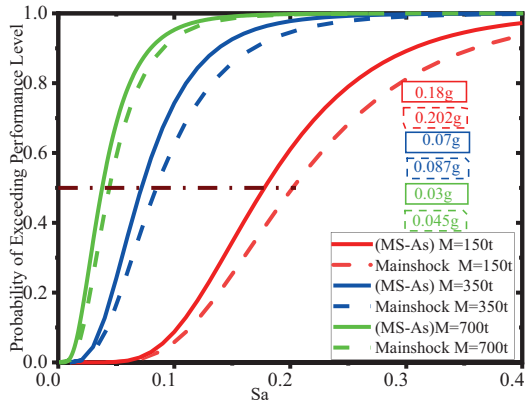


(a)Dense

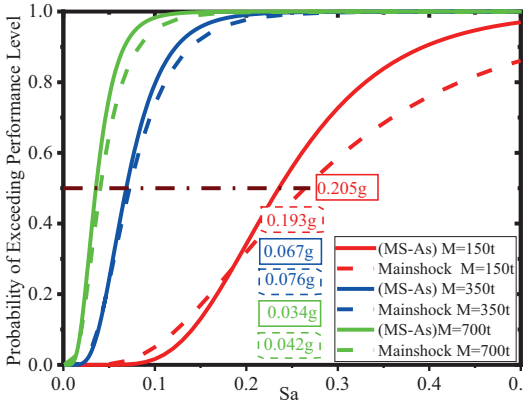


(b) Loose

Figure 14. Fragility curves of the ISPS system different mass :Mainshock+Aftershock; and Mainshock: (a) Denes; (b) Loose



(a)Soft



(b) stiff

Figure 15. Fragility curves of the ISPS system different mass :Mainshock+Aftershock; and Mainshock: (a) Soft; (b) Stiff

CONCLUSION

In this paper, the seismic evaluation of soil structure system (ISPS) with different soil, diameter and mass , subjected to sequential mainshock-aftershock records, was studied by means of the pushover analysis and IDA for generate the fragility curves. The effect of the soil type, masse, diametre of pile on ISPS system under mainshock (MS) and mainshock-aftershock (MS-AS) loading was investigated in this paper using the pushover, the IDA and the fragility assessment methods. Four type of soils (dense and loose sand, soft and stiff caly) with different masse (150t, 350t, 700t) and varing the diamtre of pile (1.5m, 2m, 3m) were considered in the study.From the findings of this research, the following conclusions can be drawn:

- In most cases, the lateral capacity of the loose gives a lower lateral capacity to dense sand, but about the ductility the loose sand more ductility. And for clay, the stiff clay show higher lateral capacity to soft clay.
- Based on both IDA and fragility assessment methods, the effect of type soil on ISPS system : for dense soil the vulnerable of mainshock-aftershock (MS-AS) loading are more damage due to mainshock loading for all diameter of the pile and the masse; But for loose sand the effect of aftershock are neglected after mainshock loading for all the diameter of the pile and the masse effect.
- The effect of clay type on ISPS system : for soft soil are more vulnerable to damage due to mainshock-aftershock (MS-AS) loading. but in the stiff clay the effect of mainshock-aftershock (MS-AS) loading for all the diameter of pile and for masse are neglected.

REFERENCE

1. **C.E. Administration,** Earthquake Site Work Outline and Technical Guidelines, Earthquake press, Beijing, 1998
2. **Chang L, Peng F, Ouyang Y, Elnashai AS, Spencer Jr BF.** Bridge seismicretrofit program planning to maximize postearthquake transportation networkcapacity. J Inf Syst 2012;18(2):75–88. http://dx.doi.org/10.1061/(ASCE)IS.1943-555X.0000082.
3. USGS, United states geological survey, 2012. <http://www.usgs.gov/>
4. **Li Y, Song R, Van De Lindt JW.** Collapse fragility of steel structures subjected to earthquake mainshock–aftershock sequences. J Struct Eng 2014.http://dx.doi.org/10.1061/(ASCE)ST.1943-541X.0001019
5. **Zhang J, Makris N.** Kinematic response functions and dynamic stiffnesses of bridgeembankments. Earthq Eng Struct Dynam 2002;31:1933–66
6. **Kotsoglou A, Pantazopoulou S**. Bridge–embankment interaction under transverse ground excitation. Earthq Eng Struct Dynam 2007;36:1719–40.
7. **Mylonakis G, Nikolaou S, Gazetas G.** Footings under seismic loading: analysis anddesign issues with emphasis on bridge foundations. Soil DynamEarthqEng2006;26:824–53.
8. **Elgamal A, Yan L, Yang Z, Conte JP.** Three-dimensional seismic response ofHumboldt Bay bridge-foundation-ground system. J Struct Eng 2008;134:1165–76.
9. **Mylonakis G, Gazetas G.** Seismic soil-structure interaction: beneficial ordetrimental? J Earthq Eng 2000/07/01 2000;4:277–301.
10. **Stefanidou SP, Sextos AG, Kotsoglou AN, Lesgidis N, Kappos AJ.** Soil-structureinteraction effects in analysis of seismic fragility of bridges using an intensity-basedground motion selection procedure. Eng Struct 2017;151:366–80.
11. **Ucak A, Tsopelas P**. Effect of soil–structure interaction on seismic isolated bridges.J Struct Eng 2008;134:1154–64.
12. **Jeremi´c B, Kunnath S, Xiong F.** Influence of soil–foundation–structure interactionon seismic response of the I-880

viaduct. Eng Struct 2004/02/01/2004;26:391–402.
13. **Xiang N, Alam MS.** Comparative seismic fragility assessment of an existing isolatedcontinuous bridge retrofitted with different energy dissipation devices. J BridgeEng 2019;24:04019070.L. Su, H.-P. Wan, Y. Dong, D. M. Frangopol, and .
14. **Yang C-SW, Werner SD, DesRoches R.** Seismic fragility analysis of skewed bridges in the central southeastern United States. Eng Struct 2015/01/15/2015;83: 116–28.
15. **Rahmani A, Taiebat M, Liam Finn WD, Ventura CE.** Evaluation of substructuring method for seismic soil-structure interaction analysis of bridges. Soil Dynam Earthq Eng 2016/11/01/2016;90:112–27.
16. **Xie Y, DesRoches R.** Sensitivity of seismic demands and fragility estimates of a typical California highway bridge to uncertainties in its soil-structure interactio modeling. Eng Struct 2019/06/15/2019;189:605–1
17. **Noori HR, Memarpour MM, Yakhchalian M, Soltanieh S.** Effects of ground motion directionality on seismic behavior of skewed bridges considering SSI. Soil Dynam Earthq Eng 2019/12/01/2019;127:105820.
18. **Mallick M, Raychowdhury P.** Seismic analysis of highway skew bridges with nonlinear soil–pile interaction. Transport Geotech 2015/06/01/2015;3:36–47.
19. **Carbonari S, Morici M, Dezi F, Gara F, Leoni G.** Soil-structure interaction effects in single bridge piers founded on inclined pile groups. Soil Dynam Earthq Eng 2017/01/01/2017;92:52–67.
20. **Gonz´ alez F, Padron ´ LA, Carbonari S, Morici M, Aznarez ´ JJ, Dezi F, et al.** Seismicresponse of bridge piers on pile groups for different soil damping models and lumped parameter representations of the foundation. Earthq Eng Struct Dynam 2019;48:306–27.
21. **Vlassis A, Spyrakos C.** Seismically isolated bridge piers on shallow soil stratum with soil–structure interaction. Comput Struct 2001;79:2847–61.
22. **Ajamy, A., Asgarian, B., Ventura, C.E., Zolfaghari, M.R.:** Seismic fragility analysis of jacket type offshoreplatforms considering soil-pile-structure interaction. Eng. Struct. 174, 198–211 (2018). https://doi.org/10.1016/j.engstruct.2018.07.066
23. **Ajamy, A., Zolfaghari, M.R., Asgarian, B., Ventura, C.E.:** Probabilistic seismic analysis of offshore platformsincorporating uncertainty in soil–pile–structure interactions. J. Constr. SteelRes. 101, 265–279 (2014). https://doi.org/10.1016/j.jcsr.2014.05.024
24. **Shafieezadeh, A., DesRoches, R., Rix, G.J., Werner, S.D.**: Three-dimensional wharf response to far-field andimpulsive near-field ground motions in liquefiable soils. J. Struct. Eng. 139(8), 1395–1407 (2013). https://doi.org/10.1061/(asce)st.1943-541x.0000642
25. **Stefanidou, S.P., Sextos, A.G., Kotsoglou, A.N., Lesgidis, N., Kappos, A.J.:** Soil-structure interaction effectsin analysis of seismic fragility of bridges using an intensity-based ground motion selection procedure. Eng. Struct. 151, 366–380 (2017). https://doi.org/10.1016/j.engstruct.2017.08.033
26. **Chara, C., Mitropoulou, C.C., Kostopanagiotis, C., Kopanos, M., Ioakim, D., Lagaros, N.D.:** Influence of soilstructure interaction on fragility assessment of building structures. In: Structures, pp. 85–98. Elsevier (2016). https://doi.org/10.1016/j.istruc.2016.02.005
27. **Wang, X., Ye, A., Ji, B.:** Fragility-based sensitivity analysis on the seismic performance of pile-group supported bridges in liquefiable ground undergoing scour potentials. Eng. Struct. 198, 109427 (2019). https://doi.org/10.1016/j.engstruct.2019.109427 program SeismoStruct v7 (SeismoSoft and 2022)

28. **Calabrese, A., Almeida, J. P., & Pinho, R.** (2010). Numericalissues in distributed inelasticity modeling of RC frameelements for seismic analysis. Journal of EarthquakeEngineering, 14(S1), 38–68.
29. **Menegotto, M., & Pinto, P.E.** (1973). Method of analysis forcyclically loaded reinforced concrete plane frames including changes in geometry and non-elastic behavior of elements under combined normal force and bending moment(pp. 15–22). Lisbon, Portugal: IASBE Proceedings
30. **Mander JB, Priestley MJN, Park R.** Theoretical stress-strain model for confinedconcrete. Struct Eng 1998;114(8):1804–26
31. **Richart, F.E., Brandtzæg, A., & Brown, R.** L. (1928). A studyof the failure of concrete under combined compressive stresses. University of Illinois Bulletin, 26(12)
32. **Pyke RM.** Nonlinear soil models for irregular cyclic loadings. J Geotech Eng Div,ASCE 1979;105(6):715–26
33. **Allotey N, Naggar MH El.** A consistent soil fatigue framework based on the number of equivalent cycles. Geotech Geol Eng 2007;26(1):65–77.
34. **Allotey N, Naggar MH E**l. Generalized dynamic Winkler model for nonlinear soil–structure interaction analysis. Can Geotech J 2008;45(4):560–73
35. **Brandenberg SJ, Boulanger RW, Kutter BL, Chang D**. Behavior of pile foundations inlaterally spreading ground during centrifuge tests. J Geotech Geoenviron Eng2005;131(11):1378–91.
36. **Dezi F, Carbonari S, Leoni G.** A model for the 3D kinematic interaction analysis ofpile groups in layered soils. Earthq Eng Struct Dyn 2009;38(11):1281–305
37. **Dezi F, Carbonari S, Morici M.** A numerical model for the dynamic analysis of inclined pile groups: a numerical model for the dynamic analysis of inclined pile groups. Earthq Eng Struct Dyn 2016;45(1):45–68.
38. **Vamvatsikos Dimitrios, Cornell C Allin**. Incremental dynamic analysis. EarthquakeEng Struct Dyn 2002;31(3):491–514
39. **Mander JB, Dhakal RP, Mashiko N, Solberg KM**. Incremental dynamic analysis applied to seismic financial risk assessment of bridges. Eng Struct2007;29(10):2662–7
40. **Chomchuen Prakit, Boonyapinyo Virote.** Incremental dynamic analysis with multimodes for seismic performance evaluation of RC bridges. Eng Struct2017;132:29–43
41. **Kazemi F, Mohebi B, Yakhchalian M.** Evaluation of the P-delta effect oncollapsecapacity of adjacent structures subjected to far-field ground motions.CivilEngJ2018;4(5):1066–73.
42. performance ofadjacent pounding structures using viscous dampers. In: The16thEuropeanConference on Earthquake Engineering; 2018. p. 18–21
43. **Kostov M.** Seismic fragility analyses. In "Regional Workshop On ExternalEventsPSA 6-10 November 2000, Sofia," 2000
44. **Duan X, Pappin JW.** "A procedure for establishing fragility functions for seismicloss estimate of existing buildings based on nonlinear pushover analysis,"in14thWorld Conference on Earthquake Engineering. Beijing: China; 2008. p. 12–7
45. **Kumitani S, Takada T.** Probabilistic assessment of buildings damage consideringaftershocks of earthquakes. 14th World Conference on EarthquakeEngineering.2008.
46. **Haran Pragalath DC, Davis R, Sarkar P.** Reliability evaluation of RC framebytwomajor fragility analysis methods. Asian J. Civil Eng. (BuildingAndHousing)2015;16:47–66.
47. Ioannou Ioanna, Douglas John, Rossetto Tiziana. Assessing the impact of groundmotion variability and uncertainty on empirical fragility

curves.SoilDynEarthquake Eng 2015;69:83–92.
48. **Kappos Andreas J, Panagopoulos Georgios, Panagiotopoulos Christos, Penelis Gregorios.** A hybrid method for the vulnerability assessment of R/CandURM buildings. Bull Earthq Eng 2006;4(4):391–413.
49. **Muntasir Billah AHM, Shahria Alam M.** Seismic fragility assessment of highway bridges: a state-of-the-art review. Struct Infrastruct Eng 2015;11(6):804–32.
50. **Ibrahim Yasser E, El-Shami Mostafa M.** Seismic fragility curves for mid-risereinforced concrete frames in Kingdom of Saudi Arabia. IES J PartA:CivilStructEng 2011;4(4):213–23.
51. **Shinozuka M, Feng MQ, Kim H-K, Kim S-H.** Nonlinear static procedurefor + fragilitycurve development. JEngMech 2000; 126 (12):1287–95.
52. **Shinozuka M, Feng M, Kim H, Uzawa T, Ueda T.** "Statistical analysis offragilitycurves. Technical Report." Multidisciplinary Center for Earthquake Engineering Research, MCEER-032003.
53. **Xue Q, Wu C-W, Chen C-C, Chen K-C.** The draft code for performance-based seismic design of buildings in Taiwan. Eng Struct 2008;30(6):1535–47.
54. COSMOSVirtualDataCenter.:⟨http://strong motioncenter.org/vdc/scripts/de

СПИСОК ЛИТЕРАТУРЫ

1. **C.E. Administration,** Earthquake Site Work Outline and Technical Guidelines, Earthquake press, Beijing, 1998
2. **Chang L, Peng F, Ouyang Y, Elnashai AS, Spencer Jr BF.** Bridge seismicretrofit program planning to maximize postearthquake transportation networkcapacity. J Inf Syst 2012;18(2):75–88. http://dx.doi.org/10.1061/(ASCE)IS.1943-555X.0000082.
3. USGS, United states geological survey, 2012. <http://www.usgs.gov/>
4. **Li Y, Song R, Van De Lindt JW.** Collapse fragility of steel structures subjected to earthquake mainshock–aftershock sequences. J Struct Eng 2014.http://dx.doi.org/10.1061/(ASCE)ST.1943-541X.0001019
5. **Zhang J, Makris N.** Kinematic response functions and dynamic stiffnesses of bridgeembankments. Earthq Eng Struct Dynam 2002;31:1933–66
6. **Kotsoglou A, Pantazopoulou S**. Bridge–embankment interaction under transverse ground excitation. Earthq Eng Struct Dynam 2007;36:1719–40.
7. **Mylonakis G, Nikolaou S, Gazetas G.** Footings under seismic loading: analysis anddesign issues with emphasis on bridge foundations. Soil DynamEarthqEng2006;26:824–53.
8. **Elgamal A, Yan L, Yang Z, Conte JP.** Three-dimensional seismic response ofHumboldt Bay bridge-foundation-ground system. J Struct Eng 2008;134:1165–76.
9. **Mylonakis G, Gazetas G.** Seismic soil-structure interaction: beneficial ordetrimental? J Earthq Eng 2000/07/01 2000;4:277–301.
10. **Stefanidou SP, Sextos AG, Kotsoglou AN, Lesgidis N, Kappos AJ.** Soil-structureinteraction effects in analysis of seismic fragility of bridges using an intensity-basedground motion selection procedure. Eng Struct 2017;151:366–80.
11. **Ucak A, Tsopelas P**. Effect of soil–structure interaction on seismic isolated bridges.J Struct Eng 2008;134:1154–64.
12. **Jeremi´c B, Kunnath S, Xiong F.** Influence of soil–foundation–structure interactionon seismic response of the I-880 viaduct. Eng Struct 2004/02/01/2004;26:391–402.
13. **Xiang N, Alam MS.** Comparative seismic fragility assessment of an existing isolatedcontinuous bridge retrofitted with different energy dissipation devices. J

BridgeEng 2019;24:04019070.L. Su, H.-P. Wan, Y. Dong, D. M. Frangopol, and .

14. **Yang C-SW, Werner SD, DesRoches R.** Seismic fragility analysis of skewed bridges in the central southeastern United States. Eng Struct 2015/01/15/2015;83: 116–28.
15. **Rahmani A, Taiebat M, Liam Finn WD, Ventura CE.** Evaluation of substructuring method for seismic soil-structure interaction analysis of bridges. Soil Dynam Earthq Eng 2016/11/01/2016;90:112–27.
16. **Xie Y, DesRoches R.** Sensitivity of seismic demands and fragility estimates of a typical California highway bridge to uncertainties in its soil-structure interactio modeling. Eng Struct 2019/06/15/2019;189:605–1
17. **Noori HR, Memarpour MM, Yakhchalian M, Soltanieh S.** Effects of ground motion directionality on seismic behavior of skewed bridges considering SSI. Soil Dynam Earthq Eng 2019/12/01/2019;127:105820.
18. **Mallick M, Raychowdhury P.** Seismic analysis of highway skew bridges with nonlinear soil–pile interaction. Transport Geotech 2015/06/01/2015;3:36–47.
19. **Carbonari S, Morici M, Dezi F, Gara F, Leoni G.** Soil-structure interaction effects in single bridge piers founded on inclined pile groups. Soil Dynam Earthq Eng 2017/01/01/2017;92:52–67.
20. **Gonz´ alez F, Padron ´ LA, Carbonari S, Morici M, Aznarez ´ JJ, Dezi F, et al.** Seismicresponse of bridge piers on pile groups for different soil damping models and lumped parameter representations of the foundation. Earthq Eng Struct Dynam 2019;48:306–27.
21. **Vlassis A, Spyrakos C.** Seismically isolated bridge piers on shallow soil stratum with soil–structure interaction. Comput Struct 2001;79:2847–61.
22. **Ajamy, A., Asgarian, B., Ventura, C.E., Zolfaghari, M.R.:** Seismic fragility analysis of jacket type offshoreplatforms considering soil-pile-structure interaction. Eng. Struct. 174, 198–211 (2018). https://doi.org/10.1016/j.engstruct.2018.07.066
23. **Ajamy, A., Zolfaghari, M.R., Asgarian, B., Ventura, C.E.:** Probabilistic seismic analysis of offshore platformsincorporating uncertainty in soil–pile–structure interactions. J. Constr. SteelRes. 101, 265–279 (2014). https://doi.org/10.1016/j.jcsr.2014.05.024
24. **Shafieezadeh, A., DesRoches, R., Rix, G.J., Werner, S.D.**: Three-dimensional wharf response to far-field andimpulsive near-field ground motions in liquefiable soils. J. Struct. Eng. 139(8), 1395–1407 (2013). https://doi.org/10.1061/(asce)st.1943-541x.0000642
25. **Stefanidou, S.P., Sextos, A.G., Kotsoglou, A.N., Lesgidis, N., Kappos, A.J.:** Soil-structure interaction effectsin analysis of seismic fragility of bridges using an intensity-based ground motion selection procedure. Eng. Struct. 151, 366–380 (2017). https://doi.org/10.1016/j.engstruct.2017.08.033
26. **Chara, C., Mitropoulou, C.C., Kostopanagiotis, C., Kopanos, M., Ioakim, D., Lagaros, N.D.:** Influence of soilstructure interaction on fragility assessment of building structures. In: Structures, pp. 85–98. Elsevier (2016). https://doi.org/10.1016/j.istruc.2016.02.005
27. **Wang, X., Ye, A., Ji, B.:** Fragility-based sensitivity analysis on the seismic performance of pile-group supported bridges in liquefiable ground undergoing scour potentials. Eng. Struct. 198, 109427 (2019). https://doi.org/10.1016/j.engstruct.2019.109427 program SeismoStruct v7 (SeismoSoft and 2022)
28. **Calabrese, A., Almeida, J. P., & Pinho, R.** (2010). Numericalissues in distributed inelasticity modeling of RC frameelements for seismic analysis. Journal of EarthquakeEngineering, 14(S1), 38–68.

29. **Menegotto, M., & Pinto, P.E.** (1973). Method of analysis forcyclically loaded reinforced concrete plane frames including changes in geometry and non-elastic behavior of elements under combined normal force and bending moment(pp. 15–22). Lisbon, Portugal: IASBE Proceedings
30. **Mander JB, Priestley MJN, Park R.** Theoretical stress-strain model for confinedconcrete. Struct Eng 1998;114(8):1804–26
31. **Richart, F.E., Brandtzæg, A., & Brown, R.** L. (1928). A studyof the failure of concrete under combined compressive stresses. University of Illinois Bulletin, 26(12)
32. **Pyke RM.** Nonlinear soil models for irregular cyclic loadings. J Geotech Eng Div,ASCE 1979;105(6):715–26
33. **Allotey N, Naggar MH El.** A consistent soil fatigue framework based on the number of equivalent cycles. Geotech Geol Eng 2007;26(1):65–77.
34. **Allotey N, Naggar MH E**l. Generalized dynamic Winkler model for nonlinear soil–structure interaction analysis. Can Geotech J 2008;45(4):560–73
35. **Brandenberg SJ, Boulanger RW, Kutter BL, Chang D**. Behavior of pile foundations inlaterally spreading ground during centrifuge tests. J Geotech Geoenviron Eng2005;131(11):1378–91.
36. **Dezi F, Carbonari S, Leoni G.** A model for the 3D kinematic interaction analysis ofpile groups in layered soils. Earthq Eng Struct Dyn 2009;38(11):1281–305
37. **Dezi F, Carbonari S, Morici M.** A numerical model for the dynamic analysis of inclined pile groups: a numerical model for the dynamic analysis of inclined pile groups. Earthq Eng Struct Dyn 2016;45(1):45–68.
38. **Vamvatsikos Dimitrios, Cornell C Allin**. Incremental dynamic analysis. EarthquakeEng Struct Dyn 2002;31(3):491–514
39. **Mander JB, Dhakal RP, Mashiko N, Solberg KM**. Incremental dynamic analysis applied to seismic financial risk assessment of bridges. Eng Struct2007;29(10):2662–7
40. **Chomchuen Prakit, Boonyapinyo Virote.** Incremental dynamic analysis with multimodes for seismic performance evaluation of RC bridges. Eng Struct2017;132:29–43
41. **Kazemi F, Mohebi B, Yakhchalian M.** Evaluation of the P-delta effect oncollapsecapacity of adjacent structures subjected to far-field ground motions.CivilEngJ2018;4(5):1066–73.
42. performance ofadjacent pounding structures using viscous dampers. In: The16thEuropeanConference on Earthquake Engineering; 2018. p. 18–21
43. **Kostov M.** Seismic fragility analyses. In "Regional Workshop On ExternalEventsPSA 6-10 November 2000, Sofia," 2000
44. **Duan X, Pappin JW.** "A procedure for establishing fragility functions for seismicloss estimate of existing buildings based on nonlinear pushover analysis,"in14thWorld Conference on Earthquake Engineering. Beijing: China; 2008. p. 12–7
45. **Kumitani S, Takada T.** Probabilistic assessment of buildings damage consideringaftershocks of earthquakes. 14th World Conference on EarthquakeEngineering.2008.
46. **Haran Pragalath DC, Davis R, Sarkar P.** Reliability evaluation of RC framebytwomajor fragility analysis methods. Asian J. Civil Eng. (BuildingAndHousing)2015;16:47–66.
47. Ioannou Ioanna, Douglas John, Rossetto Tiziana. Assessing the impact of groundmotion variability and uncertainty on empirical fragility curves.SoilDynEarthquake Eng 2015;69:83–92.
48. **Kappos Andreas J, Panagopoulos Georgios, Panagiotopoulos Christos,**

Penelis Gregorios. A hybrid method for the vulnerability assessment of R/CandURM buildings. Bull Earthq Eng 2006;4(4):391–413.

49. **Muntasir Billah AHM, Shahria Alam M.** Seismic fragility assessment of highway bridges: a state-of-the-art review. Struct Infrastruct Eng 2015;11(6):804–32.
50. **Ibrahim Yasser E, El-Shami Mostafa M.** Seismic fragility curves for mid-risereinforced concrete frames in Kingdom of Saudi Arabia. IES J PartA:CivilStructEng 2011;4(4):213–23.
51. **Shinozuka M, Feng MQ, Kim H-K, Kim S-H.** Nonlinear static procedurefor + fragilitycurve development. JEngMech 2000; 126 (12):1287–95.
52. **Shinozuka M, Feng M, Kim H, Uzawa T, Ueda T.** "Statistical analysis offragilitycurves. Technical Report." Multidisciplinary Center for Earthquake Engineering Research, MCEER-032003.
53. **Xue Q, Wu C-W, Chen C-C, Chen K-C.** The draft code for performance-based seismic design of buildings in Taiwan. Eng Struct 2008;30(6):1535–47.
54. COSMOSVirtualDataCenter.:⟨http://strong motioncenter.org/vdc/scripts/de

International Journal for Computational Civil and Structural Engineering, 19(3) 114–129 (2023)

DOI:10.22337/2587-9618-2023-19-3-114-129

NUMERICAL MODELLING OF WIND LOADS ON WINDOWS. VALIDATION FOR A HIGH-RISE SQUARE PLAN BUILDING

Oleg S. Goryachevsky

National Research Moscow State University of Civil Engineering, Moscow, RUSSIA

Abstract: This paper presents the results of numerical and experimental modelling of mean and peak pressure coefficients for window assemblies on a rectangular building. The applicability of the SST and GEKO *k*-ω turbulence models implemented in ANSYS Fluent is investigated. A simple steady-state method for determining the peak wind pressures, which utilizes the turbulence kinetic energy calculation, is shown to be sufficient for practical purposes. A comparative analysis with the values of pressure coefficients given in the Russian building code is carried out. The obtained results can be used in the design of window assemblies of typical buildings.

Keywords: computational fluid dynamics (CFD), experimental wind tunnel (WT) testing, pressure coefficients, structural aerodynamics, window assemblies

ЧИСЛЕННОЕ МОДЕЛИРОВАНИЕ ВЕТРОВЫХ ДАВЛЕНИЙ НА ОКНА. ВАЛИДАЦИЯ ДЛЯ ТИПОВОГО МНОГОЭТАЖНОГО ЗДАНИЯ КВАДРАТНОЙ ФОРМЫ

О.С. Горячевский

Национальный исследовательский Московский государственный строительный университет, г. Москва, РОССИЯ

Аннотация: В статье представлены результаты численного и экспериментального моделирование средних и пиковых аэродинамических коэффициентов для оконных конструкций прямоугольного здания. Исследуется применимость моделей турбулентности SST и GEKO *k*-ω, реализованных в программном комплексе ANSYS Fluent. Показана достаточная для практических целей точность стационарной постановки и простейшего метода определения пиковых значений ветровых давлений на основе кинетической энергии турбулентности. Проведен сопоставительный анализ со значениями аэродинамических коэффициентов, приведенных в российских нормах. Полученные результаты могут быть использованы при проектировании оконных конструкций типовых зданий.

Ключевые слова: вычислительная гидродинамика, экспериментальные испытания в аэродинамической трубе, аэродинамический коэффициент давлений, строительная аэродинамика, оконные конструкции

1. INTRODUCTION

Physical (experimental) modelling of wind loads and actions took on in its modern form in the middle of the 20th century. Tests in wind tunnels (WTs) with uniform flow began in the early 20th century [1], but the results differed significantly from field observations. The first WT with a long test section used to model atmospheric boundary layer (ABL) was built at the Colorado A&M College campus [2]. The first significant structures that were designed based on test results from the same WT (the college had already been renamed to Colorado State University) were the World Trade Centre Twin Towers in 1964 [3-4].

Large-scale studies were conducted for another 30 years to test against the full-scale (field) data in order to validate the experimental modelling results [5-10]. Important validation requirements were identified, including the reproduction of the statistical flow characteristics (mean velocities, turbulence intensity and spectrum)

[11-13], taking into account the developed similarity criteria [14] and the use of high-frequency pressure sensors [15]. Limitations were also identified, e.g., the Reynolds number independence is observed only for bluff bodies, and the deviation from field data for roofs and bodies with uncertain separation point. A review of the history of development and validation of experimental modelling of wind actions is given in [16].

Computational Fluid Dynamics is a powerful tool for analyzing wind actions and related problems (pedestrian comfort, emission propagation, snow loads, etc.) [17-18].

The first works on numerical modelling of wind actions were carried out in the 1970s. However, mass industrial application of CFD technologies was hampered by [19]:

1) colossal requirements for computational resources at the time;
2) insufficient theoretical development of turbulence models and eddy-resolving approaches;
3) lack of software available to the researching engineers;
4) lack of reliable V&V process.

Due to scientific and technological progress, by the beginning of the 21st century, favourable opportunities for industrial application of CFD technologies in the construction industry have developed. Therefore, in the early 2000s there was an explosive growth in the number of scientific studies and attempts (successful and not) to apply, verify and validate numerical modelling for the solution of problems of structural aerodynamics [20-23]. The first CFD application guidelines in structural aerodynamics from European [24] and Japanese [25] researchers were published. They contained basic recommendations for boundary conditions, size of the computational domain, turbulence models, discretization parameters, reliable numerical schemes and V&V principles.

At present, there are a number of building code recommendations on the application of computational fluid dynamics in structural aerodynamics, including the determination of wind loads [26-29]. Meanwhile, contrary to the global trend, numerical modelling of wind loads and actions has been removed from the Russian building code [30].

Among Russian-language sources, there is a deficit of high-quality literature on numerical modelling of wind actions in structural aerodynamics. The only full-fledged monograph exists [31], and the papers on modelling snow loads [32], aeroelasticity of buildings and structures [33] and estimation of pedestrian comfort parameters [34] are noteworthy.

There are three main approaches to the numerical solution of the Navier-Stokes equations [35-36]:

1) DNS (Direct Numerical Simulation), which is characterized by extremely high computational complexity, relevant only for academic problems at low Reynolds numbers;
2) LES (Large Eddy Simulation), which is used to determine transient characteristics of the flow. It has high computational complexity when the wall functions are used and even higher complexity when the boundary layer is resolved;
3) RANS (Reynolds-averaged Navier-Stokes), which is a fast but often insufficiently accurate approach for determining time-averaged flow characteristics.

In industrial applications, the hybrid RANS-LES approach [37] shows sufficiently accurate results with adequate requirements to computational resources.

With any approach utilized, the reliability of the obtained results is evaluated after V&V procedure of the numerical model against the experimental data [38]. An integrated approach with simultaneous use of numerical and experimental modelling results gives a synergistic effect, eliminating the weaknesses of each approach [39].

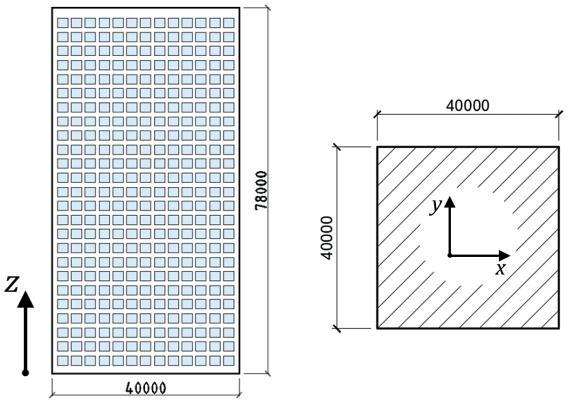
Based on qualitative experimental results, it is possible to calibrate the parameters of numerical models (usually, the coefficients of turbulence models) to obtain reliable and more

comprehensive results. Recently, the GEKO *k*-ω turbulence model has been developed, which makes it relatively easy to calibrate its parameters using experimental data [40-41].
This paper presents the results of numerical modelling of mean and peak pressure coefficients on the facades of a rectangular 25-storey building. The results of numerical modelling were compared to the experimental data obtained in the WT of NRU MSUCE for the corresponding building and the normative values of SP 20 [30].

2. METHODOLOGY

2.1. Building model description

The mean and peak pressure coefficients on the façade windows of a rectangular 25-storey building are investigated (Fig. 1). The building dimensions are $d \times d = 40 \times 40m$, and the height is $h = 75m$. Windows' dimensions are $1.75 \times 2m$, and the spacing is $2.958m$. Depth of windows in the façade is $0.23m$.



a) front view *b) top-down view*

Figure 1. Building dimensions, mm

Numerical modelling and wind tunnel tests were performed for 24 wind directions (from 0° to 345° in 15° intervals) (Fig. 2). The model's symmetry allowed to reduce the number of sensors and to estimate the modelling errors.

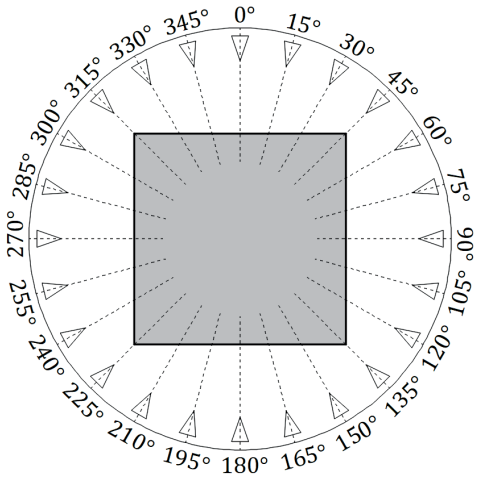


Figure 2. Design wind directions

Pressure coefficients were measured at the centroids of the window surfaces. Since each window is an independent structure, the extreme values of pressure coefficients are of practical interest:

$$c_e^{\max} = \max_j \left(c_e^j\right); \quad c_e^{\min} = \min_j \left(c_e^j\right)$$
$$c_{e,+}^{\max} = \max_j \left(c_{e,+}^j\right); \quad c_{e,-}^{\min} = \min_j \left(c_{e,-}^j\right) \tag{1}$$

where c_e^j is the external mean pressure coefficient for the j-th wind direction, and $c_{e,+(-)}^j$ is the external positive (negative) peak pressure coefficient for j-th wind direction.

2.2. Wind pressure coefficients

Pressure coefficients at the building surfaces were determined in the classical way:

$$c\left(x,y,z\right) = \frac{\Delta P(x,y,z)}{Q(h)} \tag{2}$$

where c is the generalized pressure coefficient, ΔP is the excessive wind pressure on the building façade, Q is the dynamic pressure, and x, y, z are the coordinates.
In SP 20, the pressure coefficients vary only horizontally, and the vertical variability is controlled by the equivalent height z_e [30]. Therefore, in order to accurately compare the

values of the coefficients given in SP 20 to those modelled numerically or in the WT (2), it is necessary to take into account the following relationship between them:

$$c = \frac{\Delta P}{Q} = \frac{w_0 k(z_e) c_{norm}}{w_0 k(h)} = \\ = c_{norm} \left(\frac{z_e}{10}\right)^{2\alpha} \Big/ \left(\frac{h}{10}\right)^{2\alpha} = c_{norm} \left(\frac{z_e}{h}\right)^{2\alpha} \quad (3)$$

where w_0 is the basic wind pressure, $k(z_e)$ is the height variation factor, α is the terrain factor, and c_{norm} are the values of horizontal pressure coefficients given in SP 20.

For the object of this study:

$$z_e = \begin{cases} d, & 0 < z < h - d \\ h, & z \geq h - d \end{cases} \quad (4)$$

Then:

$$c = \begin{cases} c_{norm} \left(d / h\right)^{2\alpha}, & 0 < z < h - d \\ c_{norm}, & z \geq h - d \end{cases} \quad (5)$$

As can be seen from expression (5), starting from the 13th floor and above, the values of pressure coefficients according to (2) and the building code are identical. Consequently, for the upper floors the numerical and experimental values can be compared directly. For a correct comparison of values on the lower floors it is necessary to lower the normative coefficients by a factor of 0.82, 0.77 and 0.72 for terrain types A, B and C respectively.

It should be remembered that the piecewise-constant vertical values of wind pressures given in SP 20 [30] are a simplification. In reality, the pressure coefficients are distributed over the surface continuously, forming complex three-dimensional patterns (Fig. 4). Value jumps can be observed only across the corners.

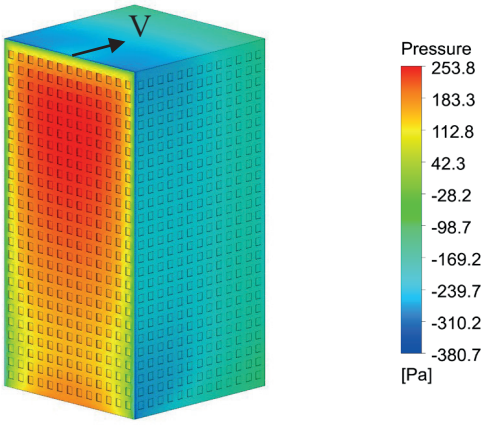


Figure 3. Numerical simulation of mean wind pressure distribution, Pa

2.3. Wind tunnel experiment description

Experimental studies were carried out in the NRU MSUCE WT by the AAISK UNPL staff. The WT has a closed circuit and a modular nine-unit fan with a testing area length of 18.9*m*.

The upstream flow velocities and reference pressures were determined 1.5*m* away from the 1:100 scale model placed in the WT testing area (Fig. 4).

Pressure sensors were placed in the middle of window openings on the 14th, 23rd and 25th floors (Fig. 5) on two sides of the model.

Pressure coefficients for each control point and wind direction were determined by statistical processing of pressure sensor readings (1000Hz frequency):

$$c_e = \frac{\Delta P_{ave}}{Q} \\ c_{e,+(-)} = \frac{\Delta P_{max(min)}}{Q} \quad (6) \\ P_{max(min)} = \Delta P_{ave} \pm 3\sigma_P$$

where ΔP_{ave}, ΔP_{max}, ΔP_{min} are average, maximum and minimum pressure values at the test points, respectively, σ_P is the wind pressure standard deviation, and Q is the dynamic pressure at the top of the model.

The experiments were carried out without roughness, as the aim was to determine the pressure coefficients with the least influence of the upstream flow turbulence possible.

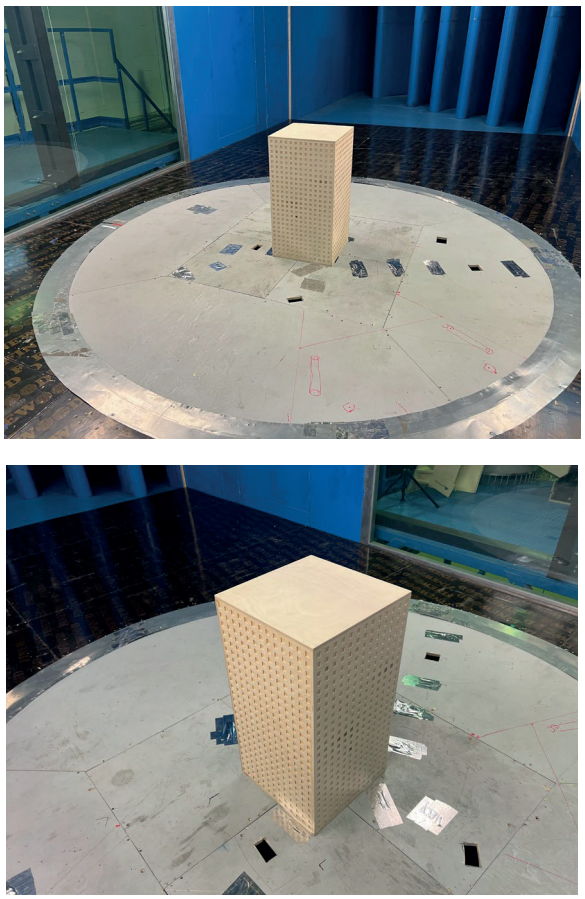


Figure 4. Building model in the WT

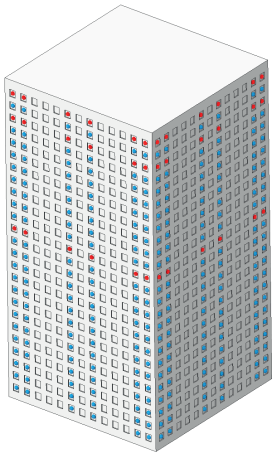


Figure 5. Pressure sensors (in red, not present on the other sides) and additional measurement points in the numerical model (in blue, present on all sides) layout

2.4. Numerical model description

The numerical model is based on the Navier-Stokes equations for incompressible Newtonian fluid with mass forces omitted:

$$\frac{\partial u_i}{\partial t}+u_j\frac{\partial u_i}{\partial x_j}=-\frac{1}{\rho}\frac{\partial p}{\partial x_i}+\frac{\mu}{\rho}\frac{\partial^2 u_i}{\partial x_i\partial x_j};\qquad \frac{\partial u_i}{\partial x_i}=0;\quad \rho,\mu=\text{const} \tag{7}$$

where u_i is the velocity components for the x_i direction, p is the pressure, ρ is the density, μ is the dynamic viscosity, and t is the time.

Direct numerical solution of equations (7) for practical problems at high Reynolds numbers is not possible due to very high computational requirements. LES approach is not considered in this paper, as well. In the present study, the Reynolds-averaged Navier-Stokes (RANS) equations are applied, obtained by decomposing the instantaneous quantities into their time-averaged and fluctuating quantities:

$$\boldsymbol{u}(\boldsymbol{x},t)=\overline{\boldsymbol{u}}(\boldsymbol{x})+\boldsymbol{u}'(\boldsymbol{x},t)\qquad p(\boldsymbol{x},t)=\overline{p}(\boldsymbol{x})+p'(\boldsymbol{x},t) \tag{8}$$

where $\boldsymbol{u}'(\boldsymbol{x},t)$, $p'(\boldsymbol{x},t)$ are the fluctuating quantities of velocity and pressure, respectively.

The resulting expressions are called the Reynolds equations:

$$\rho\overline{u}_j\frac{\partial\overline{u}_i}{\partial x_j}=\frac{\partial}{\partial x_j}\left[-\overline{p}\delta_{ij}+\mu\left(\frac{\partial\overline{u}_i}{\partial x_j}+\frac{\partial\overline{u}_j}{\partial x_i}\right)-\rho\overline{u_i'u_j'}\right] \tag{9}$$

The disadvantage of time-averaging is the appearance of second order moments $\rho\overline{u_i'u_j'}$ in (9). The additional unknown quantities form

the Reynolds stress tensor. To close the obtained equations (9), the additional hypotheses called the turbulence models are needed.

In this paper, two turbulence models are applied:

1) SST, which is widely used and proven in engineering applications [35];

2) GEKO *k*-ω, which is relatively recently implemented in ANSYS Fluent [40] with wide calibration possibilities.

Let us provide a mathematical description of the latter model:

$$\rho\frac{\partial\left(\overline{u}_j k\right)}{\partial x_j} = P_k - C_\mu \rho k\omega + \\ + \frac{\partial}{\partial x_j}\left[\left(\mu + \frac{\mu_t}{\sigma_k}\right)\frac{\partial k}{\partial x_j}\right] \tag{10}$$

$$\rho\frac{\partial\left(\overline{u}_j \omega\right)}{\partial x_j} = C_{\omega 1}F_1\frac{\omega}{k}P_k - C_{\omega 2}F_2\rho\omega^2 + \\ + \rho F_3 CD + \frac{\partial}{\partial x_j}\left[\left(\mu + \frac{\mu_t}{\sigma_\omega}\right)\frac{\partial \omega}{\partial x_j}\right] \tag{11}$$

where k is the turbulence kinetic energy (TKE), ω is the specific turbulence dissipation rate, P_k is the production of TKE, $\mu_t = \rho k/\omega$ is the eddy viscosity, $CD = \frac{2}{\sigma_\omega}\frac{1}{\omega}\frac{\partial k}{\partial x_j}\frac{\partial \omega}{\partial x_j}$, C_μ, $C_{\omega 1}$, $C_{\omega 2}$, σ_k, σ_ω are the model constants, and F_1, F_2, F_3 are the model functions, which can be calibrated through freely assignable coefficients. In this work, the value of C_{SEP} (F_1, F_2, F_3), which governs the eddy viscosity, was varied. The values of C_{SEP} = 1.00, 1.75 and 2.25 were considered.

Note that *k*-ω models have a weakness in modelling the free shear flows because of the strong dependence on the inlet turbulent characteristics [42]. Therefore, in practice, mixed BSL-SST models are used, which implement both *k*-ε and *k*-ω models in different flow regions. The separation of the regions is done by blending functions. The GEKO *k*-ω model implements a similar approach.

The following boundary conditions for the computational domain were applied:

1) the velocity profile at the inlet: $\left(\overline{\boldsymbol{u}}, \boldsymbol{n}\right) = U\left(z\right), \left(\overline{\boldsymbol{u}}, \boldsymbol{\tau}\right) = 0$ ($\boldsymbol{n}$, $\boldsymbol{\tau}$ are vectors normal and tangent to the surface, respectively, z is the height coordinate);

2) $k(z)$ and $\omega(z)$ were also specified at the inlet;

2) backflow pressure at the outlet was set to 0: $\overline{p} = 0$;

3) free slip wall conditions were set for the lateral and upper boundaries: $\left(\overline{\boldsymbol{u}}, \boldsymbol{n}\right) = 0, \left(\overline{\boldsymbol{u}}, \boldsymbol{n}\right) = 0$;

4) no-slip wall conditions were set for the ground and building surfaces: $\overline{\boldsymbol{u}} = 0$.

The standard (RMS) wind pressures were calculated using the methodology that is outlined in [31]:

$$\Delta\overline{p} + \sigma_P = \frac{\rho}{2}\left(\overline{U} + \sigma_U\right)^2$$

$$\sigma_P = \frac{\rho}{2}\left(2\overline{U}\sigma_U + \sigma_U^2\right)$$

$$\sigma_P = \left[2\frac{\sigma_U}{\overline{U}} + \left(\frac{\sigma_U}{\overline{U}}\right)^2\right]\Delta\overline{p}$$

$$\sigma_P = \left(2I_U + I_U^2\right)\Delta\overline{p} \tag{12}$$

where $\overline{U}$ is the mean wind speed, and I_U is the turbulence intensity.

In [31], the turbulence intensity is proposed to be determined from the Bernoulli's law and the turbulence isotropy:

$$I_U = \frac{\sigma_U}{\overline{U}} = \sqrt{\frac{2}{3}k} \div \sqrt{\frac{2\left|\Delta\overline{p}\right|}{\rho}} = \sqrt{\frac{\rho k}{3\left|\Delta\overline{p}\right|}}, \tag{13}$$

On the walls, the TKE value is 0. Therefore, averaged values are taken in small volumes around the wall points.

The peak pressure coefficients, then, can be estimated by the following formulas:

$$c_{e,+} = \frac{\Delta\overline{p} + \theta_{+}\sigma_P}{Q}$$
$$c_{e,-} = \frac{\Delta\overline{p} - \theta_{-}\sigma_P}{Q} \quad (14)$$

where θ+, θ- are the coefficients that can be fitted from experimental data (equal for the whole model).

Although expression (13) and the methodology for determining TKE on the walls have somewhat weak theoretical justification, in practice it allows to determine the peak pressure coefficients fairly accurately. This will be confirmed in the present study.

2.5. Numerical simulation description

ANSYS Fluent 2021R2 was used for numerical modelling, carried out at a 1:100 scale (k_s = 100), similarly to the WT experiments.

The computational domain size corresponds to a fragment of the WT testing area, with the height of 2.44m, width of 4m and length of 9.5m (Fig. 6). The inlet boundary is located 3m away from the center of the building model.

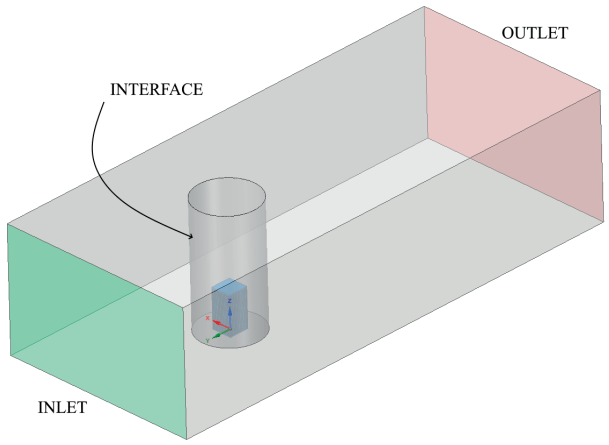


Figure 6. Computational domain

A mesh interface was established between and additional cylindrical volume around the building model and the rest of the domain, approximating the transition between non-conformal meshes. This approach avoids rebuilding the mesh between the wind direction changes, which are achieved by rotating the outer volume around the cylindrical inner volume.

The poly-hexcore finite volume mesh was created in ANSYS Fluent Meshing (Fig. 7). The cell size on the building surface is 0.0025m with 5 inflation layers, and the total number of finite volume cells is 5.75 million.

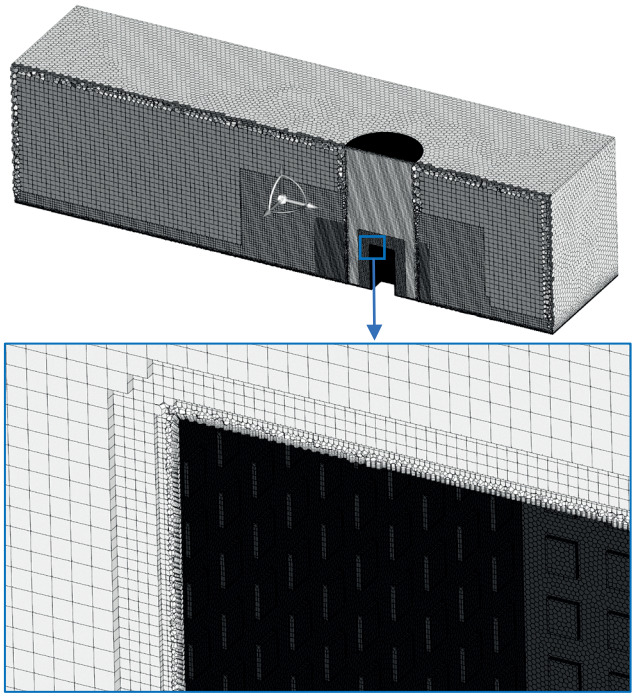


Figure 7. Finite volume mesh section

The simulations were carried out using the steady-state pseudo-transient approach, in which the transient quantities that disappeared after the time-averaging procedure are re-introduced into the equations (9-11). The time, then, is replaced by a sufficiently large pseudo-transient timestep. The relaxation coefficients ensure sufficiently fast convergence. This approach is usually more efficient compared to the direct solution of the steady-state equations.

The total number of iterations is 125. The first 75 iterations are simulated with the standard pseudo-timestep, and the last 50 iterations are simulated with a timestep reduced by a factor of 2. This approach ensures better convergence. At the end of the simulation, the scaled residuals for all conservation equations fall below $5 \cdot 10^{-4}$. Test simulations showed that increasing the number of iterations does not affect the result significantly.

Second Order Upwind numerical scheme was used for the momentum equations (9) and turbulence transport (10-11) in space and pseudo-time. The Coupled pressure-velocity solver was used.

2.6. Inlet profile characteristics

The wind speed profile (Fig. 8) and turbulence characteristics for the inlet were set similarly to those measured in the WT. The expression for wind speed was determined using the least squares method:

$$U(z) = \begin{cases} U_0 \left(z/z_0\right)^{\alpha}, & z < z_1 \\ U_0 \left(z_1/z_0\right)^{\alpha}, & z \geq z_1 \end{cases} \quad (8)$$

where U_0 = 15.6m/s, z_0 = 0.15m, z_1 = 0.32m, α = 0.10.

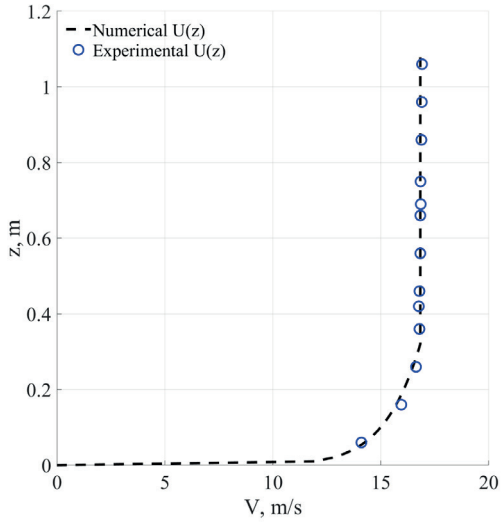


Figure 8. Numerical and experimental wind profiles

The turbulence intensity in the WT was kept constant at ~3% for z > 0.3m. For the numerical model, the intensity measured in the experiment was approximated by the least squares method, too. It was then converted to k and ω, which were set at the inlet.

3. RESULTS AND DISCUSSION

For the modelled pressure coefficients, errors were evaluated. For the experimental data, the errors mainly come from deviations in the wind direction angle due to the imperfection of the WT's rotary table mechanism, minor asymmetry in the sensors' location, and sensor measurement errors.

The scatter of experimental values was estimated by the difference between the results obtained in symmetrical zones.

For the numerical data, the errors mainly come from non-ideal iterative convergence and high gradients in the corner zones. Iterative fluctuations were considered for the last 25 iterations. The difference of the sought values was measured on a circular area with a radius of 5*mm* (approximately 30% of the window surface area).

Figs. 9-12 show floor plots of the extreme pressure coefficients' values (1). Each plot includes a diagram, which shows the location of the corresponding windows on the building. The variation of experimental values is shown by error bars, while the variation of numerical values is shown by translucent bars of the appropriate colour.

The SST and GEKO k-ω (C_{SEP} = 1.00, 1.75 and 2.25) turbulence models were considered. The coefficients in expression (14) were taken equal to θ+ = 0.25 and θ- = 2.25.

It is known that the pressure coefficients obtained from numerical simulation are often slightly higher than those from the experiments. This situation is observed even when the reference pressures are measured at

the same location. In this study, the shift effect was also detected. Therefore, a correction of the pressure coefficients by $c_{e,shift} = 0.07$ was introduced to reduce the numerical values.

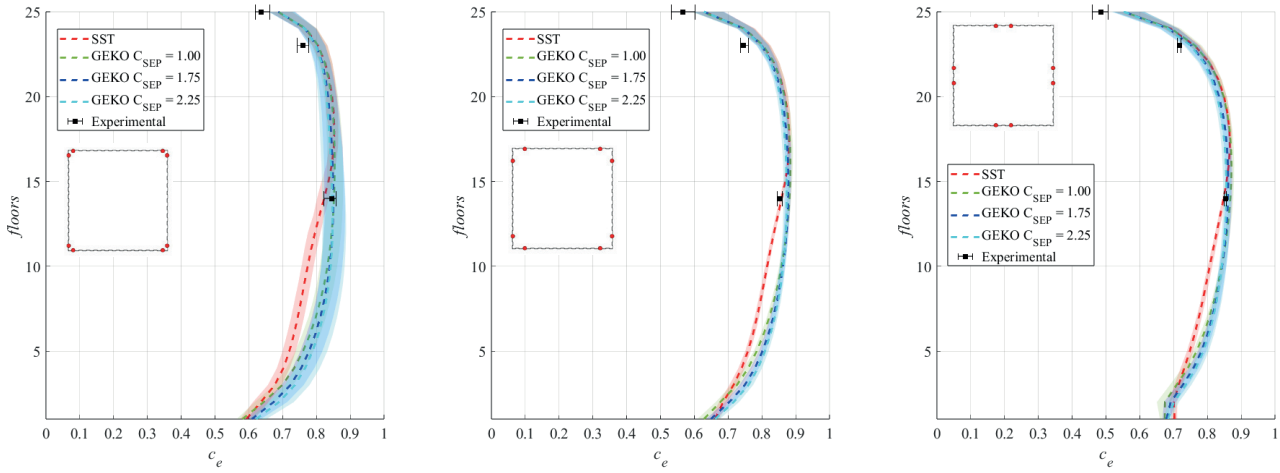


Figure 9. Floor plots of maximum positive values of mean pressure coefficient $c_e^{\max}$

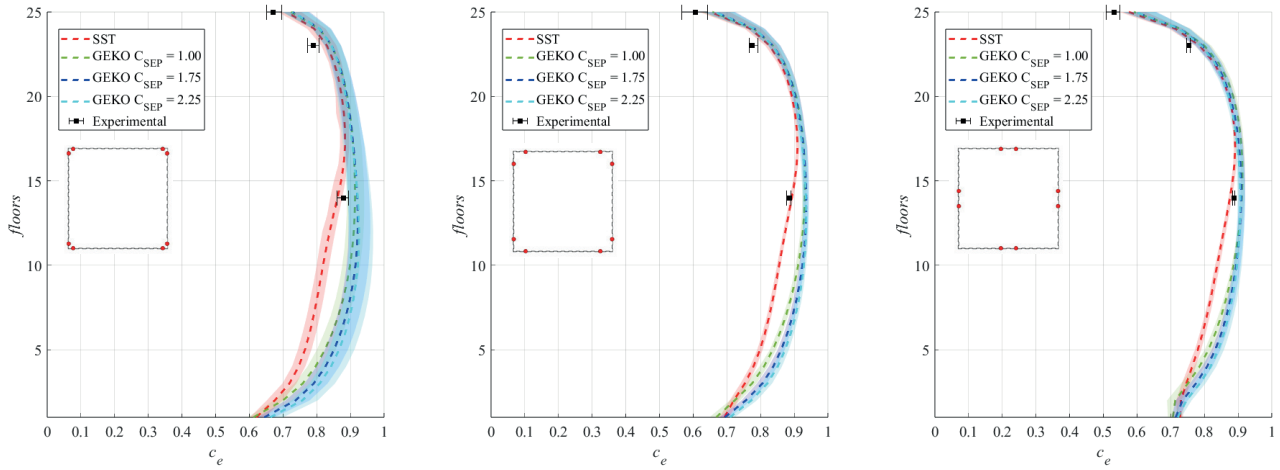


Figure 10. Floor plots of maximum positive values of peak pressure coefficient $c_{e,+}^{\max}$

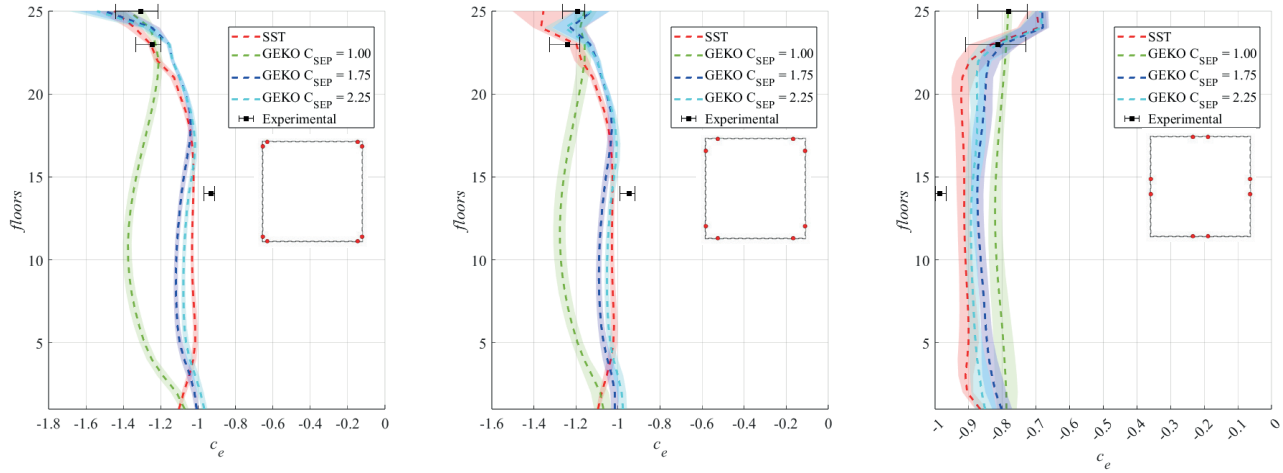


Figure 11. Floor plots of minimum negative values of mean pressure coefficient $c_e^{\min}$

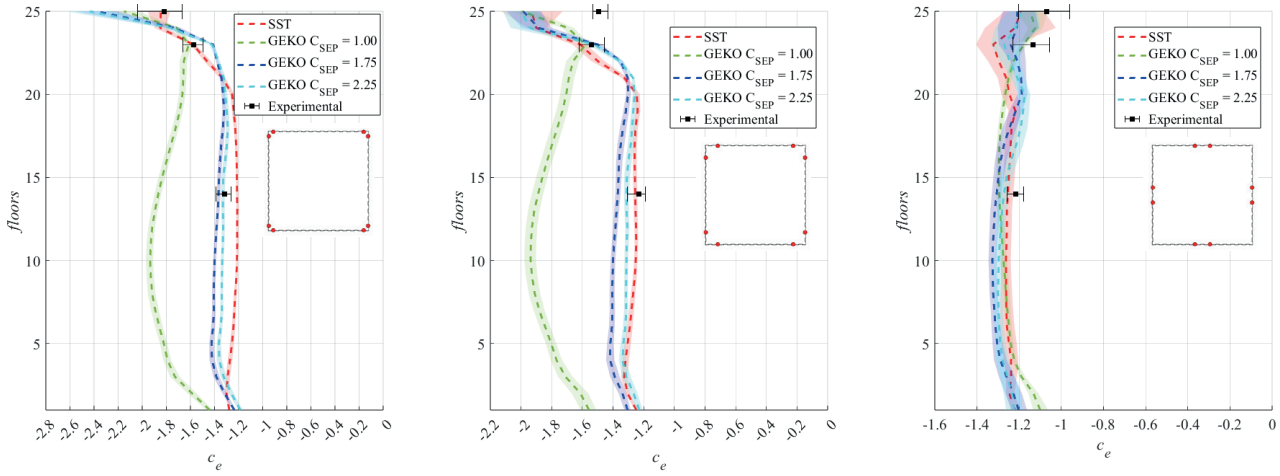


Figure 12. Floor plots of minimum negative values of peak pressure coefficient $c_{e,-}^{\min}$

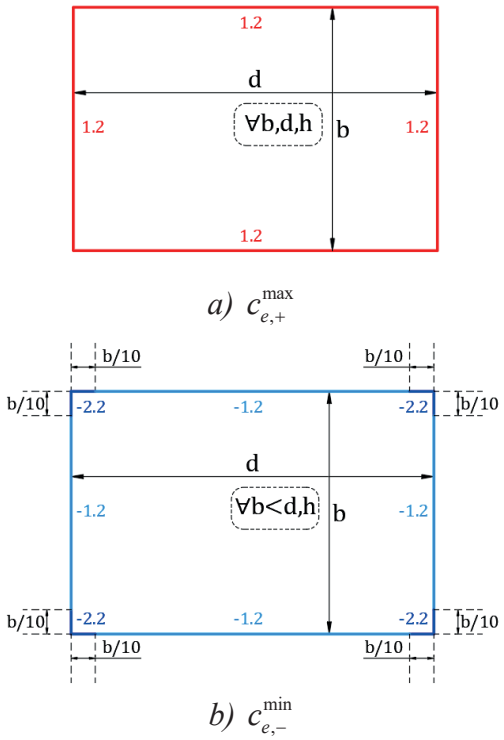
Analyzing the plots in Figs. 9-12, it can be seen that the numerical and experimental results are subject to noticeable errors. Accounting for the errors allows for a more complete analysis of the results.

1. All numerical and experimental values of $c_e^{\max}$ are in good agreement with each other (deviations <10%). For the floors below the middle one, the SST model gives slightly lower values than GEKO. However, it is not possible to establish which model is more plausible due to the lack of experimental data points.
2. All numerical and experimental values of $c_{e,+}^{\max}$ are in good agreement with each other (deviations <10%). The SST model gives slightly better results than GEKO.
3. The numerical values of $c_e^{\min}$ are significantly different between the turbulence models. GEKO at C_{SEP} = 1.00 gives the worst results (deviation from the experimental data up to 40%) for the 14th floor, but better results for the 23rd and 25th floors (fits within the experimental spread). The SST model gives the best results for the 14th floor (deviation <10%).
4. The numerical and experimental values of $c_{e,-}^{\min}$ are in good agreement with each other in the center zone of the building. However, the SST model gives slightly better results at the 14th floor, while GEKO at C_{SEP} = 1.00 gives better results at the 23rd and 25th floors.
5. In the corner zones, the numerical and experimental values of $c_{e,-}^{\min}$ correspond best for the SST model. However, the experimental data on the 25th floor for the 2nd window from the corner was not reproduced accurately enough by either turbulence model. For this point, the numerical data gives significantly overestimated values (-2.0 vs. -1.5 experimental values).

Comparison of the obtained results with paragraph B.1.17 of SP 20 [30] reveals a significantly poor design of normative schemes (Fig. 13). As such, experimental and numerical values of $c_{e,+}^{\max}$ do not reach even 1.0 anywhere, unlike the value of 1.2 the building code suggests. For the lower and upper parts of the building the values of the coefficients are much lower than for the central part.

At the corners of the 25th floor the numerical values of $c_{e,-}^{\min}$ can reach -2.6 (in the code: -2.2), although the experimental values do not exceed -2.05 (remember that this is where numerical and experimental values deviate the most). However, on other floors, $c_{e,-}^{\min}$ values

are significantly lower than normative values. For the 2nd window from the corner, both experimental and numerical values are significantly higher than the normative -1.2. For other zones of the building, $c_{e,-}^{min}$ values can be slightly higher than -1.2, reaching -1.4 in the numerical simulations.



a) $c_{e,+}^{max}$

b) $c_{e,-}^{min}$

Figure 13. Normative values of peak pressure coefficients (h is the building height)

According to SP 20 [30], the pressure coefficients and the corresponding wind loads decrease steeply at the bottom of the building. However, the modelling results show that the decrease of pressure coefficients at the bottom of the building is observed only for c_e^{max} and $c_{e,+}^{max}$, while c_e^{min} and $c_{e,-}^{min}$ remain almost constant.

The Russian building code does not contain regulations for extreme values of mean pressure coefficients, despite their necessity for the design of window assemblies. Therefore, it is not possible to carry out an appropriate comparison.

4. CONCLUSION

Comparison of the results of numerical and experimental modelling confirms that the numerical modelling of mean and peak wind loads is sufficiently reliable for practical purposes. At the same time, the possibility of numerical modelling to obtain a significantly more complete distribution of the coefficients without additional resources is demonstrated.

One of the important advantages of the proposed approach is the relatively low computational cost due to the use of the steady-state approach only. This is very important for practical problems constrained by time and budget.

However, the numerical approach used in this paper turns out to be dependent on the availability of experimental data for calibrating the turbulence models, computing the coefficients θ+, θ- and the shift factor $c_{e,shift}$. Obviously, the development of more advanced models to determine peak wind pressures independent of experimental data is required.

The GEKO *k*-ω turbulence model has shown a good ability to be calibrated with experimental data. However, to achieve better results than those obtained using the SST model, more research is required for a full calibration of the GEKO model.

The importance of error evaluation for the experimental and numerical results is demonstrated. In industrial applications and scientific research, appropriate analysis is often not performed, which can lead to dangerous underestimation of wind loads.

The extreme values of mean and peak pressure coefficients obtained in this study are recommended for use by window assembly engineers.

REFERENCES

1. **Kazakevich M.I.** Aerodinamika inzhenernyh sooruzhenij. Moscow: OAO Giprotroymost, 2014, 168 p. (in Russian)

2. **Cermak J.E., Koloseus H.J.** Lake Hefner Model Studies of Wind Structure and Evaporation. Final Report – Part II, № 54JEC22, 1954, 123 p.
3. **Davenport A.G.** The response of supertall buildings to wind // Second Century of the Skyscraper: Council on Tall Buildings and Urban Habitat, 1988, pp. 705-725.
4. **Glanz J., Lipton E.** City in the Sky: The Rise and Fall of the World Trade Center. Times Books, 2014, 480 p.
5. **Rathbun J.C.** Wind forces on a tall building // Trans. Am. Soc. Civil Eng., 1940, Volume 105, pp. 1-41.
6. **Marshall R.D.** A study of wind pressures on a single-family dwelling in model and full scale // J. Wind Eng. Ind. Aerodyn., 1975, Volume 1, pp. 177-199.
7. **Eaton K.J., Mayne J.R.** The measurement of wind pressures on two-storey houses at Aylesbury // J. Wind Eng. Ind. Aerodyn., 1975, Volume 1, pp. 67-109.
8. **Holmes J.D.** Comparison of model and full-scale tests of the Aylesbury house // Proceedings of the International Workshop on Wind Tunnel Modeling Criteria and Techniques in Civil Engineering Applications, 1982, pp. 605-618.
9. **Richardson G.M., Robertson A.P., Hoxey R.P., Surry D.** Full-scale and model investigations of pressures on an industrial/agricultural building // J. Wind Eng. Ind. Aerodyn., 1990 ,Volume 36(2), pp. 1053-1062.
10. **Hoxey R.P., Richards P.J.** Full-scale wind load measurements point the way forward // J. Wind Eng. Ind. Aerodyn, 1995, Volume 57, Issues 2-3, pp. 215-224.
11. **Monin A.S., Obukhov A.M**. Basic laws of turbulent mixing in the surface layer of the atmosphere // Contrib. Geophys. Inst. Acad. Sci. USSR, 1954, Volume 24(151), pp. 163-187 (in Russian).
12. Van der Hoven I. Power spectrum of horizontal wind speed in the frequency range from 0.0007 to 900 cycles per hour // Journal of Atmospheric Sciences, 1957 Volume 14, pp. 160-164.
13. **Davenport A.G.** The relationship of wind structure to wind loading // Proc. Conf. on Wind Effects on Buildings & Structures, HMSO, 1965, pp. 54-111.
14. **Cermak J.E.** Wind tunnel design for physical modeling of atmospheric boundary layer // Journal of the Engineering Mechanics Division, 1981, Volume 107, pp. 623-642.
15. **Rofail A.W., Kwok K.C.S.** A reliability study of wind tunnel results for cladding pressures // J. Wind Eng. Ind. Aerodyn., 1992, Volume 44, Issues 1-3, pp. 2413-2424.
16. **Cochran L., Derickson R.** A physical modeler's view of computational wind engineering // J. Wind Eng. Ind. Aerodyn., 2011, Volume 99, Issue 4, pp. 139-153.
17. **Meroney R.N., Derickson R**. Virtual reality in wind engineering: the windy world within the computer // J. Wind Eng., 2014, Volume 11, pp. 11-26.
18. **Blocken B**. Computational Fluid Dynamics for urban physics: Importance, scales, possibilities, limitations and ten tips and tricks towards accurate and reliable simulations // Build. Environ., 2015, Volume 91, pp. 219-245.
19. **Blocken B.** 50 years of computational wind engineering: past, present and future // J. Wind Eng. Ind. Aerodyn., 2014, Volume 129, pp. 69-102.
20. **Mochida A., Tominaga Y., Murakami S., Yoshie R., Ishihara T., Ooka R.** Comparison of various k-ε models and DSM applied to flow around a highrise building-report on AU cooperative project for CFD prediction of wind environment // Wind Struct. Int. J., 2002, Volume 5, pp. 227-244.
21. **Celik I.B., Ghia U., Roache P.J., Freitas C.J.** Procedure for estimation and reporting of uncertainty due to discretization in CFD

applications // J. Fluids Eng. Trans. ASME, 2008, Volume 130(7).
22. **Bruno L., Salvetti M.V., Ricciardelli F.** Benchmark on the aerodynamics of a rectangular 5:1 cylinder: an overview after the first four years of activity // J. Wind Eng. Ind. Aerodyn., 2014, Volume. 126, pp. 87-106.
23. **Thordal M.S., Bennetsen J.C., Capra S., Kragh A.K., Koss H.H.H.** Towards a standard CFD setup for wind load assessment of high-rise buildings: Part 2– Blind test of chamfered and rounded corner high-rise buildings // J. Wind Eng. Ind. Aerodyn., 2020, Volume 205, p. 104282.
24. **Franke J., Hellsten A., Schlünzen K.H., Carissimo B.** Best practice guideline for the CFD simulation of flows in the urban environment-a summary // 11th Conference on Harmonisation within Atmospheric Dispersion Modelling for Regulatory Purposes, Cambridge, UK, July 2007, 2007.
25. **Tominaga Y., Mochida A., Yoshie R., Kataoka H., Nozu T., Yoshikawa M., Shirasawa T.** AIJ guidelines for practical applications of CFD to pedestrian wind environment around buildings // J. Wind Eng. Ind. Aerodyn., 2008, Volume 96, Issues 10-11, pp. 1749-1761.
26. Guidebook of Recommendations for Wind Loads on Buildings 2 – Wind Induced Response and Load Estimation / Practical Guide of CFD for Wind Resistant Design, AIJ, 2017. (in Japanese)
27. CNR DT 207 R1/2018 Istruzioni per la valutazione delle azioni e degli effetti del vento sulle costruzioni, 2019. (in Italian)
28. ASCE/SEI 7-22 Minimum Design Loads and Associated Criteria for Building and other Structures, 2022.
29. Matematicheskoe (chislennoe)" modelirovanie vetrovyh nagruzok i vozdejstvij. Metodicheskoe posobie. Moscow: FAU «FCS», 2020, 61 p.
30. SP 20.13330.2016 Loads and actions (with changes №1-4). Moscow: FGBU «RST» 2022.
31. **Belostotsky A.M., Akimov P.A., Afanasyeva I.N.** Vychislitel'naya aerodinamika v zadachah stroitel'stva, Moscow: Izdatel'stvo ASV, 2017, 720 p. (in Russian).
32. **Britikov N.A**. Numerical modelling of snow deposits and snow transport on long-span roofs for steady and unsteady flow // International Journal for Computational Civil and Structural Engineering, 2022, Volume 18(4), pp. 23–38.
33. **Belostotsky A.M., Afanasyeva I.N., Negrozova I.Yu., Goryachevsky O.S**. Simulation of aerodynamic instability of building structures on the example of a bridge section. Part 2: solution of the problem in a coupled aeroelastic formulation and comparison with engineering estimates // International Journal for Computational Civil and Structural Engineering, 2021, Volume 17(3), pp. 24-38.
34. **Belostotsky A.M., Afanasyeva I.N., Lantsova I.Yu.** Estimation of pedestrian comfort on the basis of numerical modeling of wind aerodynamics of buildings in the environmental development // International Journal for Computational Civil and Structural Engineering, 2019, Volume 15(2), pp. 24-39.
35. **Menter F.R.** Review of the shear-stress transport turbulence model experience from an industrial perspective // J. Wind Eng. Ind. Aerodyn., 2009, Volume 23, pp. 305-316.
36. **Menter F.R.** Best Practice: Scale-Resolving Simulations in ANSYS CFD. Version 2.00. Technical paper. ANSYS, 2015, 47 p.
37. **Menter F., Hüppe A., Matyushenko A., Kolmogorov D.** An overview of hybrid RANS–LES models developed for industrial CFD // Appl. Sci., 2021, Volume 11, p. 2459, 2021.
38. **Oberkampf W.L., Trucano T.G., Hirsch C**. Verification, validation, and predictive capability in computational engineering and

physics // Appl. Mech. Rev., 2004, Volume 57, pp. 345-384.
39. **Meroney R.N.** Ten questions concerning hybrid computational/physical model simulation of wind flow in the built environment // Build. Environ., 2016, Volume 96, pp. 12-21.
40. **Menter F., Lechner R., Matyushenko A.** Best practice: Generalized k-ω (GEKO) Two-Equation Turbulence Model in ANSYS CFD: Version 1.01. Best Practice. ANSYS, 2019, 32 p.
41. **Sharkey P.S., Menter F.R.** A numerical investigation of the turbulent flow around a scale model JBC hull using the Generalized k-omega (GEKO) turbulence model // 11th International Workshop on Ship and Marine Hydrodynamics (IWSH2019), 2019.
42. **Kok J.C.** Resolving the Dependence on Freestream Values for the k-omega Turbulence Model // AIAA Journal, 2000, Volume 38(7), pp. 1292-1295.

СПИСОК ЛИТЕРАТУРЫ

1. **Казакевич М.И.** Аэродинамика инженерных сооружений. Москва: ОАО Гипростроймост, 2014, 168 с.
2. **Cermak J.E., Koloseus H.J.** Lake Hefner Model Studies of Wind Structure and Evaporation. Final Report – Part II, № 54JEC22, 1954, 123 p.
3. **Davenport A.G.** The response of supertall buildings to wind // Second Century of the Skyscraper: Council on Tall Buildings and Urban Habitat, 1988, pp. 705-725.
4. **Glanz J., Lipton E.** City in the Sky: The Rise and Fall of the World Trade Center. Times Books, 2014, 480 p.
5. **Rathbun J.C.** Wind forces on a tall building // Trans. Am. Soc. Civil Eng., 1940, Volume 105, pp. 1-41.
6. **Marshall R.D**. A study of wind pressures on a single-family dwelling in model and full scale // J. Wind Eng. Ind. Aerodyn., 1975, Volume 1, pp. 177-199.
7. **Eaton K.J., Mayne J.R.** The measurement of wind pressures on two-storey houses at Aylesbury // J. Wind Eng. Ind. Aerodyn., 1975, Volume 1, pp. 67-109.
8. **Holmes J.D**. Comparison of model and full-scale tests of the Aylesbury house // Proceedings of the International Workshop on Wind Tunnel Modeling Criteria and Techniques in Civil Engineering Applications, 1982, pp. 605-618.
9. **Richardson G.M., Robertson A.P., Hoxey R.P., Surry D.** Full-scale and model investigations of pressures on an industrial/agricultural building // J. Wind Eng. Ind. Aerodyn., 1990, Volume 36(2), pp. 1053-1062.
10. **Hoxey R.P., Richards P.J.** Full-scale wind load measurements point the way forward // J. Wind Eng. Ind. Aerodyn, 1995, Volume 57, Issues 2-3, pp. 215-224.
11. **Монин А.С., Обухов А.М.** Основные закономерности турбулентного перемешивания в приземном слое атмосферы // Труды ГЕОФИАН, 1954. № 24 (151), с. 163-187
12. **Van der Hoven I.** Power spectrum of horizontal wind speed in the frequency range from 0.0007 to 900 cycles per hour // Journal of Atmospheric Sciences, 1957 Volume 14, pp. 160-164.
13. **Davenport A.G.** The relationship of wind structure to wind loading // Proc. Conf. on Wind Effects on Buildings & Structures, HMSO, 1965, pp. 54-111.
14. **Cermak J.E**. Wind tunnel design for physical modeling of atmospheric boundary layer // Journal of the Engineering Mechanics Division, 1981, Volume 107, pp. 623-642.
15. **Rofail A.W., Kwok K.C.S.** A reliability study of wind tunnel results for cladding pressures // J. Wind Eng. Ind. Aerodyn., 1992, Volume 44, Issues 1-3, pp. 2413-2424.
16. **Cochran L., Derickson R.** A physical modeler's view of computational wind

engineering // J. Wind Eng. Ind. Aerodyn., 2011, Volume 99, Issue 4, pp. 139-153.
17. Meroney R.N., Derickson R. Virtual reality in wind engineering: the windy world within the computer // J. Wind Eng., 2014, Volume 11, pp. 11-26.
18. **Blocken B.** Computational Fluid Dynamics for urban physics: Importance, scales, possibilities, limitations and ten tips and tricks towards accurate and reliable simulations // Build. Environ., 2015, Volume 91, pp. 219-245.
19. **Blocken B.** 50 years of computational wind engineering: past, present and future // J. Wind Eng. Ind. Aerodyn., 2014, Volume 129, pp. 69-102.
20. **Mochida A., Tominaga Y., Murakami S., Yoshie R., Ishihara T., Ooka R.** Comparison of various k-ε models and DSM applied to flow around a highrise building-report on AU cooperative project for CFD prediction of wind environment // Wind Struct. Int. J., 2002, Volume 5, pp. 227-244.
21. **Celik I.B., Ghia U., Roache P.J., Freitas C.J.** Procedure for estimation and reporting of uncertainty due to discretization in CFD applications // J. Fluids Eng. Trans. ASME, 2008, Volume 130(7).
22. **Bruno L., Salvetti M.V., Ricciardelli F**. Benchmark on the aerodynamics of a rectangular 5:1 cylinder: an overview after the first four years of activity // J. Wind Eng. Ind. Aerodyn., 2014, Volume. 126, pp. 87-106.
23. **Thordal M.S., Bennetsen J.C., Capra S., Kragh A.K., Koss H.H.H.** Towards a standard CFD setup for wind load assessment of high-rise buildings: Part 2–Blind test of chamfered and rounded corner high-rise buildings // J. Wind Eng. Ind. Aerodyn., 2020, Volume 205, p. 104282.
24. **Franke J., Hellsten A., Schlünzen K.H., Carissimo B**. Best practice guideline for the CFD simulation of flows in the urban environment-a summary // 11th Conference on Harmonisation within Atmospheric Dispersion Modelling for Regulatory Purposes, Cambridge, UK, July 2007, 2007.
25. **Tominaga Y., Mochida A., Yoshie R., Kataoka H., Nozu T., Yoshikawa M., Shirasawa T.** AIJ guidelines for practical applications of CFD to pedestrian wind environment around buildings // J. Wind Eng. Ind. Aerodyn., 2008, Volume 96, Issues 10-11, pp. 1749-1761.
26. Guidebook of Recommendations for Wind Loads on Buildings 2 – Wind Induced Response and Load Estimation / Practical Guide of CFD for Wind Resistant Design, AIJ, 2017. (in Japanese)
27. CNR DT 207 R1/2018 Istruzioni per la valutazione delle azioni e degli effetti del vento sulle costruzioni, 2019. (in Italian)
28. ASCE/SEI 7-22 Minimum Design Loads and Associated Criteria for Building and other Structures, 2022.
29. Математическое (численное)" моделирование ветровых нагрузок и воздействий. Методическое пособие, М.: ФАУ «ФЦС», 2020, 61 с.
30. СП 20.13330.2016 Нагрузки и воздействия. Актуализированная редакция СНиП 2.01.07-85* (с Изменениями N 1, 2, 3, 4), М.: ФГБУ «РСТ», 2022.
31. **Белостоцкий А.М., Акимов П.А., Афанасьева И.Н.** Вычислительная аэродинамика в задачах строительства, М.: Издательство АСВ, 2017, 720 с.
32. **Бритиков Н.А.** Методика численного моделирования снегоотложений и снегопереноса на покрытиях большепролётных зданий и сооружений в стационарной и нестационарной постановках // International Journal for Computational Civil and Structural Engineering, 2022, Том 18(4), с. 23–38.
33. **Белостоцкий А.М., Афанасьева И.Н., Негрозова И.Ю., Горячевский О.С.** Моделирование аэродинамической неустойчивости строительных конструкций на примере сечения моста. Часть 2: Решение задачи в связанной

аэроупругой постановке и сопоставление с инженерными оценками // International Journal for Computational Civil and Structural Engineering, 2021, Том 17(3), с. 24-38.
34. **Белостоцкий А.М., Афанасьева И.Н., Ланцова И.Ю**. Оценка пешеходной комфортности на основе численного моделирования ветровой аэродинамики зданий в окружающей застройке // International Journal for Computational Civil and Structural Engineering, 2019, Том 15(2), с. 24-39.
35. **Menter F.R.** Review of the shear-stress transport turbulence model experience from an industrial perspective // J. Wind Eng. Ind. Aerodyn., 2009, Volume 23, pp. 305-316.
36. **Menter F.R.** Best Practice: Scale-Resolving Simulations in ANSYS CFD. Version 2.00. Technical paper. ANSYS, 2015, 47 p.
37. **Menter F., Hüppe A., Matyushenko A., Kolmogorov D.** An overview of hybrid RANS–LES models developed for industrial CFD // Appl. Sci., 2021, Volume 11, p. 2459, 2021.
38. **Oberkampf W.L., Trucano T.G., Hirsch C.** Verification, validation, and predictive capability in computational engineering and physics // Appl. Mech. Rev., 2004, Volume 57, pp. 345-384.
39. **Meroney R.N.** Ten questions concerning hybrid computational/physical model simulation of wind flow in the built environment // Build. Environ., 2016, Volume 96, pp. 12-21.
40. **Menter F., Lechner R., Matyushenko A**. Best practice: Generalized k-ω (GEKO) Two-Equation Turbulence Model in ANSYS CFD: Version 1.01. Best Practice. ANSYS, 2019, 32 p.
41. **Sharkey P.S., Menter F.R.** A numerical investigation of the turbulent flow around a scale model JBC hull using the Generalized k-omega (GEKO) turbulence model // 11th International Workshop on Ship and Marine Hydrodynamics (IWSH2019), 2019.
42. **Kok J.C.** Resolving the Dependence on Freestream Values for the k-omega Turbulence Model // AIAA Journal, 2000, Volume 38(7), pp. 1292-1295.

Goryachevsky Oleg Sergeevich, Deputy Director at A.B. Zolotov REC CM of the National Research Moscow State University of Civil Engineering; 129337, Russia, Moscow, Yaroslavskoe shosse, 26.
E-mail: osgoryachevskij@mail.ru

Горячевский Олег Сергеевич, заместитель директора НОЦ КМ им. А.Б. Золотова Национального исследовательского Московского государственного строительного университета; 129337, Россия, г. Москва, Ярославское шоссе, д. 26.
E-mail: osgoryachevskij@mail.ru

DOI:10.22337/2587-9618-2023-19-3-130-140

THE EFFECT OF SOIL DENSIFICATION ON THE ATTENUATION OF THE PHENOMENON OF SOIL LIQUEFACTION IN A PORT PROJECT IN MOROCCO

Mohamed Bziaz [1], Lahcen Bahi [1], Latifa Ouadif [1], Anas Bahi [1], Abdehak Sabihi [2], Hamou Mansouri [2]

[1] L3GIE Laboratory, Mohammadia Engineering School, B.P 765, Agdal Rabat 10090 Mohammed V University in Rabat, MOROCCOO

[2] LPEE Public Laboratory for tests and studies, Casablanca, MOROCCO

Abstract: Morocco, which is in a seismically active zone, is currently experiencing a significant development in terms of the realization of development and infrastructure projects. Therefore, reflection on soil liquefaction problems during project design is essential. The densification of soils by vibro compaction is a recent process of soil treatment, its effect is to improve the geo mechanical characteristics of the soil in this case the relative density and subsequently the reduction of the potential for liquefaction, it is a technique soil improvement in the mass, it is closely linked to the grain size of the soil to be treated, its percentage of fines less than 10% (going to 0.08 mm <10%), this technique gives the treated soil sufficient cohesion to avoid large increases in pore pressures during the earthquake. This article aims, through the study of a real case, to evaluate the effectiveness of vibro compaction to improve the relative density of the soil and consequently the reduction of the risk of liquefaction of the treated soil. The work focuses on the analysis of the SPT tests carried out before treatment and on the CPT tests of control of the vibro-compactge works carried out after execution. This study showed that this process generates an effect of improvement of the relative density and reduction of the compaction by inducing a reduction of the risk of liquefaction.

Keywords: treatment, Liquefaction, SPT, CPT, Vibro compaction, relative density

ВЛИЯНИЕ УПЛОТНЕНИЯ ПОЧВЫ НА ОСЛАБЛЕНИЕ ЯВЛЕНИЯ ЕЁ РАЗЖИЖЕНИЯ В ПОРТОВОМ ПРОЕКТЕ В МАРОККО

Мохамед Бзиаз [1], Лахсен Бахи [1], Латифа Оадиф [1], Анас Бахи [1], Абдехак Сабихи [2], Хаму Мансури [2]

[1] Лаборатория L3GIE, Инженерная школа Мохаммадии, BP 765, Агдал Рабат 10090 Университет Мохаммеда V в Рабате, Марокко

[2] Общественная лаборатория LPEE для испытаний и исследований, г. Касабланка, Марокко

Аннотация : Марокко, находящееся в сейсмически активной зоне, в настоящее время переживает значительное развитие с точки зрения реализации девелоперских и инфраструктурных проектов. Поэтому важно учитывать проблемы разжижения почвы при разработке проекта. Уплотнение грунтов путем виброуплотнения - это новейший процесс обработки грунта, его эффект заключается в улучшении геомеханических характеристик грунта, в данном случае относительной плотности и, как следствие, снижении потенциала разжижения, это метод улучшения грунта в масса, она тесно связана с размером зерен обрабатываемого грунта, его процентная доля мелких частиц менее 10% (до 0,08 мм <10%), этот метод придает обработанному грунту достаточную связность, чтобы избежать значительного увеличения пор. давления во время землетрясения. Данная статья направлена на изучение реального случая, чтобы оценить эффективность виброуплотнения для улучшения относительной плотности грунта и, следовательно, снижения риска разжижения обрабатываемого грунта. Основное внимание в работе уделяется анализу испытаний СПД, проведенных до обработки, и испытаний СРТ контроля виброуплотняющих работ, проведенных после выполнения. Это исследование показало, что этот процесс

дает эффект улучшения относительной плотности и уменьшения уплотнения, вызывая снижение риска разжижения.

Ключевые слова: обработка, сжижение, КПТ, CPT, вибропрессование, относительная плотность

1. INTRODUCTION

Carrying out projects on predominantly sandy land in seismic zones requires consideration of the liquefaction phenomenon in order to avoid unforeseen damage (Seed, 1971[2]; Robertson & Wride, 1998[3]; Boulanger & Idriss , 2008 [4]). To meet this need, the evaluation of the liquefaction potential by appropriate methods therefore becomes an important step in the design of projects in order to decide on possible treatment methods, depending on the nature of the ground treated. Our studied case is the soils of Nador in the North – East of Morocco. this soil consists of sandy deposits presenting a risk of liquefaction. after having confirmed the seismic risk by the exploitation of the SPT tests carried out on the materials in place, the vibro-compaction was carried out to fight against the phenomenon of liquefaction. The vibrations generate a temporary phenomenon of liquefaction of the ground surrounding the vibrator. In this state, the inter granular forces are almost cancelled, and the grains rearrange themselves in a denser configuration presenting better mechanical characteristics. The purpose of this article is to describe the technique as it is carried out today and to discuss the parameters to be defined and controlled to ensure the effectiveness of the liquefaction treatment process by vibro-compaction and in particular the relative density of the soil, and this through the exploitation of a companion of the CPT tests carried out after treatment of the materials.

2. PRESENTATION OF THE SITE

The site object of our study is located in the North-East of Morocco, it is the city of Nador which is known to the Mediterranean. The site is made up of permeable sandy deposits. At this location, the characterization of the soil's susceptibility to liquefaction is essential. the location of the study area is shown in figure 1.



Figure 1. Location of the study area

2.1 Geological setting

The study area is part of the Eastern Rif, and presents geological formations characterized by an upper Miocene and a lower Pleistocene belonging to the Villafranchian. These lands consist mainly of pink silts with a gravelly bed, and a small strip of a powerful Quaternary; both belonging to the Middle Quaternary.

Around the site There is a set of characteristic reliefs, formed by intermediate substrates : To the east, the volcanic Massif of Gourougou, located at the eastern limit of the site. It is 25 km long along the E-W axis and 15 km wide along the N-S axis. it culminates at 887m. It is a complex stratovolcano formed from a variety of volcanic,

basic and intermediate rocks. To the north, the Cap des Trois Fourches massif, resulting mainly from pyroclastite lava volcanism, and a set of metamorphic rocks. It culminates at 433m at the top of the tarjat.

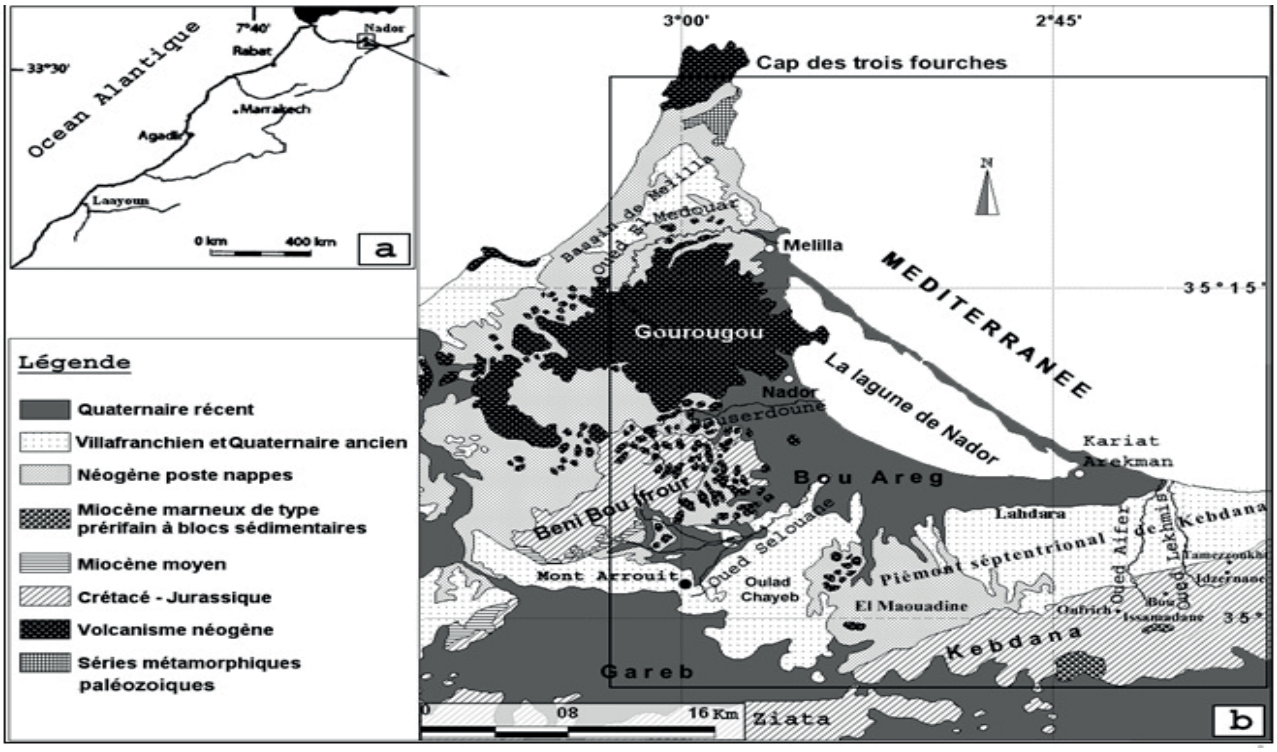


Figure 3. Extract from the geological map of the study area

2.2 The seismicity of the region

The province of Nador is part of the Rif chains, this region is the seat of a very active instrumental seismic activity, which has been verified and validated by a set of studies which have highlighted the existence of numerous active structures in the within the Rif chains.

The area planned for the port of Nador project and the watershed to which it belongs are located at the north-eastern end of the high Rif ranges, at the bay of Bettoya. It is obviously in the northern zone with medium seismicity. In addition, the Nador region is part of zone No. 3 according to the RPS 2000 revised in 2011, and therefore a maximum acceleration of 0.2 g is considered.

3. CONTEXT AND GEOTECHNICAL RECONNAISSANCE

to assess the state of compactness of the soil, an SPT test was carried out. the test result is shown in Table 1..

Table 1. SPT test result

Depth(m)	Number of shots
1.5	9
3.5	25
5.5	17
9.5	2
11.5	12
13.5	13
15.5	17
17.5	24
19.5	40
21.5	68
23.5	> 50
25.5	>50
27.5	>68
29.5	77
31.5	78
33.5	>80
35.5	>77
37.5	>83
39.5	>95
41.5	>99

The lithological section shows that the terrain of this area consists mainly of sand-based sediments up to a depth of 21.50 m. Note however the presence of a layer of alluvium between 21.50 and 22.50 m. The bedrock is made up of volcanic tuff and greyish marls up to a sounding depth of 44.30 m.
the sands encountered are loose to moderately compact, except between the depth of 19.30 m and 20.30 m where there is a dense layer of sand.

4. SOIL LIQUEFACTION RISK ASSESSMENT

In the presence of groundwater, the resistance to liquefaction of the soil is evaluated by applying the NCEER method, developed by Youd and Idriss[5], The risk of soil liquefaction is given by the safety factor F.S:

$$F.S = CRR/CSR \quad (1)$$

With: CSR: cyclic stress ratio.
CRR: cyclic resistance ratio. According to euro code 8[6], and RPS 2000 version 2011 [7], liquefaction occurs if the CRR/CSR ratio < 1.25 (2)

4.1. Cyclic Stress Ratio (CSR) Assessment

Seed and Idriss 1971[8] formulated the following equation for the calculation of the cyclic stress ratio CSR

$$CSR = \frac{\tau_{av}}{\sigma'_{v0}} = 0.65 \left(\frac{\alpha_{max}}{g}\right)\left(\frac{\sigma_{v0}}{\sigma'_{v0}}\right) r_d \quad (3)$$

Where τ_{av} is the average cyclic shear stress; α_{max} is the maximum horizontal acceleration at the ground surface; g = 9.81 m² / s is the acceleration due to gravity; σ_{v0} is the initial vertical total stress; σ'_{v0} is the initial effective vertical stress; r_d is the stress reduction factor.
The stress reduction coefficient is expressed as a function of depth by the following equations (Liao and Whitman 1986) [8]:

$$r_d = 1 - 0.00765z \quad z \leq 9{,}15m \quad (4)$$
$$r_d = 1.74 - 0.0267z \quad 9{,}15m < z \leq 23m \quad (5)$$

4.2. Evaluation of Cyclic Resistance Ratio (CRR)

The determination of cyclic soil resistance can be carried out using data obtained from in-situ tests (Standard penetration test, Cone penetration test, shear wave velocity measurement). To incorporate the effect of earthquake magnitude (duration of earthquake or number of cycles), an MSF magnitude correction factor that adjusts the CRR value to an earthquake magnitude of 7.5 will be added in the following equation which becomes as follows:

$$CRR = CRR7.5 * CM \quad (6)$$

With CM correction factor, determined according to Annex B of EN 1998-5[6], based on surface wave amplitude M

Table 2. CM correction factor, determined according to Annex B of EN 1998-5[6]

M	CM
5.50	2.86
6.00	1.20
6.50	1.69
7.00	1.30
8.00	0.67

4.3 Evaluation of Safety Factor

The standard penetration test is the most commonly used test. It consists of determining the number of strokes N necessary to sink a corer to a depth of 30 cm, while taking reworked samples indicative of the different layers crossed. This method uses the normalized standard penetration index N1.60cs For a magnitude of 7.5 an approximation of CRR is given by the formula established by Idriss and Boulanger (2006) [9-11]

$$CRR_{7.5} = \text{EXP}\left[\frac{(N1)_{60cs}}{14.1} + \left(\frac{(N1)_{60cs}}{126}\right)^2 - \left(\frac{(N1)_{60cs}}{23.6}\right)^3 + \left(\frac{(N1)_{60cs}}{25.4}\right)^4 - 2.8\right] \quad (7)$$

$$\boldsymbol{(N1)_{60cs} = (N1)_{60} + \text{EXP}\left(1.63 + \frac{9.7}{FC+0.1} - \left(\frac{15.7}{FC+0.1}\right)^2\right)} \quad (8)$$

Table 3. Safety factor for SPT-Test

Depth(m)	Nspt	CSR	CRR	FS
1.5	9	0.26	0.52	2.01
3.5	25	0.25	>4.0	>1.5
5.5	17	0.27	0.55	2.08
7.5	17	0.25	0.40	1.56
9.5	2	0.24	0.13	0.55
11.5	12	0.23	0.22	0.97
13.5	13	0.21	0.21	1.00
15.5	17	0.20	0.24	1.20
17.5	24	0.18	0.31	1.69
19.5	40	0.17	1.07	6.29
21.5	68	0.16	>4.0	>1.5
23.5	50	0.14	1.41	>1.5
25.5	50	0.13	1.73	>1.5

The safety factor calculated in table 3 leads to the conclusion that the layers between 9.00 m and 16.00 m are liquefiable.

4.4 Prediction of Seismic-Induced Settlement

Based on the curves of Ishihara and Yoshimine [12], Driss& Boulanger proposed the following empirical relationship:

$\varepsilon v = 1.5e^{(-0.025Dr,ini)}$. min {8 ;ɣ max}

$Dr,ini = \sqrt{\frac{N1(60)cs}{46}}$

If Dr,ini ≥ 39.2% ⇒ Fult = 0.032+0.047. Dr,ini - 0.0006.(Dr,ini)²

iF not Fult =+0.9524

If FS < F ult ⇒ymax→ ∞ (9)

If FS >2 ⇒y max= 0

If F ult ≤ FS ≤2 ⇒ ymax= 3.5 (2- FS)$(\frac{1-Fult}{FS-Fult})$

Table 4. Safety factor for SPT-Test

Depth(m)	Nspt	$(N1)_{60cs}$	Dr,ini	SS(cm)
1.5	9	22.51	0.70	1.15
3.5	25	39.08	0.92	0.00
5.5	17	24.76	0.73	0.41
7.5	17	23.18	0.71	0.77
9.5	2	7.46	0.40	8.77
11.5	12	16.70	0.60	2.46
13.5	13	16.27	0.60	2.38
15.5	17	18.73	0.64	1.20
17.5	24	23.42	0.71	0.31
19.5	40	34.19	0.86	0

SS : Seismic-Induced Settlement

The Seismic-Induced Settlement is about 18.00 cm.

5. SOIL TREATMENT BY VIBRO-COMPACTION

According to paragraph 3, there is a risk of liquefaction between 9.00 and 16.00 m depth. The treatment against liquefaction was done by vibro-compaction in the context of the construction of the port of Nador in Morocco, in order to improve the relative density of the materials in place.

To evaluate the effect of soil densification on liquefaction, the results of CPT tests carried out after treatment are used. Given the number of tests carried out which are more than 20 CPT tests after vibro-compaction, we will simply interpret the 7 tests which are located at the points indicated in table 5:

Table 5. Checkpoints of CPT tests after vibro compaction

Point	X	Y	CPT
1	703413.10	520974.01	CPT1
2	703392.58	520996.46	CPT2
3	307390.42	520953.30	CPT3
4	703454.86	521014.34	CPT4
5	703382.57	521052.02	CPT5
6	703410.14	520933.01	CPT6
7	703398.25	521024.51	CPT7

The determination of the relative density after vibro-compaction can be done by referring to the work of Jamiolkowski (1985) which made it possible to establish a generic correlation applicable to all types of sand and which is formulated in the following form:

$$q_c = C_0 . P_a . e^{C_1 . D_R} . \left(\frac{\sigma'_{v0}}{P_a}\right)^{C_2} \quad (10)$$

$$D_R = \frac{1}{C_1} . ln\left(\frac{{}^{q_c}/_{P_a}}{C_0 . \left(\left(\frac{\sigma'_{v0}}{P_a}\right) C_2\right)}\right) \quad (11)$$

$$\sigma'_{v0} = z . (\gamma_{sat} - \gamma_w) \quad (12)$$

$\gamma_{sat} = 21\ kPa$
$\gamma_w = 9.81\ kPa$
$P_a = 101.325\ kPa$
q_c : Measured cone resistance

DR = Relative density; σ'_{v0} : Effective vertical stress; C0 : Jamiolkowski coefficient (1985 2001); C1 : Jamiolkowski coefficient (1985 2001); C2 : Jamiolkowski coefficient (1985 2001). This work was supplemented by Jamiolkowski (2001), who proposes new coefficients C0, C1 and C2, re-evaluated:

Table 6. Coefficients C0, C1, C2 determined by Jamiolkowski in 1985 and 2001 for relations 10 and 11.

Jamiolkowski	1985	2001
C_0	11.79	17.68
C_1	2.93	3.1
C_2	0.72	0.5

The 2001 coefficients are more unfavourable in that, for an equal target relative density, they require higher values of qc than those of 1985.
The use of this formula makes it possible to trace the variation of relative density as a function of depth **(Fig3 to Fig9),** and this by exploiting the results of the CPT tests carried out after vibro-compaction.
The value of the relative density required after treatment depends on the requirements of each project, but in general it must be greater than 70%. for the case of treatment of the sand of the port of Nador by vibro-compacting the validation criteria are as follows:
1. The minimum geometric mean of the relative density measured between 0 and 4 meters depth of the CPT must be 70%
2. The minimum geometric mean relative density measured over the entire depth must be 77%
3. The values of the peak resistance qc measured must be evaluated in relation to the conformity curves **Fig: 10**. No section must decrease beyond these curves over more than 50 cm of continuous test depth
For this project the criteria mentioned above are respected for the 7 control tests and consequently the vibro-compaction has made it possible to improve the relative density of the soil and to reduce the risk of liquefaction.

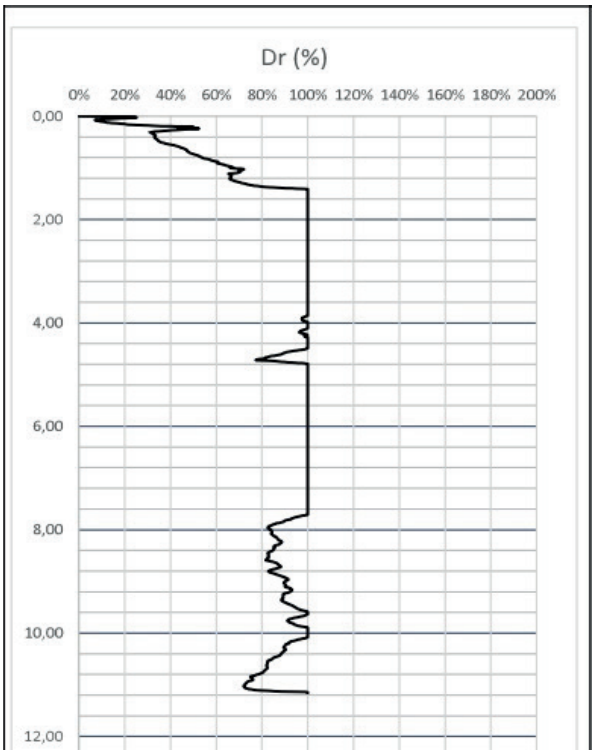


Figure 3. Relative density for CPT1 as a function of depth

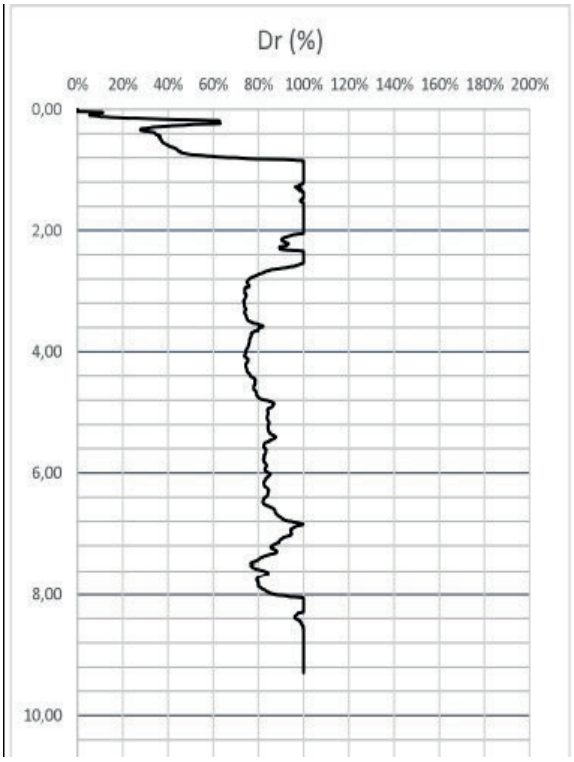


Figure 4. Relative density for CPT2 as a function of depth

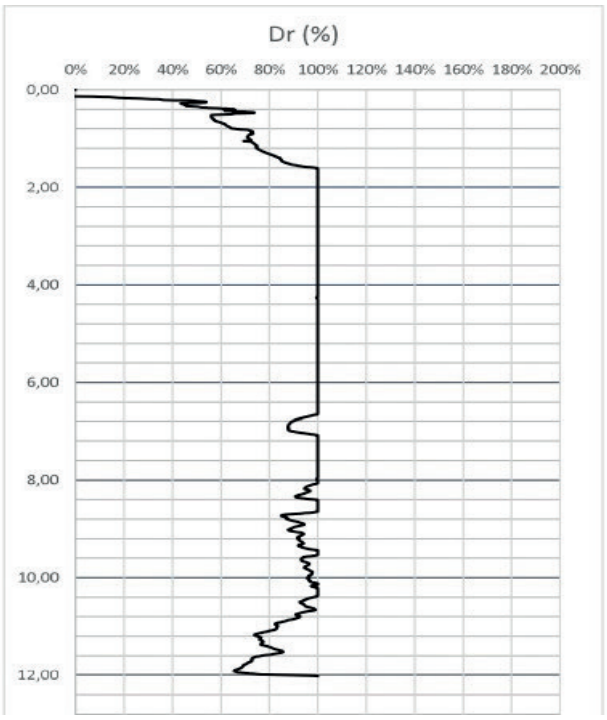


Figure 5. Relative density for CPT3 as a function of depth



Figure 6. Relative density for CPT4 as a function of depth

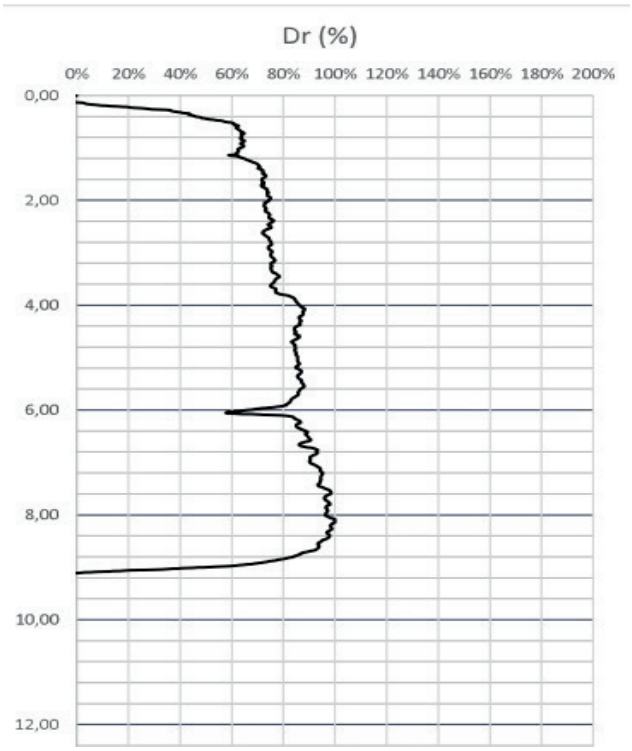


Figure 7. Relative density for CPT5 as a function of depth

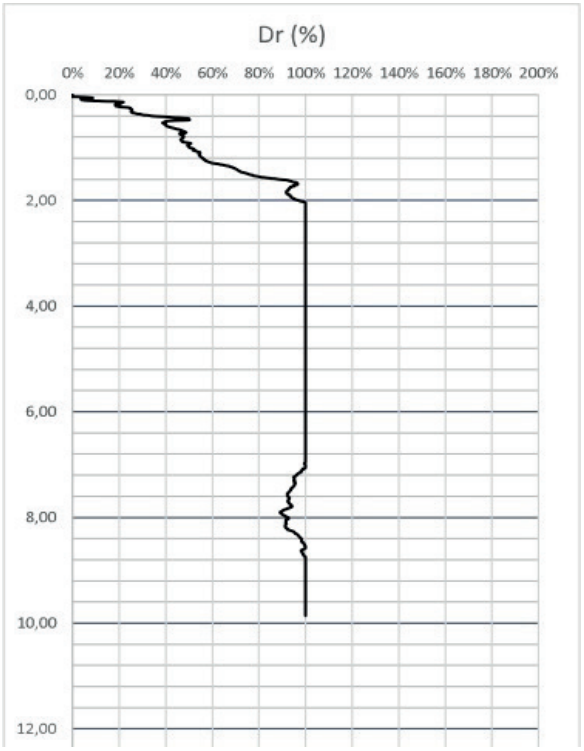


Figure 8. Relative density for CPT6 as a function of depth

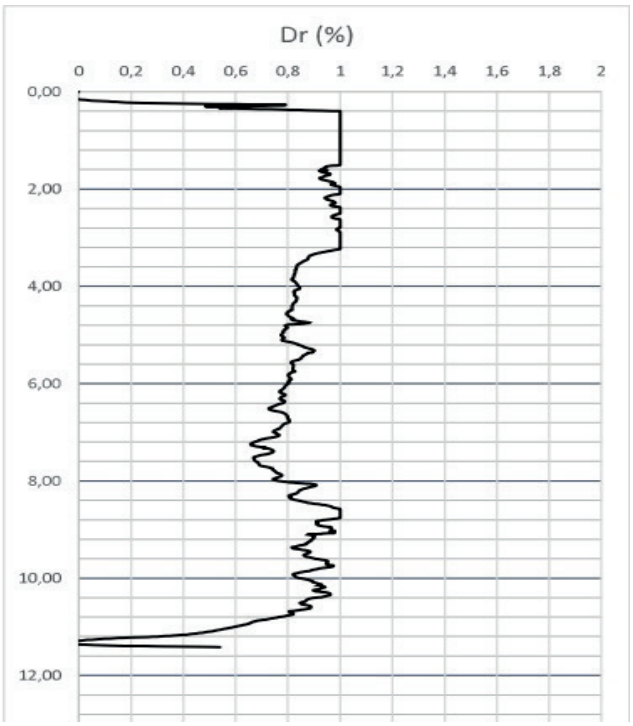


Figure 9. Relative density for CPT7 as a function of depth

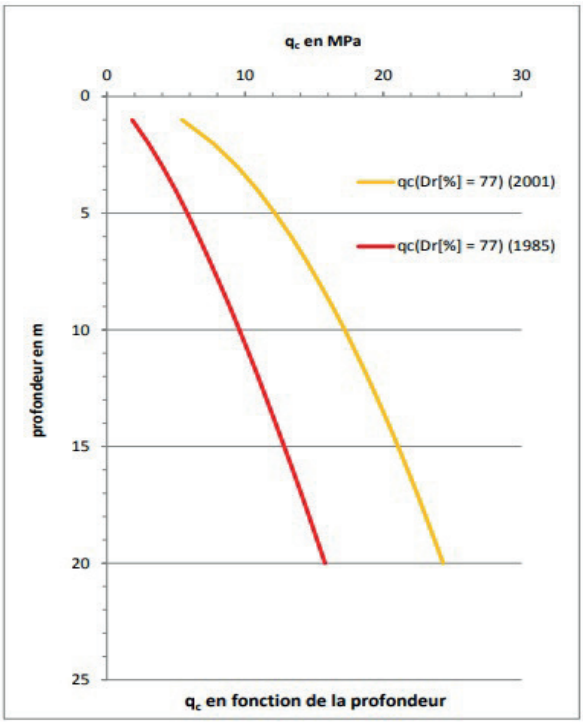


Figure 10. Correlation curves Jamiolowski Dr = 70% and Dr 77%

6. CONCLUSION

in this work we studied the soils of the port of Nador in Morocco, these soils are characterized by the existence of loose sandy deposits to moderately compact presenting a risk of liquefaction between the depths 9 m and 16 m, which was confirmed by the evaluation of the liquefaction potential and the relative density by the exploitation of the SPT tests carried out on the materials on site. the CPT tests carried out on the vibro-compacted materials have made it possible to conclude that the relative density reached after this treatment is satisfactory by inducing an improvement in the geomechanical characteristics of the treated soil and consequently the elimination of the risk of liquefaction during the earthquake

REFERENCES

1. **BZIAZ, M. - BAHI, L. - OUADIF, L. - BAHI, A - MANSOURI, H. - DOUIRI, A. - ABBACH, M**. : Evaluation of post liquefaction settlement and treatment and reinforcement of the soil by stone columns. International Journal of Innovative Research and Scientific Studies 6(1) 2023, pages: 102-114, doi: 10.53894/ijirss.v6i1.1113
2. **Seed B., Idriss I.M., 1971**. Simplified procedures for evaluating soil liquefaction potential. PROC.JSME, ASCE, Vol 97,SM9,PP 1249-1273.
3. **Robertson P.K., Wride C., 1998**. Evaluating cyclic liquefaction potential using the cone penetration test. Canadian Geotechnical Journal: 442-459.
4. **Idriss, I. M., & Boulanger, R. W. (2008).** Soil Liquefaction during Earthquakes. In Earthquake Engineering Research institute (Vol. 1). https://doi.org/10.1109/MIA.2007.322261
5. **T.L. Youd and I. M. Idriss,** "Liquefaction resistance of soils: Summary report from the 1996 NCEER and 1998 NCEER/NSF workshops on evaluation of liquefaction resistance of soils," *Journal of Geotechnical and Geoenvironmental Engineering,* vol. 127, pp. 297-313, 2001.Available at: https://doi.org/10.1061/(asce)1090-0241(2001)127:4(297).
6. **EN 1998-5, "(English): Eurocode 8**: Design of structures for earthquake resistance – Part 5: Foundations, retaining structures and geotechnical aspects [Authority: The European Union Per Regulation 305/2011, Directive 98/34/EC, Directive 2004/18/EC]. Retrieved from: https://www.phd.eng.br/wp-content/uploads/2014/11/en.1998.5.2014.pdf," 2004.
7. **RPS, "The RPS 2000 seismic building regulations**, 2011 version, department of quality and technical affairs, ministry of housing and urban policy in Morocco. Retrieved from: https://www.academia.edu/33259147," 2000.
8. **S.S.C. Liao and R.V. Whitman**, A catalog of liquefaction and Non-liquefaction occurrences during earthquakes, department of civil engineering. Cambridge, MA: Massachusetts Institute of Technology, 1986.
9. **Idriss and R. Boulanger,** "Semi-empirical procedures for evaluating liquefaction potential during earthquakes," Soil Dynamics and Earthquake Engineering, vol. 26, pp. 115-130, 2006.Available at: https://doi.org/10.1016/j.soildyn.2004.11.023.
10. **I.M. Idriss and R.W. Boulanger**, "Soil liquefaction during earthquakes," Monograph MNO-12, Earthquake

Engineering Research Institute, Oakland, CA, 2612008.

11. **I.M. Idriss and R.W. Boulanger**, SPT - based liquefaction triggering procedure, centre for geotechnical modeling, department of civil and environmental engineering. California: Universitu of California, Davis, 2010.
12. **K. Ishihara and M. Yoshimine**, "Evaluation of settlements in sand deposits following liquefaction during earthquakes," Soils and Foundations, vol. 32, pp. 173-188, 1992.Available at: https://doi.org/10.3208/sandf1972.32.173.
13. **I.M. Idriss and R.W. Boulanger**, "Semi-empirical procedures for evaluating liquefaction potential during earthquakes," presented at the 11th International Conference on Soil Dynamics and Earthquake Engineering, and 3rd International Conf. on Earthquake Geotechnical Engineering, Berkeley, USA: 32–56), 2004

СПИСОК ЛИТЕРАТУРЫ

1. **BZIAZ, M. - BAHI, L. - OUADIF, L. - BAHI, A - MANSOURI, H. - DOUIRI, A. - ABBACH, M**. : Evaluation of post liquefaction settlement and treatment and reinforcement of the soil by stone columns. International Journal of Innovative Research and Scientific Studies 6(1) 2023, pages: 102-114, doi: 10.53894/ijirss.v6i1.1113
2. **Seed B., Idriss I.M., 1971**. Simplified procedures for evaluating soil liquefaction potential. PROC.JSME, ASCE, Vol 97,SM9,PP 1249-1273.
3. **Robertson P.K., Wride C., 1998**. Evaluating cyclic liquefaction potential using the cone penetration test. Canadian Geotechnical Journal: 442-459.
4. **Idriss, I. M., & Boulanger, R. W. (2008).** Soil Liquefaction during Earthquakes. In Earthquake Engineering Research institute (Vol. 1). https://doi.org/10.1109/MIA.2007.322261
5. **T.L. Youd and I. M. Idriss,** "Liquefaction resistance of soils: Summary report from the 1996 NCEER and 1998 NCEER/NSF workshops on evaluation of liquefaction resistance of soils," *Journal of Geotechnical and Geoenvironmental Engineering,* vol. 127, pp. 297-313, 2001.Available at: https://doi.org/10.1061/(asce)1090-0241(2001)127:4(297).
6. **EN 1998-5, "(English): Eurocode 8**: Design of structures for earthquake resistance – Part 5: Foundations, retaining structures and geotechnical aspects [Authority: The European Union Per Regulation 305/2011, Directive 98/34/EC, Directive 2004/18/EC]. Retrieved from: https://www.phd.eng.br/wp-content/uploads/2014/11/en.1998.5.2014.pdf," 2004.
7. **RPS, "The RPS 2000 seismic building regulations**, 2011 version, department of quality and technical affairs, ministry of housing and urban policy in Morocco. Retrieved from: https://www.academia.edu/33259147," 2000.
8. **S.S.C. Liao and R.V. Whitman**, A catalog of liquefaction and Non-liquefaction occurrences during earthquakes, department of civil engineering. Cambridge, MA: Massachusetts Institute of Technology, 1986.

9. **Idriss and R. Boulanger,** "Semi-empirical procedures for evaluating liquefaction potential during earthquakes," Soil Dynamics and Earthquake Engineering, vol. 26, pp. 115-130, 2006. Available at: https://doi.org/10.1016/j.soildyn.2004.11.023.
10. **I.M. Idriss and R.W. Boulanger**, "Soil liquefaction during earthquakes," Monograph MNO-12, Earthquake Engineering Research Institute, Oakland, CA, 2612008.
11. **I.M. Idriss and R.W. Boulanger**, SPT - based liquefaction triggering procedure, centre for geotechnical modeling, department of civil and environmental engineering. California: Universitu of California, Davis, 2010.
12. **K. Ishihara and M. Yoshimine**, "Evaluation of settlements in sand deposits following liquefaction during earthquakes," Soils and Foundations, vol. 32, pp. 173-188, 1992.Available at: https://doi.org/10.3208/sandf1972.32.173.
13. **I.M. Idriss and R.W. Boulanger**, "Semi-empirical procedures for evaluating liquefaction potential during earthquakes," presented at the 11th International Conference on Soil Dynamics and Earthquake Engineering, and 3rd International Conf. on Earthquake Geotechnical Engineering, Berkeley, USA: 32–56), 2004

DOI:10.22337/2587-9618-2023-19-3-141-154

SEISMIC VULNERABILITY ASSESSMENT FOR BUILDINGS OF PORT BLAIR CITY USING RAPID VISUAL SCREENING AS A TOOL

Mr. Adharsh G. [1*], Dr. R. Sivakumar[2], Dr. K.S. Satyanarayanan[3]

[1*]**Affiliation 1:** S.A Engineering College, Poonamallee, Avadi Road Veeraraghavapuram, Thiruverkadu, Tamil Nadu, INDIA

[1*]**Affiliation 2:** Research Scholar, Department of Civil Engineering, Faculty of Engineering and Technology, SRM Institute of Science and Technology, SRM Nagar, Kattankulathur, Chengalpattu, Chennai TN, INDIA

[2] Department of Civil Engineering, Faculty of Engineering and Technology, SRM Institute of Science and Technology, SRM Nagar, Kattankulathur, Chengalpattu, Chennai TN, INDIA

[3] Department of Civil Engineering, Faculty of Engineering and Technology, SRM Institute of Science and Technology, SRM Nagar, Kattankulathur, Chengalpattu, Chennai TN, INDIA

[1*] Corresponding Author Email: profadharshg82072@gmail.com

Abstract: Andaman and Nicobar Islands is one of the most earthquake experienced areas around the world subjected to frequent earthquakes which is being the area of study using rapid visual screening (RVS) method by google maps and field visit as well. Although the google maps and internet sources can be used to cover up 80 percent data required for assessing and quantifying the RVS score but a field visit was made for extracting more relevant data for a detailed study. Port Blair municipal area was narrowed down for the screening since it had the greatest number of buildings. It was found that the moment resisting frames have been used in most of the buildings. RC moment resisting frames, load bearing structures, steel structures and wooden structures were studied in the screening and score was awarded. Gleaned from the score it was derived that old buildings are more susceptible for higher damage in near future then the recently constructed building.

Keywords: Damage assessment, Port Blair city, Rapid visual screening, Vulnerability assessment

ОЦЕНКА СЕЙСМИЧЕСКОЙ УЯЗВИМОСТИ ЗДАНИЙ В ГОРОДЕ ПОРТ-БЛЭР С ИСПОЛЬЗОВАНИЕМ МЕТОДА БЫСТРОГО ВИЗУАЛЬНОГО СКРИНИНГА

Адхарш Г. [1]*, Сивакумар Р. [2], Сатьянараянан К.С. [3]

[1]* инженерный колледж, Пунамалли, Авади Роуд, Вирарагхавапурам, Тируверкаду, штат Тамилнад, ИНДИЯ; Институт науки и технологий, Нагар, Каттанкулатур, Ченгалпатту, Ченнаи, штат Тамилнад, ИНДИЯ

[2] Институт науки и технологии, Нагар, Каттанкулатур, Ченгалпатту, Ченнаи, штат Тамилнад, ИНДИЯ

[3] Институт науки и технологии, Нагар, Каттанкулатур, Ченгалпатту, Ченнаи, штат Тамилнад, ИНДИЯ

[1*] Email: profadharshg82072@gmail.com

Аннотация: Андаманские и Никобарские острова - один из наиболее сейсмоопасных районов мира, подверженный частым землетрясениям, и именно здесь проводилось исследование с использованием метода быстрого визуального скрининга (БВС) по картам Google и с выездом на место. Хотя карты Google и интернет-источники могут быть использованы для получения 80% данных, необходимых для оценки и проведения БВС, для получения более релевантных данных для детального исследования был проведен выезд на место. Муниципальный район Порт-Блэр был выбран для обследования, поскольку в нем находится наибольшее количество зданий. Было обнаружено, что в большинстве зданий использовались каркасы рамного типа. В ходе обследования были изучены железобетонные рамы, несущие конструкции, стальные и деревянные конструкции и выполнена оценка. На основании

полученных оценок было сделано заключение, что старые здания более подвержены большим разрушениям в ближайшем будущем, чем недавно построенные.

Ключевые слова: Оценка ущерба, город Порт-Блэр, быстрое визуальное обследование, оценка уязвимости

1 INTRODUCTION

Andaman & Nicobar Islands lying in the Bay of Bengal is significantly one of the most vulnerable regions in terms of seismicity,[30] around the globe and is placed in zone V of Indian seismic zones. As per the national center of seismology, In India frequent earthquake occurs around the Islands in the Bay of Bengal Sea with an average of 30 earthquakes [27] [13] [28] every month *Source* After [25] [22] The Islands have also reached a population of 4 lakhs and have a high flow of tourists all over the world all these parameters show the importance of seismic studies in the Andaman & Nicobar Islands *Source* After Sarmah & Das, (2018) Port Blair which is the capital of the Andaman & Nicobar Islands is a fast-developing city that mainly is the home of the majority of reinforced concrete (RC) framed structures[19] [31] [32-34] Although the municipal regulatory board of the islands has set limitations on the height and number of floors for the RC structures as 15m or G+4 respectively, it was observed that the anchorage reinforcement was not adopted in 90% of the RC framed structures specified in IS13920:2016 ductile detailing for RC framed structures in Zone V[22-23] [26] Yadollahi.et.al.2012).[7] Though there are some studies for the geotechnical studies on the Islands unfortunately no study is found on the damage and risk assessment of the RC framed structures which is of high importance.[14] Fig 1 shows the epicenter distribution of the Andaman and Nicobar Islands where it is clearly shown the density of epicenters with a magnitude range of 6.5 – 8. A survey was conducted in the port Blair region for the existing buildings using rapid visual screening (RVS) developed by FEMA [15] *Source* After Federal Emergency Management Agency (2017) for the assessment of various types of buildings which were then used for classifying the buildings as per the damage conditions and suggestions were made or the building for further evaluation.[20] [21][24][29]

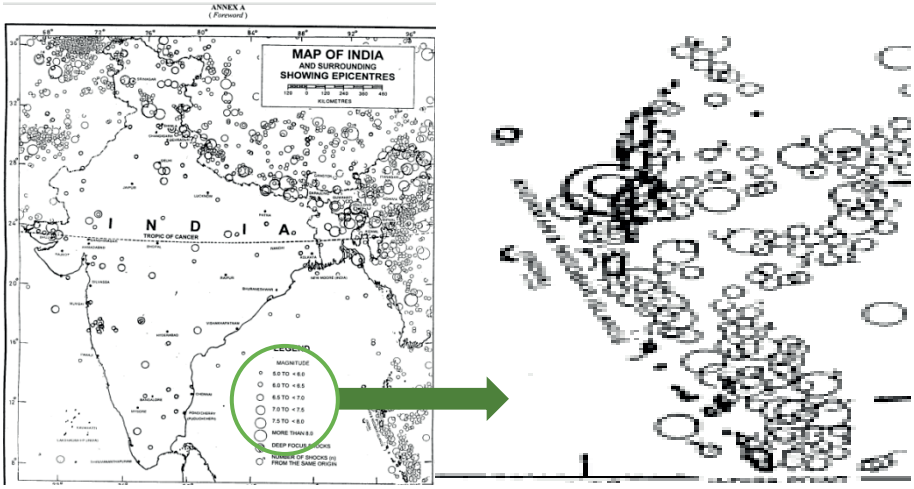


Figure 1. Epicenter distribution of Andaman and Nicobar Islands

2. LITERATURE REVIEW

Moustafa moufid Kasim and Salmia Beddu in 2021 approached the RVS method through a web-based method, where they used Google maps for data collection without physically going to the site. Around 500 buildings were selected and segregated as per plan irregularity and vertical irregularity which was taken from the street view function. A hazard map was plotted and further, it was directed for a detailed study *Source* After [18]
Additionally, Tanya Sharma and Sutapa Das in 2019 [1] conducted the rapid visual screening for 100 buildings which were randomly selected and categorized in 9 major vulnerability parameters using US FEMA *Source* After Federal Emergency Management Agency (2017) guideline

3. STUDY AREA

3.1 Geological & Soil profile

The Andaman & Nicobar Island group, situated 1200 km south east of the mainland in the Bay of Bengal *Source* After [6] The main agricultural soils are found in the valleys and are of alluvial and colluvial origin and sandy clay to sandy loam in texture *Source* After Subramani & Gangaiah. The pH of soils is normal for 55.3 and 72.4 % soils of Andaman and Nicobar districts *Source* After Subramani & Gangaiah.

3.2 Seismic History

The Islands have experienced numerous earthquakes in its life span. Although the numbers are not recorded precisely before 19th century. In this paper the seismic events pre–and post-independence are discussed. On 26 June 1941 a huge magnitude earthquake occurred with an epicentral distance of 60kM from South Andaman causing major and damages to masonry structures including the collapse of cellular jail's central watch tower *source* after [6]. Till the 2004 earthquake there was not a substantial high magnitude earthquake recorded which were almost less than 6 (M<6), however a moderate earthquake was recorded 20 January 1992 with a magnitude of 6.9, and a similar earthquake again hit the islands with a magnitude of 6.5 on 13 September 2002. On 2004 the islands experienced its highest magnitude earthquake ever recorded of 9.3. after the 2004 earthquake many seismic events were recorded with mild magnitude till date.

4.SCREENING METHODOLOGY

The study aimed to create a hazard profile of Port Blair city. As this was the city's first study of its kind, the building samples were chosen randomly within a zone. The RC framed buildings are generally susceptible to getting damaged if it has irregularity of shape in plan and elevation, hence two types of screening methods were adopted

4.1 Google earth images (GEI)

Google Earth images (GEI) is a free source through which the area and the dimensions of the building can be calculated for preliminary screening. Using GEI, it was found that most of the RC buildings were symmetrical in shape. Around 100 buildings were selected from higher altitudes as samples by switching the satellite view to terrain view in GEI from the study area randomly and only 5 buildings had plan irregularity. The preliminary survey using GEI showed buildings are vulnerable due to plan irregularity as 5%.



Figure 2. Building sampling using Google earth images (GEI)

4.2 Rapid Visual Screening (RVS

RVS method is one of the most widely used methods for initial screening of buildings that are in seismic zones, since it is simple, anyone with no technical knowledge can survey the buildings and fill out the form *source* after [4]. The RVS form was generated by the federal emergency management agency (FEMA) which created it for low, moderate, and high seismic zones and as far as the Indian version of RVS is concerned it has been modified for masonry buildings and RC structures for five different seismic zones. The survey forms can be customized as per the need which is the major advantage of the tool *Source* after [11]

4.3 Building possession

All the buildings were roped into 10 categories according to their building possession- Residential, Commercial, Industrial, Government, Office, School, Hospital, Religious, Storage, Transportation, Unknown and Mixed Use

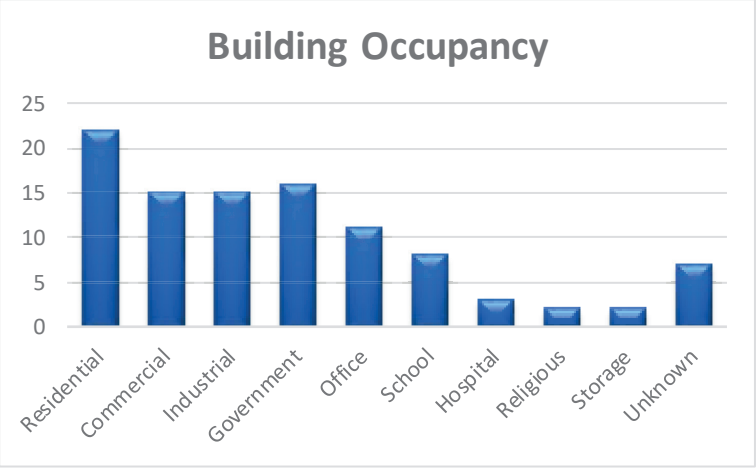


Figure 3. Distribution contribution of building occupancy

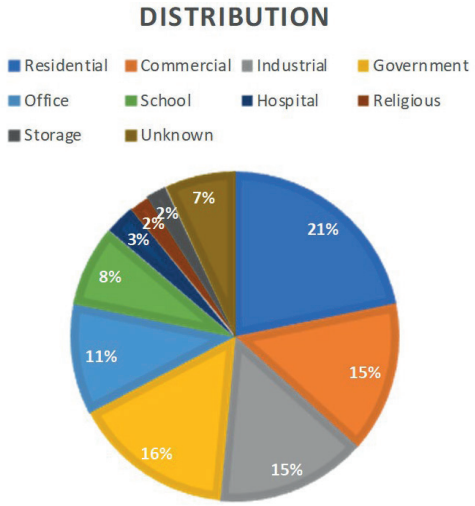
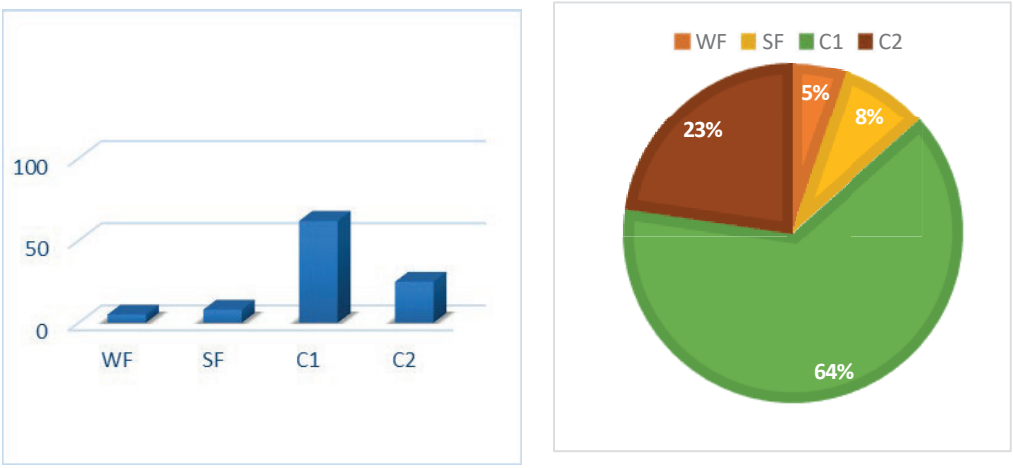


Figure 4. Percentage Distribution of building occupancy

4.4 Building Type

On account to the survey conducted only 5 types of building were found in the city which were wood frame (WF), Steel frames (SF), Concrete moment resisting frame (C1), Concrete frame with masonry infill (C2). Figure 5 shows the distribution of the 100 building samples distribution according to its building type. Most of the buildings were newly constructed due to the increase in tourism and steel structures were limited and very few truss and bridge decks were made of steel elements. Wooden structures were very less in numbers with only single storey buildings.



(a) *(b)*

Figure 5. (a) Distribution contribution of building type (b) Percentage distribution of building type

4.5 Building sample

In Port Blair city, a total of 75 building was surveyed using the RVS sheet. The sample consisted of 60 RCC buildings with normal slabs and steel roof trusses and 10 other types of buildings which were non-engineered buildings with low-risk profiles consisting of timber structures. The RCC buildings sampled were a mixture of old buildings to newly constructed buildings. As the city is now a tourism hub, most RC buildings were private hotels and residencies. The buildings were observed for 3 to 5 minutes and the survey form was filled *source* after [12]



a) *b)* *c)*

Figure 5. (a) area covered in the city (b) & (c) Elevation and external condition of building samples

5. DETAILED VISUAL INVESTIGATION

The buildings were further investigated to find if any deep damage traces are found in the structure. As a result, it was observed that out of 75 sampled structure 3 buildings were damaged severely in the beam column section and required immediate repairing. The damaged buildings were constructed well before 30 years as per the local sources. The major damage was found in the buildings after the 2004 earthquake as per local sources. A high magnitude earthquake may cause severe damage and lead the deterioration of the structures [16] As per the local construction engineer no buildings were constructed with refence to IS codes source after [17], (Yang & Goettel,et.al.2007), (Yadollahi, et al.2012).



(a) *(b)* *(c)*

Figure 6. (a), (b) & (c) Damaged beam and column in three different schools of Port Blair

6. BUILDING CONSTRUCTION REQUIRED

According to IS13920:2016 the required ductile detailing in seismic zone V, in an external joint, all the longitudinal bars shall be well provided with anchorage length away from the inner face of the column, equal to the development length in tension plus 10 times the bar diameter minus the allowance for 90-degree bend(‘s) and in internal joints both face bars of the beam shall be taken continuously through the column *Source* after BIA (1996)

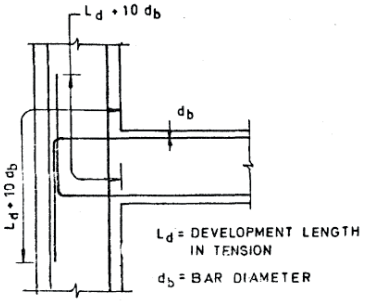


Figure 7. Beam-column joint required in a highly seismic area building [3]

7. STATE OF DAMAGE AND RVS SCORE

As per the data analyzed in the sheets, RVS scores were calculated. The score suggests the damage level of the building in the near future due to earthquake or other dynamic loads with respect to all the parameters

Table 1. RVS score and potential damage of building with reference to European Macro-seismic Scale (EMS-98) source after Graziani, et al., (2019)

RVS Score	Potential Damage	Damage Description
RS < 0.3	Most likely to get Class 5 damage; Very high chance of Class 4 damage	**Destruction** (In-depth structural system damage) Ground floor collapse (e.g., building wings)
0.3 < RS < 0.7	Most likely to get Class 4 damage; Very high chance of Class 3 damage	**Very hefty damage** (Substantial structural system damage, massive non-structural damage) Heavy cracks in structural elements with concrete compression failure and steel fractures; bond failure of reinforcing bars; camber of columns.
0.7 < RS < 2.0	Most likely to get Class 3 damage; Very high chance of Class 2 damage	**Substantial to hefty damage** (Average structural damage, hefty non-structural damage) Column cracks and beam-column joints, at coupled wall joints, concrete cover spalling and buckling of reinforced bars.
2.0 < RS < 3.0	Most likely to get Class 2 damage; Very high probability of Class 1 damage	**Medium Damage** (Minor structural damage, medium non-structural damage) Cracks in structural members.
RS > 3.0	Most likely to get Class 1 damage	**Negligible to minor damage** (Nil structural damage, minor non-structural damage) Hair cracks in the upper layer over frame members or in walls at the base. Hair cracks in partition walls and infills.

Table 2 RVS score performance of buildings

RVS Score	Damage Class	Number of buildings			
		WF	SF	C1	C2
RS < 0.3	5	0	0	1	1
30.3 < RS < 0.7	4	0	0	16	2

RVS Score	Damage Class	Number of buildings			
		WF	SF	C1	C2
0.7 < RS < 2.0	3	0	0	15	6
2.0 < RS < 3.0	2	2	3	19	4
RS > 3.0	1	3	5	11	12

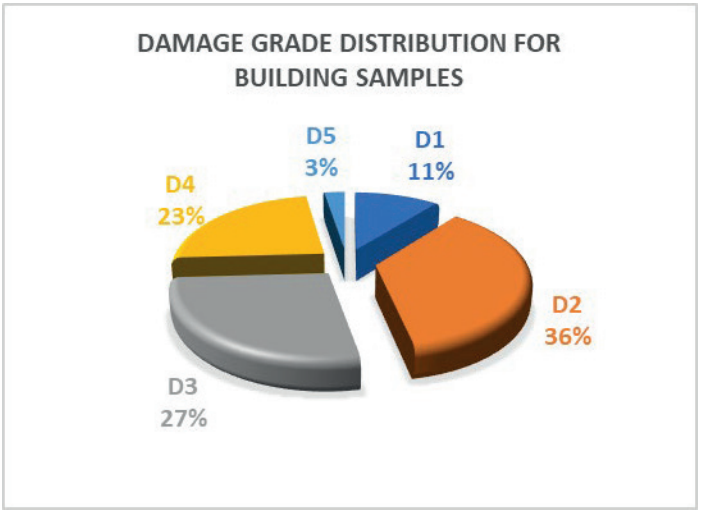


Figure 6. Damage grade distribution of all the building samples assessed

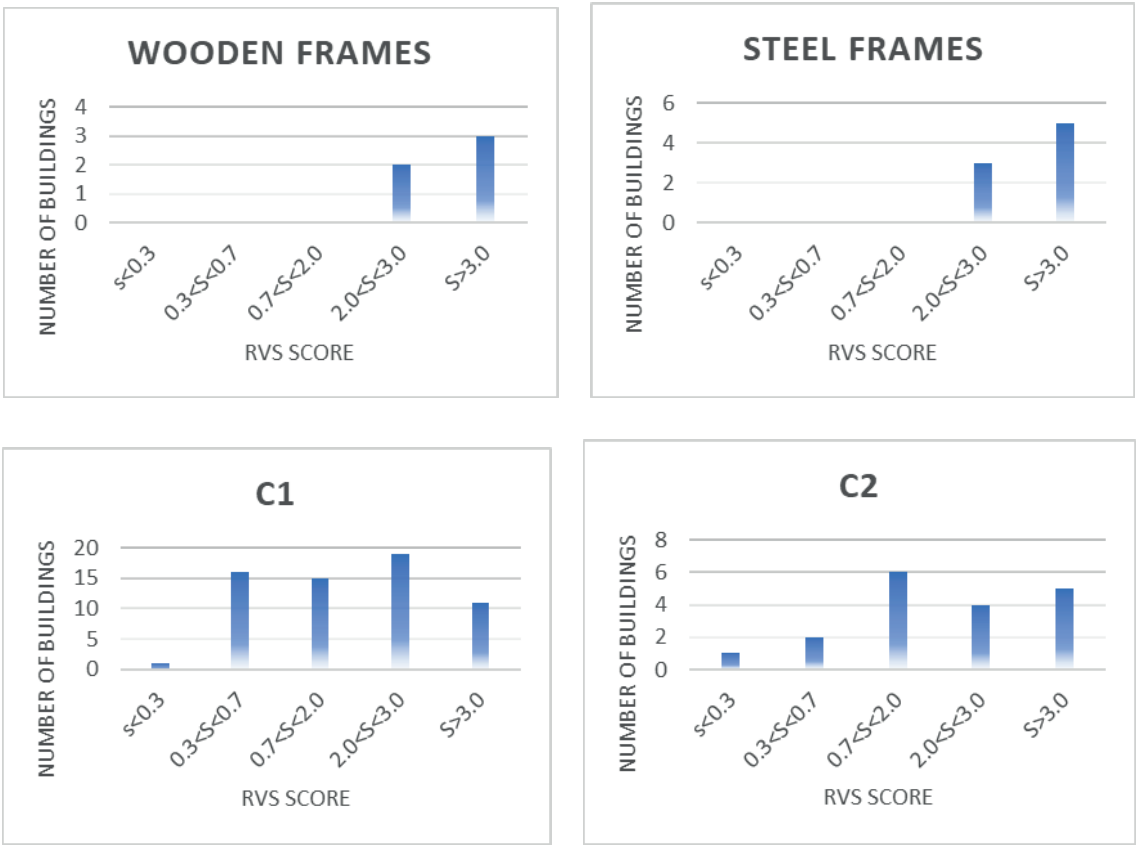


Figure 7. RVS score of corresponding building types

A total of 5 wooden frames were assessed during RVS out of which two buildings showed three buildings were used as ware houses which substantially showed grade 2 damage and two buildings that were not much used in the past showed grade 1 damage. 8 steel frames were observed in which were mostly used as workshops and motor garages, 3 frames were drafted under grade 2 damage where a slight crack were observed near the steel column and connected walls though the remaining 5 trusses were classified under grade one damage due to zone severity.

The majority of the building in the inspected area were found to be moment resisting RC frames(C1) in which 62 buildings were visited for screening. 11 framed buildings were grouped in grade 1 damage due to their plan and elevation regularity. 19 buildings were grouped under grade 2 damage due their plan and vertical irregularity being the reason of grading in the majority of building which were also constructed in sloped areas. The C1 type building were less in numbers in which 1, 2, 6, 4, and 12 number of buildings were grouped under grade 5, 4, 3, 2, and 1 respectively.[8] [9] [10].

8. CONCLUSION

For the development and safety of the residents of Port Blair city and due to the large inflow of tourism every year in the Islands, it is very important to study the remaining area of the city for the damage assessment and present conditions of the building. As the survey was conducted within a small scale of 75 buildings most of the buildings were residential and a very small percentage of buildings were used for commercial purposes. The following points were concluded after the study using RVS as a tool to measure the damage of buildings in the future.

1. The Rapid visual screening tool could be used for the initial screening of buildings through google maps where the plan irregularity in plan can be find out and further study can be done if the full-scale picture is available through internet sources of all the buildings of the selected area.
2. All though the Port Blair city has shown a steady growth in their infrastructure development and doesn't show much negative values while screening but the construction practice adopted in the Islands doesn't meet the regulations of IS13920:2016 of ductile design.
3. The old buildings which were observed were 50 years old in average which showed significant damage in the crucial areas such as beam column joint.
4. As the city is of national importance, more detailed visual screening and deep inspection is needed for the buildings which showed the sign of vulnerability during the present study

REFERENCES

1. **Alam, N., Alam, M.S., Tesfamariam, S.** (2012). Buildings' seismic vulnerability assessment methods: a comparative study. *Natural hazards*, *62*, 405-424.
2. **Angeletti, P., Bellina, A., Guagenti, E., Moretti, A., Petrini, V.** (1988, August). Comparison between vulnerability assessment and damage index, some results. In *Proceedings of the 9th World Conference on Earthquake Engineering* (Vol. 7, pp. 181-186).
3. **Bandopadhyay, P.C., Carter, A.** (2017). Chapter 2 Introduction to the geography and geomorphology of the Andaman–Nicobar Islands. *Geological Society, London, Memoirs*, *47*(1), 9-18.
4. **Bhalkikar, A., Kumar, R.P.** (2021, February). A comparative study of different rapid visual survey methods used for seismic assessment of existing buildings. In *Structures* (Vol. 29, pp. 1847-1860). Elsevier.

5. New Zealand Society for Earthquake Engineering (1998-). (2014). *Assessment and improvement of the structural performance of buildings in earthquakes: Prioritisation, initial evaluation, detailed assessment, improvement measures: Recommendations of a NZSEE study group on earthquake risk buildings*. New Zealand Society for Earthquake Engineering.
6. **Bandopadhyay, P.C., Carter, A.** (2017). Chapter 6 geological framework of the Andaman–Nicobar Islands. *Geological Society, London, Memoirs*, *47*(1), 75-93.
7. **Chourasia, A., Singh, S.K., Singhal, S., Singh, D., & Chauhan, N.** (2021). Detailed vulnerability assessment and seismic upgradation of non-engineered masonry building. *Journal of Structural Integrity and Maintenance*, *6*(2), 123-134.
8. Federal Emergency Management Agency (US) (Ed.). (2017). *Rapid visual screening of buildings for potential seismic hazards: a handbook*. Government Printing Office.
9. **Golla, A.P.S., Bhattacharya, S.P., Gupta, S.** (2020). The accessibility of urban neighborhoods when buildings collapse due to an earthquake. *Transportation research part D: transport and environment*, *86*, 102439.
10. **Graziani, L., Del Mese, S., Tertulliani, A., Arcoraci, L., Maramai, A., & Rossi, A.** (2019). Investigation on damage progression during the 2016–2017 seismic sequence in Central Italy using the European Macroseismic Scale (EMS-98). *Bulletin of Earthquake Engineering*, *17*, 5535-5558.
11. **Harirchian, E., Lahmer, T.** (2019, October). Earthquake hazard safety assessment of buildings via smartphone app: A comparative study. In *IOP Conference Series: Materials Science and Engineering* (Vol. 652, No. 1, p. 012069). IOP Publishing.
12. **Harith, N.S.H., Jainih, V., Ladin, M.A., Adiyanto, M.I.** (2021). Assessing the vulnerability of Kota Kinabalu buildings. *Civil Engineering Architecture*, *9*, 68-77.
13. **Hassan, A.F., Sozen, M.A.** (1997). Seismic vulnerability assessment of low-rise buildings in regions with infrequent earthquakes. *ACI structural journal*, *94*(1), 31-39.
14. **Ilki, A., Comert, M., Demir, C., Orakcal, K., Ulugtekin, D., Tapan, M., Kumbasar, N.** (2014). Performance based rapid seismic assessment method (PERA) for reinforced concrete frame buildings. *Advances in structural engineering*, *17*(3), 439-459.
15. **Ishack, S., Bhattacharya, S.P., Maity, D.** (2021). Rapid Visual Screening method for vertically irregular buildings based on Seismic Vulnerability Indicator. *International Journal of Disaster Risk Reduction*, *54*, 102037.
16. **Jain, S.K., Murty, C.V.R.** (2005). Proposed draft provisions and commentary on ductile detailing
17. **Jain, S., Mitra, K**., K of RC structures subjected to seismic forces. *IITK/GSDMA, EQ11-v4 & EQ16-v3 IIT, Kanpur*. umar, M., & Shah, M. (2010, July). A rapid visual seismic assessment procedure for RC frame buildings in India. In *Proceedings of the 9th US National and 10th Canadian Conference on Earthquake Engineering, Toronto, ON, Canada* (Vol. 29).
18. **Kassem, M.M., Beddu, S., Ooi, J.H., Tan, C.G., Mohamad El-Maissi, A., Mohamed Nazri, F.** (2021). Assessment of seismic building vulnerability using rapid visual screening method through web-based application for Malaysia. *Buildings*, *11*(10), 485.
19. **Micozzi, F., Scozzese, F., Ragni, L., Dall'Asta, A.** (2022). Seismic reliability of base isolated systems: sensitivity to design choices. *Engineering Structures*, *256*, 114056.
20. **Miyamoto, H.K., Gilani, A.S., Wada, A.** (2012). The 2011 Eastern Japan earthquake: Facts and reconstruction recommendations. *Proc. 15 WCEE*.

21. **Papadrakakis, M., Fragiadakis, M., Plevris, V.** Risk Assessment of Historic Residential Brick-Masonry Buildings in Vienna by Rapid-Visual-Screening.
22. **Rahman, N., Ansary, M.A., Islam, I.** (2015). GIS based mapping of vulnerability to earthquake and fire hazard in Dhaka city, Bangladesh. *International journal of disaster risk reduction*, *13*, 291-300.
23. **Rai, D.C.** (2005). Review of documents on seismic evaluation of existing buildings. *Department of Civil Engineering, Indian Institute of Technology Kanpur India*.
24. **Rai, P.K., Singh, P., Mishra, V.N., Resilience, S.C.** (2021). *Recent technologies for disaster management and risk reduction*. Springer International Publishing.
25. **Sarmah, T., Das, S.** (2018). Earthquake vulnerability assessment for RCC buildings of Guwahati city using rapid visual screening. *Procedia engineering*, *212*, 214-221.
26. **Shah, M.F., Ahmed, A., Kegyes-B, O.K.** (2016, November). A Case Study Using Rapid Visual Screening Method to Determine the Vulnerability of Buildings in two Districts of Jeddah, Saudi Arabia. In *Proceedings of the 15th international symposium on new technologies for urban safety of mega cities in Asia, Tacloban, Philippines* (pp. 7-9).
27. **Sinha, A.K.** (2022). Rapid visual screening vulnerability assessment method of buildings: a review. *International Journal of Advanced Technology and Engineering Exploration*, *9*(88), 326.
28. **Sinha, R., Goyal, A.** (2004). A national policy for seismic vulnerability assessment of buildings and procedure for rapid visual screening of buildings for potential seismic vulnerability. *Report to Disaster Management Division, Ministry of Home Affairs, Government of India, Hindistan*, 1-9.
29. **Sinha, R., Goyal, A.** (2004). A national policy for seismic vulnerability assessment of buildings and procedure for rapid visual screening of buildings for potential seismic vulnerability. *Report to Disaster Management Division, Ministry of Home Affairs, Government of India, Hindistan*, 1-9.
30. **Takahashi, A., Tago, S., Ilki, A., Okada, T.** (2004, August). Seismic capacity evaluation of existing reinforced concrete buildings in turkey (effect of retrofit). In *Proceedings of 13th world conference on earthquake engineering, Canada: Vancouver* (pp. 1-6).
31. **Visuvasam, J., Simon, J., Chandrasekar, R.** (2017). Seismic vulnerability assessment of existing residential building at Vellore. *Int J Civ Eng Technol*, *8*(4), 604-610.
32. **Yadollahi, M., Adnan, A., Zin, R.M.** (2012). Seismic vulnerability functional method for rapid visual screening of existing buildings. *Archives of Civil Engineering*, 363-377.
33. **Yakut, A.** (2004). Preliminary seismic performance assessment procedure for existing RC buildings. *Engineering Structures*, *26*(10), 1447-1461.
34. **Yang, Y., Goettel, K.A.** (2007). *Enhanced rapid visual screening (E-Rvs) method for prioritization of seismic retrofits in Oregon*. Portland, OR, USA: Oregon Department of Geology and Mineral Industries.

СПИСОК ЛИТЕРАТУРЫ

1. **Alam, N., Alam, M.S., Tesfamariam, S.** (2012). Buildings' seismic vulnerability assessment methods: a comparative study. *Natural hazards*, *62*, 405-424.
2. **Angeletti, P., Bellina, A., Guagenti, E., Moretti, A., Petrini, V.** (1988, August). Comparison between vulnerability assessment and damage index, some results. In *Proceedings of the 9th World Conference on Earthquake Engineering* (Vol. 7, pp. 181-186).
3. **Bandopadhyay, P.C., Carter, A.** (2017). Chapter 2 Introduction to the geography and geomorphology of the Andaman–

Nicobar Islands. *Geological Society, London, Memoirs*, *47*(1), 9-18.

4. **Bhalkikar, A., Kumar, R.P.** (2021, February). A comparative study of different rapid visual survey methods used for seismic assessment of existing buildings. In *Structures* (Vol. 29, pp. 1847-1860). Elsevier.
5. New Zealand Society for Earthquake Engineering (1998-). (2014). *Assessment and improvement of the structural performance of buildings in earthquakes: Prioritisation, initial evaluation, detailed assessment, improvement measures: Recommendations of a NZSEE study group on earthquake risk buildings*. New Zealand Society for Earthquake Engineering.
6. **Bandopadhyay, P.C., Carter, A.** (2017). Chapter 6 geological framework of the Andaman–Nicobar Islands. *Geological Society, London, Memoirs*, *47*(1), 75-93.
7. **Chourasia, A., Singh, S.K., Singhal, S., Singh, D., & Chauhan, N.** (2021). Detailed vulnerability assessment and seismic upgradation of non-engineered masonry building. *Journal of Structural Integrity and Maintenance*, *6*(2), 123-134.
8. Federal Emergency Management Agency (US) (Ed.). (2017). *Rapid visual screening of buildings for potential seismic hazards: a handbook*. Government Printing Office.
9. **Golla, A.P.S., Bhattacharya, S.P., Gupta, S.** (2020). The accessibility of urban neighborhoods when buildings collapse due to an earthquake. *Transportation research part D: transport and environment*, *86*, 102439.
10. **Graziani, L., Del Mese, S., Tertulliani, A., Arcoraci, L., Maramai, A., & Rossi, A.** (2019). Investigation on damage progression during the 2016–2017 seismic sequence in Central Italy using the European Macroseismic Scale (EMS-98). *Bulletin of Earthquake Engineering*, *17*, 5535-5558.
11. **Harirchian, E., Lahmer, T.** (2019, October). Earthquake hazard safety assessment of buildings via smartphone app: A comparative study. In *IOP Conference Series: Materials Science and Engineering* (Vol. 652, No. 1, p. 012069). IOP Publishing.
12. **Harith, N.S.H., Jainih, V., Ladin, M.A., Adiyanto, M.I.** (2021). Assessing the vulnerability of Kota Kinabalu buildings. *Civil Engineering Architecture*, *9*, 68-77.
13. **Hassan, A.F., Sozen, M.A.** (1997). Seismic vulnerability assessment of low-rise buildings in regions with infrequent earthquakes. *ACI structural journal*, *94*(1), 31-39.
14. **Ilki, A., Comert, M., Demir, C., Orakcal, K., Ulugtekin, D., Tapan, M., Kumbasar, N.** (2014). Performance based rapid seismic assessment method (PERA) for reinforced concrete frame buildings. *Advances in structural engineering*, *17*(3), 439-459.
15. **Ishack, S., Bhattacharya, S.P., Maity, D.** (2021). Rapid Visual Screening method for vertically irregular buildings based on Seismic Vulnerability Indicator. *International Journal of Disaster Risk Reduction*, *54*, 102037.
16. **Jain, S.K., Murty, C.V.R.** (2005). Proposed draft provisions and commentary on ductile detailing
17. **Jain, S., Mitra, K**., K of RC structures subjected to seismic forces. *IITK/GSDMA, EQ11-v4 & EQ16-v3 IIT, Kanpur*. umar, M., & Shah, M. (2010, July). A rapid visual seismic assessment procedure for RC frame buildings in India. In *Proceedings of the 9th US National and 10th Canadian Conference on Earthquake Engineering, Toronto, ON, Canada* (Vol. 29).
18. **Kassem, M.M., Beddu, S., Ooi, J.H., Tan, C.G., Mohamad El-Maissi, A., Mohamed Nazri, F.** (2021). Assessment of seismic building vulnerability using rapid visual screening method through web-based application for Malaysia. *Buildings*, *11*(10), 485.
19. **Micozzi, F., Scozzese, F., Ragni, L., Dall'Asta, A.** (2022). Seismic reliability of

base isolated systems: sensitivity to design choices. *Engineering Structures*, *256*, 114056.

20. **Miyamoto, H.K., Gilani, A.S., Wada, A.** (2012). The 2011 Eastern Japan earthquake: Facts and reconstruction recommendations. *Proc. 15 WCEE*.
21. **Papadrakakis, M., Fragiadakis, M., Plevris, V.** Risk Assessment of Historic Residential Brick-Masonry Buildings in Vienna by Rapid-Visual-Screening.
22. **Rahman, N., Ansary, M.A., Islam, I.** (2015). GIS based mapping of vulnerability to earthquake and fire hazard in Dhaka city, Bangladesh. *International journal of disaster risk reduction*, *13*, 291-300.
23. **Rai, D.C.** (2005). Review of documents on seismic evaluation of existing buildings. *Department of Civil Engineering, Indian Institute of Technology Kanpur India*.
24. **Rai, P.K., Singh, P., Mishra, V.N., Resilience, S.C.** (2021). *Recent technologies for disaster management and risk reduction*. Springer International Publishing.
25. **Sarmah, T., Das, S.** (2018). Earthquake vulnerability assessment for RCC buildings of Guwahati city using rapid visual screening. *Procedia engineering*, *212*, 214-221.
26. **Shah, M.F., Ahmed, A., Kegyes-B, O.K.** (2016, November). A Case Study Using Rapid Visual Screening Method to Determine the Vulnerability of Buildings in two Districts of Jeddah, Saudi Arabia. In *Proceedings of the 15th international symposium on new technologies for urban safety of mega cities in Asia, Tacloban, Philippines* (pp. 7-9).
27. **Sinha, A.K.** (2022). Rapid visual screening vulnerability assessment method of buildings: a review. *International Journal of Advanced Technology and Engineering Exploration*, *9*(88), 326.
28. **Sinha, R., Goyal, A.** (2004). A national policy for seismic vulnerability assessment of buildings and procedure for rapid visual screening of buildings for potential seismic vulnerability. *Report to Disaster Management Division, Ministry of Home Affairs, Government of India, Hindistan*, 1-9.
29. **Sinha, R., Goyal, A.** (2004). A national policy for seismic vulnerability assessment of buildings and procedure for rapid visual screening of buildings for potential seismic vulnerability. *Report to Disaster Management Division, Ministry of Home Affairs, Government of India, Hindistan*, 1-9.
30. **Takahashi, A., Tago, S., Ilki, A., Okada, T.** (2004, August). Seismic capacity evaluation of existing reinforced concrete buildings in turkey (effect of retrofit). In *Proceedings of 13th world conference on earthquake engineering, Canada: Vancouver* (pp. 1-6).
31. **Visuvasam, J., Simon, J., Chandrasekar, R.** (2017). Seismic vulnerability assessment of existing residential building at Vellore. *Int J Civ Eng Technol*, *8*(4), 604-610.
32. **Yadollahi, M., Adnan, A., Zin, R.M.** (2012). Seismic vulnerability functional method for rapid visual screening of existing buildings. *Archives of Civil Engineering*, 363-377.
33. **Yakut, A.** (2004). Preliminary seismic performance assessment procedure for existing RC buildings. *Engineering Structures*, *26*(10), 1447-1461.
34. **Yang, Y., Goettel, K.A.** (2007). *Enhanced rapid visual screening (E-Rvs) method for prioritization of seismic retrofits in Oregon*. Portland, OR, USA: Oregon Department of Geology and Mineral Industries.

Mr. Adharsh G. **Affiliation 1:** Assistant Professor, Department of Civil Engineering, S.A Engineering College, Poonamallee, Avadi Road Veeraraghavapuram, Thiruverkadu, Tamil Nadu, INDIA; **Affiliation 2:** Research Scholar, Department of Civil Engineering, Faculty of Engineering and Technology, SRM Institute of Science and Technology, SRM Nagar, Kattankulathur, 603203, Chengalpattu, Chennai TN, INDIA. Email: profadharshg82072@gmail.com

Dr. R. Sivakumar, Professor, Department of Civil Engineering, Faculty of Engineering and Technology,

SRM Institute of Science and Technology, SRM Nagar, Kattankulathur, 603203, Chengalpattu, Chennai TN, INDIA. Email: profadharshg82072@gmail.com

Dr. K.S. Satyanarayanan Professor, Department of Civil Engineering, Faculty of Engineering and Technology, SRM Institute of Science and Technology, SRM Nagar, Kattankulathur, 603203, Chengalpattu, Chennai TN, INDIA. Email: profadharshg82072@gmail.com

Адхарш Г., доцент, кафедра гражданского строительства, инженерный колледж, Пунамалли, Авади Роуд, Вирарагхавапурам, Тируверкаду, штат Тамилнад, Индия; Научный сотрудник, кафедра гражданского строительства, факультет инженерии и технологий, Институт науки и технологий, Нагар, Каттанкулатур, 603203, Ченгалпатту, Ченнаи, штат Тамилнад, Индия. Эл. почта: profadharshg82072@gmail.com

Сивакумар Р., профессор кафедры гражданского строительства инженерно-технологического факультета Института науки и технологии, Нагар, Каттанкулатур, 603203, Ченгалпатту, Ченнаи, штат Тамилнад, Индия. Эл. почта: profadharshg82072@gmail.com

Сатьянараянан К.С., профессор кафедры гражданского строительства инженерно-технологического факультета Института науки и технологии, Нагар, Каттанкулатур, 603203, Ченгалпатту, Ченнаи, штат Тамилнад, Индия. Эл. почта: profadharshg82072@gmail.com

International Journal for Computational Civil and Structural Engineering, 19(3) 155–164(2023)

DOI:10.22337/2587-9618-2023-19-3-155-164

LOCALIZATION OF SOLUTION OF THE PROBLEM OF THREE-DIMENSIONAL THEORY OF ELASTICITY WITH THE USE OF B-SPLINE DISCRETE-CONTINUAL FINITE ELEMENT METHOD

Marina L. Mozgaleva, Pavel A. Akimov

National Research Moscow State University of Civil Engineering, Moscow, RUSSIA

Abstract: Localization of solution of the problem of three-dimensional theory of elasticity with the use of B-spline discrete-continual finite element method (specific version of wavelet-based discrete-continual finite element method) is under consideration in the distinctive paper. The original operational continual and discrete-continual formulations of the problem are given, some actual aspects of construction of normalized basis functions of a B-spline are considered, the corresponding local constructions for an arbitrary discrete-continual finite element are described, some information about the numerical implementation and an example of analysis are presented.

Keywords: localization, wavelet-based discrete-continual finite element method, B-spline discrete-continual finite element method, discrete-continual finite element method, finite element method, B-spline, numerical solution, three-dimensional theory of elasticity, structural analysis

ЛОКАЛИЗАЦИЯ РЕШЕНИЯ ТРЕХМЕРНОЙ ЗАДАЧИ ТЕОРИИ УПРУГОСТИ НА ОСНОВЕ ВЕЙВЛЕТ-РЕАЛИЗАЦИИ ДИСКРЕТНО-КОНТИНУАЛЬНОГО МЕТОДА КОНЕЧНЫХ ЭЛЕМЕНТОВ С ИСПОЛЬЗОВАНИЕМ B-СПЛАЙНОВ

М.Л. Мозгалева, П.А. Акимов

Национальный исследовательский Московский государственный строительный университет, г. Москва, РОССИЯ

Аннотация: В настоящей статье рассматривается локализация решения трехмерной задачи теории упругости на основе вейвлет-реализации дискретно-континуального метода конечных элементов с использованием B-сплайнов. Приведены исходные операторные континуальная и дискретно-континуальная постановки задачи, рассмотрены некоторые актуальные вопросы построения нормализованных базисных функций B-сплайна, описаны соответствующие локальные построения для произвольного дискретно-континуального конечного элемента, представлены некоторые сведения о численной реализации и пример расчета.

Ключевые слова: локализация, вейвлет-реализация метода конечных элементов, дискретно-континуальный метод конечных элементов, метод конечных элементов, B-сплайны, численное решение, трехмерная задача теории упругости, расчеты конструкций

INTRODUCTION

Numerical solution of the problem of three-dimensional theory of elasticity with the use of B-spline version of so-called discrete-continual finite element method (DCFEM) [1-4] has been already considered in [1]. Systematic literature review has been presented in [1] as well. In this

regard, let us immediately move on to the main material of the distinctive paper.

1. FORMULATIONS OF THE PROBLEM

Let the constancy of the parameters of the problem be in the direction corresponding to x_3 (main direction). The operational formulation of the problem with the use of so-called method of extended domain [5], taking into account the selection of the main direction, is determined by the equation [6]:

$$L\,\overline{u} = \overline{\overline{F}}, \quad 0 \le x_1 \le \ell_1,\ 0 \le x_2 \le \ell_2,\ 0 \le x_3 \le \ell_3, \tag{1.1}$$

where we have

$$L = -L_{vv}\,\partial_3^2 + L_{uv}\,\partial_3 + L_{uu}; \tag{1.2}$$

$$L_{uu} = \partial_1^* \begin{bmatrix} 2\mu+\lambda & 0 & 0 \\ 0 & \mu & 0 \\ 0 & 0 & \mu \end{bmatrix} \partial_1 + \partial_1^* \begin{bmatrix} 0 & \lambda & 0 \\ \mu & 0 & 0 \\ 0 & 0 & 0 \end{bmatrix} \partial_2 + \partial_2^* \begin{bmatrix} 0 & \mu & 0 \\ \lambda & 0 & 0 \\ 0 & 0 & 0 \end{bmatrix} \partial_1 + \partial_2^* \begin{bmatrix} \mu & 0 & 0 \\ 0 & 2\mu+\lambda & 0 \\ 0 & 0 & \mu \end{bmatrix} \partial_2; \tag{1.3}$$

$$L_{uv} = \partial_1^* \begin{bmatrix} 0 & 0 & \lambda \\ 0 & 0 & 0 \\ \mu & 0 & 0 \end{bmatrix} + \partial_2^* \begin{bmatrix} 0 & 0 & 0 \\ 0 & 0 & \lambda \\ 0 & \mu & 0 \end{bmatrix} - \begin{bmatrix} 0 & 0 & \mu \\ 0 & 0 & 0 \\ \lambda & 0 & 0 \end{bmatrix} \partial_1 - \begin{bmatrix} 0 & 0 & 0 \\ 0 & 0 & \mu \\ 0 & \lambda & 0 \end{bmatrix} \partial_2; \tag{1.4}$$

$$L_{vv} = \begin{bmatrix} \mu & 0 & 0 \\ 0 & \mu & 0 \\ 0 & 0 & 2\mu+\lambda \end{bmatrix}; \tag{1.5}$$

$$\overline{\overline{F}} = \theta\overline{F} + \delta_\Gamma \bar{f}; \tag{1.6}$$

$$\theta(x_1,x_2,x_3) = \begin{cases} 1, & (x_1,x_2,x_3) \in \Omega \\ 0, & (x_1,x_2,x_3) \notin \Omega; \end{cases} \tag{1.7}$$

$$\delta_\Gamma(x_1,x_2,x_3) = \partial\theta / \partial\overline{n}; \tag{1.8}$$

ℓ_1, ℓ_2, ℓ_3 are corresponding dimensions of extended domain (linear dimensions of considering structure); $x = (x_1, x_2, x_3)$; x_1, x_2, x_3 are Cartesian coordinates; μ and λ are Lame parameters; Ω is the domain, occupied by structure;

$$\Omega = \{ (x_1, x_2): \quad 0 < x_1 < \ell_1; \quad 0 < x_2 < \ell_2; \quad 0 < x_3 < \ell_3 \}; \tag{1.9}$$

$\theta(x_1, x_2, x_3)$ is characteristic function of domain Ω; $\delta_\Gamma = \delta_\Gamma(x_1, x_2, x_3)$ is the delta function of boundary $\Gamma = \partial\Omega$; $\overline{n} = [\, n_1 \;\; n_2 \;\; n_3 \,]^T$ is boundary normal vector; $\overline{F}$ is the load vector in domain Ω; $\bar{f}$ is the corresponding boundary load vector; $\overline{u}$ is the vector of displacements (unknown vector function),

$$\overline{u} = \begin{bmatrix} u_1 \\ u_2 \\ u_3 \end{bmatrix}; \tag{1.10}$$

$\partial_s = \partial / \partial x_s,\ s = 1, 2;\ \partial_s^* = -\partial / \partial x_s,\ s = 1, 2.$

Let us introduce the following notations

$$\overline{v} = \partial_3\overline{u} = \begin{bmatrix} v_1 \\ v_2 \\ v_3 \end{bmatrix}; \tag{1.11}$$

$$\overline{u}' = \partial_3\overline{u}; \quad \overline{v}' = \partial_3\overline{v}. \tag{1.12}$$

Thus we can rewrite (1.1):

$$L_{uu}\,\overline{u} + L_{uv}\overline{v} - L_{vv}\partial_3\overline{v} = \overline{\overline{F}}. \tag{1.13}$$

Finally we obtain system of differential equations with operational coefficients:

$$\begin{cases} \overline{u}' = \overline{v} \\ \overline{v}' = L_{vv}^{-1} L_{uu} \overline{u} + L_{vv}^{-1} L_{uv} \overline{v} - L_{vv}^{-1} \overline{\overline{F}} \end{cases} \quad (1.14)$$

or

$$\overline{z}' = \widetilde{L}\overline{z} + \overline{\overline{F}}\,, \quad (1.15)$$

where

$$\widetilde{L} = \begin{bmatrix} 0 & E \\ L_{vv}^{-1} L_{uu} & L_{vv}^{-1} L_{uv} \end{bmatrix}; \quad \overline{\overline{F}} = \begin{bmatrix} 0 \\ -L_{vv}^{-1} \overline{\overline{F}} \end{bmatrix}; \quad (1.16)$$

$$\overline{z} = \begin{bmatrix} \overline{u} \\ \overline{v} \end{bmatrix}; \quad E = \begin{bmatrix} 1 & 0 & 0 \\ 0 & 1 & 0 \\ 0 & 0 & 1 \end{bmatrix}; \quad (1.17)$$

The system of equations (1.15) is supplemented by boundary conditions, which are set in sections with coordinates $x_3^1 = 0$ and $x_3^2 = \ell_3$.

2. SOME GENERAL ASPECTS OF FINITE ELEMENT APPROXIMATION

The discrete component of the numerical solution is represented by directions along the axes x_1 and x_2. The fulfilment within the element (rectangular element) is the same for all components of the vector function $\overline{U}$ (see (1.4)) Let's divide the interval $(0, \ell_1)$ into $N_{e,1}$ parts and interval $(0, \ell_2)$ into $N_{e,2}$ parts (sides of elements); $h_{e,1} = \ell_1 / N_{e,1}$ is the length of the side of the element in the direction x_1; $h_{e,2} = \ell_2 / N_{e,2}$ is the length of the side of the element in the direction x_2. Let us number the elements with a multi-index $i_e = (i_{e,1}, i_{e,2})$, where $i_{e,1} = 1, ..., N_{e,1}$ is the number in the first direction (x_1); $i_{e,2} = 1, ..., N_{e,2}$ is the number in the second direction (x_2).

We will also divide each side of the element $i_e = (i_{e,1}, i_{e,2})$ into and parts $N_{h,e,1}(i_{e,1})$ and $N_{h,e,2}(i_{e,2})$, respectively. It should be noted that $N_{h,e,1}(i_{e,1})$ and $N_{h,e,2}(i_{e,2})$ are of greater importance on the localization (of solution) elements than on the other elements. Let us denote the number of nodes on the element in the first and the second directions as

$$N_{p,1}(i_{e,1}) = N_{h,e,1}(i_{e,1}) + 1;$$

$$N_{p,2}(i_{e,2}) = N_{h,e,2}(i_{e,2}) + 1.$$

Thus, the total number of nodes on the element with this discretization is equal to

$$N_p(i_e) = N_{p,1}(i_{e,1}) N_{p,2}(i_{e,2}).$$

3. LOCAL CONSTRUCTIONS FOR ARBITRARY FINITE ELEMENT

Let us represent fulfilment on the element $i_e = (i_{e,1}, i_{e,2})$ for the p-th component of the vector function ($p = 1, 2, 3$)

$$u_p(x_1, x_2) = w(t_1, t_2) =$$

$$= \sum_{j_2=1}^{N_{p,2}(i_{e,2})} \sum_{j_1=1}^{N_{p,1}(i_{e,1})} \varphi_{j_2}^{m_2(i_{e,2})}(t_2) \varphi_{j_1}^{m_1(i_{e,1})}(t_1) \cdot \alpha_p^{(j_2, j_1)}, \quad (2.1)$$

where

$$x_1(i_{e,1}) \le x_1 \le x_1(i_{e,1}) + h_{e,1};$$

$$x_2(i_{e,2}) \le x_2 \le x_2(i_{e,2}) + h_{e,2};$$

$$t_1 = (x_1 - x_1(i_{e,1})) / h_{e,1}, \quad 0 \le t_1 \le 1;$$

$$t_2 = (x_2 - x_2(i_{e,2})) / h_{e,2}, \quad 0 \le t_2 \le 1;$$

$\varphi_j^m(t)$ is the j-th basis function of the B-spline of degree m (see, for example, [7, 8]).

In this case, we have the following relations:

$$\partial_1 = \frac{\partial}{\partial x_1} = \frac{1}{h_{e,1}} \cdot \frac{\partial}{\partial t_1}; \quad \partial_2 = \frac{\partial}{\partial x_1} = \frac{1}{h_{e,2}} \cdot \frac{\partial}{\partial t_2}; \quad (2.2)$$

$$dx_1 = h_{e,1} \cdot dt_1; \quad dx_2 = h_{e,2} \cdot dt_2; \quad (2.3)$$

Let us define the parameters $\alpha_p^{(j_2,j_1)}$ in terms of the nodal unknowns on the element $i_e=(i_{e,1},\ i_{e,2})$:

$$u_p^{(i_2,i_1)}(x_{i,1},\ x_{i,2})=w(t_{i,1},\ t_{i,2})=$$
$$=\sum_{j_2=1}^{N_{p,2}(i_{e,2})}\sum_{j_1=1}^{N_{p,1}(i_{e,1})}\varphi_{j_2}^{m_2(i_{e,2})}(t_{i,2})\varphi_{j_1}^{m_1(i_{e,1})}(t_{i,1})\cdot\alpha_p^{(j_2,j_1)};$$
$$x_{i_1}=x_1(i_{e,1})+\frac{h_{e,1}}{N_{p,1}(i_{e,1})-1}(i_1-1);$$
$$x_{i_2}=x_2(i_{e,2})+\frac{h_{e,2}}{N_{p,2}(i_{e,2})-1}(i_2-1);$$
$$t_1=(x_1-x_1(i_{e,1}))/h_{e,1}=$$
$$=\left[x_1(i_{e,1})+\frac{h_{e,1}}{N_{p,1}(i_{e,1})-1}(i_1-1)-x_1(i_{e,1})\right]/h_{e,1}=$$
$$=\frac{i_1-1}{N_{p,1}(i_{e,1})-1};$$
$$t_2=\frac{i_2-1}{N_{p,2}(i_{e,2})-1}.$$

We obtain a system of linear algebraic equations

$$T\overline{\alpha}_p^{i_e}=\overline{u}_p^{i_e},\qquad(2.4)$$

where we have

$T=\{t_{i,j}\}_{i,j=1,\ldots,N_p(i_e)}$:

$$t_{i,j}=\varphi_{j_2}^{m_2(i_{e,2})}(t_{i_2})\cdot\varphi_{j_1}^{m_1(i_{e,1})}(t_{i_1})$$

does not depend on p;

$$\overline{\alpha}_p=\{\alpha_p^j\}=\{\alpha_p^{j_2,j_1}\};\quad \overline{u}_p^{i_e}=\{u_p^i\}=\{u_p^{i_2i_1}\};$$
$$i=i_1+N_{p,1}(i_{e,1})\cdot(i_2-1),$$
$$i_2=1,\ \ldots,N_{p,2}(i_{e,2}),\quad i_1=1,\ \ldots,N_{p,1}(i_{e,1});$$
$$j=j_1+N_{p,1}(i_{e,1})\cdot(j_2-1),$$
$$j_2=1,\ \ldots,N_{p,2}(i_{e,2}),\quad j_1=1,\ \ldots,N_{p,1}(i_{e,1}).$$

Then we have

$$\overline{\alpha}_p^{i_e}=T^{-1}\overline{u}_p^{i_e}.\qquad(2.5)$$

Let us introduce the following notations:

$$\overline{u}^{i_e}=\begin{bmatrix}\overline{u}^1\\ \vdots\\ \overline{u}^{N_p(i_e)}\end{bmatrix}$$

are the nodal values of the vector function on the element i_e;

$$\overline{u}^i=\begin{bmatrix}u_1^i\\ u_2^i\\ u_3^i\end{bmatrix}$$

is the value of the vector function at the i-th node on the element i_e;

$$\overline{u}_p^{i_e}=\begin{bmatrix}u_p^1\\ \vdots\\ u_p^{N_p(i_e)}\end{bmatrix}$$

are the nodal values of the p-th component of the vector function on the element i_e ($p=1,\ 2,\ 3$).

Let P be a permutation matrix such that

$$P\overline{u}^{i_e}=\begin{bmatrix}\overline{u}_1^{i_e}\\ \overline{u}_2^{i_e}\\ \overline{u}_3^{i_e}\end{bmatrix}.\qquad(2.6)$$

Since for a permutation matrix $P^{-1}=P^T$, the inverse transformation has the form

$$\overline{u}^{i_e}=P^T\begin{bmatrix}\overline{u}_1^{i_e}\\ \overline{u}_2^{i_e}\\ \overline{u}_3^{i_e}\end{bmatrix}.\qquad(2.7)$$

To construct local stiffness matrices corresponding to the operators L_{uu}, L_{uv}, L_{vv}, we consider bilinear forms, taking into account representation (2.1) and relations (2.2)-(2.3) on the form functions:

$$\begin{aligned}
&\overline{u}(x_1,\ x_2)=\overline{w}(t_1,\ t_2)=\\
&\quad=\sum_{k_2=1}^{N_{p,2}(i_{e,2})}\sum_{k_1=1}^{N_{p,1}(i_{e,1})}\varphi_{k_2}^{m_2(i_{e,2})}(t_2)\varphi_{k_1}^{m_1(i_{e,1})}(t_1)\cdot\overline{\alpha}^k;\\
&\overline{y}(x_1,\ x_2)=\overline{q}(t_1,\ t_2)=\\
&\quad=\sum_{k_2=1}^{N_{p,2}(i_{e,2})}\sum_{k_1=1}^{N_{p,1}(i_{e,1})}\varphi_{k_2}^{m_2(i_{e,2})}(t_2)\varphi_{k_1}^{m_1(i_{e,1})}(t_1)\cdot\overline{\beta}^k;
\end{aligned}\tag{2.8}$$

$$x_1(i_{e,1})\le x_1\le x_1(i_{e,1})+h_{e,1};$$

$$x_2(i_{e,2})\le x_2\le x_2(i_{e,2})+h_{e,2};$$

$$0\le t_1,\ t_2\le 1;$$

$$\overline{\alpha}^k=\begin{bmatrix}\alpha_1^k\\ \alpha_2^k\\ \alpha_3^k\end{bmatrix};\quad \overline{\beta}^k=\begin{bmatrix}\beta_1^k\\ \beta_2^k\\ \beta_3^k\end{bmatrix};$$

$$k=k_1+N_{p,1}(i_{e,1})\cdot(k_2-1);$$

$$k_2=1,...,N_{p,2}(i_{e,2});\quad k_1=1,...,N_{p,1}(i_{e,1});$$

$$\begin{aligned}
&B_{vv}(\overline{u},\overline{y})=(L_{vv}\overline{u},\overline{y})=\\
&=\int_{x_2(i_{e,2})}^{x_2(i_{e,2})+h_{e,2}}\int_{x_1(i_{e,1})}^{x_1(i_{e,1})+h_{e,1}}\left(\begin{bmatrix}\mu&0&0\\0&\mu&0\\0&0&2\mu+\lambda\end{bmatrix}\overline{u},\overline{y}\right)dx_1dx_2=\\
&=h_{e,2}h_{e,1}\int_0^1\int_0^1\left(\begin{bmatrix}\mu&0&0\\0&\mu&0\\0&0&2\mu+\lambda\end{bmatrix}\overline{u},\overline{y}\right)dt_1dt_2=\\
&=\sum_{i_2=1}^{N_{p,2}(i_{e,2})}\sum_{i_1=1}^{N_{p,1}(i_{e,1})}\sum_{j_2=1}^{N_{p,2}(i_{e,2})}\sum_{j_1=1}^{N_{p,1}(i_{e,1})}\gamma_{i,j}\times\\
&\times\left(\begin{bmatrix}\mu&0&0\\0&\mu&0\\0&0&2\mu+\lambda\end{bmatrix}\overline{\alpha}^j,\overline{\beta}^i\right),
\end{aligned}$$

where we have

$$\begin{aligned}
\gamma_{i,j}=&h_{e,1}\int_0^1\varphi_{j_1}^{m_1(i_{e,1})}(t_1)\cdot\varphi_{i_1}^{m_1(i_{e,1})}(t_1)dt_1\times\\
&\times h_{e,2}\int_0^1\varphi_{j_2}^{m_2(i_{e,2})}(t_2)\cdot\varphi_{i_2}^{m_2(i_{e,2})}(t_2)dt_2.
\end{aligned}\tag{2.9}$$

Let us denote

$$\Gamma=\{\gamma_{i,j}\}_{i,j=1,...,N_p(i_e)};\quad G=(T^{-1})^T\Gamma T^{-1}.\tag{2.10}$$

Then, taking into account dependences (2.5) and (2.6), the following chain of equalities is valid

$$\begin{aligned}
&B_{vv}(\overline{u},\overline{y})=<L_{vv}\overline{u},\overline{y}>=\mu(\Gamma\overline{\alpha}_1^{i_e},\overline{\beta}_1^{i_e})+\\
&+\mu(\Gamma\overline{\alpha}_2^{i_e},\overline{\beta}_2^{i_e})+(2\mu+\lambda)(\Gamma\overline{\alpha}_3^{i_e},\overline{\beta}_3^{i_e})=\\
&=\mu((T^{-1})^T\Gamma T^{-1}\overline{u}_1^{i_e},\overline{y}_1^{i_e})+\\
&+\mu((T^{-1})^T\Gamma T^{-1}\overline{u}_2^{i_e},\overline{z}_2^{i_e})+\\
&+(2\mu+\lambda)((T^{-1})^T\Gamma T^{-1}\overline{u}_3^{i_e},\overline{z}_3^{i_e})=\\
&=\left(\begin{bmatrix}\mu G&0&0\\0&\mu G&0\\0&0&(2\mu+\lambda)G\end{bmatrix}\begin{bmatrix}\overline{u}_1^{i_e}\\ \overline{u}_2^{i_e}\\ \overline{u}_3^{i_e}\end{bmatrix},\begin{bmatrix}\overline{z}_1^{i_e}\\ \overline{z}_2^{i_e}\\ \overline{z}_3^{i_e}\end{bmatrix}\right)=\\
&=\left(P^T\begin{bmatrix}\mu G&0&0\\0&\mu G&0\\0&0&(2\mu+\lambda)G\end{bmatrix}P\overline{u}^{i_e},\overline{z}^{i_e}\right)=\\
&=(K_{vv}^{i_e}\overline{u}^{i_e},\overline{z}^{i_e}).
\end{aligned}$$

Thus, the local stiffness matrix $K_{vv}^{i_e}$ corresponding to the operator L_{vv} has the form

$$K_{vv}^{i_e}=P^T\begin{bmatrix}\mu G&0&0\\0&\mu G&0\\0&0&(2\mu+\lambda)G\end{bmatrix}P.\tag{2.11}$$

Similarly, one can obtain local stiffness matrices corresponding to the operators L_{uu} and L_{uv}. We present here the final formulas.

The operator L_{uu} corresponds to

$$K_{uu}^{i_e} = K_{uu,1}^{i_e} + K_{uu,2}^{i_e} + K_{uu,3}^{i_e} + K_{uu,4}^{i_e}, \quad (2.12)$$

where we have

$$K_{uu,1}^{i_e} = P^T \begin{bmatrix} (2\mu+\lambda)G_1 & 0 & 0 \\ 0 & \mu G_1 & 0 \\ 0 & 0 & \mu G_1 \end{bmatrix} P;$$

$$G_1 = (T^{-1})^T \Gamma_1 T^{-1}; \quad \Gamma_1 = \{\gamma_{1,i,j}\}_{i,j=1,\ldots,N_p(i_e)};$$

$$\gamma_{1,i,j} = \frac{1}{h_{e,1}} \int_0^1 \frac{d\varphi_{j_1}^{m_1(i_{e,1})}}{dt_1}(t_1) \cdot \frac{d\varphi_{i_1}^{m_1(i_{e,1})}}{dt_1}(t_1) dt_1 \times \times h_{e,2} \int_0^1 \varphi_{j_2}^{m_2(i_{e,2})}(t_2) \cdot \varphi_{i_2}^{m_2(i_{e,2})}(t_2) dt_2; \quad (2.13)$$

$$K_{uu,2}^{i_e} = P^T \begin{bmatrix} 0 & \lambda G_2 & 0 \\ \mu G_2 & 0 & 0 \\ 0 & 0 & 0 \end{bmatrix} P;$$

$$G_2 = (T^{-1})^T \Gamma_2 T^{-1}; \quad \Gamma_2 = \{\gamma_{2,i,j}\}_{i,j=1,\ldots,N_p(i_e)};$$

$$\gamma_{2,i,j} = \int_0^1 \varphi_{j_1}^{m_1(i_{e,1})}(t_1) \cdot \frac{d\varphi_{i_1}^{m_1(i_{e,1})}}{dt_1}(t_1) dt_1 \times \times \int_0^1 \frac{d\varphi_{j_2}^{m_2(i_{e,2})}}{dt_2}(t_2) \cdot \varphi_{i_2}^{m_2(i_{e,2})}(t_2) dt_2; \quad (2.14)$$

$$K_{uu,3}^{i_e} = P^T \begin{bmatrix} 0 & \mu G_3 & 0 \\ \lambda G_3 & 0 & 0 \\ 0 & 0 & 0 \end{bmatrix} P;$$

$$G_3 = (T^{-1})^T \Gamma_3 T^{-1}; \quad \Gamma_3 = \{\gamma_{3,i,j}\}_{i,j=1,\ldots,N_p(i_e)};$$

$$\gamma_{3,i,j} = \int_0^1 \frac{d\varphi_{j_1}^{m_1(i_{e,1})}}{dt_1}(t_1) \cdot \varphi_{i_1}^{m_1(i_{e,1})}(t_1) dt_1 \times \times \int_0^1 \varphi_{j_2}^{m_2(i_{e,2})}(t_2) \cdot \frac{d\varphi_{i_2}^{m_2(i_{e,2})}}{dt_2}(t_2) dt_2; \quad (2.15)$$

$$K_{uu,4}^{i_e} = P^T \begin{bmatrix} \mu G_4 & 0 & 0 \\ 0 & (2\mu+\lambda)G_4 & 0 \\ 0 & 0 & \mu G_4 \end{bmatrix} P;$$

$$G_4 = (T^{-1})^T \Gamma_4 T^{-1}; \quad \Gamma_4 = \{\gamma_{4,i,j}\}_{i,j=1,\ldots,N_p(i_e)};$$

$$\gamma_{4,i,j} = \frac{1}{h_{e,1}} \int_0^1 \varphi_{j_1}^{m_1(i_{e,1})}(t_1) \cdot \varphi_{i_1}^{m_1(i_{e,1})}(t_1) dt_1 \times \times h_{e,2} \int_0^1 \frac{d\varphi_{j_2}^{m_2(i_{e,2})}}{dt_2}(t_2) \cdot \frac{d\varphi_{i_2}^{m_2(i_{e,2})}}{dt_2}(t_2) dt_2. \quad (2.16)$$

The operator L_{uv} corresponds to

$$K_{uv}^{i_e} = K_{uv,1}^{i_e} + K_{uv,2}^{i_e} - K_{uv,3}^{i_e} - K_{uv,4}^{i_e}, \quad (2.17)$$

where we have

$$K_{uv,1}^{i_e} = P^T \begin{bmatrix} 0 & 0 & \lambda D_1 \\ 0 & 0 & 0 \\ \mu D_1 & 0 & 0 \end{bmatrix} P;$$

$$D_1 = (T^{-1})^T \Delta_1 T^{-1}; \quad \Delta_1 = \{\delta_{1,i,j}\}_{i,j=1,\ldots,N_p(i_e)};$$

$$\delta_{1,i,j} = \int_0^1 \varphi_{j_1}^{m_1(i_{e,1})}(t_1) \cdot \frac{d\varphi_{i_1}^{m_1(i_{e,1})}}{dt_1}(t_1) dt_1 \times \times h_{e,2} \int_0^1 \varphi_{j_2}^{m_2(i_{e,2})}(t_2) \cdot \varphi_{i_2}^{m_2(i_{e,2})}(t_2) dt_2; \quad (2.18)$$

$$K_{uv,2}^{i_e} = P^T \begin{bmatrix} 0 & 0 & 0 \\ 0 & 0 & \lambda D_2 \\ 0 & \mu D_2 & 0 \end{bmatrix} P;$$

$$D_2 = (T^{-1})^T \Delta_2 T^{-1}; \quad \Delta_2 = \{\delta_{2,i,j}\}_{i,j=1,\ldots,N_p(i_e)};$$

$$\delta_{2,i,j} = h_{e,1} \int_0^1 \varphi_{j_1}^{m_1(i_{e,1})}(t_1) \cdot \varphi_{i_1}^{m_1(i_{e,1})}(t_1) dt_1 \times \times \int_0^1 \varphi_{j_2}^{m_2(i_{e,2})}(t_2) \cdot \frac{d\varphi_{i_2}^{m_2(i_{e,2})}}{dt_2}(t_2) dt_2; \quad (2.19)$$

$$K_{uv,3}^{i_e} = P^T \begin{bmatrix} 0 & 0 & \mu D_3 \\ 0 & 0 & 0 \\ \lambda D_3 & 0 & 0 \end{bmatrix} P;$$

$$D_3 = (T^{-1})^T \Delta_3 T^{-1}; \quad \Delta_3 = \{\delta_{3,i,j}\}_{i,j=1,\ldots,N_p(i_e)};$$

$$\delta_{3,i,j} = \int_0^1 \frac{d\varphi_{j_1}^{m_1(i_{e,1})}}{dt_1}(t_1) \cdot \varphi_{i_1}^{m_1(i_{e,1})}(t_1) dt_1 \times \times h_{e,2} \int_0^1 \varphi_{j_2}^{m_2(i_{e,2})}(t_2) \cdot \varphi_{i_2}^{m_2(i_{e,2})}(t_2) dt_2; \quad (2.20)$$

$$K_{uv,4}^{i_e} = P^T \begin{bmatrix} 0 & 0 & 0 \\ 0 & 0 & \mu D_4 \\ 0 & \lambda D_4 & 0 \end{bmatrix} P;$$

$$D_4 = (T^{-1})^T \Delta_4 T^{-1}; \quad \Delta_4 = \{\delta_{4,i,j}\}_{i,j=1,\ldots,N_p(i_e)};$$

$$\delta_{4,i,j} = h_{e,1} \int_0^1 \varphi_{j_1}^{m_1(i_{e,1})}(t_1) \cdot \varphi_{i_1}^{m_1(i_{e,1})}(t_1) dt_1 \times \times h_{e,2} \int_0^1 \frac{d\varphi_{j_2}^{m_2(i_{e,2})}}{dt_2}(t_2) \cdot \varphi_{i_2}^{m_2(i_{e,2})}(t_2) dt_2; \quad (2.21)$$

3. EXAMPLE OF ANALYSIS

3.1. Formulation of the problem.

As a model example, let us consider the determination of the displacements of a three-dimensional beam, fixed along the side faces in three directions, under the influence of a load concentrated in the center (Figure 3.1).

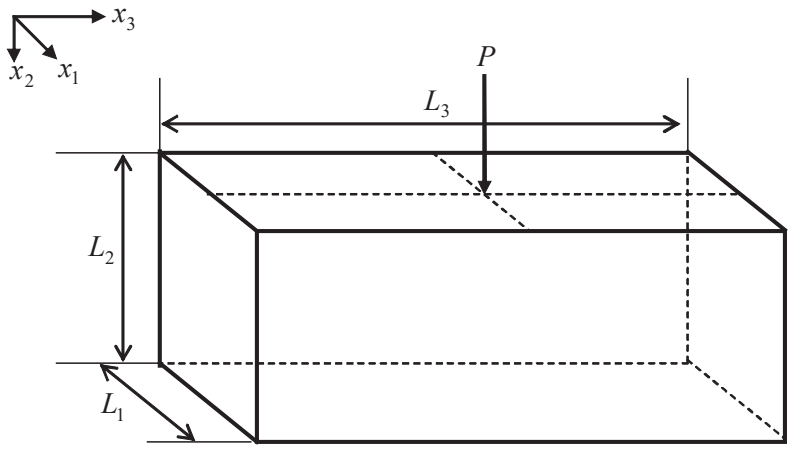


Figure 3.1. Example of analysis.

Let us consider the following geometric parameters:

$$L_1 = L_2 = 3.6 \text{ m}; \; L_3 = 8 \text{ m}.$$

Let us consider the following design parameters of material of the beam: coefficient of elasticity $E = 26500 \cdot 10^4$ kN/m^2; Poisson's ratio $\nu = 0.15$. Let external load parameter be equal to $P = 100$ kN.

3.2. Structural analysis with allowance for localization.

Let us determine the localization of the solution in the zone of application of the load. Let us set

$$N_{e,1} = N_{e,2} = 4$$

is the number of elements in each discrete direction. The lengths of the element are equal to

$$h_{e,1} = \ell_1 / N_{e,1} = 3.6 / 4 = 0.9; \quad h_{e,2} = h_{e,1} = 0.9.$$

Let us set the fulfilment by directions (Figure 3.2):

$$N_{p,1}(1) = N_{p,1}(4) = 2$$

is the fulfilment in the first direction by a spline of the first order: $m_1(1) = m_1(4) = 1$;

$$N_{p,1}(2) = N_{p,1}(3) = 4$$

is the fulfilment in the first direction by a spline of the third order: $m_1(2) = m_1(3) = 3$;

$$N_{p,2}(1) = N_{p,2}(2) = 4$$

is the fulfilment in the second direction by a spline of the third order: $m_2(1) = m_2(2) = 3$;

$$N_{p,2}(3) = N_{p,2}(4) = 2$$

is the fulfilment in the second direction by a spline of the first order: $m_1(3) = m_1(4) = 1$.

Thus, the localization area includes elements with numbers (2, 1), (3, 1), (2, 2), (3, 2).

The total number of nodes of the mesh is equal to $N_p = 9 \cdot 9 = 81$.

The total number of unknown nodal displacements is equal to $N_d = 3 \cdot 81 = 243$.

Total number of nodal unknowns is equal to $N_U = 2 \cdot 243 = 486$.

Figures 3.3 and 3.4 graphically represent selected examples of the obtained solution results. Let us use the following notations:

$$h_2 = h_{e,2} / 3 = 0.9 / 3 = 0.3$$

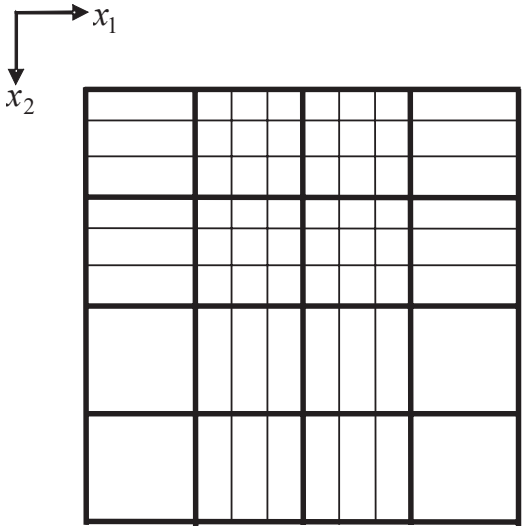
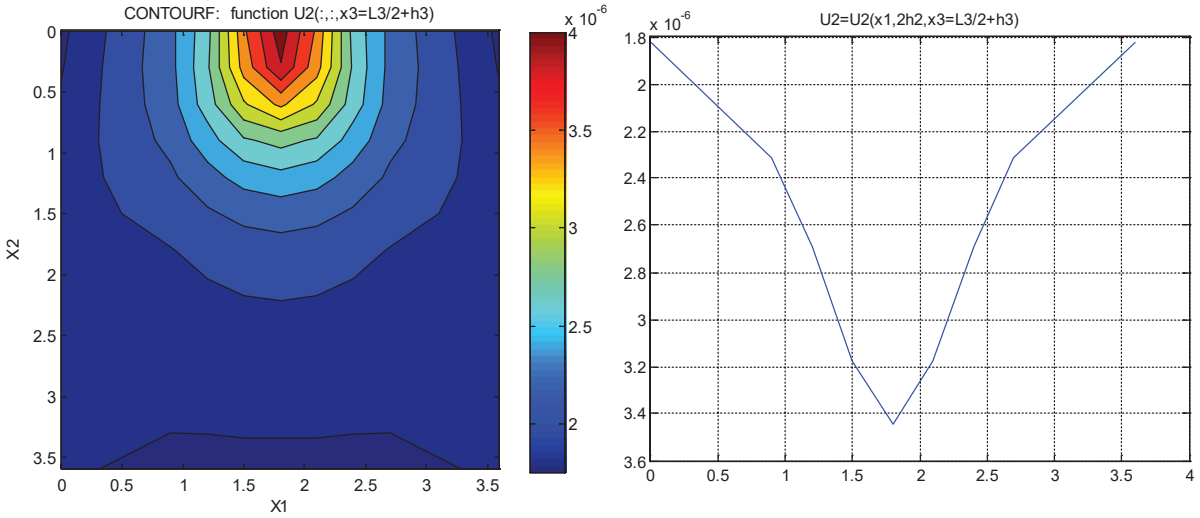


Figure 3.2. Mesh discretization with allowance for localization.



a) b)

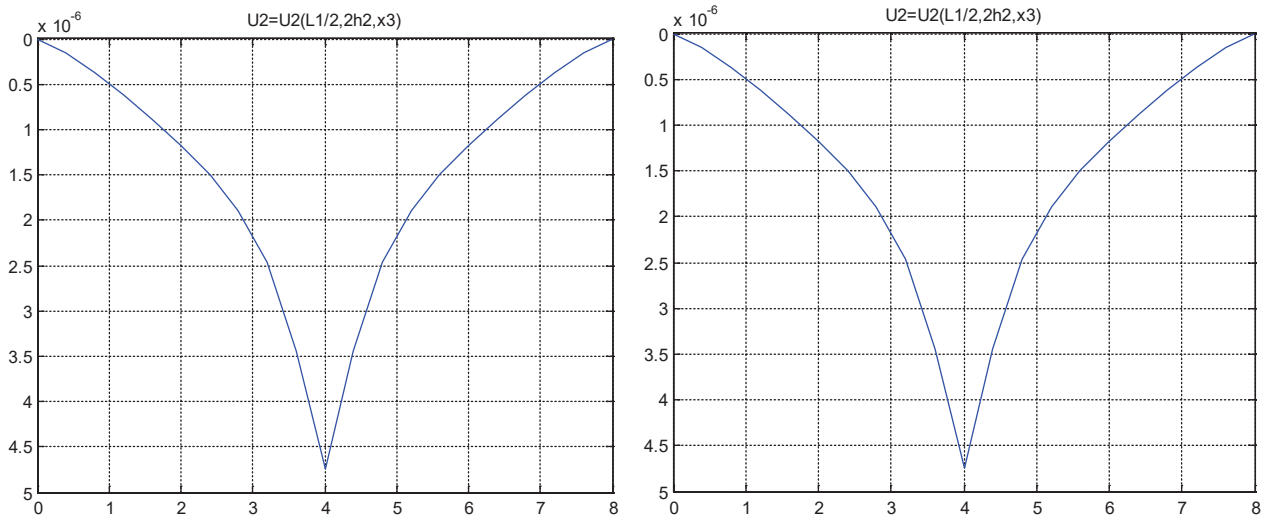
Figure 3.3. Nodal displacements u_2:

a) in section $x_3 = \ell_3 / 2 + h_3$; b) in section and at the level $x_2 = 2h_2$

is the step of discretization of the finite element in the localization area in the second direction (x_2);

– step of printing the result along the continual direction (x_3).

$$h_3 = \ell_3 / 20 = 8 / 20 = 0.4$$



a) b)

Figure 3.4. Displacements along continual direction for $x_1 = \ell_1 / 2$ *and* $x_2 = 2h_2$ *: a) component* u_2 *; b) component* u_3 *.*

REFERENCES

1. **Mozgaleva M.L., Akimov P.A., Kaytukov T.B.** Localization of solution of the problem of two-dimensional theory of elasticity with the use of discrete-continual finite element method. // International Journal for Computational Civil and Structural Engineering, 2021, Vol. 17, Issue 2, pp. 83-104.
2. **Akimov P.A., Mozgaleva M.L., Kaytukov T.B.** Numerical solution of the problem of isotropic plate analysis with the use of B-spline discrete-continual finite element method. // // International Journal for Computational Civil and Structural Engineering, 2020, Vol. 16, Issue 4, pp. 14-28.
3. **Akimov P.A., Mozgaleva M.L., Kaytukov T.B.** Numerical solution of the problem of beam analysis with the use of B-spline finite element method. // International Journal for Computational Civil and Structural Engineering, 2020, Vol. 16, Issue 3, pp. 12-22.
4. **Akimov P.A., Sidorov V.N.** Correct Method of Analytical Solution of Multipoint Boundary Problems of Structural Analysis for Systems of Ordinary Differential Equations with Piecewise Constant Coefficients. // Advanced Materials Research Vols. 250-253, 2011, pp. 3652-3655.
5. **Akimov P.A., Mozgaleva M.L.** Method of Extended Domain and General Principles of Mesh Approximation for Boundary Problems of Structural Analysis. // Applied Mechanics and Materials, 2014, Vols. 580-583, pp. 2898-2902.
6. **Lur'e A.I.** Teorija uprugosti [Theory of Elasticity]. Moscow, Nauka, 1970, 939 pages (in Russian).
7. **Dobeshi I.** Desjat' lekcij po vejvletam [Ten lectures on wavelets]. Izhevsk: NIC «Regu-

ljarnaja i haoticheskaja dinamika», 2001, 464 pages (in Russian).
8. **Chui K.** Vvedenie v vejvlety [Introduction to wavelets]. Moscow, Mir, 2001, 412 pages (in Russian).

СПИСОК ЛИТЕРАТУРЫ

1. **Mozgaleva M.L., Akimov P.A., Kaytukov T.B.** Localization of solution of the problem of two-dimensional theory of elasticity with the use of discrete-continual finite element method. // International Journal for Computational Civil and Structural Engineering, 2021, Vol. 17, Issue 2, pp. 83-104.
2. **Akimov P.A., Mozgaleva M.L., Kaytukov T.B.** Numerical solution of the problem of isotropic plate analysis with the use of B-spline discrete-continual finite element method. // // International Journal for Computational Civil and Structural Engineering, 2020, Vol. 16, Issue 4, pp. 14-28.
3. **Akimov P.A., Mozgaleva M.L., Kaytukov T.B.** Numerical solution of the problem of beam analysis with the use of B-spline finite element method. // International Journal for Computational Civil and Structural Engineering, 2020, Vol. 16, Issue 3, pp. 12-22.
4. **Akimov P.A., Sidorov V.N.** Correct Method of Analytical Solution of Multipoint Boundary Problems of Structural Analysis for Systems of Ordinary Differential Equations with Piecewise Constant Coefficients. // Advanced Materials Research Vols. 250-253, 2011, pp. 3652-3655.
5. **Akimov P.A., Mozgaleva M.L.** Method of Extended Domain and General Principles of Mesh Approximation for Boundary Problems of Structural Analysis. // Applied Mechanics and Materials, 2014, Vols. 580-583, pp. 2898-2902.
6. **Лурье А.И.** Теория упругости. – М.: Наука, 1970. – 939 с.
7. **Добеши И.** Десять лекций по вейвлетам. – Ижевск: НИЦ «Регулярная и хаотическая динамика», 2001. – 464 с.
8. **Чуи К.** Введение в вейвлеты. – М.: Мир, 2001. – 412 с.

Marina L. Mozgaleva, Senior Scientist Researcher, Dr.Sc.; Professor of Department of Applied Mathematics, National Research Moscow State University of Civil Engineering; 26, Yaroslavskoe Shosse, Moscow, 129337, Russia; phone/fax +7(499) 183-59-94; Fax: +7(499) 183-44-38; Email: marina.mozgaleva@gmail.com.

Pavel A. Akimov, Full Member of the Russian Academy of Architecture and Construction Sciences, Professor, Dr.Sc.; Rector of National Research Moscow State University of Civil Engineering; 26, Yaroslavskoe Shosse, Moscow, 129337, Russia; phone: +7(495) 651-81-85; Fax: +7(499) 183-44-38; E-mail: AkimovPA@mgsu.ru, rector@mgsu.ru, pavel.akimov@gmail.com.

Taymuraz B. Kaytukov, Advisor of the Russian Academy of Architecture and Construction Sciences, Associate Professor, Ph.D.; Vice-Rector, Associate Professor Department of Applied Mathematics, National Research Moscow State University of Civil Engineering; 26, Yaroslavskoe Shosse, Moscow, 129337, Russia; phone: +7(499) 929-52-29; fax: +7(499) 183-59-94; Email: KaytukovTB@mgsu.ru.

Мозгалева Марина Леонидовна, старший научный сотрудник, доктор технических наук; профессор кафедры прикладной математики Национального исследовательского Московского государственного строительного университета; 129337, Россия, г. Москва, Ярославское шоссе, дом 26; телефон/факс: +7(499) 183-59-94; Email: marina.mozgaleva@gmail.com.

Акимов Павел Алексеевич, академик РААСН, профессор, доктор технических наук; ректор Национального исследовательского Московского государственного строительного университета; 129337, Россия, г. Москва, Ярославское шоссе, дом 26; телефон: +7(495) 651-81-85; факс: +7(499) 183-44-38; Email: AkimovPA@mgsu.ru, rector@mgsu.ru, pavel.akimov@gmail.com.

Кайтуков Таймураз Батразович, советник РААСН, доцент, кандидат технических наук; проректор, профессор кафедры прикладной математики Национального исследовательского Московского государственного строительного университета; 129337, Россия, г. Москва, Ярославское шоссе, дом 26; телефон: +7(499) 929-52-29; факс: +7(499) 183-44-38; Email: KaytukovTB@mgsu.ru.

International Journal for Computational Civil and Structural Engineering, 19(3) 165–172(2023)

DOI:10.22337/2587-9618-2023-19-3-165-172

NUMERICAL SIMULATION OF THE STRESS-STRAIN STATE OF A LARGE-SPAN STRUCTURE WITH JOINTS WITH GAP UNDER THE SEISMIC LOADS IN A TRANSIENT DYNAMIC

Alexander M. Belostotsky, Andrei S. Pavlov, Alexandr I. Nagibovich

National Research Moscow State University of Civil Engineering, Moscow, RUSSIA

Abstract: The article presents the results of numerical simulation of a unique long-span structure subjected to seismic loads. The roof and facade of structures were connected to reinforced concrete base with joints with gaps. The simulation was realized for ideal model and model with gap imperfections. Various modeling approaches for the joints and the resulting dynamic response were examined.

Keywords: Long-span structures, seismic response, joints with gaps

ЧИСЛЕННОЕ МОДЕЛИРОВАНИЕ НАПРЯЖЕННО-ДЕФОРМИРОВАННОГО СОСТОЯНИЯ БОЛЬШЕПРОЛЕТНОГО СООРУЖЕНИЯ С ЛЮФТАМИ В ОПОРАХ С УЧЕТОМ СЕЙСМИЧЕСКИХ ВОЗДЕЙСТВИЙ В НЕЛИНЕЙНОЙ ДИНАМИЧЕСКОЙ ПОСТАНОВКЕ

А.М. Белостоцкий, А.С. Павлов, А.И. Нагибович

Национальный исследовательский Московский государственный строительный университет, г. Москва, РОССИЯ

Аннотация: В актуальной статье представлены результаты численного моделирования уникального сооружения, подвергающегося сейсмическому воздействию, включающего большепролетные конструкции покрытия и другие ограждающие конструкции, связанные с железобетонным основанием через опорные части с конструктивными люфтами/зазорами. Проведена оценка динамической реакции сооружения в идеализированной постановке и при наличии несовершенств узлов. Рассмотрены различные варианты моделирования узлов и реализуемой динамической реакции.

Ключевые слова: Большепролетные конструкции, сейсмическая реакция сооружения, опорные части с люфтами

1. INTRODUCTION

Current modern approaches to numerical modeling of unique buildings and structures are oriented towards detailed and physically accurate reproduction of the construction itself, taking into account initial imperfections and the actual operational scheme of the components.

The consideration of imperfections becomes especially important for tasks involving the direct modeling of the behavior of a structure subjected to dynamic influences, such as seismic loads of the ultimate level or emergency actions leading to progressive collapse. These situations may force the structure to operate in a critically unstable state, for which standard methods of assessing load-bearing capacity have limited applicability. It is necessary in these cases to ensure the stability and survivability of the structure and to eliminate the possibility of its collapse.

Based on various domestic and international normative documents and research, two main types of imperfections can be identified:

– Imperfections of the shape of structural elements (various deviations from straightness or theoretical shape);
– Imperfections of the joints (the actual stiffness of joints, structural nonlinearity of joints in the form of contact opening, or the possibility of free movement due to clearances).

Accounting for shape imperfections in modern normative documents, such as Russian Codes, Eurocodes, ACI, and others, can be done through coefficients determined based on initial eccentricities and element sizes or through direct modeling of imperfections by adjusting the shape of the analytical model.

Research related to the consideration of the actual project scheme of joint operation has been conducted by teams from the Melnikov Central Research and Design Institute of Steel Structures (CNIIIPSK), including the work of N.N. Streletsky, VNIIPI Promstalkonstruktsiya, and the work of V.V. Kalenov and A.B. Pavlov [4]. G.G. Kashevarova's work [5] is also relevant in this context. Expert assessments of the actual joint operation schemes in the collapse of large-span structures have been the focus of research by A.M. Belostotsky [1-3] and teams from the R&D Center StaDyO and NOC KM MGSU, and among others.

In this current article, we will consider one of the numerical modeling approaches for the behavior of joints, the structural design of which allows for clearances or gaps, resulting in limited free movement of the structure.

2. PROBLEM'S FORMULATION

The large-span structure is located in a seismic zone. The normative seismicity of the construction site is assessed at 9 points for soils of category II in terms of seismic properties. According to the results of geophysical studies, the revised seismicity of the construction site is numerically rated at 8 points.

The object is a building with a complex geometric shape, featuring an outstanding cantilevered open terrace with a length of 35.2 meters. The building's roof is designed as a spatial steel truss structure supported by steel columns, with overhanging edges on all sides and a canopy over the main entrance and terrace. The approximate overall dimensions in plan are 124.8 by 207.0 meters.

The steel roof elements span the entire volume of the building and consist of a spatial grid structure comprising longitudinal and transverse trusses. The support for the roofing is provided by a reinforced concrete frame and steel columns, which, in turn, rest on the reinforced concrete structure of the frame and the steel structure of the cantilever.

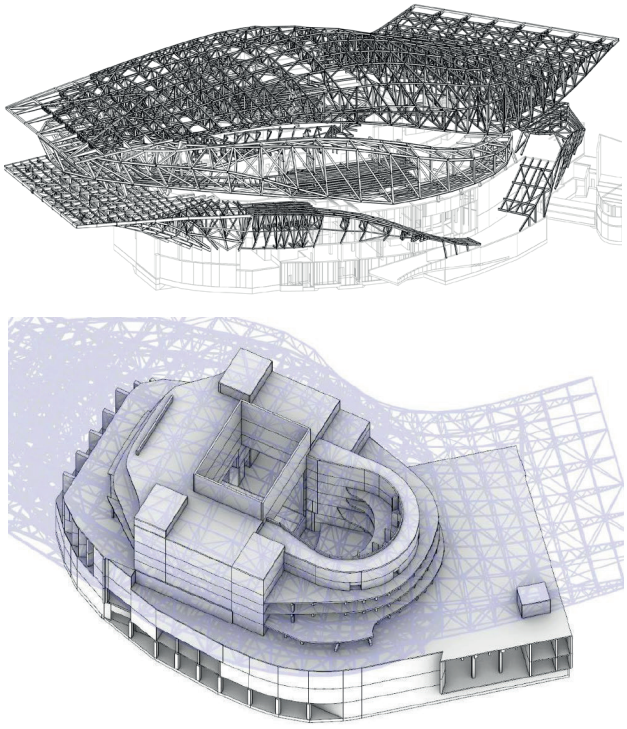


Figure 1. Structural views

The steel elements of the 35.2-meter cantilever consist of longitudinal and transverse trusses made of welded elements. Support for the facade is provided through steel inclined struts on the reinforced concrete frame and the cantilever structure, as well as through cantilever support of the facade elements on the reinforced concrete frame. The steel elements of the structure are made of welded I-beam sections and circular pipes.

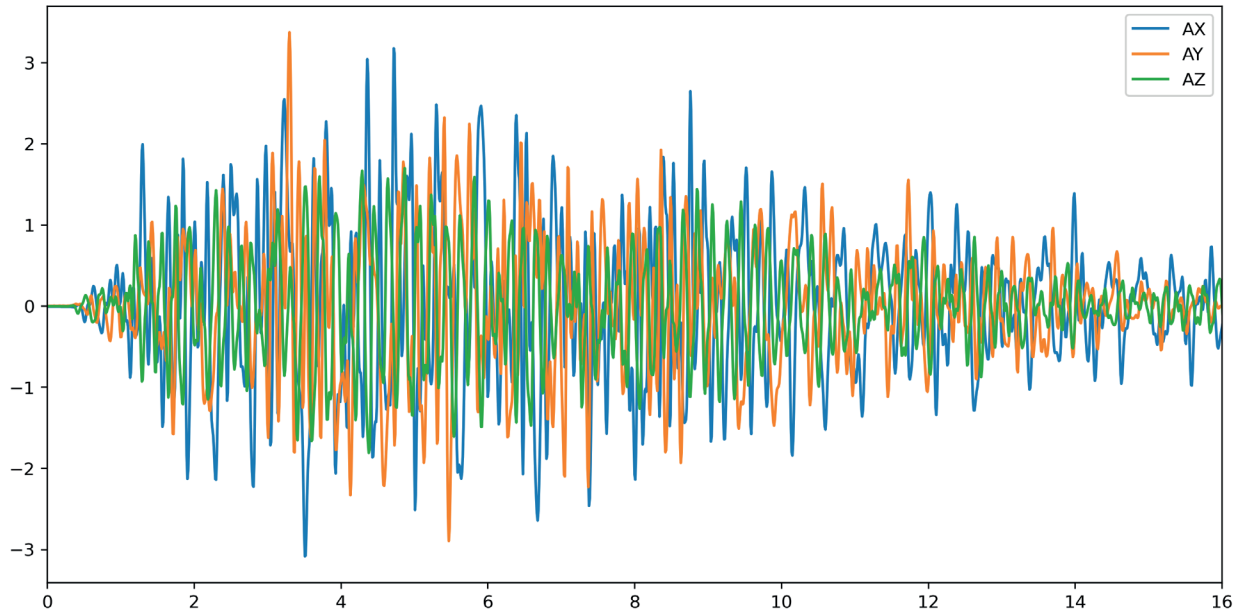


Figure 2. Accelerograms for seismic loads for X, Y, Z directions (acceleration, m/sec^2 vs time, sec)

The joints that connect the steel roof and facades with the reinforced concrete structures of the operational part of the structure are designed as hinged movable and fixed joints with clearances/gaps normal to the base of the joint. Preliminary calculations using linear spectral theory have shown that, in addition to compressive reactions, tensile forces may occur at these joints, leading to cyclic opening/closing of the gap and essentially bidirectional impact loads. Assessing the contribution of the dynamic impact component to the overall stress-strain state of the structure and joints within the framework of linear spectral theory is impossible.

Taking this into account, experimental numerical modeling of the structure was performed in a transient dynamic using direct integration of dynamic equations in time with an implicit scheme, considering physical, geometric, and structural nonlinearities.

The base excitation considered was seismic loading based on a three-component ground motion record of the ultimate level (Level KZ) with a structure responsibility factor (K0) of 1.3, in accordance with current regulatory requirements.

3. MODELS AND THEIR PROPERTIES

The analysis of the structure's behavior was performed in a dynamic setup using the Newmark method with standard integration parameters [7], considering physical and geometric nonlinearities. Damping was implemented in the analytical model using Rayleigh damping. For steel structures, the determination of the "alpha" and "beta" parameters was performed with damping set at 2% of critical damping, while for reinforced concrete; it was set at 5% of critical damping.

Considering the complexity of the structural design and the independent vibrations of structural segments, the Rayleigh damping range was considered in the range of f_1 = 1.381 Hz, up to 33 Hz.

Number of natural mode	Natural frequency, Hz
1	1.381
2	1.5744
3	1.6095
4	1.9641
5	2.0974
6	2.1176

Number of natural mode	Natural frequency, Hz
7	2.183
8	2.2404
9	2.2691
10	2.2841

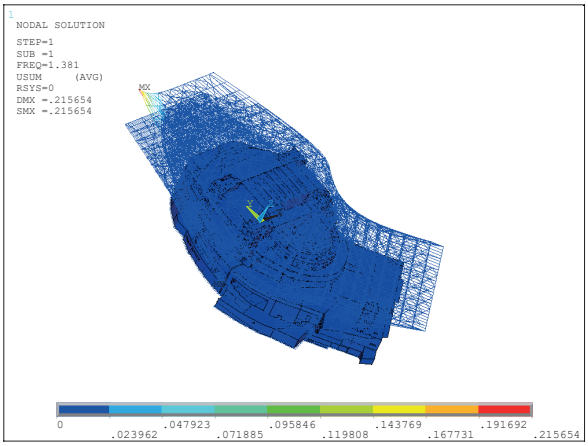


Figure 3. First natural mode of structure

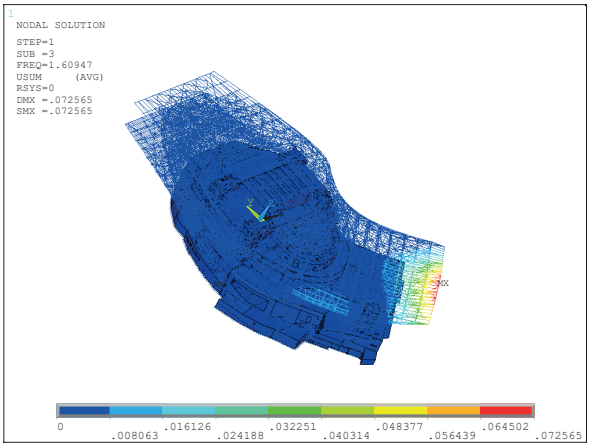


Figure 4. Third natural mode of structure

The calculations were realized with ANSYS Mechanical software package. In the analysis the following elements were used:

– structural beam elements BEAM188 based on Timoshenko's theory with corrections for shear and seven degrees of freedom at each node (three translations, three rotations, and one out-of-plane degree of freedom)

– thin-walled shell elements SHELL181 in the Mindlin-Reissner form with full integration (for representing wall and slab reinforced concrete structures).

The modeling of joints was done using discrete spring elements. Several options were considered beforehand:

- A variable stiffness spring elements (multi-linear form) COMBIN39.
- Two springs oriented in different directions along local axes with clearances, using COMBIN40 elements.
- The combination of the COMBIN40 spring element with a contact element node-to-node.

Table 1. Axial stiffness of springs for middle range of triaxial displacement-force curve for COMBIN39

Joint type	Axial stiffness, kN/m	Gap, mm
A	744580	1.8
B	372080	2
G	764050	2.6
D1	1583440	2.6
D2	1187500	2.6
D3	791560	2.6
D4	372080	1.7
D5	372080	1.7
E	555670	2.4

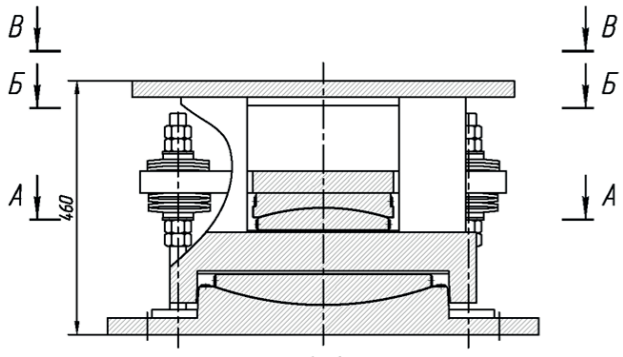


Figure 5. Section of Joint type A

The COMBIN40 options showed a good force-displacement relation during verification modeling. However, during the actual dynamic analysis, they encountered unconvergence issues.

The use of finite elements of the COMBIN39 type was chosen as optimal. The behavior of the supporting joints with clearances was represented in the form of a three-linear displacement-stiffness diagram. The stiffness of the extreme

segments was equivalent to the longitudinal stiffness of the connected structures, while the middle segment was assumed to have the stiffness of disc springs introduced into the structural node to reduce the influence of clearances on the stress-strain state of the structure.

Figure 5 displays a graph of force verification in the element relative to the displacement of one of the structure's nodes. In the 0-2 interval, a compressive load is applied to the node, followed by unloading. In the 2-3 interval, a displacement equal to the clearance is applied, followed by equivalent tensile loading in stage 1.

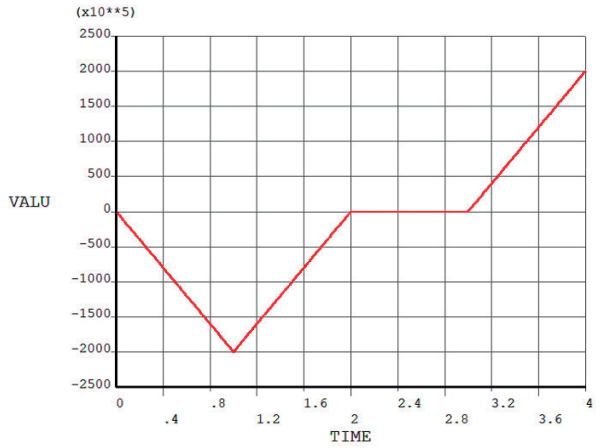


Figure 6. Force-loading stage relationship for COMBIN39 as joint with gaps

It's worth noting that the stiffness ratio between the middle and extreme segments of the diagram spans several orders of magnitude, which, in turn, affects the convergence of the solution when transitioning from the "stiff" portion of the curve to the "soft" portion and vice versa.

4. RESULTS AND DISCUSSION

The conducted computational studies indicate that small clearances/gaps in the joints, allowing limited movement of the structure as a rigid body, have a minimal impact on the resulting stress-strain state of the entire system.

According to the performed computational studies, the joints with clearances have relations describing the stress-strain state over time that are similar to those of the model without them (top diagrams in Figure 7 and 8).

Some joints only work in compression, while others experience momentary detachments accompanied by dynamic impact. Such dynamic loading of the system does not qualitatively affect the overall deformation over time, but it leads to local rapidly decaying high-frequency oscillations (visible in the graphs as local densifications of the deformation curves).

It's worth noting that the high-frequency noise generated by the "impacts" of the structure after introducing clearances is more pronounced for joints with higher contact stiffness. Additionally, for these temporary segments, convergence issues arise, necessitating a reduction in the integration step.

To improve convergence and maintain a stable time integration step in this case, two approaches can be applied:

1. Adjust the reduced stiffness of the deformation curve segments for COMBIN39 elements that represent the behavior of joints with closed gaps.
2. Use non-standard integration parameters for the Newmark method [7] to smooth the solution for high-frequency oscillation regions:

$$\alpha = \frac{1}{4}(1+\gamma)^2$$

$$\beta = \frac{1}{2} + \gamma,$$

γ — amplitude decay factor with recommended value between 0.05 and 0.1 for high and moderated speed dynamic processes [6].

For some joints, accounting for the behavior of disc springs and gaps results in a reduction of detachment forces if the displacement does not reach the gap size. For certain elements, such as joint B (element 510493), E (506798), and E (506792), the detachment forces increase from 8.6% to 31.5%. For elements D2 (506805), D2 (506788), D4 (506787), D3 (506806), D2 (506803), and D4 (506804), the increase in compressive forces ranges from 7.3% to 37.8%. Large values correspond to joints with initially small support reactions.

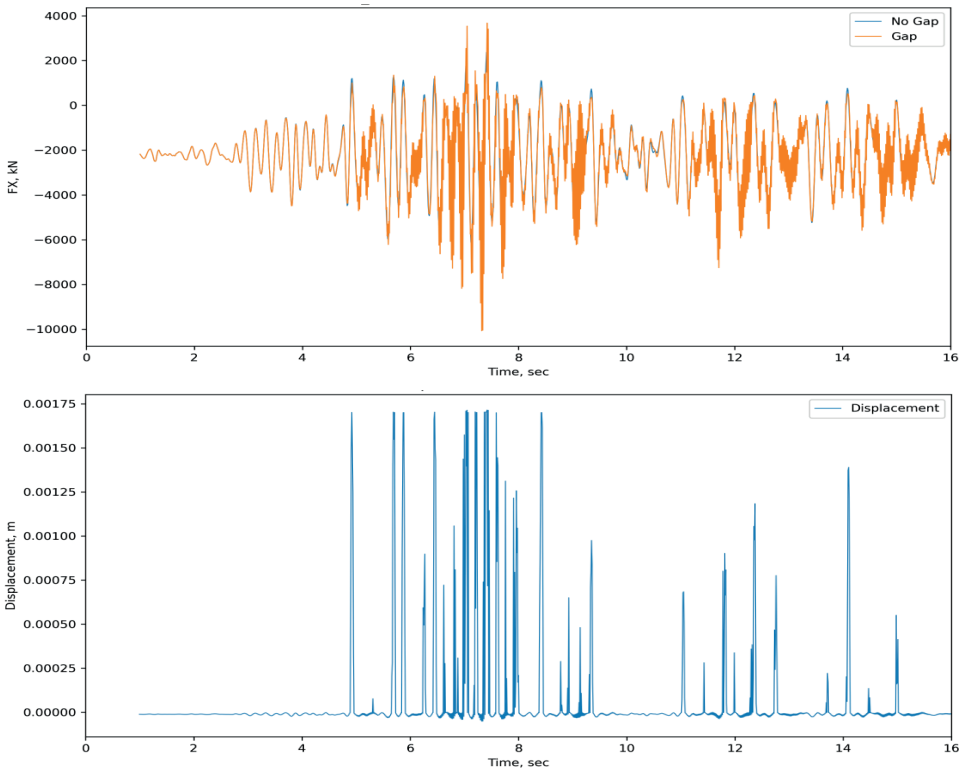


Figure 7. Joint reaction and gap displacement versus time for element 506791 (top — axial reaction vs time, bottom — axial displacement between joint plates vs time)

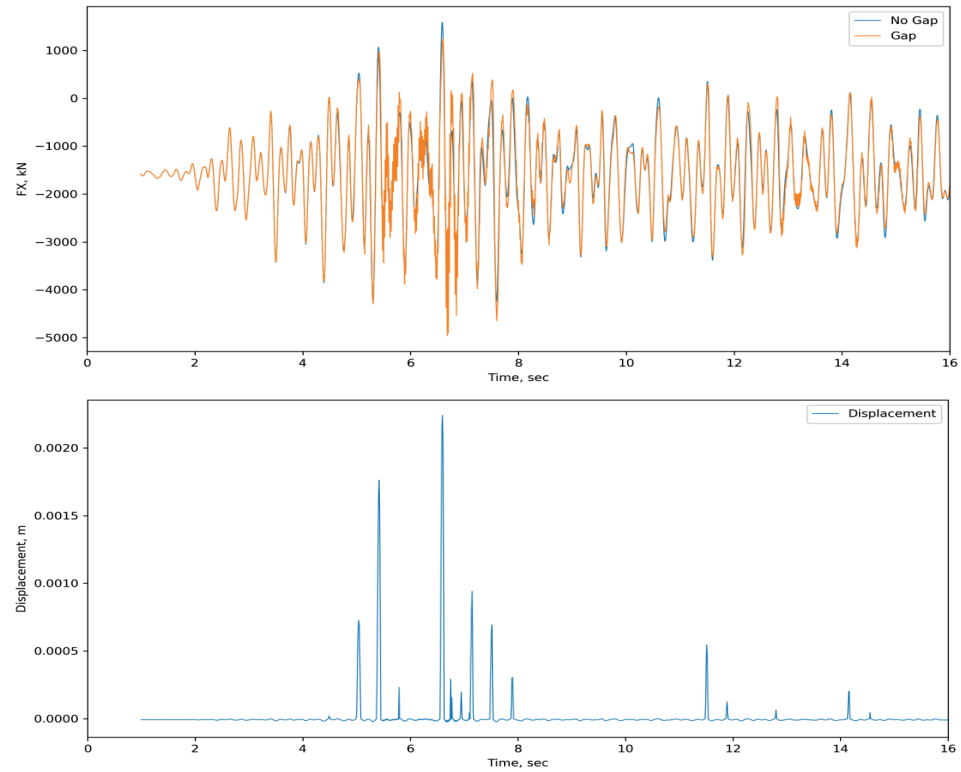


Figure 8. Joint reaction and gap displacement versus time for element 506808 (top — axial reaction vs time, bottom — axial displacement between joint plates vs time)

In most cases, the amplitude of compression/detachment forces is close to those obtained from the model without accounting for the behavior of joints with clearances.
The influence on shear reactions and the change in their amplitude values is insignificant and does not exceed an average of 2%.

CONCLUSION

A methodology for modeling buildings and structures with joints that have clearances/gaps, subjected to cyclic dynamic seismic loading, has been proposed. Approaches for maintaining a stable time step and reducing the computational costs of the iterative solution process have also been presented.
Based on the results of the performed calculations of large-span structure under seismic loading using three-component ground motion records with direct integration of dynamic equations over time, considering physical, geometric, and structural nonlinearities, it is currently possible to use linear elastic models, calculated using linear spectral theory, for modeling structures that include joints with small clearances/gaps.

ACKNOWLEDGEMENTS

This research was supported by Ministry of Science and Higher Education of the Russian Federation (project No. FSWG-2023-0004, “A system of territorial seismic protection of critical infrastructure facilities based on granular metamaterials with the properties of wide-range phonon crystals”).

REFERENCES

1. **Belostotsky, A.M.** Analysis of the causes of the collapse of the roof structures of the SOK Transvaal-Park / A. M. Belostotsky, S.I. Dubinsky // ANSYS Solutions. Russian edition. – 2007. – №4. – P. 5-12.
2. **Belostotsky, A. M.** Analysis of the causes of the collapse of the roof structures of the SOK Transvaal-Park. Part 1. Problem Statement and Numerical Simulation Methodology. Part 2. Simulation of loads / A. M. Belostotsky // Vestnik MGSU. – 2006. – №3. – P. 20-40.
3. **Belostotsky, A.M.** Numerical modeling in expert studies of the causes of collapse and local collapse of structures of large-span buildings / A.M. Belostotsky // Intern. J. for Computational Civil and Structural Engineering. – 2008. – Vol. 4. – Iss. 2. – P. 26–28.
4. Recommendations for the design of shear bolted steel structures. VNIPI Promstalkonstruktsia, CNIIPSK im. Melnikova — 1990.
5. **Kashevarova, G.G.** Comparison of the bearing capacity and deformability of flanged beam-to-column junctions for different flange thicknesses / G.G. Kashevarova, M.P.Son, A. D. Zemlyanuhin // Sovremennie technologii v stroitelstve. Theoria i praktika.. – 2020. – V. 1. – P. 44-49. – EDN JRUIXN.
6. **T.J.R. Hughes.** The Finite Element Method Linear Static and Dynamic Finite Element Analysis. Prentice-Hall, Inc. Englewood Cliffs, NJ. – 1987.
7. **N.M. Newmark.** "Method of Computation for Structural Dynamics". ASCE Journal of Engineering Mechanics Division. Vol. 85. 67-94. 1959.
8. **ANSYS. Mechanical APDL Theory Reference. 2021.**

СПИСОК ЛИТЕРАТУРЫ

1. **Белостоцкий, А.М.** Анализ причин обрушения конструкций покрытия СОК «Трансвааль-парк» / А. М. Белостоцкий, С.И. Дубинский // ANSYS Solutions. Русская редакция. – 2007. – №4. – С. 5–12.

2. **Белостоцкий, А.М.** Анализ причин обрушения конструкций покрытия СОК «Трансвааль-парк». Часть 1. Постановка задачи и методология численного моделирования. Часть 2. Моделирования нагрузок и воздействий / А.М. Белостоцкий // Вестник МГСУ. – 2006. – №3. – С. 20-40.
3. **Белостоцкий, А.М.** Численное моделирование в экспертных исследованиях причин обрушения и локального разрушения конструкций большепролетных зданий / А.М. Белостоцкий // Intern. J. for Computational Civil and Structural Engineering. – 2008. – Vol. 4. – Iss. 2. – P. 26–28.
4. Рекомендации по проектированию работающих на сдвиг болтовых соединений стальных строительных конструкций. ВНИПИ Промстальконструкция, ЦНИИПСК им. Мельникова – 1990 г.
5. **Кашеварова, Г. Г.** Сравнение несущей способности и деформативности фланцевых узлов примыкания балки к колонне при разных толщинах фланца / Г.Г. Кашеварова, М.П. Сон, А.Д. Землянухин // Современные технологии в строительстве. Теория и практика. – 2020. – Т. 1. – С. 44-49. – EDN JRUIXN.
6. **T.J.R. Hughes.** The Finite Element Method Linear Static and Dynamic Finite Element Analysis. Prentice-Hall, Inc. Englewood Cliffs, NJ. – 1987.
7. **N.M. Newmark.** "Method of Computation for Structural Dynamics". ASCE Journal of Engineering Mechanics Division. Vol. 85. 67-94. 1959.
8. **ANSYS. Mechanical APDL Theory Reference. 2021.**

Alexander M. Belostotsky – DSc, Professor, Full Member of the Russian Academy of Architecture and Construction Sciences, Scientific adviser at A.B. Zolotov REC CM of the National Research Moscow State University of Civil Engineering; 129337, Russia, Moscow, Yaroslavskoe shosse, 26. E-mail: amb@stadyo.ru

Andrey S. Pavlov – CSc, Department head at A.B. Zolotov REC CM of the National Research Moscow State University of Civil Engineering; 129337, Russia, Moscow, Yaroslavskoe shosse, 26. E-mail: a.pvlv@yandex.ru

Alexandr I. Nagibovich – CSc, Director at A.B. Zolotov REC CM of the National Research Moscow State University of Civil Engineering; 129337, Russia, Moscow, Yaroslavskoe shosse, 26. E-mail: nagibovich@yandex.ru

Белостоцкий Александр Михайлович – д.т.н., профессор, академик РААСН, научный руководитель НОЦ КМ им. А.Б. Золотова Национального исследовательского Московского государственного строительного университета; 129337, Россия, г. Москва, Ярославское шоссе, д. 26. E-mail: amb@stadyo.ru

Павлов Андрей Сергеевич – к.т.н, руководитель отдела НОЦ КМ им. А.Б. Золотова Национального исследовательского Московского государственного строительного университета; 129337, Россия, г. Москва, Ярославское шоссе, д. 26. E-mail: a.pvlv@yandex.ru

Нагибович Александр Игоревич – к.т.н, директор НОЦ КМ им. А.Б. Золотова Национального исследовательского Московского государственного строительного университета; 129337, Россия, г. Москва, Ярославское шоссе, д. 26. E-mail: nagibovich@yandex.ru

International Journal for Computational Civil and Structural Engineering, 19(3) 173–183(2023)

DOI:10.22337/2587-9618-2023-19-3-173-183

DEVELOPMENT OF COMPUTATIONAL SCHEMES OF GENERALIZED KINEMATIC DEVICES THAT PRECISELY REGULATE THE NATURAL FREQUENCY SPECTRUM OF ELASTIC SYSTEMS WITH A FINITE NUMBER OF DEGREES OF MASS FREEDOM, IN WHICH THE DIRECTIONS OF MOTION ARE PARALLEL, BUT DO NOT LIE IN THE SAME PLANE PART 1: THEORETICAL FOUNDATIONS

Leonid S. Lyakhovich [1], Pavel A. Akimov [2], Zaur R. Galyautdinov [1], Andrey S. Plyaskin [1]

[1] Tomsk State University of Architecture and Civil Engineering, Tomsk, RUSSIA

[2] National Research Moscow State University of Civil Engineering, Moscow, RUSSIA

Abstract: To date, for some elastic systems with a finite number of degrees of mass freedom, in which the directions of mass movement are parallel and lie in the same plane, methods have been developed for creating additional generalized targeted constraints and generalized targeted kinematic devices. Each generalized targeted constraint increases, and each generalized targeted kinematic device reduces the value of only one selected natural frequency to a predetermined value, without changing the remaining natural frequencies and natural modes. Earlier, for elastic systems with a finite number of degrees of mass freedom, in which the directions of mass motion are parallel, but do not lie in the same plane (for example, plates), an approach for the computing of a matrix of additional stiffness and a method for the development of computational schemes of additional generalized targeted constraints were developed. Also earlier, for such systems, an approach was proposed for the computing of a special matrix with allowance for additional inertial forces that determine a generalized targeted kinematic device. At the same time, the method of development of computational schemes of kinematic devices was not proposed. The distinctive paper is devoted to approach, that makes it possible to develop computational schemes of generalized targeted kinematic devices for such systems as well. A variant of the computational scheme of constraint for the rod system with one degree of activity, is considered. Some special properties of such targeted kinematic devices are revealed.

Keywords: localization, natural frequency, natural mode, additional generalized targeted constraint, stiffness coefficients, inertial forces, generalized targeted kinematic device

ФОРМИРОВАНИЕ РАСЧЕТНЫХ СХЕМ ОБОБЩЕННЫХ КИНЕМАТИЧЕСКИХ УСТРОЙСТВ, ПРИЦЕЛЬНО РЕГУЛИРУЮЩИХ СПЕКТР ЧАСТОТ СОБСТВЕННЫХ КОЛЕБАНИЙ УПРУГИХ СИСТЕМ С КОНЕЧНЫМ ЧИСЛОМ СТЕПЕНЕЙ СВОБОДЫ МАСС, У КОТОРЫХ НАПРАВЛЕНИЯ ДВИЖЕНИЯ ПАРАЛЛЕЛЬНЫ, НО НЕ ЛЕЖАТ В ОДНОЙ ПЛОСКОСТИ

Л.С. Ляхович [1], П.А. Акимов [2], З.Р. Галяутдинов [1], А.С. Пляскин [1]

[1] Томский государственный архитектурно-строительный университет, г. Томск, РОССИЯ

[2] Национальный исследовательский Московский государственный строительный университет, г. Москва, РОССИЯ

Аннотация: К настоящему времени для некоторых упругих систем с конечным числом степеней свободы масс, у которых направления движения масс параллельны и лежат в одной плоскости, разработаны методы создания дополнительных обобщенных прицельных связей и обобщенных прицельных кинематических

устройств. Каждая обобщённая прицельная связь увеличивает, а каждое обобщенное прицельное кинематическое устройство уменьшает величину лишь одной выбранной собственной частоты до наперед заданного значения, не изменяя при этом остальные собственные частоты и формы собственных колебаний. Ранее для упругих систем с конечным числом степеней свободы масс, у которых направления движения масс параллельны, но не лежат в одной плоскости (например, пластины), разработан подход образования матрицы дополнительных жесткостей и метод формирования расчетных схем дополнительных обобщенных прицельных связей. Также ранее для таких систем предложен подход образования матрицы учета действия дополнительных инерционных сил, определяющих обобщенное прицельное кинематическое устройство. При этом способ формирования расчетных схем кинематических устройств, предложен не был. В данной статье предлагается подход, позволяющий формировать расчетные схемы обобщенных прицельных кинематических устройств и для таких систем. Рассмотрен вариант расчетной схемы связи, представленный стержневой системой с одной степенью активности. Выявлены некоторые особые свойства таких прицельных кинематических устройств.

Ключевые слова: частота собственных колебаний, форма собственных колебаний, дополнительная обобщенная прицельная связь, коэффициенты жесткости, инерционные силы, обобщенное прицельное кинематическое устройство

INTRODUCTION

As is known [1-9], one of the methods for releasing a certain frequency interval from one or more natural frequencies can be the introduction of generalized targeted constraints and generalized targeted kinematic devices. In the mentioned research works, for elastic systems with a finite number of degrees of freedom of masses, in which the directions of mass motion are parallel and lie in the same plane (for example, elastic rods), methods and algorithms for development of targeted constraints and generalized targeting kinematic devices were proposed. In [3-9] for systems with a finite number of degrees of freedom of masses, in which the directions of mass motion are parallel, but do not lie in the same plane, an approach is proposed to the computing of a matrix of additional stiffness coefficients with allowance for targeted constraints and an algorithm for development of computational scheme for this constraint. For generalized targeted kinematic devices an approach to the computing of a special matrix with allowance for additional inertial forces was also considered. Besides, a method for development of computational schemes of kinematic devices for such systems has not been proposed.

The distinctive paper contains description of an algorithm that makes it possible to develop computational schemes of kinematic devices for such systems as well. A variant of the computational scheme, represented by a statically determinate rod system with one degree of activity, is considered. Some special properties of such kinematic devices have been revealed. The possibility of taking into account the influence of the elastic properties of the rods of a kinematic device on the values of the natural frequencies and the coordinates of natural modes is considered.

Let us present, in accordance with [4, 5], the algorithm of computing of corresponding matrix with allowance for additional inertial forces. For the considering systems (for instance, Figure 1*a*), the main system of the displacement method is selected (Figure 1*b*). The equations of the displacement method are written in the conventional form for systems with a finite number of degrees of freedom

$$\begin{aligned}
&(r[1,1]+m[1]\omega^2)v_\omega[1,j]+r[1,2]v_\omega[2,j]+\ldots+r[1,q]v_\omega[q,j]+\ldots+r[1,n]v_\omega[n,j]=0\\
&r[2,1]v_\omega[1,j]+(r[2,2]+m[2]\omega^2)v_\omega[2,j]+\ldots+r[2,q]v_\omega[q,j]+\ldots+r[2,n]v_\omega[n,j]=0\\
&\ldots\ldots\ldots\ldots\ldots\ldots\ldots\ldots\ldots\ldots\ldots\ldots\ldots\ldots\ldots\ldots\ldots\ldots\ldots\ldots\ldots\ldots\ldots\ldots\ldots\ldots\ldots\ldots\\
&r[n,1]v_\omega[1,j]+r[n,2]v_\omega[2,j]+\ldots+r[n,q]v_\omega[q,j]+\ldots+(r[n,n]+m[n]\omega^2)v_\omega[n,j]=0
\end{aligned} \qquad (1)$$

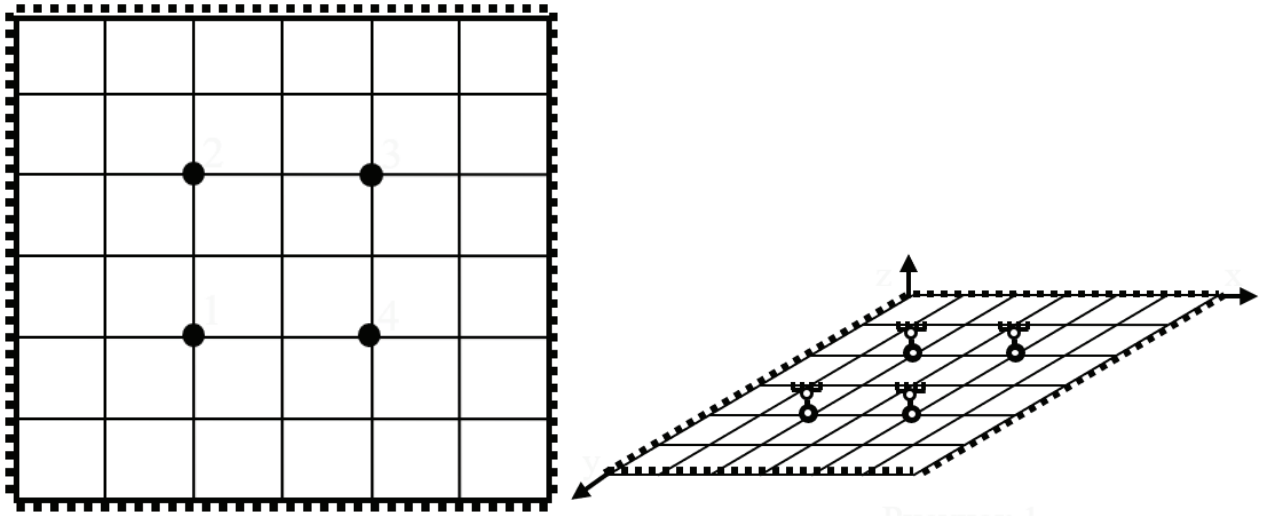


Figure 1. Considering system: a) initial problem; b) the main system of the displacement method.

In (1) the quantities $r[i,k]$ form a matrix of stiffness coefficients $A=\|r[i,k]\|$; the mass values $m[i]$ form a diagonal matrix $M=\|m[i]\|$; ω is the natural frequency of the system; $v_\omega[k,j]$ are displacements in the direction of movement of the masses in the j th ($j=1,2,..,q,,..,n$) form of natural oscillations.

Roots of the equation

$$\left|A-\omega^2 M\right|=0 \tag{2}$$

determine the natural frequency spectrum of the system

$$\omega[1],\omega[2],...,\omega[q-1],\omega[q],\omega[q+1],...\omega[n]. \tag{3}$$

In [4], [5] it is shown that a kinematic device with one degree of activity transmits a generalized impact inertial force to the considering type of structure, which reduces the value of only one natural frequency to a given value ω_S, leaving the remaining frequencies of the spectrum unchanged.

The device is formed on the basis of a special matrix with allowance for additional inertial forces

$$M_0=M_{m0}*M_m, \tag{4}$$

where we have

$$M_m=\|m_0[i,k]\|_{i,k=1}^n. \tag{5}$$

The matrix M_0 has special properties [4], [5]. If the introduced kinematic device is "targeted" at the q th natural frequency, then the coefficients of the matrix M_m ($\|m_0[i,k]\|_{i,k=1}^n$) are orthogonal to the coordinates of the natural modes corresponding to the remaining frequencies of the spectrum. That is

$$\sum_{k=1}^{n} m_0[i,k]*v_\omega[k,j]=0, \quad (i=1,2,..,n,\ j=1,2,..,q-1,q+1,..,n). \tag{6}$$

In relation to the q th natural frequency, at which the kinematic device is "targeted" we have

$$\sum_{k=1}^{n} m_0[i,k]*v_\omega[k,q]\neq 0, \quad (i=1,2,..,n). \tag{7}$$

In [4], [5] it is shown that conditions (5) and (6) will be satisfied by the coefficients

$$m_0[i,k]=m[i]m[k]v_\omega[i,q]v_\omega[k,q]. \tag{8}$$

The value of the multiplier M_{m0} is found as the root of the equation

$$\left|(A-\omega_S^2 * M)-M_{m0} * (\omega_S^2 * M_m)\right| = 0 . \quad (9)$$

The value M_{m0} is determined by the dependency

$$M_{m0} = \frac{\sum_{i=1}^{n}\sum_{k=1}^{n}(a[i,k]-\omega_S^2 m[i,k])v_\omega[i,(q)]v_\omega[k,(q)]}{\sum_{i=1}^{n}\sum_{k=1}^{n}\omega_S^2 m_0[i,k]v_\omega[i,(q)]v_\omega[k,(q)]} \quad (10)$$

Result of solving the equation

$$\left|A-\omega^2(M+M_{m0}M_m)\right| = 0 \quad (11)$$

must confirm that the natural modes have not changed, and the "target" frequency has decreased to the value ω_S.

Kinematic device, which will correspond to a special matrix of coefficients with allowance for additional inertial forces

$$M_0 = M_{m0}M_m , \quad M_m = \left\|m_0[i,k]\right\|_{i,k=1}^{n} , \quad (12)$$

should ensure the relationship between nodal displacements is the same as between the coordinates of the q th natural mode of the original system. In [2, 4, 5] it is also shown that such a relationship will be realized if the kinematic device transmits inertial forces $\bar{R}[i](i=1,..,n)$ to the nodes, the ratios between which are proportional to the ratios between the forces

$$R_0[i] = m[i]v_\omega[i,q] . \quad (13)$$

The magnitude of the forces $\bar{R}[i](i=1,..,n)$ [2] is determined from the relation

$$\bar{R}[i] = \sum_{k=1}^{n} M_{mO}\omega_S^2 m_0[i,k]v_\omega[k,(q)] . \quad (14)$$

Computational schemes of generalized targeted kinematic devices are multivariate and depend on the geometry of the base system, the location of the masses and other features of the object.

One of the options for the computational scheme of a generalized targeted kinematic device can be a statically determined hinge-rod system, to which additional mass M_{add} is applied.

The geometry of the computational scheme is determined by the lengths of the main racks installed in the nodes where the masses are located, in the direction of movement of the masses $l_{st}[i]$ $(i=1,2,..,n)$, the coordinates of the node X_0, Y_0, Z_0 for applying the additional mass, as well as the coordinates $X[i], Y[i], Z[i]$ of the articulated fixed supports located outside the original system and determining the directions of the additional rods connecting the tops of some of the main racks with these supports.

After forming a matrix M_0 of coefficients of additional inertial forces (4), (5), (8), (10) and a setting of values $\bar{R}_0[i]$ (12), it is required, by varying the lengths of the racks $l_{st}[i]$ $(i=1,2,..,n)$ and coordinates X_0, Y_0, Z_0, $X[i], Y[i], Z[i]$ to find their values at which the inertial forces $N_{st}[i](i=1,..,n)$ in racks, will be equal to the forces $\bar{R}_0[i](i=1,..,n)$ with the accepted level of approach.

Thus, it is proposed to solve the problem of forming a computational scheme of a kinematic device based on minimizing the sum of the squares of the differences between the inertial forces arising in the main racks in the process of forming the kinematic device, and the quantities $\bar{R}[i](i=1,..,n)$, the relationships between which will be proportional to the relationships between the forces $\bar{R}_0[i](i=1,..,n)$. To do this, in the space of varied parameters $l_{st}[i]$ $(i=1,2,..,n)$, X_0, Y_0, Z_0, $X[i], Y[i], Z[i]$ the target function is selected

$$f_0 = \sum_{i=1}^{i=n} (Nst[i] - \overline{R}[i])^2 . \qquad (15)$$

To assess the proximity of the target function (14) to the minimum, a small value OOO is assigned.

In accordance with the above, a version of the computational scheme of the kinematic device is formed in the form as a statically determinable hinged-rod system. In this case, the computational scheme should provide the additional mass with only one degree of freedom, namely the ability to move in parallel with the movements of the remaining masses in the process of natural oscillations.

According to the design conditions, the length of one of the main racks (for example, the g th rack) is specified. Let's call this rack the base one, $l_{st}[g] = l_{st0}[g]$. The initial values of the remaining variable parameters are selected, that is, the lengths of the racks

$$\overline{l}_{st}[i] \ (i = 1,2,..,(g-1),(g+1),..,n)$$

and coordinates X_0, Y_0, Z_0, $X[i], Y[i], Z[i]$.

These steps determine the initial geometry of the computational model of the kinematic device.

To further solve the problem, it is necessary to choose a method for finding the minimum of the target function (15) (steepest descent [10-15], random search [16-18], or others).

The algorithm for implementing further steps to develop the computational model of the kinematic device is similar to the algorithm of development of the computational model of the targeted constraints [6-9].

The first step. Increments are set to variable lengths of racks

$$l_{st}[i] = \overline{l}_{st}[i] + \Delta l (i = 1,2,..,(g-1),(g+1),..,n)$$

and coordinates

$$X_0 = X_0 + \Delta X_0 , \quad Y_0 = Y_0 + \Delta Y_0 ,$$

$$Z_0 = Z_0 + \Delta Z_0 ;$$

$$X[i] = X[i] + \Delta X[i], \quad Y[i] = Y[i] + \Delta Y[i],$$

$$Z[i] = Z[i] + \Delta Z[i], (i = 1,2,...n_1) ;$$

Thus, the geometry of the computational scheme of the kinematic device is updated.

The second step. A system of equilibrium equations is compiled to determine the forces in the elements of the updated computational scheme of a statically determinate kinematic device.

The third step. From the equilibrium equations, the forces in the elements of the computational scheme of the kinematic device are found.

The fourth step. The value of the target function (15) is computed.

The fifth step. If we have $f_0 > OOO$, then in accordance with the chosen method of searching for the minimum of the target function (15), the varied parameters and thereby the computational scheme of the kinematic device and the system of equilibrium equations are adjusted. Then we go to the third step and the process continues.

The sixth step. If the value f_0 is less than a preselected small value OOO, then the process ends, and the computational scheme of the targeted kinematic device is developed with a given error (OOO).

Within development a computational scheme or creation of targeted constraints situations are known in which the values of the lengths of the main racks turn out to be of different signs. Structurally, such a computational scheme is almost impossible to implement. In these cases, within creation of targeted constraints, the constraint shifted in the direction of mass movement in a positive or negative direction by an amount at which the lengths of all main racks became of the same sign [7, 9]. Within development of computational scheme of kinematic devices, a similar the solution is not always applicable in such situations.

Allowance for the features of kinematic devices, when the above situation occurs, represents a separate problem and will be considered separately in subsequent paper.

Let us consider an approach to determining the value of additional mass (M_{add}) from the condition that the kinetic energy of additional inertial forces is equal to the work of the inertial force created by the additional mass during natural vibrations.

It is obvious that the kinetic energy of additional inertial forces (E_k) is determined by the dependence

$$E_k = M_{m0}\left[\sum_{i=1}^{n}\sum_{k=1}^{n}\omega_S^2 m_0[i,k]v_\omega[i,(q)]v_\omega[k,(q)]\right]. \quad (16)$$

Inertial force created by additional mass is equal to

$$N_{in}(t) = -M_{add}\frac{\partial^2 v(t)}{(\partial t)^2}. \quad (17)$$

Movement of additional mass in (17) is equal to

$$v(t) = v_m \sin(\omega_S t). \quad (18)$$

In (18) the amplitude value of the movement of additional mass during vibrations.

From (17) and (18) it follows that the amplitude value of the inertial force created by the additional mass

$$N_{in} = M_{add} v_m \omega_S^2. \quad (19)$$

Equating the kinetic energy of additional inertial forces (16) to the work of the inertial force N_{in} on displacement v_m, we obtain $E_k = N_{in} v_m$ or $E_k = v_m^2 \omega_S^2$. Thus, we get

$$M_{add} = \frac{M_{m0}\left[\sum_{i=1}^{n}\sum_{k=1}^{n}\omega_S^2 m_0[i,k]v_\omega[i,(q)]v_\omega[k,(q)]\right]}{M_{add} v_m^2 \omega_S^2}. \quad (20)$$

In order to use dependence (20) it is necessary to determine firstly the displacement value v_m.

Let us consider the option of determining the value v_m under the condition that the kinematic device moves as an absolutely rigid body only due to the displacement of the nodes in which the masses of the original system are located. To do this, in the generated scheme of the kinematic device, a unit force is introduced in the node for applying additional mass, directed parallel to the movement of the masses. The action of this force determines the forces in the main racks

$$N_{st,1}[i] \quad (i = 1,2,..,n).$$

The movements of the nodes, where the main racks are installed, are determined by the coordinates of the shape of the natural mode corresponding to the frequency at which the kinematic device is 'targeted"

$$\mathbf{v_\omega[i,(q)] \quad (i = 1,2,..,n)}.$$

Thus, we have

$$v_m = \sum_{i=1}^{n} v_\omega[i,(q)]N_{st,1}[i], \quad (21)$$

M_{add} is determined by (20). The determination did not take into account the compliance of the kinematic device rods. Therefore, the result of changes in the spectrum of natural frequencies will depend on the rigidity parameters of its elements.

Let us consider the possibility of taking into account the influence of the compliance of the rods of the kinematic device on the amount of movement of additional mass. Let us denote the amplitude of movement of additional mass during oscillations by $v_{m,0}$. The value $v_{m,0}$ consists of two components

$$v_{m,0} = v_m + v_{m,d}, \quad (22)$$

where v_m is the component corresponding to the movement of the kinematic device as an absolutely rigid body (21); $v_{m,d}$ is the component of the movement of additional mass corresponding to the deformation of the rods of the kinematic device.

In order to determine $v_{m,d}$ the forces in all the rods of the developed diagram of the kinematic device from the action of a unit force introduced at the node of application of additional mass and directed parallel to the movement of the masses

$$N_{st,1}[i], N_{p,1}[j], N_{d,1}[k].$$

are found.

Here $N_{st,1}[i], N_{p,1}[j], N_{d,1}[k]$ are the corresponding forces are in the racks, belt rods and additional rods. The amplitude values of the forces

$$N_{st}[i], N_p[j], N_d[k],$$

that arise during natural vibrations in the rods of the kinematic device are determined at the end of the process of its creation. It should be noted that $N_{st}[i], N_p[j], N_d[k]$ are respectively the forces in the racks, belt rods and additional rods. Since the linear theory of small vibrations is used, the forces in the rods of the kinematic device are determined according to the undeformed scheme.

Thus, the displacement $v_{m,d}$ is determined by the constraint

$$v_{md} = \left[\sum_{i=1}^{n} \frac{N_{st}[i] N_{st,1}[i] \left| l_{st}[i] \right|}{EF_{st}[i]} + \right. \\ + \sum_{j=1}^{n_2} \frac{N_p[j] N_{p,1}[j] l_p[j]}{EF_p[j]} + \\ \left. + \sum_{k=1}^{n_1} \frac{N_d[k] N_{d,1}[j] l_d[k]}{EF_d[k]} \right], \quad (23)$$

where $E, F_{st}[i], F_p[j], F_d[k]$ are respectively the elastic modulus of the material of the kinematic device and the cross-sectional area of the racks, belt and additional rods.

The total displacement is presented in (22).

The expression for determining the amplitude value of the inertial force created by the additional mass can be written in the following form

$$N_{in,0} = M_{add} v_{m,0} \omega_S^2. \quad (24)$$

The energy balance is now based on the equality of the sum of the kinetic energy of additional inertial forces (E_k) and the potential energy of deformation of the rods of the kinematic device (E_d) to the work of the inertial force $N_{in,0}$ on displacement $v_{m,0}$. This condition takes the form

$$E_k + E_d = N_{in,0} v_{m,0} = M_{add} v_{m,0}^2 \omega_S^2; \quad (25)$$

$$v_{md} = \left[\sum_{i=1}^{n} \frac{N_{st}^2[i] l_{st}[i]}{EF_{st}[i]} + \sum_{j=1}^{n_2} \frac{N_p^2[j] l_p[j]}{EF_p[j]} + \right. \\ \left. + \sum_{k=1}^{n_1} \frac{N_d^2[k] l_d[k]}{EF_d[k]} \right]. \quad (26)$$

Finally, we have

$$M_{add} = \frac{E_k + E_d}{v_{m,0}^2 \omega_S^2}. \quad (27)$$

Before the formation of the kinematic device, a system with n degrees of freedom was considered. Let us call the natural frequencies of this system (3) "basic". If the kinematic device is created in such a way that the additional mass is able to move only in parallel with the movements of the remaining masses, then only one more degree of freedom is added to the considering system. Thus, the considering system has $(n+1)$ degrees of freedom. This circumstance causes the appearance of another "additional" natural frequency.

The targeting of the kinematic device is realized only in relation to the "basic" natural frequencies. The value of the "additional" natural frequency depends on the compliance parameters of the rods of the kinematic device and can be either

greater than the values of all “basic” frequencies or less than any of them.

REFERENCES

1. **Lyahovich L.S., Maletkin O.Ju.** O pricel'nom regulirovanii sobstvennyh chastot uprugih system [On targeted control of natural frequencies of elastic systems]. // Izvestija vuzov. Stroitel'stvo i arhitektura, 1990, No. 1, pp. 113-117 (In Russian).
2. **Lyahovich L.S.** Osobye svojstva optimal'nyh sistem i osnovnye napravlenija ih realizacii v metodah rascheta sooruzhenij [Special properties of optimal systems and the main directions of their implementation in the methods of structural analysis]. Tomsk, TGASU, 2009. – 372 pages (In Russian).
3. **Lyakhovich L.S., Akimov P.A.** Aimed control of the frequency spectrum of eigenvibrations of elastic plates with a finite number of degrees of freedom of masses by superimposing additional constraints. // International Journal for Computational Civil and Structural Engineering, 2021, Volume 17, Issue 2, pp. 76-82.
4. **Lyakhovich L.S., Akimov P.A.** Aimed control of the frequency spectrum of eigenvibrations of elastic plates with a finite number of degrees of freedom by introducing additional generalized kinematic devices. // International Journal for Computational Civil and Structural Engineering, 2021, Volume 17, Issue 3, pp. 14-20.
5. **Akimov P.A, Lyahovich L.S.** Pricel'noe regulirovanie spektra chastot sobstvennyh kolebanij uprugih plastin s konechnym chislom stepenej svobody mass putem vvedenija dopolnitel'nyh obobshhennyh svjazej i obobshhennyh kinematicheskih ustrojstv [Precision control for eigen-frequency of elastic plates with finite number of mass degrees of freedom by using additional generalized connections and kinematic devices]. // Vestnik Tomskogo gosudarstvennogo arkhitekturno-stroitel'nogo universiteta. Journal of Construction and Architecture, 2021, Vol. 23, No. 4, pp. 57-67 (In Russian).
6. **Lyakhovich L.S., Akimov P.A.** About Development of Computational Schemes of Some Additional Constraints for Elastic Systems. Part 1: Theoretical Foundations [О формировании расчетных схем некоторых дополнительных связей для упругих систем. Часть 1: Теоретические основы подхода]. // Promyshlennoe i Grazhdanskoe Stroitelstvo, 2022, No. 9, pp. 4-10 (in Russian).
7. **Lyakhovich L.S., Akimov P.A.** About Development of Computational Schemes of Some Additional Constraints for Elastic Systems. Part 2: Samples of Analysis [О формировании расчетных схем некоторых дополнительных связей для упругих систем. Часть 2: Примеры расчетов]. // Promyshlennoe i Grazhdanskoe Stroitelstvo, 2022, No. 9, pp. 4-10 (in Russian).
8. **Lyakhovich L.S., Akimov P.A.** Formation of Computational Schemes of Additional Targeted Constraints That Regulate The Frequency Spectrum of Natural Oscillations of Elastic Systems With a Finite Number of Degrees of Mass Freedom, the Directions of Movement of Which are Parallel, But Do Not Lie in the Same Plane. Part 1: Theoretical Foundations. // International Journal for Computational Civil and Structural Engineering, 2022, Volume 18, Issue 2, pp. 183-193.
9. **Lyakhovich L.S., Akimov P.A.** Formation of Computational Schemes of Additional Targeted Constraints That Regulate The Frequency Spectrum of Natural Oscillations of Elastic Systems With a Finite Number of Degrees of Mass Freedom, the Directions of Movement of Which are Parallel, But Do Not Lie in the Same Plane. Part 2: The First Sample of Analysis. // International Journal for Computational Civil and Structural Engineering, 2022, Volume 18, Issue 3, pp. 137-146.
10. **Bertola M.** Nonlinear steepest descent approach to orthogonality on elliptic curves. //

Journal of Approximation Theory, 2022, Vol. 276, 105717.
11. **Chen Z., Fang Y., Kong X., Dehg L.** Identification of multi-axle vehicle loads on beam type bridge based on minimal residual norm steepest descent method. // Journal of Sound and Vibration, 2023, Vol. 563, 117866.
12. **Lapucci M., Mansueto P.** Improved front steepest descent for multi-objective optimization. // Operations Research Letters, 2023, Vol. 51, Issue 3, pp. 242-247.
13. **Mittal G., Gibi A.K.** A modified steepest descent method for solving non-smooth inverse problems. // Journal for Computational and Applied Mathematics, 2023, Vol. 424, 114997.
14. **Mittal G., Gibi A.K.** Convergence analysis of an optimally accurate frozen multi-level projected steepest descent iteration for solving inverse problems. // Journal of Complexity, 2023, Vol. 75, 101711.
15. **Ren Q.** Seismic acoustic full waveform inversion based on the steepest descent method and simple linear regression analysis. // Journal of Applied Geophysics, 2022, Vol. 203, 104686.
16. **Do B., Ohsaki M.** A random search for discrete robust design optimization of linear-elastic steel frames under interval parametric uncertainty. // Computers & Structures, 2021, Vol. 249, 106506.
17. **Oztas G.Z., Erdem S.** Random search with adaptive boundaries algorithm for obtaining better initial solutions. // Advances in Engineering Software, 2022, Vol. 169, 103141.
18. Wosniack M.E., Raposo E.P., Viswanathan G.M., da Luz M.G.E. A parallel algorithm for random searches. // Computer Physics Communications, 2015, Vol. 196, pp. 390-397.

СПИСОК ЛИТЕРАТУРЫ

1. **Ляхович Л.С., Малеткин О.Ю.** О прицельном регулировании собственных частот упругих систем. // Известия вузов. Строительство и архитектура, 1990, № 1, с. 113-117.
2. **Ляхович Л.С.** Особые свойства оптимальных систем и основные направления их реализации в методах расчета сооружений. Монография. – Томск: Издательство ТГАСУ, 2009. - 372 с.
3. **Lyakhovich L.S., Akimov P.A.** Aimed control of the frequency spectrum of eigenvibrations of elastic plates with a finite number of degrees of freedom of masses by superimposing additional constraints. // International Journal for Computational Civil and Structural Engineering, 2021, Volume 17, Issue 2, pp. 76-82.
4. **Lyakhovich L.S., Akimov P.A.** Aimed control of the frequency spectrum of eigenvibrations of elastic plates with a finite number of degrees of freedom by introducing additional generalized kinematic devices. // International Journal for Computational Civil and Structural Engineering, 2021, Volume 17, Issue 3, pp. 14-20.
5. **Акимов П.А., Ляхович Л.С.** Прицельное регулирование спектра частот собственных колебаний упругих пластин с конечным числом степеней свободы масс путем введения дополнительных обобщенных связей и обобщенных кинематических устройств. // Вестник Томского государственного архитектурно-строительного университета, 2021, том 23, № 4, с. 57-67.
6. **Ляхович Л.С., Акимов П.А.** О формировании расчетных схем некоторых дополнительных связей для упругих систем. Часть 1. Теоретические основы подхода. // Промышленное и гражданское строительство, 202, №9, с. 4-10.
7. **Ляхович Л.С., Акимов П.А., Мешеулов Н.В.** О формировании расчетных схем некоторых дополнительных связей для упругих систем. Часть 2. Примеры расчёта. // Промышленное и гражданское строительство, 2022, №9, с. 11-19.

8. **Lyakhovich L.S., Akimov P.A.** Formation of Computational Schemes of Additional Targeted Constraints That Regulate The Frequency Spectrum of Natural Oscillations of Elastic Systems With a Finite Number of Degrees of Mass Freedom, the Directions of Movement of Which are Parallel, But Do Not Lie in the Same Plane. Part 1: Theoretical Foundations. // International Journal for Computational Civil and Structural Engineering, 2022, Volume 18, Issue 2, pp. 183-193.
9. **Lyakhovich L.S., Akimov P.A.** Formation of Computational Schemes of Additional Targeted Constraints That Regulate The Frequency Spectrum of Natural Oscillations of Elastic Systems With a Finite Number of Degrees of Mass Freedom, the Directions of Movement of Which are Parallel, But Do Not Lie in the Same Plane. Part 2: The First Sample of Analysis. // International Journal for Computational Civil and Structural Engineering, 2022, Volume 18, Issue 3, pp. 137-146.
10. **Bertola M.** Nonlinear steepest descent approach to orthogonality on elliptic curves. // Journal of Approximation Theory, 2022, Vol. 276, 105717.
11. **Chen Z., Fang Y., Kong X., Dehg L.** Identification of multi-axle vehicle loads on beam type bridge based on minimal residual norm steepest descent method. // Journal of Sound and Vibration, 2023, Vol. 563, 117866.
12. **Lapucci M., Mansueto P.** Improved front steepest descent for multi-objective optimization. // Operations Research Letters, 2023, Vol. 51, Issue 3, pp. 242-247.
13. **Mittal G., Gibi A.K.** A modified steepest descent method for solving non-smooth inverse problems. // Journal for Computational and Applied Mathematics, 2023, Vol. 424, 114997.
14. **Mittal G., Gibi A.K.** Convergence analysis of an optimally accurate frozen multi-level projected steepest descent iteration for solving inverse problems. // Journal of Complexity, 2023, Vol. 75, 101711.
15. **Ren Q.** Seismic acoustic full waveform inversion based on the steepest descent method and simple linear regression analysis. // Journal of Applied Geophysics, 2022, Vol. 203, 104686.
16. **Do B., Ohsaki M.** A random search for discrete robust design optimization of linear-elastic steel frames under interval parametric uncertainty. // Computers & Structures, 2021, Vol. 249, 106506.
17. **Oztas G.Z., Erdem S.** Random search with adaptive boundaries algorithm for obtaining better initial solutions. // Advances in Engineering Software, 2022, Vol. 169, 103141.
18. Wosniack M.E., Raposo E.P., Viswanathan G.M., da Luz M.G.E. A parallel algorithm for random searches. // Computer Physics Communications, 2015, Vol. 196, pp. 390-397.

Leonid S. Lyakhovich, Full Member of the Russian Academy of Architecture and Construction Sciences, Professor, DSc, Professor of Department of Structural Mechanics, Tomsk State University of Architecture and Building; 2, Solyanaya St., 2, Tomsk, 634003, Russia; E-mail: lls@tsuab.ru

Pavel A. Akimov, Full Member of the Russian Academy of Architecture and Construction Sciences, Professor, Dr.Sc.; Rector of National Research Moscow State University of Civil Engineering; 26, Yaroslavskoe Shosse, Moscow, 129337, Russia; phone: +7(495) 651-81-85; Fax: +7(499) 183-44-38; E-mail: AkimovPA@mgsu.ru, rector@mgsu.ru, pavel.akimov@gmail.com.

Zaur R. Galyautdinov, Associate Professor, DSc, Professor of Department of Reinforced Concrete and Stone Structures, Tomsk State University of Architecture and Building; 2, Solyanaya St., 2, Tomsk, 634003, Russia;
E-mail: gazr@yandex.ru.

Andrey S. Plyaskin, Associate Professor, Ph.D., Head of Department of Metal and Wooden Structures, Tomsk State University of Architecture and Building; 2, Solyanaya St., 2, Tomsk, 634003, Russia;
E-mail: plyaskinandrei@mail.ru.

Ляхович Леонид Семенович, академик РААСН, профессор, доктор технических наук, профессор кафедры строительной механики, Томский государственный архитектурно-строительный университет; 634003, Россия, г. Томск, Соляная пл. 2;
E-mail: lls@tsuab.ru

Акимов Павел Алексеевич, академик РААСН, профессор, доктор технических наук; ректор Национального исследовательского Московского государственного строительного университета; 129337, Россия, г. Москва, Ярославское шоссе, дом 26;
телефон: +7(495) 651-81-85; факс: +7(499) 183-44-38;
Email: AkimovPA@mgsu.ru, rector@mgsu.ru, pavel.akimov@gmail.com.

Галяутдинов Заур Рашидович, доцент, доктор технических наук, доцент кафедры железобетонных и каменных конструкций, Томский государственный архитектурно-строительный университет; 634003, Россия, г. Томск, Соляная пл. 2; E-mail: gazr@yandex.ru.

Пляскин Андрей Сергеевич, доцент, кандидат технических наук, заведующий кафедрой металлических и деревянных конструкций, Томский государственный архитектурно-строительный университет; 634003, Россия, г. Томск, Соляная пл. 2;
E-mail: plyaskinandrei@mail.ru.